République Algérienne Démocratique et Populaire
Ministère de l'Enseignement Supérieur et de la Recherche Scientifique

Université Batna 2 – Mostefa Ben Boulaïd
Faculté de Technologie
Département de Génie Civil

Thèse

Préparée au sein du laboratoire de recherche LGC-ROI, UB2.

Présentée pour l'obtention du diplôme de :

Doctorat en Génie Civil
Option : Géotechnique et Ouvrages d'Art en Interaction

Sous le Thème :

Analyse Numérique du Comportement d'une Conduite sur un Versant Non-Saturé Instable de Grande Hauteur. Cas de la Conduite AEP de Ain Tinn-Mila.

(Numerical Analysis of Pipeline Behavior on High Unstable Unsaturated Slope. Case of AEP pipe of Ain Tinn-Mila.)

Présentée par :

BOUATIA Mohammed

Devant le jury composé de :

Mr. KARECH Toufik	Prof.	Université de Batna 2	Président
Mr. DEMAGH Rafik	Prof.	Université de Batna 2	Rapporteur
Mme. DERRICHE Zohra	Prof.	ENSTP	Co-Rapporteur
Mr. BAHEDDI Mohamed	Prof.	Université de Batna 2	Examinateur
Mr. BENMEBAREK Sadok	Prof.	Université de Biskra	Examinateur
Mr. KHEMISSA Mohamed	Prof.	Université de M'sila	Examinateur
Mlle. BAHLOUL Ouassila	MCA.	Université de Batna 2	Invitée

Juin 2021

Abstract

On the path to development, third world countries, including Algeria, continue to face their own problems. Important part of these encountered problems are linked to the safety and serviceability of many infrastructures built to meet the strong demand of the population which is continuously growing. To this end, the present thesis focuses on the application of unsaturated soil mechanics to study the stability of unsaturated slopes and the behavior of buried pipelines in expansive soils located in a sloping unsaturated area where the Aine-Tine slope located in Mila basin constitute the site of the study.

Pipelines are linear infrastructures which are usually used around the world to transport fluids such as gas and water in the purpose of addressing strong hydraulic and energy inequalities that characterize many countries. In Algeria, the Beni-Haroun dam was built in the province of Mila to ensure hydraulic safety and remedy a strong hydrological inequality that characterizes the eastern part of the country comprising the following provinces: Mila, Constantine, Batna and Khenchela. This was done by burying more than 600 km of pipes of different diameters in the Quaternary basin of the province of Mila, resulting in the creation of a new system consisting of pipe and soil which are two different materials with different characteristics. The pipeline systems necessitate a deep understanding of the mechanism of soil structure interaction because they are generally buried at a shallow depth where they are exposed to the wetting and drying processes and subjected to the variation of the shear strength and stiffness of such soil. As many research did the unfavorable case considered in the studies and designs of the interaction of pipelines with the burial soil was the saturated conditions. However, it not the always the case as confirmed in this thesis and in many new researches as cited in the literature review chapter.

Starting with the verification of the stability of the slope using the software FLAC 3D, the slope was found to be in a critical stability. After that, the unsaturated soil mechanics was considered to verify the effect of the suction on the shear strength of Aine-Tine slope where the fitting parameters of the SWCC played a key role in the variation of the factor of safety.

In the second part of the thesis, numerical investigations were carried out to analyze the effect of expansion movement under precipitation, where it was found that the decrease of suction has a significant effect on the internal forces appeared along the pipeline ring. The obtained results can offer a reliable platform to understand and justify the possible causes of the water leakage points along the pipeline. The simulation was undertaken using GEOSLOPE Software of GeoStudio co ltd, and considering the transverse and longitudinal cross sections of the pipeline. It was verified that the duration of the rain and the initial profile of suction has a proportional effect on the deformation and internal forces happened on the pipeline.

The last part of the thesis was oriented to study the effect of the permanent ground deformations that can follow the surficial slope failures in the Aine-Tine slope especially during the winter season when large amount of the apparent cohesion due to the present suction can be lost under the saturation process during the rain. Numerical investigation was carried out to study

the interaction of pipeline with soil under the effect of large increment of displacements which passes through the centerlines of the pipeline. The rigidity of pipeline and the profile of the suction was considered.

The studies and results presented in the present thesis showed that the consideration of the unsaturated behavior of soils in mandatory especially in countries like Algeria where the arid and semi-arid climate characterize the whole region which give a large variation of the suction present in surficial layers of such region between the summer and winter which lead to very important effect on the interaction of the pipelines with their burial depths. The results of the thesis are promising to be used by engineers and future researchers for using the unsaturated soil mechanics.

ملخص

على طريق التنمية، لا تزال دول العالم الثالث، بما في ذلك الجزائر، تواجه مشاكلها الخاصة. يرتبط جزء مهم من هذه المشكلات التي تمت مواجهتها بسلامة وإمكانية الخدمة للعديد من البنى التحتية التي تم إنشاؤها لتلبية الطلب القوي للسكان الذي يتزايد باستمرار. وتحقيقا لهذه الغاية، تركز الأطروحة الحالية على تطبيق ميكانيكا التربة غير المشبعة لدراسة استقرار المنحدرات غير المشبعة وسلوك خطوط الأنابيب المدفونة في التربة الممتدة الموجودة في منطقة منحدرة غير مشبعة حيث يشكل منحدر عين الطين الواقع في حوض ميلة موقع الدراسة.

خطوط الأنابيب هي عبارة عن بنى تحتية خطية تُستخدم عادةً في جميع أنحاء العالم لنقل السوائل مثل الغاز والمياه بغرض معالجة عدم المساواة القوية في المياه والطاقة التي تميز العديد من البلدان. في الجزائر، تم بناء سد بني هارون في ولاية ميلة لضمان السلامة المائية ومعالجة التفاوت الهيدرولوجي القوي الذي يميز الجزء الشرقي من البلاد والذي يضم المقاطعات التالية: ميلة وقسنطينة وباتنة وخنشلة. وقد تم ذلك عن طريق دفن أكثر من 600 كيلومتر من الأنابيب بأقطار مختلفة في الحوض الرباعي لمقاطعة ميلة، مما أدى إلى إنشاء نظام جديد يتكون من الأنابيب والتربة وهما مادتان مختلفتان لهما خصائص مختلفة.

تتطلب أنظمة خطوط الأنابيب فهمًا عميقًا لآلية تفاعل بين التربة والمنشأة لأنها تُدفن عمومًا على عمق ضحل حيث تتعرض لعمليات الترطيب والتجفيف وتتعرض لتغير قوة القص وكذا صلابة التربة. كما فعلت العديد من الأبحاث، كانت الحالة غير المواتية التي تم أخذها في الاعتبار في الدراسات والتصميمات الخاصة بتفاعل الأنابيب مع تربة الدفن هي الظروف المشبعة. ومع ذلك، ليس هذا هو الحال دائمًا كما تم تأكيده في هذه الأطروحة وفي العديد من الأبحاث الجديدة كما هو مذكور في فصل مراجعة الأدبيات.

في البداية تم التحقق من ثبات المنحدر باستخدام برنامج FLAC 3D ، حيث وجد ان المنحدر في حالة استقرار حرج. بعد ذلك، تم النظر في ميكانيكا التربة غير المشبعة للتحقق من تأثير الشفط على قوة القص لمنحدر Aine-Tine حيث لعبت معلمات التركيب الخاصة بـ SWCC دورًا رئيسيًا في تباين عامل الأمان.

في الجزء الثاني من الرسالة تم إجراء استقصاءات عددية لتحليل تأثير حركة التمدد تحت هطول الأمطار حيث تبين أن انخفاض الشفط له تأثير كبير على القوى الداخلية التي ظهرت على طول حلقة خط الأنابيب. يمكن أن توفر النتائج التي تم الحصول عليها منصة موثوقة لفهم وتبرير الأسباب المحتملة لنقاط تسرب المياه على طول خط الأنابيب. تم إجراء المحاكاة باستخدام GEOSLOPE Software of GeoStudio، مع مراعاة المقاطع العرضية والطولية لخط الأنابيب. تم التحقق من أن مدة المطر والمظهر الأولي للشفط لهما تأثير نسبي على التشوه والقوى الداخلية التي حدثت على خط الأنابيب.

كان الجزء الأخير من الرسالة موجهًا لدراسة تأثير التشوهات الدائمة للأرض التي يمكن أن تتبع فشل المنحدرات السطحية في منحدر Aine-Tine خاصة خلال فصل الشتاء حيث يمكن فقد قدر كبير من التماسك الظاهري بسبب الشفط الحالي تحت عملية التشبع أثناء المطر. تم إجراء دراسة عددية لدراسة تفاعل خط الأنابيب مع التربة تحت تأثير الزيادة الكبيرة في النزوح الذي يمر عبر الخطوط المركزية لخط الأنابيب. تم النظر في صلابة خط الأنابيب وملف الشفط.

أظهرت الدراسات والنتائج المقدمة في الأطروحة الحالية أن النظر في السلوك غير المشبع للتربة إلزامي خاصة في بلدان مثل الجزائر حيث يميز المناخ الجاف وشبه الجاف المنطقة بأكملها مما يعطي تباينًا كبيرًا في الامتصاص الموجود في الطبقات السطحية من هذه المنطقة بين الصيف والشتاء مما يؤدي إلى تأثير مهم للغاية في تفاعل الأنابيب مع تربة الدفن. نتائج الأطروحة واعدة لاستخدامها من قبل المهندسين والباحثين المستقبليين لاستخدام ميكانيكا التربة غير المشبعة.

Résumé :

Sur la voie du développement, les pays du tiers monde, dont l'Algérie, continuent de faire face à leurs propres problèmes. Une partie importante de ces problèmes rencontrés est liée à la sécurité et à l'aptitude au service de nombreuses infrastructures construites pour répondre à la forte demande de la population qui ne cesse de croître. À cette fin, la présente thèse se concentre sur l'application de la mécanique des sols non saturés pour étudier la stabilité des pentes non saturées et le comportement des canalisations enfouies dans des sols expansifs situés dans une zone non saturée en pente où la pente Aine-Tine située dans le bassin de Mila constitue le site de l'étude.

Les pipelines sont des infrastructures linéaires qui sont généralement utilisées dans le monde pour transporter des fluides tels que le gaz et l'eau dans le but de remédier aux fortes inégalités hydrauliques et énergétiques qui caractérisent de nombreux pays. En Algérie, le barrage de Beni-Haroun a été construit dans la province de Mila pour assurer la sécurité hydraulique et remédier à une forte inégalité hydrologique qui caractérise la partie orientale du pays comprenant les provinces suivantes : Mila, Constantine, Batna et Khenchela. Cela a été fait en enterrant plus de 600 km de tuyaux de différents diamètres dans le bassin quaternaire de la province de Mila, aboutissant à la création d'un nouveau système composé de tuyaux et de sol qui sont deux matériaux différents avec des caractéristiques différentes. Les systèmes de canalisations nécessitent une compréhension approfondie du mécanisme d'interaction de la structure du sol car ils sont généralement enfouis à une faible profondeur où ils sont exposés aux processus de mouillage et de séchage et soumis à la variation de la résistance au cisaillement et de la rigidité de ce sol. Comme beaucoup de recherches l'ont fait, le cas défavorable considéré dans les études et les conceptions de l'interaction des pipelines avec le sol d'enfouissement était les conditions saturées. Cependant, ce n'est pas toujours le cas comme cela est confirmé dans cette thèse et dans de nombreuses nouvelles recherches citées dans le chapitre de la revue de la littérature.

A partir de la vérification de la stabilité de la pente à l'aide du logiciel FLAC 3D, la pente s'est avérée être dans une stabilité critique. Après cela, la mécanique des sols non saturés a été considérée pour vérifier l'effet de la succion sur la résistance au cisaillement de la pente Aine-Tine où les paramètres d'ajustement du SWCC ont joué un rôle clé dans la variation du facteur de sécurité.

Dans la deuxième partie de la thèse, des investigations numériques ont été menées pour analyser l'effet du mouvement d'expansion sous les précipitations, où il a été constaté que la diminution de la succion a un effet significatif sur les forces internes apparues le long de l'anneau de la canalisation. Les résultats obtenus peuvent offrir une plateforme fiable pour comprendre et justifier les causes possibles des points de fuite d'eau le long de la canalisation. La simulation a été

entreprise à l'aide du logiciel GEOSLOPE de GeoStudio, et en tenant compte des sections transversales et longitudinales du pipeline. Il a été vérifié que la durée de la pluie et le profil initial d'aspiration ont un effet proportionnel sur la déformation et les efforts internes survenus sur la canalisation.

La dernière partie de la thèse a été orientée vers l'étude de l'effet des déformations permanentes du sol qui peuvent suivre les ruptures de talus de surface dans la pente Aine-Tine en particulier pendant la saison hivernale où une grande partie de la cohésion apparente due à la succion actuelle peut être perdue sous le processus de saturation pendant la pluie. Une enquête numérique a été menée pour étudier l'interaction de la canalisation avec le sol sous l'effet de grands incréments de déplacements qui passent par les axes médians de la canalisation. La rigidité de la canalisation et le profil de la succion ont été considérés.

Les études et résultats présentés dans la présente thèse ont montré que la prise en compte du comportement insaturé des sols est obligatoire surtout dans des pays comme l'Algérie où le climat aride et semi-aride caractérise l'ensemble de la région ce qui donne une grande variation de la succion présente dans les couches superficielles d'une telle région entre l'été et l'hiver qui conduisent à un effet très important sur l'interaction des pipelines avec leurs profondeurs d'enfouissement. Les résultats de la thèse sont prometteurs pour être utilisés par les ingénieurs et les futurs chercheurs pour utiliser la mécanique des sols non saturés.

To my beloved family, my dear father Messaoud, my dear mother Djemaa, my dear sisters Ahlam and Hassina and to my dear brother Ameur.

First of all, thanks to Allah for everything.

Secondly, the opportunity to pursue my PhD studies would not have been possible without the guidance of my supervisors, Pr. Rafik DEMAGH, and Pr. Zohra DERRICHE. I would like to express my deepest appreciation to my supervisor Pr. Rafik DEMAGH for his continuous motivation, patience, and encouragement throughout my doctoral study. I owe my deepest gratitude to my co-supervisor, Pr. Zohra DERRICHE, for providing great insights and timely encouragements. Their ability in explaining phenomena that occur within the soil, in a simple way, has been undoubtedly helpful during this work, particularly, during the hardest time of the study. I have been continuously encountering countless obstacles and challenges from ground up, which can never be overcome without their constructive and enlightening suggestions. Thank you very much dear professors for the countless hours of revision and advice on shaping this thesis. I would like to express the deepest appreciation to both of my supervisors at Universiti Teknologi Malaysia Pr. Aminaton MARTO and Pr. Azman KASSIM for their unconditional and continuous support during my internship at the GEOTROPIK center, UTM. The financial support received from the Algerian Ministry of Higher Education and Scientific Research (MESRS), is gratefully acknowledged here (Ref. PNE 628-2019).

I am also grateful to Professors Toufik KARECH, Rafik DEMAGH, Zohra DERRICHE, Mohamed BAHEDDI, Sadok BENMEBAREK, Mohamed KHEMISSA and Dr. Ouassila BAHLOUL for serving as jury members and for their insightful criticism and guidance. Your comments were valuable for improving this thesis.

I am grateful to Professors Rafik DEMAGH, Mohamed BAHEDDI, Toufik KARECH, Farid HAMOUD, KADID Abdelkrim and LAMAMRA Kheireddine for giving me the first year preparatory courses to this research.

Thank you very much to the whole staff of the university of Mostefa ben Boulaid Batna 2, I can't forget your efforts with us in particular the CIVIL ENGINEERING DEPARTMENT and the INSTITUTE OF EARTH AND UNIVERSE SCIENCES.

My thanks also to Mr. KACEM (PDG-SETS) and Mr. BELATEL (DP-SETS), to Mr. SIDHOUM of the GEF-SIDHOUM Sebti, to Mr. CHEROUAL of the DRE-Mila and to Mr. DEMAGH (Ing. LNHC) and the group of the in situ investigation of the LNHC Batna. My gratitude is to the engineering team at the SETS Sétif company; Nacer, Nabyl, Houssine, Lotfi, Cherif, Mehieddine, and Djahid, they always encouraged me during my study. Special appreciations to my dear sisters Rachida (ENSTP-Kouba) and Leila (SETS) for their continuous support. My appreciations to my colleagues for their friendship and support. They include; DEBBABI, KHANNOUF, OUARGLI, LARGUECHE, HAMMACHI.

To my family, my day and night support, thank you very much.

I know I forgot to name some of you, but your support will never be forgotten.

LIST OF CONTENT

ABSTRACT ii
DEDICATION vi
ACKNOWLEDGMENTS vii
LIST OF CONTENTS viii
LIST OF FIGURES xi

GENERAL INTRODUCTION 1

Background 2
Objectives of the study 8
Novelty 9
Thesis layout 9

CHAPTER ONE 10

1. Literature review 11
1.1. Introduction 11
1.2. Unsaturated soils 11
1.2.1. The importance of the climate 13
1.2.2. Typical profile of unsaturated soils: 14
1.2.3. Soil Water Characteristic Curve SWCC 15
1.2.4. Permeability function of unsaturated soil 16
1.2.5. Stress state variables 17
1.2.6. Shear strength of unsaturated soils 18
1.2.7. Volume change of unsaturated soils 20
1.2.8. Young's modulus variation 21
1.3. Slope stability 24
1.3.1. Slope failure definition 24
1.3.2. Factor of safety concepts 24
1.3.3. Type of slopes: 25
1.3.4. Nomenclature of landslides 26
1.3.5. Movement classification 27
1.3.6. Sequence or repetition of movements 31
1.3.7. Distribution and style of landslides activity 32
1.3.8. Landslide causes 34
1.3.9. Slope failures and water 35
1.3.10. Slope failures and earthquakes 35
1.3.11. Methods of slope stability analysis 36
1.3.12. Infinite Slope Procedure 37
1.3.13. Shear strength method SRM 38
1.4. Pipeline systems 39
1.4.1. Advantages of pipelines 40
1.4.2. Components of pipelines: 40
1.4.3. Types of pipelines 40
1.4.4. Connections (Joints) 42

1.4.5. Pipeline loadings 43
1.4.6. Behavior of buried pipelines 44
1.4.7. Soil pipeline interaction modelization 50
1.4.8. Buried pipeline interaction with expansive soils 52
1.4.9. Buried pipeline subjected to Permanent Ground Deformations (PGD) 56
1.5. Conclusion 62
1.6. References 63
CHAPTER TWO 69
2. Aine-Tine slope investigations 71
2.1. Information background 71
2.2. Aine-Tine slope description 71
2.2.1. Introduction 71
2.2.2. Geographic situation 71
2.2.3. Topographic conditions 72
2.2.4. Geological conditions 73
2.2.5. Geotechnical background 76
2.2.6. Climatic conditions 81
2.2.7. Conclusion 82
2.3. Aine-Tine Slope Stability Verification (PART I) 83
2.3.1. Introduction 83
2.3.2. Geometry 83
2.3.1. FISH language 85
2.3.2. FISH language with FLAC 2D and 3D 87
2.3.3. Results and discussion 90
2.3.4. Location of the slip surface using Shear Strain Increment 93
2.3.5. Interaction of our site with other infrastructures 94
2.3.6. Conclusion 96
2.4. Shallow Layer Stability Analysis of Unsaturated Slopes (PART II) 98
2.4.1. Introduction 98
2.4.2. Infinite slope procedure: 100
2.4.1. Soil Water Characteristic Curve SWCC 102
2.4.2. The Aine Tine slope: 104
2.4.3. Results and discussion 107
2.4.4. Conclusion 110
2.5. References 111
CHAPTER THREE 115
3. Structural Behavior of Pipelines Buried in Expansive Soils under Rainfall Infiltration 116
3.1. Background information 116
3.2. Introduction 116
3.3. Methodology 120

3.4. The study area 122
3.5. Finite element analysis using SIGMA/W 123
3.6. Transverse behavior 125
3.7. Numerical Model 125
3.7.1. Model geometry 125
3.7.2. Boundary conditions 126
3.8. The Aine-Tine Clay 126
3.8.1. Hydraulic property functions, SWCC and K 127
3.8.1. Modulus of elasticity variation with respect to suction 128
3.9. The pipeline 129
3.9.1. Interface between the soil and the pipeline 130
3.9.2. The Moment of inertia of the pipeline 130
3.10. Results and discussion 131
3.10.1. Suction variations 131
3.10.2. Soil volume changes (Heave) 132
3.10.3. Radial forces 135
3.11. Longitudinal behavior 139
3.11.1. Numerical model 139
3.12. Results and discussion (Longitudinal forces) 139
3.12.1. Heave 139
3.12.2. Longitudinal forces 141
3.13. Conclusion 145
3.14. References 147

CHAPTER FOUR 150

4. Numerical Analysis of Buried Water Supply Pipelines Subjected to Shallow PGD 151
4.1. Background information 151
4.2. Introduction 151
4.3. Permanent ground deformations PGD 154
4.4. Recent Seismic Activity in the Mila province 157
4.5. Numerical Model 159
4.6. Material characteristics 161
4.6.1. Clay 161
4.6.2. Pipeline 161
4.7. Results and discussion 162
4.7.1. Soil deformations. 162
4.7.1. Pipeline displacements and ovalization 163
4.7.2. Radial forces 166
4.8. Conclusion 168
4.9. References 170

SUMMARY AND CONCLUSIONS 172

Summary 173

Conclusion..... 173
Recommendations for future works: 175

REFERENCES 176

FIGURES :

Figure -1. Population growth in Algeria 1962-2019 2
Figure -2. the idea of the dam..... 3
Figure -3. Beni Haroun dam water transport networks (Semmane et al., 2012) 4
Figure -4. Water leakage point recorded at the Aine-Tine slope..... 4
Figure -5. Map of globe climate zoning (Fredlund and Rahardjo, 1993)..... 5
Figure -6. Typical profile of saturation of a soil profile 6
Figure -7. Pipeline landslides (a) transverse (b) longitudinal (IITK-GSDMA, 2007) 7
Figure -8. Vertical pipe movement in winter and summer (Rajeev et al., 2012) 8
Figure -9. Research scheme.....9

Figure 1-1. (a) Categorization of soil mechanics (b) Soil skeleton.....12

Figure 1-2 the world's map of arid environments (Fredlund and Rahardjo, 1993) 14
Figure 1-3. Soil water characteristic curve for 3 different types of soils 16
Figure 1-4. Variations of the water content in unsaturated soil..... 17
Figure 1-5. Shear strength envelope for unsaturated soils (Al-Khazaali et al., 2018)..... 19
Figure 1-6. Constitutive surfaces for (a) soil structure and (b) water phase of an unsaturated soil (Vu and Fredlund, 2004) 21
Figure 1-7. Factors related to the slope stability analysis (Abramson et al., 2002) 24
Figure 1-8. (a) Direct shear test box, (b) soil specimens as sheared along the slope failure surface 25
Figure 1-9. Mohr-Coulomb envelope (a) Soil element (b) Stress vector (c) Shear strength envelope 25
Figure 1-10. Main groups of engineered slopes 26
Figure 1-11. Geometry of a landslide. 27
Figure 1-12. Slope movements type: Falls 28
Figure 1-13. Slope movements type: Topples 28
Figure 1-14. Slope movements type: Rotational slides 29
Figure 1-15. Slope movements type: Translational slides..... 29
Figure 1-16. Slope movements type: Lateral spreading 29
Figure 1-17. Slope movements type: Flows 30
Figure 1-18. Classification of sequence of movements..... 31
Figure 1-19. Various definitions of the FoS 36
Figure 1-20. Aspects ration of failure mass..... 37
Figure 1-21. Force acting on a slice (Infinite slope formulation)..... 38
Figure 1-22. Bell-and-spigot joint used in Pretension concrete cylinder pipe 43
Figure 1-23 Pipeline hoop: (a) terminology; (b) ring internal forces. 44
Figure 1-24. Backfill deformation: (a) flexible pipe; (b) rigid pipe 45
Figure 1-25. Stress–strain curve for steel 47
Figure 1-26. Pipeline deformation under (a) uniform radial loads (b) invert and crown punctual loads (in the case of unconfined pipeline) 47

Figure 1-27. Pipeline deformation under (a) uniform radial loads (b) invert and crown punctual loads (in the case of partially confined pipeline) 48
Figure 1-28. Typical examples of performance limits for the pipe and their location 48
Figure 1-29. Steel pipe ovalization due to fault offset (foot) (a) 0.375-inch (b) 0.75-inch wall thickness (ALA, 2005) 49
Figure 1-30. Deformed shape of a pipeline for fault displacement d=1-4 m 49
Figure 1-31. Deformation of pipeline ring under vertical concentrated loading 50
Figure 1-32. (a) Finite element model (b) BNFF model 51
Figure 1-33. Continuous pipe-soil model for (a) longitudinal and (b) transverse ground deformation 51
Figure 1-34. Model of beam embedded in an elastic foundation locally displaced laterally. 51
Figure 1-35. Segmented pipe-soil model for (a) longitudinal and (b) transverse ground deformation 52
Figure 1-36. Schematic of pipe–soil movement due to moisture change 53
Figure 1-37. Experimental and numerical models 53
Figure 1-38. External stresses acting on deflected buried pipe 54
Figure 1-39. Large-scale experimental model 54
Figure 1-40. Beam spring model used by Kouretzis et al. (2015) 55
Figure 1-41. Numerical model (Saadeldin et al., 2015) 55
Figure 1-42. Principal PGDs on pipelines considering the orientation (ALA, 2005) (IITK-GSDMA, 2007) 56
Figure 1-43. Scheme and numerical models (Rajani and Morgenstern, 1993) 57
Figure 1-44. (a) 3D and (b) 2D Laboratory testing of pipeline at the Cornell University NEES . 58
Figure 1-45. The 36-inch pipeline in Colombia subjected to sliding on a steep slope (Palmer et al., 1999) 59
Figure 1-46. Model used by Rajani et al. (1996) 59
Figure 1-47. Finite element model (Roy et al., 2016) 60
Figure 1-48. Finite element model (Vazouras et al., 2012) 60
Figure 1-49. Numerical model used Al-Khazaali et al. (2018) 61
Figure 1-50. The full test setup and a graphical illustration of the test setup (Vanapalli and Al-Khazaali, 2019) 61
Figure 2-1 Aine-Tine area location 72
Figure 2-2 The Aine-Tine Slope details 72
Figure 2-3 Aine-Tine area Topographic background 73
Figure 2-4. Mila's basin lithology (Athmania et al., 2010) 74
Figure 2-5. Principal geological formations Outcrop Inside Mila Province (Athmania et al., 2010) 75
Figure 2-6. Aine-Tine Area Geologic background 76
Figure 2-7. Shallow layer soil constitution 77
Figure 2-8 visit on the site 77
Figure 2-9 Sieve analysis 78

Figure 2-10 Plasticity index on Casagrande chart 78
Figure 2-11 Peak and Residual cohesion 79
Figure 2-12 Peak and Residual friction angle 79
Figure 2-13. The GWT of Aine-Tine site and its profile of suction 80
Figure 2-14. SPT Results 81
Figure 2-15. SPT location on the site of Aine-Tine. 81
Figure 2-16. Ombrothermal curve of the Hamala-Grarem station (1984-1997) (Chettah, 2009) . 82
Figure 2-17. The scheme of the geometry construction 84
Figure 2-18. Topographic data of the cross section elevations 85
Figure 2-19. The FISH function to built the geometry 86
Figure 2-20. Function of the geometry creation 87
Figure 2-21. DEM of the Aine-Tine Slope 87
Figure 2-22. Cross section profiles P1, P2 and P3 (Bouatia and Demagh, 2019) 88
Figure 2-23. 3D numerical model of Ain-Tine slope. 89
Figure 2-24. Geotechnical models 89
Figure 2-25. Vector of displacements in 2D cross sections 91
Figure 2-26. Y-Displacements magnitudes in 2D cross sections 92
Figure 2-27. XYZ Displacements in 3D 93
Figure 2-28. Location of the slip surface with SSI=2e-3 94
Figure 2-29. Location of the slip surface with SSI=4e-3 94
Figure 2-30. Location of the slip surface with SSI=6e-3 94
Figure 2-31. Interaction of the Aine Tine pipeline with the duplication of the RN79. 95
Figure 2-32. Primitive mesh shapes of the 3D model 95
Figure 2-33. Shell structural element to build the pipeline geometry 96
Figure 2-34. Details of the 3D model of the duplication of the RN79 highway 96
Figure 2-35. Relationship of shear strength and suction 98
Figure 2-36 Force equilibrium scheme in infinite slope procedure 101
Figure 2-37 Soil Water Characteristic Curve SWCC. 103
Figure 2-38 Suction profile within Aine-Tine shallow layer 104
Figure 2-39 Effect of parameter $\boldsymbol{a}$ on the SWCC ($\boldsymbol{n}$=2, $\boldsymbol{m}$=1) 105
Figure 2-40 Effect of parameter $\boldsymbol{n}$ on the SWCC ($\boldsymbol{a}$=10, $\boldsymbol{m}$=1) 106
Figure 2-41 Effect of parameter $\boldsymbol{m}$ on the SWCC ($\boldsymbol{a}$=10, $\boldsymbol{n}$=2) 106
Figure 2-42 FoS variations with respect to the parameter $\boldsymbol{a}$ at the top of the shallow layer 108
Figure 2-43 FoS variations with respect to the parameter $\boldsymbol{a}$ at the bottom of the shallow layer 108
Figure 2-44 FoS variations with respect to the parameter $\boldsymbol{n}$ at the top of the shallow layer 109
Figure 2-45 FoS variations with respect to the parameter $\boldsymbol{n}$ at the bottom of the shallow layer 109
Figure 2-46 FoS variations with respect to the parameter $\boldsymbol{m}$ at the top of the shallow layer 110
Figure 2-47 FoS variations with respect to the parameter $\boldsymbol{m}$ at the bottom of the shallow layer 110
Figure 3-1. Relationship of swelling pressure and percent swell with soil suction 116
Figure 3-2. Suction variation versus time (Ito et al., 2014) 117

Figure 3-3. Measured and predicted values of (a) τp–s relationships; (b) E–s relationships of Bukit Timah Granite (Han and Vanapalli, 2016) 118
Figure 3-4. A typical void ratio constitutive surface plotted in semi logarithmic scale (Vu and Fredlund, 2004) 119
Figure 3-5. Mila Province «swelling-shrinkage» susceptibility map (Athmania et al., 2010).... 121
Figure 3-6 Water leakage point at Aine-Tine site 122
Figure 3-7 Research flowchart of the present paper 122
Figure 3-8 Geological formations outcrop statistical distribution inside Mila Province 123
Figure 3-9. Aine-Tine area location 124
Figure 3-10. Finite element model and pipeline cross-section detail 126
Figure 3-11. The profiles of initial suction conditions P1, P2, P3 and P4 and Aine-Tine GWT details 127
Figure 3-12 Hydraulic characteristics of unsaturated Regina expansive clay (Adem and Vanapalli, 2013) 128
Figure 3-13 Hydraulic characteristics of Aine Tine soil 129
Figure 3-14 Detail of the interface 130
Figure 3-15. Cross sections adopted in longitudinal and transverse calculation 131
Figure 3-16. Evolution of soil suction with rainfall time for the suction profiles P1, P2, P3 and P4 132
Figure 3-17. Vector and maximum displacements for different initial suction after 30 days of rainfall infiltration 133
Figure 3-18. Y-Displacement values at the Invert, Crown and Top surface for P1, P2, P3 and P4 133
Figure 3-19. Deformed mesh around the pipeline perimeter (x5 magnitude) 134
Figure 3-20. Axial force FA distribution along pipeline perimeter (kN) with time 136
Figure 3-21. Shear force FS distribution along pipeline perimeter (kN) with time 137
Figure 3-22. Transverse bending Moment distribution along pipeline perimeter (kN) with time 138
Figure 3-23. Longitudinal finite element model 139
Figure 3-24. Expansion of clayey soil of Aine Tine slope 140
Figure 3-25. Vertical heave distribution on Top surface (m) with time 140
Figure 3-26. The maximum vertical displacement at the exposed part to the rain 141
Figure 3-27. Longitudinal axial forces distribution along pipeline (kN) with time 142
Figure 3-28. X-displacement at the central part of the model 143
Figure 3-29. Final X-displacement at the central part of the model after 30 days of rainfall 143
Figure 3-30. Longitudinal Shear forces distribution along pipeline (kN) with time 144
Figure 3-31. Longitudinal bending moment distribution along pipeline (kN) with time 145
Figure 3-32. Cross section ovalization 146
Figure 4-1. pipeline elbows subjected to pull-out forces (Vazouras and Karamanos, 2017)..... 152
Figure 4-2. Five pipe locations for DC Sand tests (P1 to P5) and one pipe location for Geba Sand test (P1G) (Zhang and Askarinejad, 2019) 153

Figure 4-3. (a) Strong down warping of the pipeline (b) Schematic diagram of the generation of forces and cracks at the boundary of the landslide induced by the deformation of the pipeline (Feng et al., 2015) 153
Figure 4-4. The final deformation of the pipeline (Feng et al., 2015) 154
Figure 4-5. Pattern of transverse and longitudinal permanent ground deformation (IITK-GSDMA, 2007) 155
Figure 4-6. Pipeline subjected to transverse PGD (IITK-GSDMA, 2007) 156
Figure 4-7. Positional relationship between pipeline and landslide and hazard analysis (Wu et al., 2014) 157
Figure 4-8. Recent Seismic Activity in the Mila province (CRAAG, 2020) 158
Figure 4-9. The7th august 2020 earthquake effects 159
Figure 4-10. Finite element model and pipeline cross-section detail 160
Figure 4-11. Details of boundary conditions 160
Figure 4-12. Contour of displacements after 2 m of sliding movement (a) flexible (b) rigid pipeline 163
Figure 4-13. Vertical displacements at the ground surface 164
Figure 4-14. Deformed mesh after 0.5, 1 and 2m of PGD for flexible and rigid pipeline 164
Figure 4-15. Displacement and deformation of pipeline and 0.5, 1 and 2 m PGD magnitudes .. 165
Figure 4-16. Axial force distribution for Flexible and Rigid pipeline under different PGDs. 166
Figure 4-17. Shear force distribution for Flexible and Rigid pipeline under different PGDs. 167
Figure 4-18. Bending moment distribution for Flexible and Rigid pipeline under different PGDs. 168

TABLES

Table 1-1 Effective stress equations for unsaturated soils 18
Table 1-2. Sub-classes of slope failures (Dikau et al., 1996) (Cruden and Varnes, 1996)..... 31
Table 1-3. Distribution of the activity of landslides 33
Table 1-4. Style of the activity of landslides 34
Table 1-5. Classification of main causes of landslides 35
Table 1-6. Static equilibrium conditions satisfied by Limit Equilibrium Methods 37
Table 1-7. Pipeline classification considering the ways of assembling 42
Table 1-8. Limit states of pipeline systems 44
Table 1-9. Key specifications for rigid and flexible pipes (Al-Khazaali et al., 2018). 45
Table 1-10. Description of the resulted deformations 48
Table 2-1 Capture of the Unified Soil Classification System (USCS) 79
Table 2-2. Correlation between relative density NSPT and Bulk density (Teng, 1962) 81
Table 2-3. Slope Mechanical Parameters (LNHC-Batna, 2016) 89
Table 2-4 FoS with 2D simulations 90
Table 2-5 Geotechnical parameters. 106

Table 3-1. Aine-Tine clay geotechnical parameters 128
Table 3-2. Aine-Tine pipeline parameters 129
Table 3-3. Longitudinal tension and compression stresses developed at the end of simulation . 142
Table 3-4. Longitudinal shear stresses developed at the end of simulation 144
Table 4-1. Common natural hazards causing PGD 155
Table 4-2. Aine-Tine clay geotechnical parameters 161
Table 4-3. Aine-Tine pipeline parameters 162
Table 4-4. Ovalization values for flexible and rigid values under different PGD magnitudes. .. 166
Table 4-5. Maximum shear forces at 0.5, 1 and 2m of PGD magnitudes (flexible and rigid pipeline) 167

GIS: Geographic Information System

SSI: Soil Structure Interaction

SRM: Strength Reduction Method

FOS: Factor of Safety

PGD: Permanent Ground Deformations

PWP: Pore Water Pressure

GWT: Ground Water Table

τ: Shear strength

τ_p: peak shear strength

σ: total stress

σ': effective stress

u_w: pore water pressure

u_a: pore air pressure

p'': pore-water pressure deficiency,

ψ: a parameter with values ranging from zero to one

χ: a parameter related to the degree of saturation of soil

p'': negative pore-water pressure taken as positive value

β: a statistical factor measured experimentally

θ_w : Volumetric water content

h : Total head

t: time

c': is the effective cohesion.

φ' : the effective angle of friction.

φ^b and φ'': the angle of shearing resistance with respect to matric suction.

GIS : Geographic Information System.

INCT : Institut National de Cartographie et de Télédetection.

DEM: Digital Elevation Model

PWP: Pore water pressure

VWC: Volumetric Water Content

AEV: Air Entry Value

LNHC : Laboratoire Nationale de L'Habitat et de la Construction

USCS: Unified Soil Classification System

CRAAG: Algerian Center of Research in Astronomy, Astrophysics and Geophysics

B R G M: Bureau of Geological and Mining Research

GWT: Ground Water Table

F_A: Axial forces

F_S: Shear forces

M_B: Bending moment

SWCC: Soil Water Characteristic Curve

k: Permeability

K_{sat}: Saturated permeability

E_{unsat}: Unsaturated Young's modulus

E_{sat}: Saturated Young's modulus

P_a: Atmospheric air pressure

e: void ratio

w: water content

GENERAL INTRODUCTION

Background

Algeria is a developing country located in the north of Africa, with more than 2 million km^2 of area, it is the largest country on the continent. Algeria has experienced a monotonous increase in urbanization due to a significant population growth since the independence (1962) (Figure -1). This is due to the improvement of living conditions which have followed a confident and continued economic capacities of the country especially energetic resources (oil and gas). For the last decades, the construction of new or expansion of existing infrastructures were the main actions of the work programs of the different Algerian governments to meet the increasing needs of the new populations. Generally, the location of citizen groups and their demographic growth are conditioned by many factors such as security and climatic condition. One of the key factors that help governments to stabilize the citizens is the water availability. The latter can be assured by natural water sources and dug wells which are traditional sources and they are largely sufficient in the case of small to medium population groups. Constructing much important and more budget-consuming infrastructures such as dams is necessary when considering to satisfy regional water needs (one or a group of neighboring provinces).

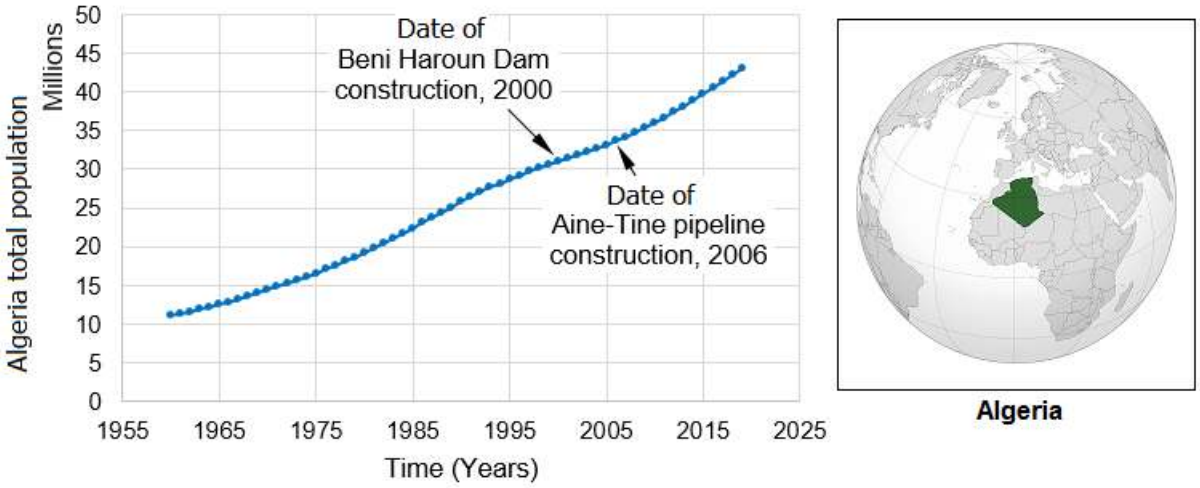

Figure -1. Population growth in Algeria 1962-2019 (https://www.banquemondiale.org/fr/country/algeria)

The north-east region of Algeria is facing an important water resource shortage. In order to help people to keep their locations, the Algerian government decided to build the Beni-Haroun dam (1983) as the biggest hydraulic project in the history of Algeria to resolve many problems mainly related to the water availability and the basin of Mila (Mila, Algeria) was found to be the best location in terms of the morphological conditions for this mega project (Figure -2, Figure -3). The construction of the dam was completed at the onset of the third millennium (2001). The dam was constructed with the rolled compacted concrete technique. It has a finished height level of 120 m. The dam was designed to achieve a maximum volume capacity of 0.96 billion m^3 and can extend to 1 billion m^3 capacity (i.e., 1 billion was achieved in 2012). In order to supply drinking water to several regions bordering the province of Mila facing water shortage, in particular the provinces of Jijel, Constantine, Oum el Bouaghi, Batna and Khenchela. The dam provides also a significant amount of irrigation water for 30000 hectares of farms in plain lands like plain of Teleghma, Chemoura (www.anbt.dz).

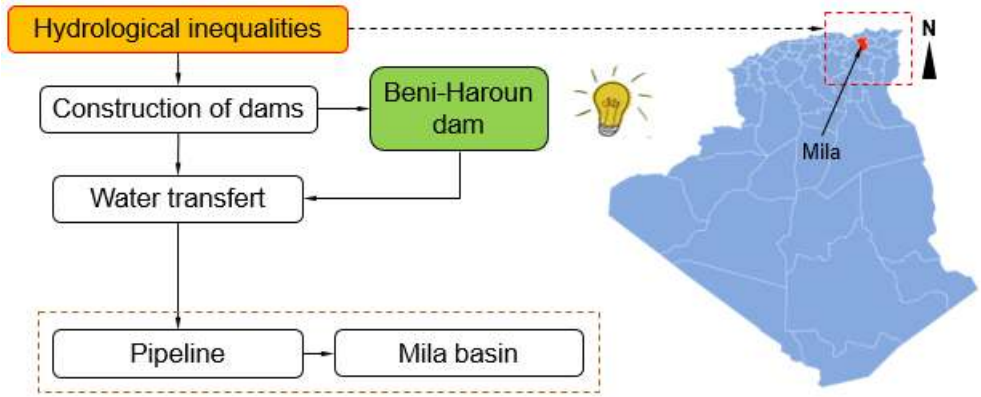

Figure -2. the idea of the dam

Dams are complex infrastructures that contain both the body of the dams (embankments) which is built generally in the paths of large valleys to serve as artificial barriers to collect the water and they contain also the different appendices to transport water. Big dams are mostly completed by different hydraulic constructions that work to transport water from the dam to the consumer centers such as pumping stations. Pipeline networks are one of the essential elements that are required to transport water towards pumping stations and then deliver it to the consumption centers such as urban area, factories as well as farms which are located at different directions and distances.

Pipelines are usually buried at shallow depth within the soil in order to protect them from different possible external actions in one hand and can be chemical such as corrosion or mechanical such as faults and slope failures, on the other hand, to facilitate the repair operations. Under certain conditions the external loadings can be a serious source of damages which consequently lead to the complete destruction of these linear structures or the disruption of their normal operations. The most known external loads will be discussed later in this thesis. Pipeline systems are constructed using different types of materials which include polyethylene, plastic, reinforced concrete or steel. Pipelines can be used pipes to transport and distribute vital energy resources (fuel) and water.

The Figure -3 shows the Beni-Haroun dam location; the route and the elevation profile of the main pipeline of water transport that links the main reservoir of the dam with the reservoir of Oued Athmania which is the starting point of the distribution line that goes towards the southern provinces. From the elevation profile it can be seen the difficult topographic conditions that the pipeline is going through to transport the water. It starts from less than an altitude of Z= 250m at the Beni-Haroun dam to reach an altitude of more than 750 m when arriving to the second reservoir. Following the construction of the pipeline network (2006), including the one which crosses the Aine-Tine slope which has an elevation of about 650 m, many water leakage points were rapidly recorded, the worst one being observed at the Aine-Tine slope (Figure -4).

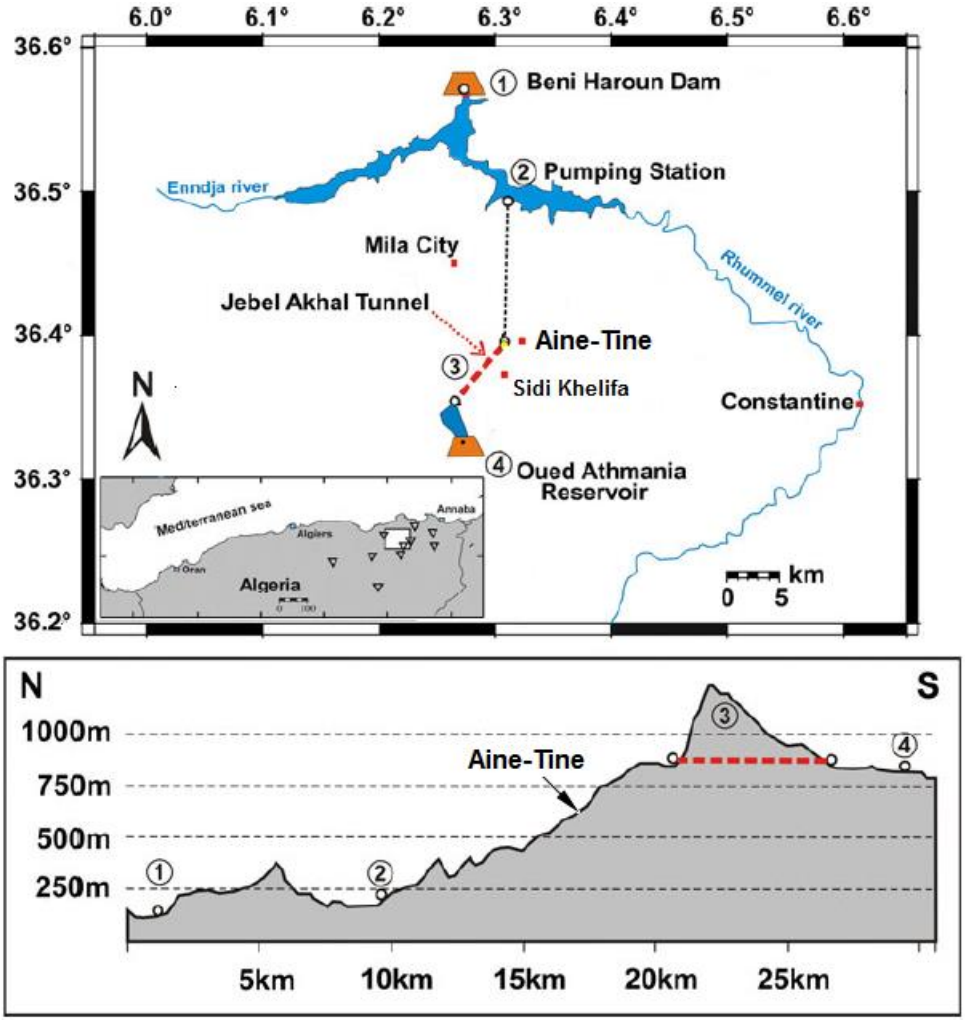

Figure -3. Beni Haroun dam water transport networks (Semmane et al., 2012)

Figure -4. Water leakage point recorded at the Aine-Tine slope

Around the world, pipelines transport oil, gas and water by crossing surficial layers of different geological formations. Figure -5 shows the distribution of the ground surface of the world in terms of aridity which can strongly governs the behavior of soils sensitive to the water content. The aridity index is a numerical indicator of the degree of dryness of the climate of the region when evaporation levels exceed the rainfall levels. It helps to identify and delimit lands to effectively use them for agriculture activities. In Algeria, it can be seen that excluding the coastal strip, the northern part of the country has mainly a semi-arid climate which is characterized by a considerable seasonal deficits of rainfall quantities. This phenomenon results in the strong unsaturation of the soils in the shallow layers especially during the summer period where high evapotranspiration occurs, reducing the water content levels of soils which will be raised in the next rainy season. Unfortunately, when these changes of the water content levels occur in a clayey soil that covers the surficial layer of Mila basin, the soil is sensitive to climatic conditions such as rainfall.

Few years after the construction of the pipeline network, the region of Mila get more attention to the authorities because the shallow unsaturated layer of the Mila basin exhibited numerous natural hazards presented as frequent instabilities in natural slopes and expansion movements which were defined by experts as the main causes of many recorded damages along the pipeline routes. From the previous discussion, it can be concluded that these geotechnical problems are principally related to many factors such as climatic conditions as well as geological and morphological characteristics where it should be studied to help engineers and decision makers to understand and predict the logic causes of the risks happened on these budget consuming infrastructures.

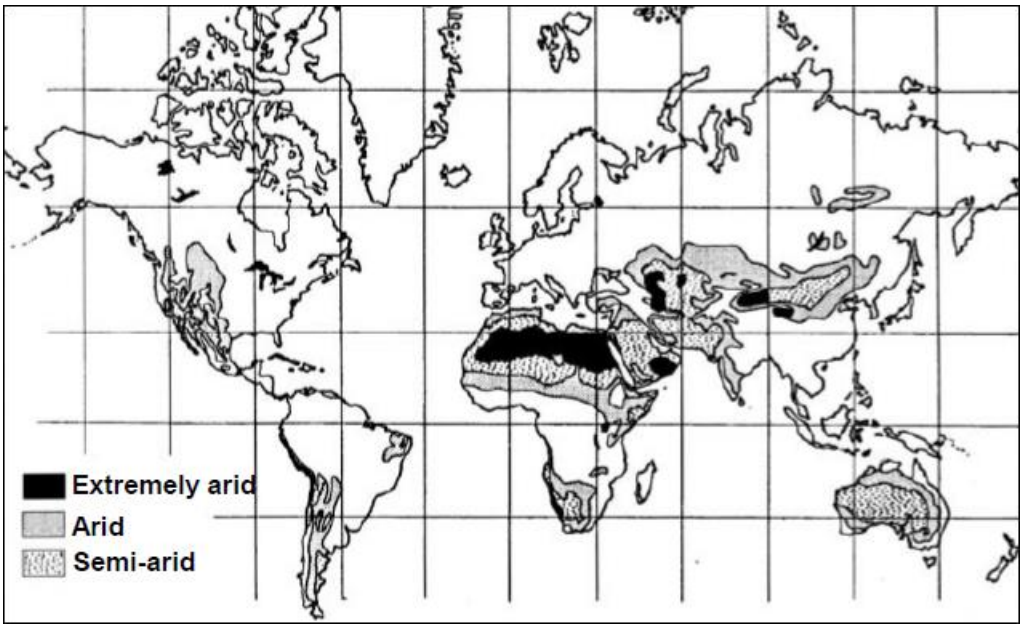

Figure -5. Map of globe climate zoning (Fredlund and Rahardjo, 1993)

In effect, the province of Mila is classified as geotechnical problem prone area. Interesting published works have been carried out by Athmania et al. (2010) to study the clay and marl formation susceptibility in this province. In the same direction, Merghadi et al. (2018) established a landslide susceptibility maps at the Mila basin. Roads are also suffering from the swelling

movements of Mila expansive soils (Afès and Didier, 2000). The area of Mila is still an active subject for professionals and research community.

Due to the interaction of pipelines with the induced permanent ground deformations (PGD), that must have occurred within the unsaturated surficial soils of the Mila basin, the pipeline network of Beni-Haroun dam knew repetitive damages taking the form of leakage points along the pipeline routes. During the rainy season, the problem worsens and the leakage rate recorded increases. The key parameters that control the soil-structure mechanical behavior under static loads are the soil and interface shear strength and modulus of elasticity, E (Al-Khazaali, 2019). It was found in many published researches that these parameters are inversely related to the moisture content of the embedding soil (Oh et al., 2009) (Vanapalli and Oh, 2010) (Adem and Vanapalli, 2014). The principle of this phenomenon was explained by Han et al. (2016) by defining the contribution of the suction (i.e., negative pore water pressure) as an energy potential with a tension stress on soil skeleton that holds the soil particles and their packets together providing resistance to elastic and plastic deformations within the soil. The suction values depend on the degree of saturation S. The natural water content w_n of an unsaturated soil is less than the saturated water content w_{sat} ($S < 100\%$) and it is related to the depth at which the soil is located from the ground water table (GWT). As shown in Figure -6, the typical profile of the saturation state consists of two zones; saturated and unsaturated zones where they are located below and above the GWT, respectively.

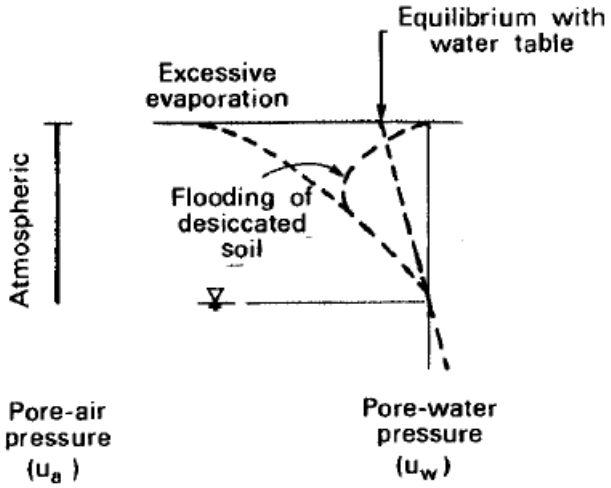

Figure -6. Typical profile of saturation of a soil profile

The water table can move up due to infiltration of rain precipitation or lowered under evapotranspiration action which lead to variation of the water content of the soil and consequently result in the effects on the SSI analysis. Unlike the unsaturated soils, the behavior of saturated soils was intensively studied. The Figure -7 shows a typical pipeline subjected to PGD due to landslide where the Figure -7 (a) shows the case of transverse PGD where the bending efforts at the right and left side of the sliding mass constitute the main loadings on the pipeline and the Figure -7 (b) depicts the case of a pipeline subjected to a longitudinal PGD. The pipeline is subjected to axial efforts with compression at the toe of the slope and tension at the scarping location.

In the Mila basin, the PGD that follow the failures of natural slopes can be triggered by losses of shear strength due rainfall precipitations which cause the reduction of the suction contribution

through the apparent cohesion (Qi and Vanapalli, 2015). Failure of natural slopes can also be triggered by seismic shakings which has become the cause of many damages that occurred on the Mila basin (Semmane et al., 2012) that can follow the large PGD in these last years. Recently, the province have known a swarm of earthquakes with magnitudes of last two events have reached M=4.5, 4.9 (CRAAG, 2020) the last two years.

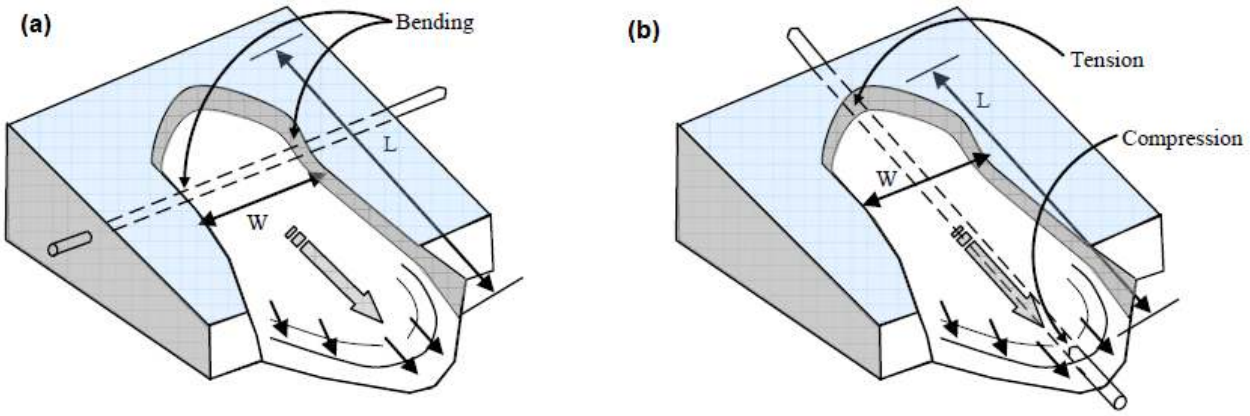

Figure -7. Pipeline landslides (a) transverse (b) longitudinal (IITK-GSDMA, 2007)

Civil engineering-related problems associated with unsaturated expansive soils are various and are still causing many damages to structures such as buried pipelines. Around the world, the expansive soils are typically distributed in semi-arid and arid regions which cover 66.5 million km^2 (Achten et al., 2013) representing about 49% of the total land area available on our planet (Holmgren, 2006). The Mila basin is classified as semi-arid and the GWT is generally located between 10 and 15 m depth (Athmania et al., 2010) due to the significant water evaporation in comparison to infiltration. Due to these reasons the use of the unsaturated soil mechanics is mandatory to study the SSI in this area where the behavior of such soils is significantly influenced by the capillary stress or matric suction (Al-Khazaali, 2019).

In the literature of unsaturated soil mechanics, two stress state variables; which are the net normal stress and the soil suction were introduced and then used by many researchers for the last six decades to analyze the mechanical behavior of unsaturated soils such as shear strength and stiffness. Therefore, the determination of these stresses is essential to study the SSI problems in unsaturated soils. Most of studies relate the unsaturated soil behavior to the soil water characteristic curve $SWCC$, which is a characteristic function that relates the degree of saturation S or the volumetric water content θ to the suction $(u_a - u_w)$ to describe the variation of the shear strength and stiffness with the water content.

Limited researches have been carried out to consider the unsaturated soil behavior in the SSI problems that consider buried pipelines as structures which interact with the surrounding soil due to the consideration of many standards such as the Seismic Guidelines for Water Pipelines of the American Lifelines Alliance (ALA, 2005) and the Guidelines for seismic design of buried pipelines of the Indian institute (IITK-GSDMA, 2007) that the saturation state is the most unfavorable condition to design buried pipeline. This is however not always the case as reported by Alkhazaali et al. (2018). Figure -8 shows the effect of the climate conditions on pipelines buried in expansive

soils where the shrink/swell movements that occurred within the surficial layers can cause additional loads to the pipeline.

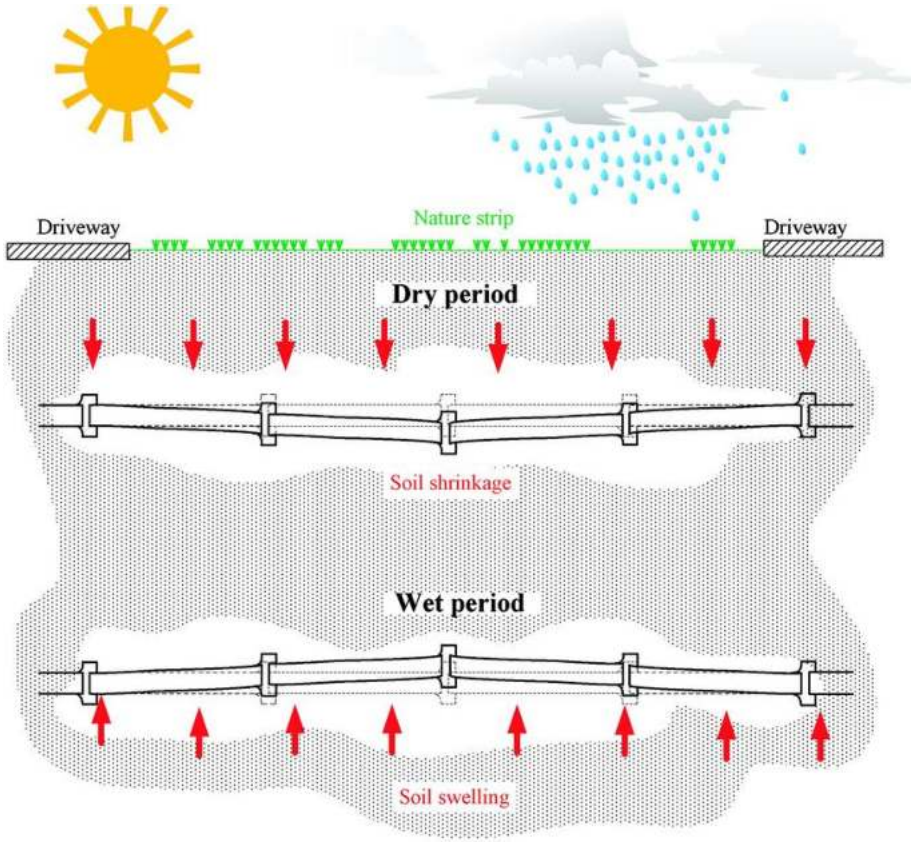

Figure -8. Vertical pipe movement in winter and summer (Rajeev et al., 2012)

It was found that limited researches were carried out to investigate the SSI considering the unsaturated soil mechanics and pipeline as a structure buried in arid and semi-arid region. The scientific community started to take care of this issue only in the recent decade (Al-Khazaali, 2019). Many studies have reported the importance of taking in consideration the effect of the suction on soil pipeline interaction. The surrounding soil may exert higher stresses and provoke damages as a result of shrink / swell movements and PGDs of shallow slope failures in unsaturated soils.

Objectives of the study

This study addresses the evaluation of the stability of the Aine-Tine slope which is one of the landslide prone slope at the Mila basin as related to the structural behavior of the pipeline of water transport that comes from the Beni-Haroun dam and which is buried in the unsaturated soils of the region. The objectives of the present study are summarized in the scheme presented in the Figure -9 where the main goals are as follows:

- The assessment of the Aine-Tine slope stability through two and three dimensional numerical analyses using the Mohr-Coulomb soil behaviour models. The FLAC software was used to carry out this part of the analysis.
- By taking into consideration the unsaturated behavior of the soils of the Mila basin an analysis is undertaken to explain the numerous slope instabilities that were recorded in the

eastern part of the Algerian territory which is characterized as a semi-arid climate area due to the seasonal variation of water content over the year.

- The study of the effect of rainfall precipitation on the stability of unsaturated slope using the infinite formulation procedure which consider the shallow failures which is common in the case of unsaturated slopes subjected to rainfall infiltration.
- Using the SIGMA/W software, the effect of suction on the structural behavior of a pipeline buried in expansive soils (i.e., Aine-Tine slope) is analyzed in order to understand the causes of the numerous water leakage points along the pipeline profile.
- Define two-dimensional plane strain numerical models to analyze the structural behavior of buried pipelines subjected to permanent ground deformations (PGD).

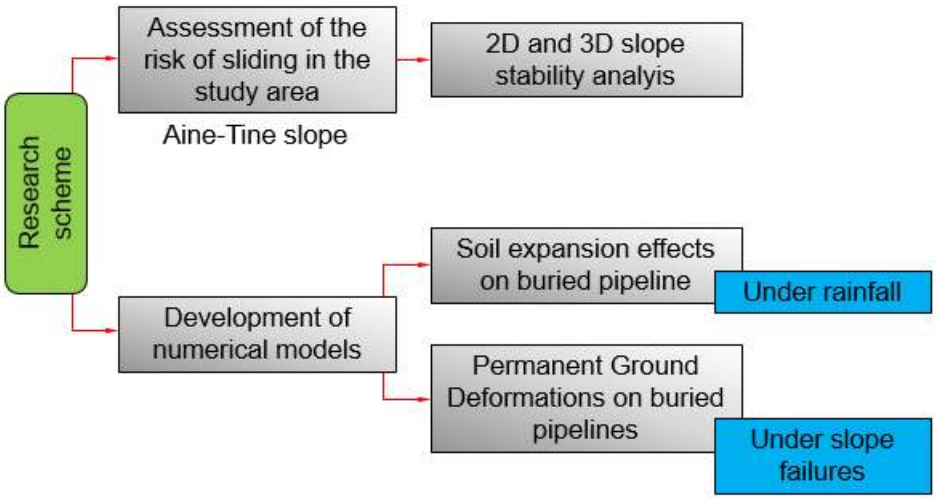

Figure -9. Research scheme.

Novelty

The unsaturated behavior of expansive soils is not taken in consideration during:

- The investigations of the stability of natural slopes.
- The design of linear infrastructures such as buried pipelines in natural slopes,

For these reasons, the present thesis will help the Algerian scientific community to understand and consider the unsaturated soil mechanics when studying slope stability problems and the stability of pipelines in arid and semi-arid regions.

Thesis layout

The work is undertaken and presented following a rigorous scientific methodology. The present thesis is structured into two parts:

Part 1: Assessment of the Aine Tine slope stability considering the unsaturated soil behavior.

Part 2: Analysis of the structural behavior of pipelines buried in expansive soils subjected to (1) expansion movements due to rainfall infiltrations and (2) permanent ground deformations due to shallow failures considering unsaturated soil mechanics.

General introduction exposes the problem addressed and presents the relevant information background. The chapter presents then the objectives of the study, the novelties expected, and the manuscript organization;

Chapter one presents a thorough literature review in general terms in relation to established researches and analyses of unsaturated soils, slope stability analyses and soil-pipeline system interactions. For as far as specific aspects of soil or pipeline system behaviors background information that underlay certain issues are presented in subject dedicated chapter.

Chapter two discusses the slope stability of the Aine-Tine slope which is carried out through two parts; the first part is a verification using the strength reduction method (SRM) implemented within the FLAC tool. The stability was studied considering 2D and 3D numerical models constructed using the powerful option offered by the Itasca software called the FISH language which allow the users to freely control their models. The second part discusses the unsaturated slope stability of Aine-Tine slope considering the effect of the SWCC fitting parameters on the variation of the factor of safety (FoS) of the shallow layer of Aine-Tine slope where buried pipelines are usually embedded.

Chapter three addresses the structural behavior of buried pipelines subjected to the soil vertical expansion movements due to rainfall infiltration. A section of pipeline of Beni-Haroun dam system buried at Aine-Tine expansive soils with 800 mm dimeter was considered. Using the SIGMA/W software, the effect of the rainfall duration and the initial suction profile expressed as different depths of the groundwater table were considered to study the internal forces applied on the pipe ring.

Chapter four presents the effect of permanent ground deformations caused by shallow layer displacements which are very common in the unsaturated slope especially after earthquakes shaking or intense rainfall infiltration. The rigidity of the pipeline and the magnitude of the PGD were considered to study the pipe deformation and to predict the magnitude of the internal forces that occur on the pipe perimeter. This part of the study was undertaken using SIGMA/W software tool.

Summary and conclusion presents the summary and conclusions of the research undertaken in this thesis. Recommendations for future work have also been proposed, which will mainly focus on taking into account 3D analyzes of the interaction between unsaturated slopes and the various structures that may exist considering the unsaturated behavior of soils in the Mila basin under real precipitation records of that characterizes the arid and semi-arid climate.

Chapter 01

LITERATURE REVIEW

1. Literature review

1.1. Introduction

The process of soil response influencing motion of the structure and vice-versa is termed as soil-structure interaction (SSI) (Anand and Satish Kumar, 2018). Scientific and professional communities are faced with many complex problems related to the stability and the ease of operation of infrastructures which lead to very harsh economic and environmental effects and, consequently, the need to be solved efficiently with the lowest costs. Overcoming these problems requires having as much information as possible on the behavior of these infrastructures involving the soil and the structure as such the study should combine structural mechanics and Geomechanics in order to understand the SSI problems (Kausel, 2010). These issues lead to over-conservative designs when ignoring one of the aspects that play a key role in the behavior of the system. Water mains are part of the infrastructures concerned by the SSI because of many related geotechnical problems (i.e., buried structures, linear structures), in particular the water supply network of the Beni-Haroun dam which will be the focus of this study.

Soils in arid and semi-arid regions where the Ground Water Table (GWT) is generally deep seated within the soil show variations in their behavior with respect to water content due to the contribution of capillary stress or matrix suction to shear strength and rigidity of the soil (Biot, 1941) (Fredlund and Morgenstern, 1976) (Vu and Fredlund, 2004) (Vanapalli et al., 1996) (Khalili and Khabbaz, 1998) (Karube and Kawai, 2001) (Oh et al., 2009) (Adem and Vanapalli, 2014a) (Han et al., 2016) (Zhang et al., 2018) (Akin and Likos, 2020). Under the increasing needs to describe and simulate the behavior of the unsaturated soils, the extension of the principles of the saturated soil mechanics gave very reliable results, as was reported by many researchers who worked on this subject such as (Bishop, 1959) (Burland, 1964) (Fredlund et al., 1978) (Fredlund et al., 1996) (Vanapalli et al., 1996) (Sawangsuriya A. et al., 2009) (Lu and Kaya, 2014).

In this chapter, coherent discussion of the basic concepts that are useful to understand the behavior of pipelines buried in unsaturated soils located at sloping area, was presented as follow:

- Unsaturated soils
- Slope stability
- Pipeline systems

Only general aspects of soil and soil pipeline systems are presented in this chapter. More specific information will be found in subject dedicated chapter.

1.2. Unsaturated soils

Soil mechanics is the science which relates the engineering mechanics with the soil characteristics (Fredlund and Rahardjo, 1993) to adapt and exploit the soils found at or near the surface of the earth in order to assist the human and facilitate his life by predicting risks, minimizing costs and ensure the durability of his projects.

This can be done starting from the description of soil and understanding its behaviour until the application of mechanical engineering technics. During the time, many researchers said that the said definition of soil mechanics is broad because it can cover many types of soil and consequently,

the term of "classic soil mechanics" appears which interested in the application of the engineering mechanics on the saturated soils which have been the emphasis in soil mechanic researches where the voids of the soil skeleton are filled with water. The extension of the world and the increasing demand to use new unknown earth regions push the professional and the research communities to explore and use new types of soils, this is expressed by many organized meetings and conferences around the world to discuss the different challenges faced while utilizing the new lands and areas covered by these types of soils and find best and common ways to resolve the induced problems due to the basic differences in the behaviour of those soils.

In practice, it was found that the application of the principles and concepts of the classic soil mechanic dealing with the saturated soils cannot describe the soils of large confronted areas where three phases are present simultaneously in such unsaturated soils (Lambe and Whitman 1979) which results in a non-classic behaviour as compared with saturated soils.

In the last decades, the differentiation between the saturated and the unsaturated soils becomes indispensable due to the basic differences first in their nature and second in their engineering behaviour. For these reasons, the research community subdivides the soil mechanics field into two portions dealing with saturated and unsaturated soils, separately, as shown in Figure 1-1 . An unsaturated skeleton presents the three constitutive phases of a soil where the pore-water pressure (PWP) is negative especially in the dry environments which characterize the arid and semi-arid climates.

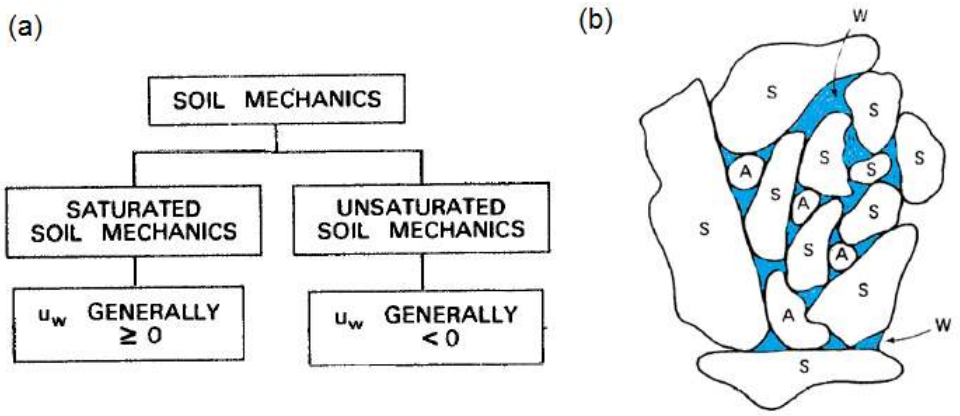

Figure 1-1. (a) Categorization of soil mechanics (b) Soil skeleton (Holtz and Kovacs, 1981)

In general, soils are multiphase materials where any mass of soil consists of a collection of solid particles as the principle phase with voids in between. The void within the soil is defined as including two phases 1) water and 2) air. In the case of saturated soils, the voids are totally occupied by water but in the case of unsaturated soils the voids are partially filled with water as illustrated in Figure 1-1, and the behaviour of such soils is mainly related to the distribution of these two fluids water and air within the soil skeleton. The distribution of these two fluids in the voids is related to many factors such as the grain size distribution and the climate. Gravel, sand, silt and the clay are the main classes present in the natural shallow layers which cover large areas of the earth, when they are located above the GWT they are normally unsaturated. The clayey soil behaviour is the most related to the unsaturated conditions which makes such soils very influenced by the variation of the water content usually induced by the climate conditions. *Many international*

conferences and meetings have been held to treat the problems related to the unsaturated soils. **Shear strength** and **volume change** are two specifically related problems to the unsaturated behaviour which depend on the degree of saturation.

As an example, for an unsaturated clayey soil subjected to a changing environment due to a rainfall precipitation may show volume changes which can be a decrease in the case of collapsible soils or it can take the form of increase in the case of expansive soils where the phenomenon is called swelling. The PWP in both of the above cases is negative but the direction of the response is totally different (Up and Down) whereas they are associated with an increase in the PWP.

The second example is that the same soils located above the GWT can present two different shear strength values under two different degrees of saturation. In their book, Fredlund and Rahardjo (1993) have explained many problem types where the application of the unsaturated soil mechanics is mandatory, these examples are as follow:

- Construction of dams and the control of their serviceability
- Natural slopes subjected to environmental changes
- Stability of vertical or near vertical excavations
- Lateral earth pressures
- Bearing capacity for shallow foundations
- Ground movements involving expansive soils
- Collapsing soils

The unsaturated soils discipline has been more investigated in the last decades because of the enormous human and economic losses related to the disasters and damages caused as a result of the interaction of such soils with the infrastructures such as roads, dams and pipelines, as these infrastructures support the global economy of the cities and facilitate the different sides of the human life. One of the most influenced infrastructures by the unsaturated behaviour of soils around the world are pipelines of fluid transportation (i.e., Water and Gas).

The interaction between the unsaturated soil and the pipelines was and still the subject of many number of theses and published papers that address the different aspects and views of the effects of such soils on the pipelines bodies under different loading and deformation conditions such as landslides, shrink and swell movements, vehicle traffic, precipitation, faults …. In order to understand and analyze and predict the behavior of pipelines constructed on and buried within such soils and then consequently to help the designers and the decision makers to make correct decisions and protect human life and ensure the durability of the economic resources for the future generations.

1.2.1. The importance of the climate

Climate and its components such as precipitation and temperature which are defined as the contributing factors that exert an important role in the behaviour of the unsaturated soils. Because of the main relation of this factors with the variations of the water content within the unsaturated soil skeleton which control the mechanical and the elastic properties of the soil. The scientific community defined the upward and the downward fluxes to describe the water movement out of and into the soil, respectively where, the upward fluxes can be happening by the evaporation or by

evapotranspiration through the vegetative cover (i.e., tree leaves). On the other hand, the downward fluxes are represented by the different forms of precipitations such as rainfall or irrigation activities. The two processes change the PWP within the unsaturated soil either by firstly, decreasing the PWP following a drying process especially during the dry season (i.e., summer) or secondly, the increasing of the PWP following a wetting process during the wet season (i.e., winter) resulting in the desaturation and the saturation of the soil with the upward and the downward fluxes, respectively.

Arid regions where the unsaturated soils are generally located are approximately found in each continent as shown in Figure 1-2, these regions are generally characterized by an annual deficit between the upward and the downward fluxes of water. Algeria is located in north Africa. In its large territory act three types of climates as follow: extremely arid in the south of the country including many provinces such as Tamanrasset, Ouargla, Bechar, Adrar and Tindouf and semi-arid climate covers the northern provinces which are close to the Mediterranean Sea coast and between the two the arid climate covers many interne provinces.

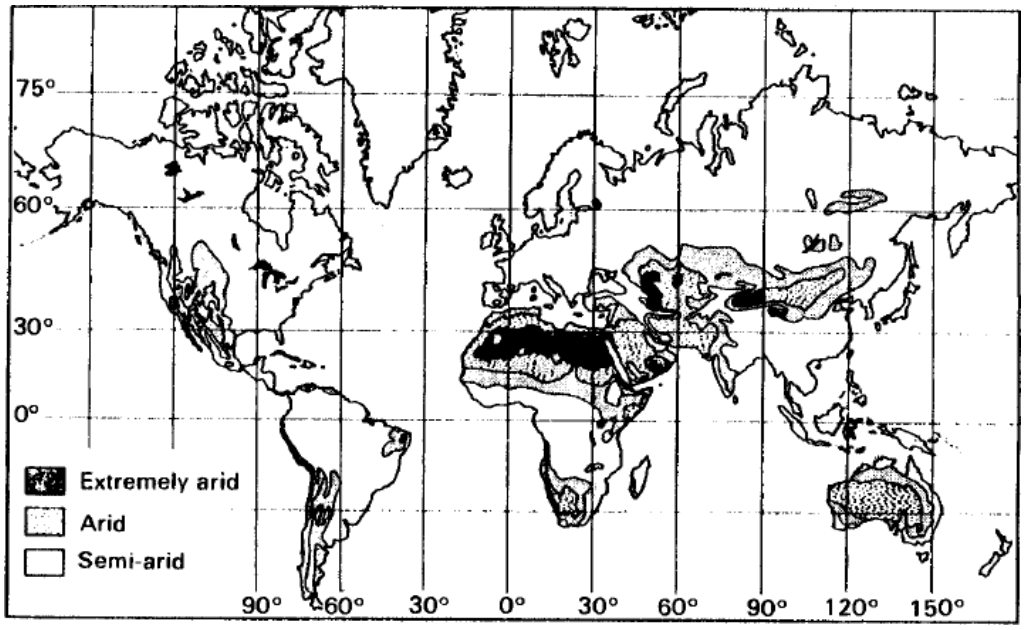

Figure 1-2 the world's map of arid environments (Fredlund and Rahardjo, 1993)

The GWT in the arid and the semi-arid regions is usually located at deep depth, as an example the GWT of the site of this study (Aine-Tine municipality, Mila province) is generally located at 15 m depth (Athmania et al., 2010). The PWP of the soils located above the GWT is negative and it is influenced by the wetting and the drying processes especially in the surficial layers. As a results, changes will occur on the volume and the shear strength of such soils.

Swelling soils are the most peculiar example to describe the effect of volume changes induced by PWPs variation under wetting processes. On the other side, the losses of the shear strength induced by the increase of the PWP induced by rainfall events have caused numerous slope instabilities around the world (Zhang et al., 2011a).

These two phenomena (i.e. volume change and shear strength losses) induced by variation of the PWPs, which is also related to many practical applications, indicates the important role that

negative pore pressures play in controlling the mechanical behaviour of unsaturated soils (Fredlund and Rahardjo, 1993) (Murray and Sivakumar, 2010).

1.2.2. Typical profile of unsaturated soils:

The main factor that brings a soil to be unsaturated is the climate conditions. In general, an unsaturated soil which has negative PWPs can occur in any geological deposit (lacustrine, residual and so on.). Clayey soils exhibit a dependent behavior to the climate variations especially in terms of shear strength and volume change. Based on many published works (Fredlund and Morgenstern, 1976). Biot (1941) is one of the first scientists who highlighted the existence of a relationship between the behaviour of soils in terms of volume change and their water content, During his studies about the three dimensional consolidation of unsaturated soils. In Fredlund and Rahardjo (1993) book, two example of typical unsaturated soils found in two different environment are illustrated which are

- Tropical residual soil found in tropical regions and
- Expansive soils found in arid and semi-arid climates.

In the following section of this thesis, the phenomena related to the second example will be explained considering the site of Aine-Tine slope profile. In general, expansive soils have high plasticity (i.e. high liquid limit) and are relatively stiff and dense. The expansive nature of a soil is most obvious near to the ground surface.

1.2.3. Soil Water Characteristic Curve SWCC

The SWCC for a soil is defined as the relationship between water content and suction that develops within the soil (Williams, 1982) and it is the most fundamental and important soil property in unsaturated soil mechanics (Satyanaga et al., 2013). Numerous equations have been proposed in the literature to represent the SWCC ((Brooks and Corey, 1964) (van Genuchten, 1980), (McKee and Bumb, 1987), (Fredlund and Xing, 1994), (Vanapalli et al., 1996)). The shape of the SWCC is very dependent to the grain size distribution of a soil (Figure 1-3) , therefore, Fredlund et al. (2002) presented a procedure for estimating the SWCC from information on the grain-size distribution properties of a soil.

Aung et al. (2001) reported that soils with different textures and pore-size distributions have different SWCCs. As shown in Figure 1-3, sandy soils usually have a low air-entry value and a steep slope of the SWCC. Silty soils and sandy soils usually have a similar shape of SWCC. However, the air-entry value of silty soils is higher than that of sandy soils due to the presence of smaller pores. Clayey soils have air-entry values higher than those of sandy and silty soils and residual water contents that cannot be visually identified.

In the last period the most used model to define the SWCC are the van Genuchten model (1980) and the Fredlund and Xing (1994) which are presented respectively in Equation 1 and Equation 2.

$$\theta = \theta_r + \frac{\theta_s - \theta_r}{\left[1+\left(\frac{(u_a-u_w)}{a}\right)^n\right]^m} \qquad \text{Equation 1}$$

$$\theta = C\left\{\frac{\theta_s}{\ln\left[\left(e+\left(\frac{(u_a-u_w)}{a}\right)^n\right)\right]^m}\right\} \quad \text{Equation 2}$$

Where, θ is the volumetric water content, θ_s is the volumetric water content at saturation, θ_r is the volumetric water content at residual water content, a is a suction related to the Air Entry Value (AEV), m and n are fitting parameters which control the shape of the SWCC (n: soil parameter which control the slope at the inflection point on the SWCC and m: soil parameter related to the residual water content), C is a correction factor written as follow:

$$C = \left[1 - \ln\left\{1 + \frac{(u_a-u_w)}{C_r}\right\}/\ln\left\{1 + \frac{1000000}{C_r}\right\}\right] \quad \text{Equation 3}$$

Where, C is the residual suction corresponding to the residual water content θ_r. The van Genuchten model was used by Zeng et al. (2020) and Bouatia et al. (2020) during their studies to investigate the effect of cracks on the SWCC of surficial layers which affect the stability of colluvial soils and to investigate the effect of the heave under rainfall infiltration on buried pipeline, respectively.

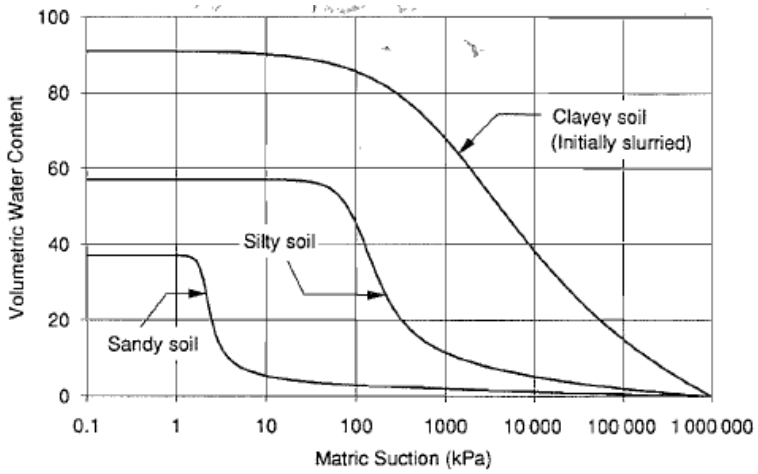

Figure 1-3. Soil water characteristic curve for 3 different types of soils

1.2.4. Permeability function of unsaturated soil

Permeability of saturated soils where pores are totally filled with water is a function of void ratio e only. Based on Darcy's law and the mass conservation for water flow, the three-dimensional water flow in unsaturated soil can be described as follow (Fredlund and Rahardjo, 1993):

$$\frac{\partial}{\partial x}\left(k\frac{\partial h}{\partial x}\right) + \frac{\partial}{\partial y}\left(k\frac{\partial h}{\partial y}\right) + \frac{\partial}{\partial z}\left(k\frac{\partial h}{\partial z}\right) = -\frac{\partial \theta_w}{\partial t} \quad \text{Equation 4}$$

where x, y, z are three Cartesian coordinates; θ_w is the volumetric water content; k is the unsaturated hydraulic conductivity or permeability; and h is the total head. For unsaturated soils, the coefficient of permeability with respect to water k_w is a function of both void ratio e and water content w due the existence of air in the pores of unsaturated soils.

$$k_w = fct\ (e, w) \quad \text{Equation 5}$$

The permeability function is a function of the degree of saturation (Huang et al., 1998). The variation of suction is due to the variation of the water content that can be caused by many causes (i.e., precipitation, irrigation activities). Consequently, the hydraulic conductivity of the unsaturated soils needs to be described due to its dependency to the degree of filling of pores as seen in Figure 1-4.

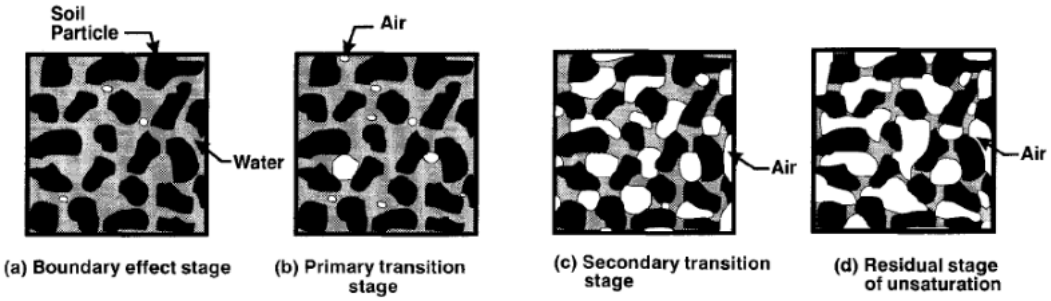

Figure 1-4. Variations of the water content in unsaturated soil

Several equations have been proposed in the literature to estimate the coefficient of permeability from the SWCC to define the function of permeability of an unsaturated soil (Gardner, 1958), (van Genuchten, 1980), (Fredlund et al., 1994), (Leong and Rahardjo, 1997). The most used permeability functions are as follow:

a) Van Genuchten (1980) equation:

$$k_w = k_s \frac{\left[1-\left(a(u_a-u_w)^{(n-1)}\right)\left(1+(a(u_a-u_w)^n)^{-m}\right)\right]^2}{1+(a(u_a-u_w)^n)^{m/2}} \qquad \text{Equation 6}$$

b) Fredlund et al. (1994) equation:

$$k_w = k_s \left\{\frac{1}{\ln\left(e+\left(\frac{(u_a-u_w)}{a}\right)^n\right)}\right\}^m \qquad \text{Equation 7}$$

c) Leong and Rahardjo (1997) equation

$$k_w = k_s \left\{\frac{1}{\ln\left(e+\left(\frac{(u_a-u_w)}{a}\right)^n\right)}\right\}^{mp} \qquad \text{Equation 8}$$

The parameter p can be evaluated using the permeability measured data. The van Genuchten (1980) equation was used by Bouatia et al. (2020) to simulate the water seepage within the Aine-Tine unsaturated soils (Chapter three).

1.2.5. Stress state variables

Hoping that the principle of effective stress would be applicable in the case of unsaturated soil as for saturated soils, many effective stress equations have been proposed to describe the behavior of unsaturated soils (Table 1-1), in order to get a reliable similar equation as the one used for the saturated soil proposed by Terzaghi (1936).

Table 1-1 Effective stress equations for unsaturated soils

Concept	Author	Equation	
Saturated	(Terzaghi, 1936)	$\sigma' = \sigma - u_w$	
Unsaturated	(Corney et al. 1958)	$\sigma' = \sigma - \beta' u_w$	
	(Bishop 1959)	$\sigma' = (\sigma - u_a) + \chi\,(u_a - u_w)$	χ: a parameter related to the degree of saturation of soil
	(Aitchison, 1961)	$\sigma' = \sigma + \psi p''$	p'': pore-water pressure deficiency, ψ: a parameter with values ranging from zero to one
	(Jennings, 1961)	$\sigma' = \sigma + \beta p''$	p'': negative PWP taken as positive value β: a statistical factor measured experimentally

However, the developed equations of effective stress have lacked theoretical justification and have not proven satisfactory, as demonstrated by their limited application to engineering analyses. To describe the unsaturated soil behavior, three combinations of stress state variables are possible which are as follow (Fredlund and Morgenstern, 1976):

a) $(\sigma - u_a)$ and $(u_a - u_w)$
b) $(\sigma - u_w)$ and $(u_a - u_w)$
c) $(\sigma - u_w)$ and $(\sigma - u_a)$

Where, σ is the total normal stress, u_a is the air pore pressure, u_w is the PWP, $(\sigma - u_a)$ is the net normal stress, $(\sigma - u_w)$ is the effective stress, $(u_a - u_w)$ matric suction. In the purpose of developing models of the volume change of unsaturated soils, the first combination was the subject of the uniqueness verification where good agreement between the calculated and the results of measured values of heaves carried out on the Regina clay (Canada). More detailed discussion can be found in the next sections.

1.2.6. Shear strength of unsaturated soils

In the case of an unsaturated soil, the stress circle corresponding to the failure conditions must be plotted on a three-dimensional diagram to consider the effect of suction. The axes in the horizontal plane are the stress state variables and the ordinate is the shear strength (Fredlund et al., 1978) (Figure 1-5). The vertical plane of $(\sigma - u_w)$ versus shear strength, with $(u_a - u_w)$ equal to zero, corresponds to the case where the soil is saturated. If the soil has a positive matrix suction, i.e. $(u_a - u_w)$ is greater than zero, a third dimension is required to plot the stress circle.

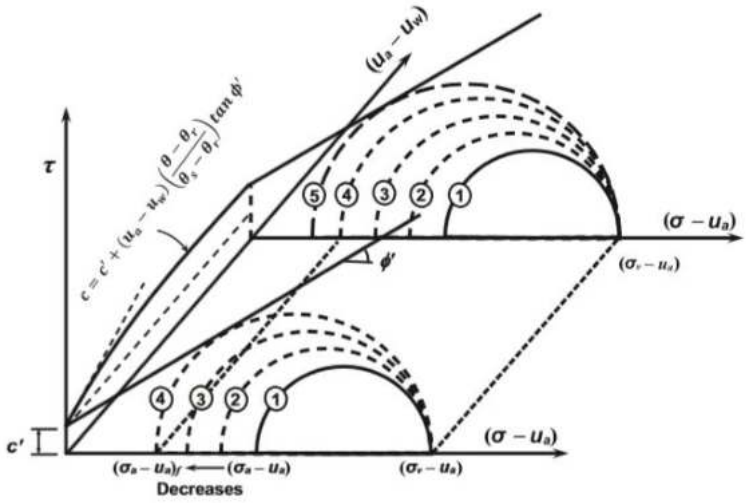

Figure 1-5. Shear strength envelope for unsaturated soils (Al-Khazaali et al., 2018)

Considering the 2nd combination of stress state variables $((\sigma - u_w), (u_a - u_w))$ the shear strength of an unsaturated soil is written as appeared in the 1st form the (Equation 9) and when considering the 1st combination $((\sigma - u_a), (u_a - u_w))$ the equation of shear strength becomes as shown in the 2nd form (Equation 10)

a) 1st form:

$$\tau = c' + (\sigma - u_w)\tan\varphi' + (u_a - u_w)\tan\varphi'' \quad \text{Equation 9}$$

b) 2nd form:

$$\tau = c' + (\sigma - u_a)\tan\varphi' + (u_a - u_w)\tan\varphi^b \quad \text{Equation 10}$$

Where τ is the shear strength of the unsaturated soil, c' is the effective cohesion of the saturated soil, φ' is the effective angle of friction for a saturated soil and φ^b and φ'' is the angle of shearing resistance with respect to matric suction. Fredlund et al. (1978) suggested that the second form called the linear shear strength equation of unsaturated soil is better than the first.

Recently, Vanapalli et al. (1996) developed new models

$$\tau = [c' + (u_a - u_w)\tan\varphi'] + (u_a - u_w)[(\Theta^{\kappa})(\tan\varphi')] \quad \text{Equation 11}$$

Where, κ is fitting parameter and Θ is normalized water content $(\Theta = \theta/\theta_s)$. The authors also proposed two other forms without using the fitting parameter κ which are as follow:

a) With respect to degree of volumetric water contents:

$$\tau = [c' + (\sigma - u_a)\tan\varphi'] + (u_a - u_w)\left[(\tan\varphi')\left\{\frac{\theta - \theta_r}{\theta_s - \theta_r}\right\}\right] \quad \text{Equation 12}$$

b) With respect to degree of saturation:

$$\tau = [c' + (\sigma - u_a)\tan\varphi'] + (u_a - u_w)\left[(\tan\varphi')\left\{\frac{S - S_r}{100 - S_r}\right\}\right] \quad \text{Equation 13}$$

The above two equations (Equation 12 and Equation 13) allow the designer to include the effect of SWCC on the variation of the shear strength. In the same year (1996), Fredlund et al. developed an equation by using the fitting parameter κ as follow:

$$\tau = c' + (\sigma - u_a)\tan\varphi' + (u_a - u_w)[\Theta(u_a - u_w)]^{\kappa}\tan\varphi' \quad \text{Equation 14}$$

Experimental determination of the value of the shear strength of an unsaturated soil is costly and time-consuming, some empirical models for predicting the shear strength of unsaturated soils are available in the literature and can provide a satisfactory accuracy for slope stability analysis. The chapter two include more details about the use of these equation to calculate the FoS of infinite unsaturated slopes.

1.2.7. Volume change of unsaturated soils

Biot (1941) was the first scientist who highlighted the existence of relationship between the behaviour of soils in terms of volume change and their water content during his studies about the three dimensional consolidation of unsaturated soils. In the same direction of studying the volume change of unsaturated soils, many researchers have worked on estimating the volume changes by developing model and equation that relate volume change with respect of the net normal stress and soil suction $(u_a - u_w)$ (i.e., (Bishop and Blight, 1963) (Matyas and Radhakrishna, 1968) (Brackley, 1971)). Vu and Fredlund (2004) proposed a method to predict 1D, 2D and 3D heave in expansive soils which consider the first combination of stress state variables discussed above where the volume change that occurs in a unit volume soil specimen can be predicted using two consecutive equations, the first for the soil structure is as follow:

$$\varepsilon = \frac{1}{v}\frac{\partial v}{\partial(\sigma - u_a)}\, d(\sigma - u_a) + \frac{1}{v}\frac{\partial v}{\partial(u_a - u_w)}\, d(u_a - u_w) \quad \text{Equation 15}$$

And the second proposed equation for volumetric water content variation:

$$\theta_w = \frac{1}{v}\frac{\partial v_w}{\partial(\sigma - u_a)}\, d(\sigma - u_a) + \frac{1}{v}\frac{\partial v_w}{\partial(u_a - u_w)}\, d(u_a - u_w) \quad \text{Equation 16}$$

Where v is the unit volume and v_w is the volume of water in the element. Using the elasticity parameters, the constitutive relationship for the soil structure can be written in an incremental elasticity form (Fredlund and Rahardjo, 1993):

$$d\varepsilon_{ij} = \frac{1+v}{E}d\left(\sigma_{ij} - \delta_{ij}u_a\right) - \frac{v}{E}d(\sigma_{kk} - 3u_a)\delta_{ij} + \frac{d(u_a - u_w)}{H}\delta_{ij} \quad \text{Equation 17}$$

The two-dimensional (x, y) matrix form of the stress-strain relationship is implemented in SIGMA/W which is one of the modules of GeoStudio software suite proposed by GeoSlope International Ltd (2007) and it can be written as follow:

$$\begin{Bmatrix}\Delta\varepsilon_x\\ \Delta\varepsilon_y\\ \Delta\gamma_{xy}\end{Bmatrix} = \frac{1}{E}\begin{bmatrix}1 & -\mu & 0\\ -\mu & 1 & 0\\ 0 & 0 & 2(1+\mu)\end{bmatrix}\begin{Bmatrix}\Delta(\sigma_x - u_a)\\ \Delta(\sigma_y - u_a)\\ \Delta(\tau_{xy})\end{Bmatrix} + \frac{1}{H}\begin{bmatrix}1 & 0 & 0\\ 0 & 1 & 0\\ 0 & 0 & 1\end{bmatrix}\begin{Bmatrix}\Delta(u_a - u_w)\\ \Delta(u_a - u_w)\\ \Delta(u_a - u_w)\end{Bmatrix} \quad \text{Equation 18}$$

Where ε_x, ε_y and γ_{xy} are the normal and shear strain components, σ_x, σ_y and τ_{xy} are the normal and shear stress components, E is the Young's modulus of the soil structure. H is the elasticity modulus with respect to a change in suction and μ is the Poisson's ratio. H is estimated adopting the relationship $H = E/(1-2\mu)$. This equation is similar in form to the constitutive equation presented by Biot (1941).

The developed equations (Vu and Fredlund, 2004) were tested firstly to simulate the effect of water leakage from a pipe under a flexible cover and the second was used to simulate the infiltration of water from the ground surface. The constitutive relationship for the soil structure is presented graphically in the form of a constitutive surface in Figure 1-6 (a). The coefficients of volume change, m_1^s and m_2^s, are slopes on the soil structure constitutive surface and can be obtained by differentiating the surface with respect to net normal stress and matric suction, respectively.

$$\boldsymbol{m_1^s = \frac{\partial \varepsilon_v}{\partial(\sigma_{mean} - u_a)} = \frac{1}{(1+e_0)} \frac{\partial e}{\partial(\sigma_{mean} - u_a)}} \quad \text{Equation 19}$$

$$\boldsymbol{m_1^s = \frac{\partial \varepsilon_v}{\partial(u_a - u_w)} = \frac{1}{(1+e_0)} \frac{\partial e}{\partial(u_a - u_w)}} \quad \text{Equation 20}$$

The constitutive relationship for the water phase is presented graphically as the constitutive surface in Figure 1-6 (b). The coefficients of water volume change, m_1^w and m_2^w, indicate the amount of water taken on or released by the soil because of a change in the net normal stress and matric suction.

$$\boldsymbol{m_1^w = \frac{\partial \theta_w}{\partial(\sigma_{mean} - u_a)}} \quad \text{Equation 21}$$

$$\boldsymbol{m_2^w = \frac{\partial \theta_w}{\partial(u_a - u_w)}} \quad \text{Equation 22}$$

Where $\theta_w = V_w/V_0$ is the volumetric water content.

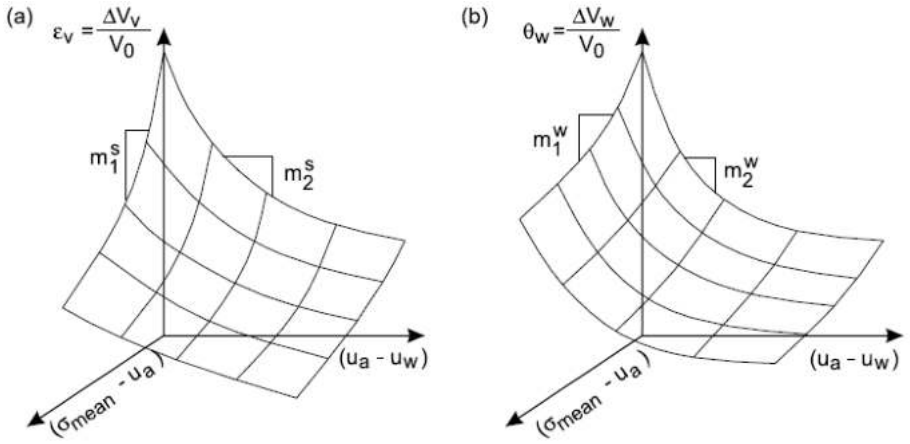

Figure 1-6. Constitutive surfaces for (a) soil structure and (b) water phase of an unsaturated soil (Vu and Fredlund, 2004)

1.2.8. Young's modulus variation

Han et al. (2016) defined the suction as an energy potential with a tension stress on soil skeleton that holds the soil particles and their packets together providing resistance to elastic and

plastic deformations. Suction will improve the performance of many materials at certain water content such the one used in pavement design codes and defined as the optimum proctor.

Many studies report that the modulus of elasticity increases with suction (Rampino et al., 2000) (Meilani et al., 2005) (Oh et al., 2009) (Sawangsuriya A. et al., 2009) (Vu and Fredlund, 2011) (Adem and Vanapalli, 2014b) (Liu et al., 2019). The Young's modulus is an essential parameter in the calculation of geotechnical problems (i.e. volume change calculation), it connects the stresses to the deformations. Using a constant elasticity modulus in either saturated or unsaturated geotechnical conditions does not reflect the reality in unsaturated soils. Unsaturated soil behavior has become a challenging subject to researchers and practitioners (Rahardjo et al., 2011).

Several semi-empirical models have been developed based on experimentation and calibration by numerical simulations to predict the modulus of elasticity based on the information about the soil water content. Soil moisture can be expressed through two state parameters which are the degree of saturation S or the volumetric water content θ_w. Using two state variables, which are the net normal stress $(\sigma - u_a)$ and suction $(u_a - u_w)$, Fredlund and Morgenstern (1976) have confirmed that two constitutive relations are required to describe the volume change behavior of an unsaturated soil. While the first equation is relative to the soil structure and the second is for the change of volume of water in the soil. For sandy soils, Oh et al. (2009) have proposed a simple semi empirical model with two fitting parameters α and β to predict the modulus of elasticity with respect to the suction information. This model demands saturated modulus of elasticity E_{sat} and the SWCC and the definition of two fitting parameters α and β. As a result of this study, α=2.5 and β=1 can give an acceptable estimation of the unsaturated elastic moduli in the case of sand.

$$E_{unsat} = E_{sat}\left[1 + \alpha \frac{(u_a - u_w)}{(P_a/100)}\left(S^{\beta}\right)\right] \qquad \text{Equation 23}$$

Where, E_{unsat} is the modulus of elasticity under unsaturated conditions, E_{sat} is the modulus of elasticity under saturated conditions, α and β are fitting parameters, and P_a is atmospheric pressure (i.e., 100kPa). Oh et al. (2009) defined a value of β=1 for sandy soils where the plasticity is very low ($I_p = 0$).

One year later, the same model have been extended by Vanapalli and Oh (2010) to be applicable for soils with plasticity index less than 16%, where they found that β=1 and 2 are suitable for coarse and fine grained soils, respectively. In which concern the parameter α, they presented a lower and upper boundary functions with respect to the plasticity index $\alpha_{Lower,Upper}$=$fct(I_P)$. This model was used by Adem and Vanapalli (2013) to predict the 1-D heave over time due to suction variation following a rainfall infiltration, and assuming the values 2 and 0.1 for α and β, respectively. It is also named the VO model and used by Al-Khazaali and Vanapalli (2020) to study the axial response of soil-pipeline interaction subjected to axial displacement, in saturated and unsaturated sand conditions using numerical model in the commercial software, SIGMA/W software to simulate physical model.

In this study, the parameters α and β took the values 1 and 0.8, respectively. But this model is not capable to describe soils with high plasticity index (i.e. Clays). Due to the high sensitivity of cohesive soils and the large need to manage these soils in different construction projects, the need

to define their elastic modulus variation with respect to moisture content is increased. Following this tendency, an extension of the VO model is made by Adem and Vanapalli (2014b) based on the encouraging results obtained in their paper (2013). Where it is found that the modulus of elasticity of unsaturated expansive soils estimated using the fitting parameters β=2 and α=0.05 to 0.15 provided reasonable estimations of the variations of soil heave (Adem and Vanapalli, 2014b). In this study, β=2 and α=0.1 are adopted for clayey soils to carry out the soil-pipeline interaction study in Aine Tine area. α=0.1 represents the middle of the range from 0.05 to 0.15.

1.3. Slope stability

The primary purpose of the slope stability analysis is to contribute on the safe and economic design of excavations, embankments, earth dams and landfills. Identification of critical geological, material, environmental and economic parameters that will affect the project is essential. In addition to the understanding of the nature, magnitudes and the frequency of potential slope problems, The analysis of slopes takes into account a variety of factors (see Figure 1-7):

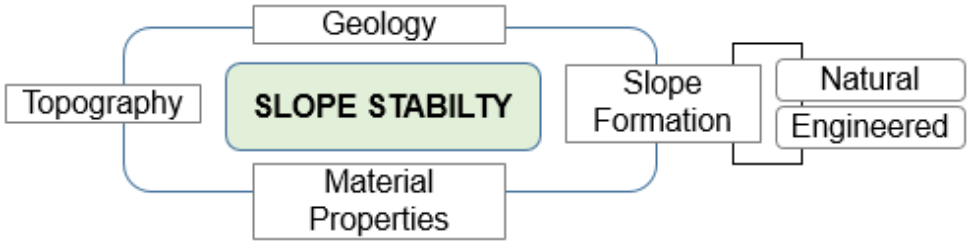

Figure 1-7. Factors related to the slope stability analysis (Abramson et al., 2002)

1.3.1. Slope failure definition

The slope failure as presented in the website of the Geological Society comprises many definitions of the term **landslide**, as follow:

- Cruden (1991) for the UNESCO Working Party on World Landslide Inventory, said that the term landslide denotes "the movement of a mass of rock, debris or earth down a slope".
- Varnes (1978) indicated that slope movement would be a better comprehensive term as it did not infer process. Varnes defined a landslide as 'a downward and outward movement of slope forming materials under the influence of gravity'.
- Brunsden (1984) preferred the term mass movement and distinguished this from mass transport as being a process which did not require a transporting medium such as water, air or ice (Dikau et al., 1996). The phenomena described as landslides are not limited to either the "land" or to "sliding", and usage of the word has implied a much more extensive meaning than its component parts suggest. Ground subsidence and collapse are excluded.

1.3.2. Factor of safety concepts

Factors of safety provide a quantitative indication of slope stability. A value of F = 1.0 indicates that a slope is on the boundary between stability and instability (Duncan et al., 2014) where the factors tending to make the slope stable are in balance with those tending to make the slope unstable. The most widely used and most generally useful definition of the factor of safety (FoS) in slope stability is:

$$\boldsymbol{FoS} = \frac{\boldsymbol{shear\ strength\ of\ the\ soil}}{\boldsymbol{shear\ stress\ required\ for\ equilibrium}} \qquad \text{Equation 24}$$

The factor of safety is defined as the ratio between the mobilized shear stress τ and the shear strength developed in a surface failure τ_f. The formula is given in Equation 25.

$$FoS = \tau_f / \tau \qquad \text{Equation 25}$$

Where τ is the mobilzed shear stress and τ_f is the maximum shear strength which can be developed in the slip surface. The formula of the shear strength can be estimated by using the Mohr-Coulomb failure criterion as can be seen in the Equation 26

$$\tau_f = c + \sigma_n \tan \varphi \qquad \text{Equation 26}$$

Where c and φ represent the cohesion and the internal friction angle of the considered soil at the slip plane and σ_n represent the normal stress that are calculated at the slip surface. The most known test to measure the shear strength parameters is the direct shear test (see Figure 1-8) in the purpose to simulate the shearing stresses within the slip plane to draw the Mohr-Coulomb envelop and finally to get the shear strength parameters (c, φ) as illustrated in the Figure 1-9.

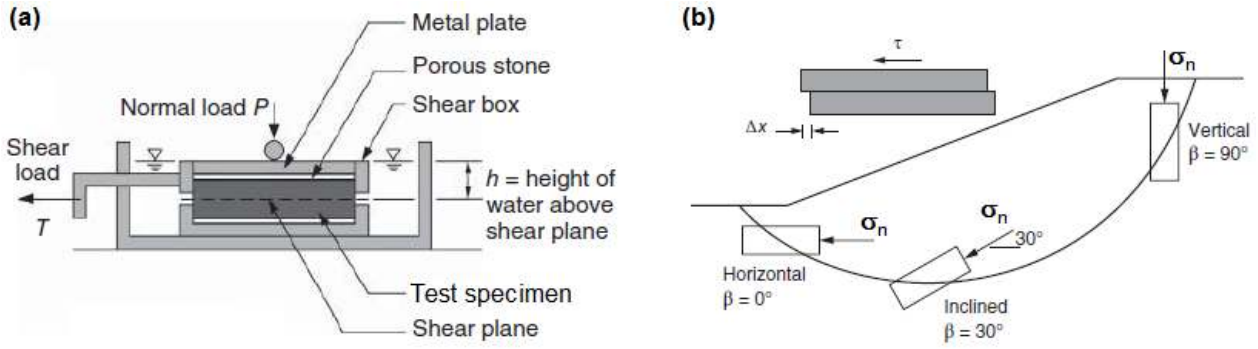

Figure 1-8. (a) Direct shear test box, (b) soil specimens as sheared along the slope failure surface

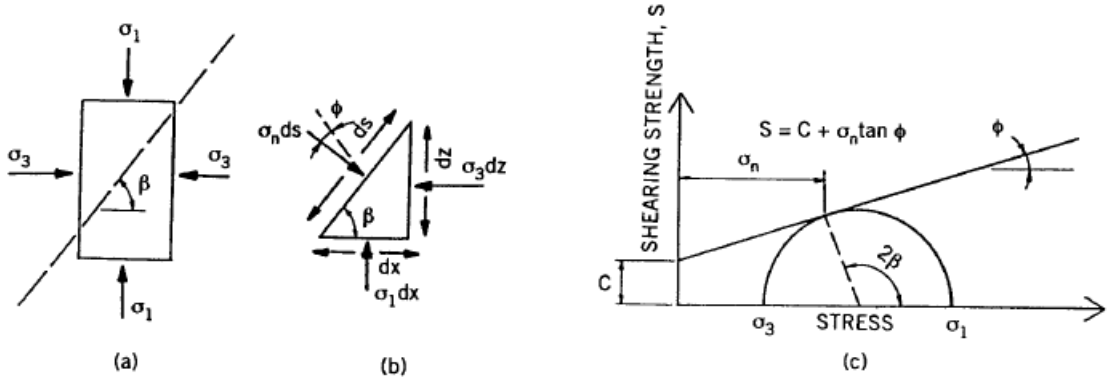

Figure 1-9. Mohr-Coulomb envelope (a) Soil element (b) Stress vector (c) Shear strength envelope (Abramson et al., 2002)

1.3.3. Type of slopes:

The classification of slope is a mandatory step to deal with slopes, it serves as a language between specialist. In the literature, slopes can be classified according to many criteria. where in the following section they will be classified in terms of the origin of creation:

1.3.3.1. Natural slopes:

The slopes formed due to natural processes and that exist naturally are called natural slopes, which exist in hilly areas. Many infrastructures intersect ridges and valleys, and these landscape can be prone to slope stability problems. Natural slopes may suddenly fail because of changes in (1) topography (2) seismicity (3) groundwater flows (4) loss of strength (5) stress changes (6) and

weathering. Generally, these failures are not understood because little study is undertaken until the failure makes it necessary. In many instances, significant uncertainty exists about the stability of a natural slope.

1.3.3.2. Engineered slopes:

The engineered slopes are modified natural slopes or new constructed slopes where the effect of man intervene by modifying principally the geometry. As seen in the Figure 1-10, the engineered slopes were categorized by Abramson et al. (2002) in three main groups (1) Fills (embankments), (2) Cut slopes and (3) Landfills where cut and fill slopes are involved.

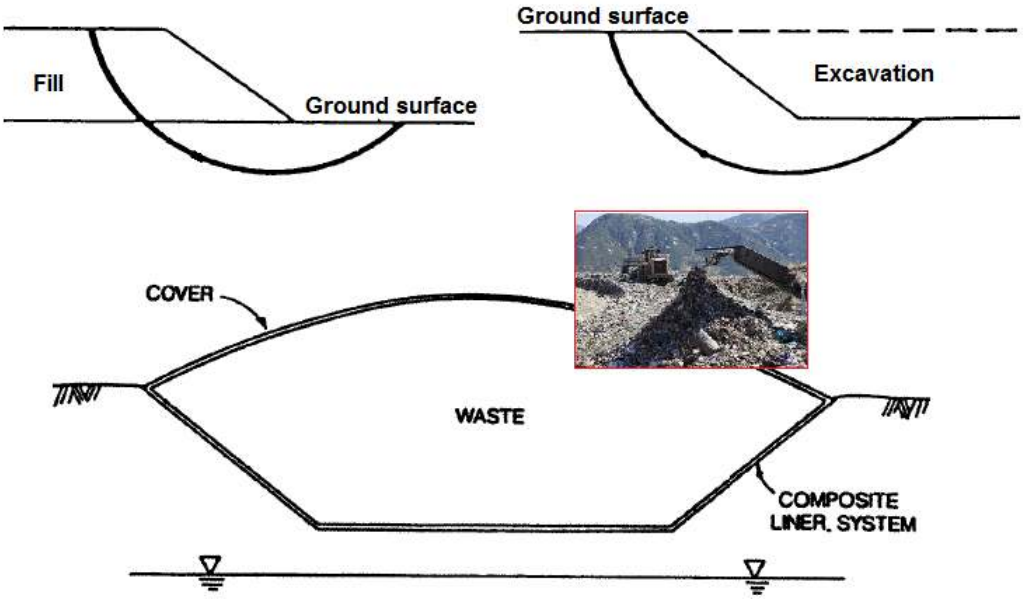

Figure 1-10. Main groups of engineered slopes

1.3.4. Nomenclature of landslides

Landslides nomenclature is a very important element in the geotechnical studies. It's a unified languages used by specialists to facilitates the different operations in the slope stability analyses. In the case of the waste type, as seen in Figure 1-10, the top surface (Cover) appears curved while in other cases it may be planar of complex where the failed material starts from a zone of depletion and deposits in the accumulation zone. the definition of the principle parts of a landslide as seen in Figure 1-11 is prepared based on the de Blasio (2011) works. The **crown** of the landslide identifies the region adjacent to the highest parts of the failed mass. The **scarp** is the steep failure surface between the failed body and the terrain. Several **minor scarps** due to internal shearing may also punctuate the main landslide body.

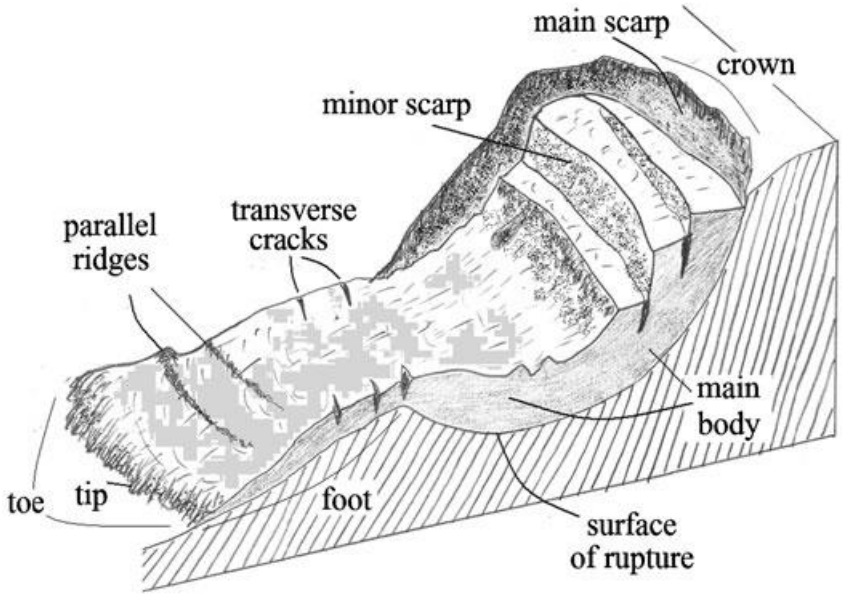

Figure 1-11. Geometry of a landslide.

The **failure surface** identifies the interface at the base of the landslide where the material has slid. The **foot** is the material deposited in the accumulation zone, beyond the failure surface. The landslide deposit ends with a **toe**, which is the line (usually bent) between the accumulated material and the untouched terrain. The **tip** is the point of the landslide deposit farthest from the crown. Some landslides exhibit transverse tension cracks in the region of the foot closest to the scarp. Closer to the toe, transverse **ridges** are sometimes formed. The right and left flanks of the landslide are identified by standing with shoulders to the crown.

1.3.5. Movement classification

Various systems of landslide classification have been proposed such as the one of Varne (1978) which is updated by Hunger et al. (2014). Varne (1978) subdivided the occurred movements on the ground surface into SIX classes based on the visual description of the movement like geometry as well as the shape and the way of the movement along the slope and some other characteristics like speed of the movement. The way of the movement means volume and granular constitution of the displaced material, trajectory, shape of the failure surface and how the failure propagates along the slope.

1.3.5.1. Falls

In falls, a mass of any size is detached from a steep slope or cliff, along a surface on which little or no shear displacement takes place, and descends mostly through the air by free fall, leaping, bounding, or rolling. Movements are very rapid to extremely rapid and may or may not be preceded by minor movements leading to progressive separation of the mass from its source.

Figure 1-12. Slope movements type: Falls

1.3.5.2. Topples

This kind of movement consists of the forward rotation of a unit or units about some pivot point, below or low in the unit, under the action of gravity and forces exerted by adjacent units or by fluids in cracks. Topples can develop in many rock types. This class of movement may or may not culminate in either falling or sliding, depending on the geometry of the failing mass and the orientation and extent of the discontinuities.

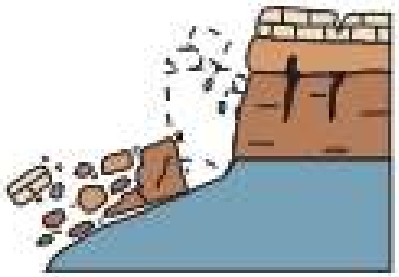

Figure 1-13. Slope movements type: Topples

1.3.5.3. Slides

In this class of movement, the movement consists of shear strain and displacement along one or several surfaces that are visible or may reasonably be inferred, or within a relatively narrow zone. The movement may be progressive; that is, shear failure may not initially occur simultaneously over what eventually becomes a defined surface, of rupture, but rather it may propagate from an area of local failure. The displaced mass may slide beyond the original surface of rupture onto what had been the original ground surface, which then becomes a surface of separation. Slides were subdivided into: (a) those in which the material in motion is not greatly deformed and consists of one or a few units. (b) those in which the material is greatly deformed or consists of many semi-independent units. These subtypes were further classed into rotational slides and planar slides. Distinction between rotational and translational sliding:

The rotary movement of a slump, if the surface of rupture dips into the hill at the foot of the slide, tends to restore equilibrium in the unstable mass; the driving moment during movement decreases and the slide may stop moving.

A translational slide, however, may progress indefinitely if the surface on which it rests is sufficiently inclined and as long as the shear resistance along this surface remains lower than the more or less constant driving force.

— Rotational slides: Rotational slides: The commonest examples of rotational slides are little deformed slumps, which are slides along a surface of rupture that is curved concavely upward. The movement in slumps takes place only along internal slip surfaces which forms together with the exposed scarps a spoon-shape. Since rotational slides occur most frequently in fairly homogeneous materials, their incidence among constructed embankments and fills, and hence their interest to engineers, has perhaps been high relative to other types of failure, and their methods of analysis have in the past been more actively studied.

— Translational slides: In translational sliding the mass progresses out or down and out along a more or less planar or gently undulatory surface and has little of the rotary movement like in slumps. The moving mass commonly slides out on the original ground surface.

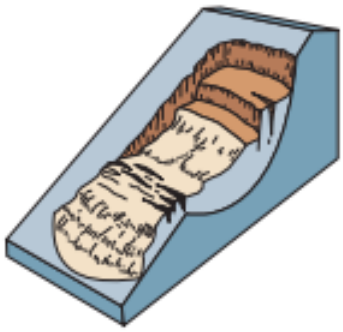

Figure 1-14. Slope movements type: Rotational slides

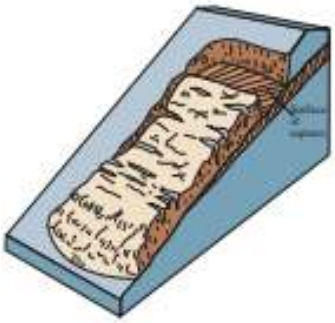

Figure 1-15. Slope movements type: Translational slides

1.3.5.4. Lateral spreading

In spreads, the dominant mode of movement is lateral extension accommodated by shear or tensile fractures. Two types may be distinguished.

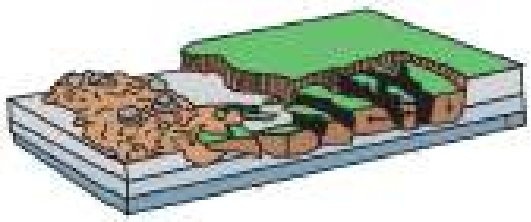

Figure 1-16. Slope movements type: Lateral spreading

— **First**: Distributed movements result in overall extension but without a recognized or well-defined controlling basal shear surface or zone of plastic flow. These appear to occur predominantly in bedrock, especially on the crests of ridges.

— **Second**: Movements may involve fracturing and extension of coherent material, either bedrock or soil, owing to liquefaction or plastic flow of subjacent material. The coherent upper units may subside, translate, rotate, or disintegrate, or they may liquefy and flow. The mechanism of failure can involve elements not only of rotation and translation but also of flow; hence, lateral spreading failures of this type may be

properly regarded as complex. They form, however, such a distinctive and dominant species in certain geologic situations that specific recognition seems worthwhile.

1.3.5.5. Flows

Many examples of slope movement cannot be classed as falls, topples, slides, or spreads. In unconsolidated materials, these generally take the form of fairly obvious flows, either fast or slow, wet or dry.

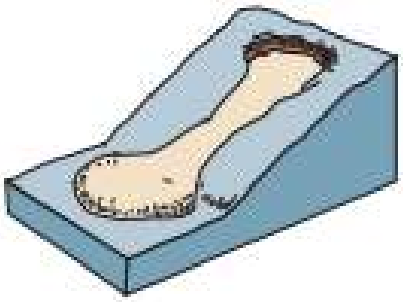

Figure 1-17. Slope movements type: Flows

1.3.5.6. Complex movements

This class of movement is the combination of two or more principal types of movements. More often than not, slope movements involve a combination of one or more of the principal types of movement described above, either within various parts of the moving mass or at different stages in development of the movements. The above classification was considered to be happened in three different materials which are rocks, debris and soil. It consequently yields eighteen (18) subclasses of slope failures as shown in Table 1-2 where those written in bold are the most probable in literature according to de Blasio (2011).

Table 1-2. Sub-classes of slope failures (Dikau et al., 1996) (Cruden and Varnes, 1996)

TYPES OF MOVEMENT		TYPES OF MATERIAL		
		ROCK (Bedrock)	ENGINEERING SOILS	
			Debris (Predominantly coarse)	Earth (Predominantly fine)
Falls		***Rock fall.***	Debris fall	Earth fall
Topples		***Rock topple.***	Debris topple	Earth topple
Slides	Translational	***Rock slide.***	Debris slide	Earth slide
	Rotational	***Rock slump.***	***Debris slump.***	***Earth slump.***
Lateral spreads		***Lateral rock spread.***	Debris spread	***Earth spread.***
Flows		Rock flow Deep creep	Debris flow	Earth flow
			Soil creep	
Complex		Combination of two or more principal types of movement		

1.3.6. Sequence or repetition of movements

The term **retrogressive** has been used almost consistently for slides or flow failures that begin at a local area, usually along a slope, and enlarge or retreat opposite to the direction of movement of the material by spreading of the failure surface, successive rotational slumps, falls, or liquefaction of the material. On the other hand, the term **progressive** has been used to indicate extension of the failure (a) downslope (b) upslope (but not specifically upslope only) and (c) either upslope or downslope, or unspecified.

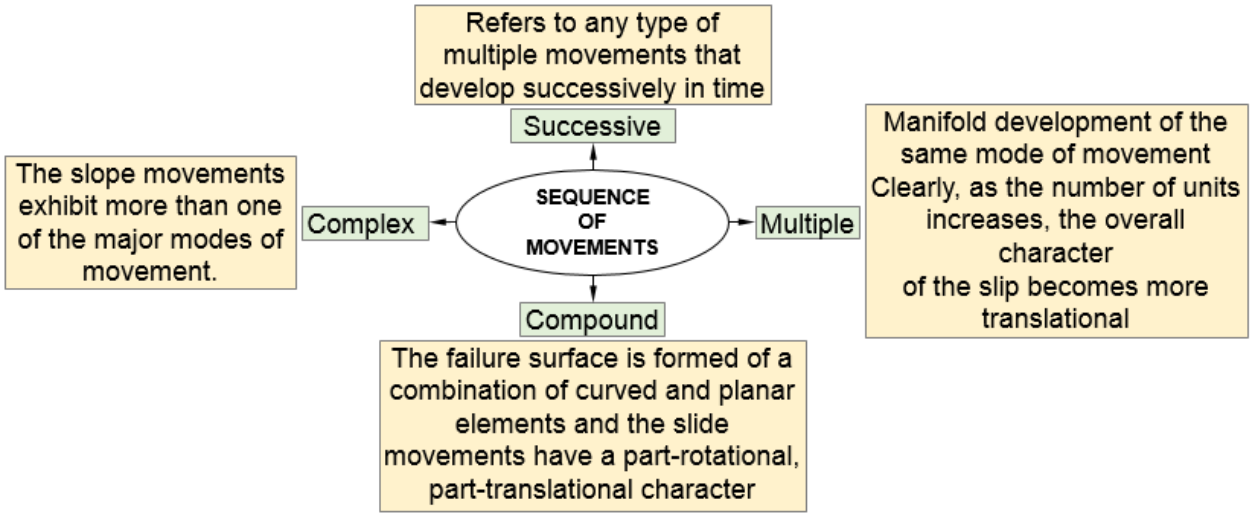

Figure 1-18. Classification of sequence of movements.

Varne (1978) suggested that the term **progressive** be used for failure that is either advancing or retreating or both simultaneously, that the term retrogressive be used only for retreating failures, and that failures that enlarge in the direction of movement be referred to simply as advancing

failures. The terms complex, composite, compound, multiple, and successive have been used in different ways by various authors. Figure 1-18 shows the definitions suggested by Varne (1978).

1.3.7. Distribution and style of landslides activity

1.3.7.1. Distribution

Based on Cooper (2007) the distribution of the activity of landslides can be divided into seven classes as follow (1) advancing; (2) retrogressive; (3) enlarging; (4) diminishing; (5) confined; (6) moving; (7) widening. The same classification was adopted by the International Geotechnical Societies UNESCO Working Party on World Landslide Inventory WP/WLI (1993) and also used by the Geological Society of London (https://www.geolsoc.org.uk). Table 1-3 presents short definitions and figures illustration for each class of distribution.

1.3.7.1. Style

Following the works published by Cooper (2007), the style of the activity of landslides can be divided into five (05) classes as follow: (1) Complex; (2) Composite; (3) Successive; (4) Single; (5) Multiple. The same classification was adopted by the International Geotechnical Societies UNESCO Working Party on World Landslide Inventory WP/WLI (1993) and also used by the Geological Society of London (https://www.geolsoc.org.uk). Table 1-4 presents short definitions and figures illustration for each class of activity.

Table 1-3. Distribution of the activity of landslides

Type of the activity	Figure (Cooper et al., 2007)
Advancing: In an advancing landslide the rupture surface is extending in the direction of movement.	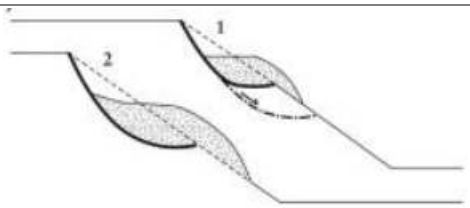
Retrogressive: In a retrogressive landslide the rupture surface is extending in the direction opposite to the movement of the displaced material.	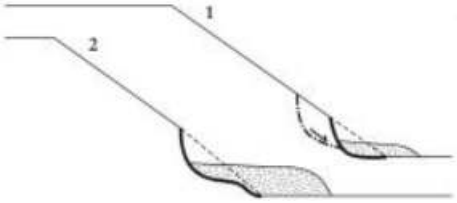
Enlarging: in an enlarging landslide the rupture surface of the landslide is extending in two or more directions.	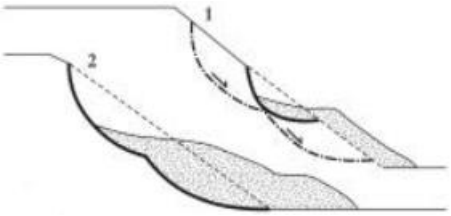
Diminishing: In a diminishing landslide the volume of displaced material is decreasing.	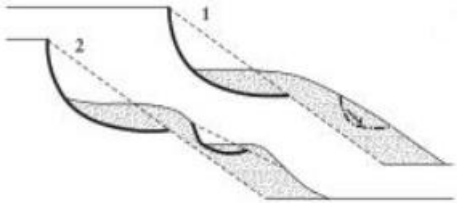
Confined: In a confined landslide there is a scarp but no rupture surface visible at the foot of the displaced mass.	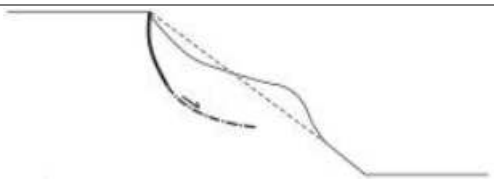
Moving: In a moving landslide the displaced material continues to move without any visible change in the rupture surface and the volume of the displaced material.	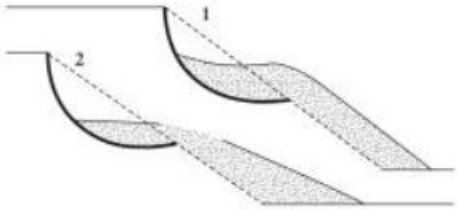
Widening: In a widening landslide the rupture surface is extending into one or both flanks of the landslide.	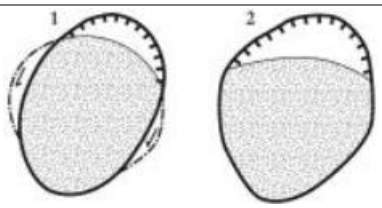

Dashed line: Original ground surface. **Gray color**: Extent of the displaced material.

Table 1-4. Style of the activity of landslides

Type of the activity	Figure (Cooper et al., 2007)
Complex: A complex landslide exhibits at least two types of movement (falling, toppling, sliding, spreading and flowing) in sequence. In the example shown a gneiss and a pegmatite vein toppled with valley incision. Alluvial deposits fill the valley bottom. After weathering had weakened the toppled material some of the displaced mass slid further downslope.	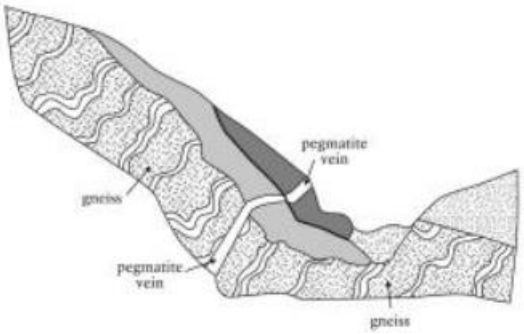
Composite: A composite landslide exhibits at least two types of movement simultaneously in different parts of the displacing mass. In the example shown the limestones have slid on the underlying shales causing toppling below the toe of the slide rupture surface.	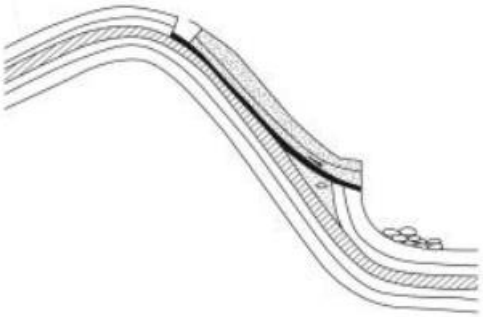
Successive: A successive landslide is the same type as a nearby, earlier landslide, but does not share displaced material or rupture surface with it. In the example shown the later slide AB is the same type as CD but does not share displaced material or a rupture surface with it.	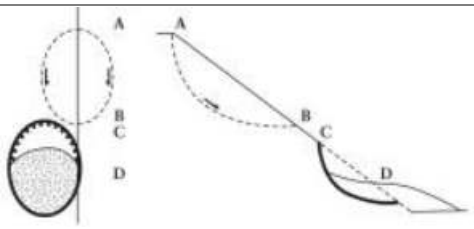
Single: A single landslide is a single movement of displaced material.	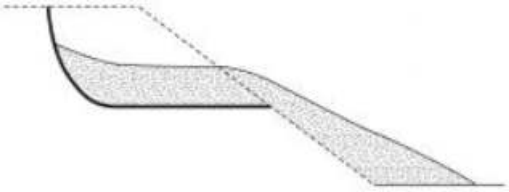
Multiple: A multiple landslide shows repeated development of the same type of movement.	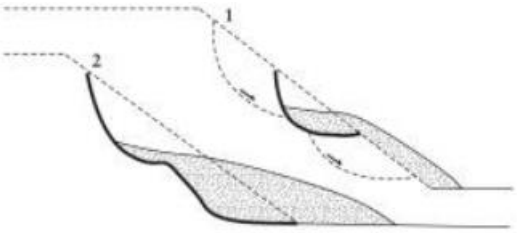

Dashed line: Original ground surface. **Gray color**: Extent of the displaced material

1.3.8. Landslide causes

Slope failures can be triggered under the effect of many factors from different sources which are summarized by Highland (2004) as follow (Table 1-5):

Table 1-5. Classification of main causes of landslides

Source of the cause	Causes
Geological causes	• Weak or sensitive materials • Weathered materials • Sheared, jointed, or fissured materials • Adversely oriented discontinuity (bedding, schistosity, fault, unconformity, contact, and so forth) • Contrast in permeability and/or stiffness of materials
Morphological causes	• Tectonic or volcanic uplift Glacial rebound • Fluvial, wave, or glacial erosion of slope toe or lateral margins • Subterranean erosion (solution, piping) • Deposition loading slope or its crest • Vegetation removal (by fire, drought) • Thawing • Freeze-and-thaw weathering • Shrink-and-swell weathering
Human causes	• Excavation of slope or its toe • Loading of slope or its crest • Drawdown (of reservoirs) • Deforestation • Irrigation • Mining • Artificial vibration • Water leakage from utilities

1.3.9. Slope failures and water

Slope saturation by water is a primary cause of landslides. This effect can occur in the form of intense **rainfall**, snowmelt, changes in GWT levels, and water level changes along coastlines, earth dams, and the banks of lakes, reservoirs, canals, and rivers.

1.3.10. Slope failures and earthquakes

Many mountainous areas that are vulnerable to landslides have also experienced at least moderate rates of earthquake occurrence in recorded times. The occurrence of earthquakes in steep landslide-prone areas greatly increases the likelihood that landslides will occur, due to ground shaking alone or shaking-caused dilation of soil materials, which allows rapid infiltration of water.

1.3.11. Methods of slope stability analysis

1.3.11.1. Limit equilibrium methods

The FoS can be defined in three ways: Limit equilibrium, force equilibrium and moment equilibrium (Abramson et al., 2002). Two different approaches are used to satisfy static equilibrium in the limit equilibrium analysis procedures. Some procedures consider equilibrium for the entire mass of soil bounded beneath by an assumed slip surface and above by the surface of the slope. In these procedures, equilibrium equations are written and solved for a single free body. The Infinite Slope procedure and the Swedish slip circle method are examples of such **single-free-body** procedures.

In other procedures the soil mass is divided into a number of vertical or horizontal slices, and equilibrium equations are written and solved for each slice. These procedures, termed **procedures of slices**, include such methods as the Ordinary Method of Slices, the Simplified Bishop procedure, and Spencer's procedure. Three static equilibrium conditions are available

- Equilibrium of forces in the vertical direction $\sum F_y = 0$
- Equilibrium of forces in the horizontal direction $\sum F_x = 0$
- Equilibrium of moments about any point $\sum M_Z = 0$

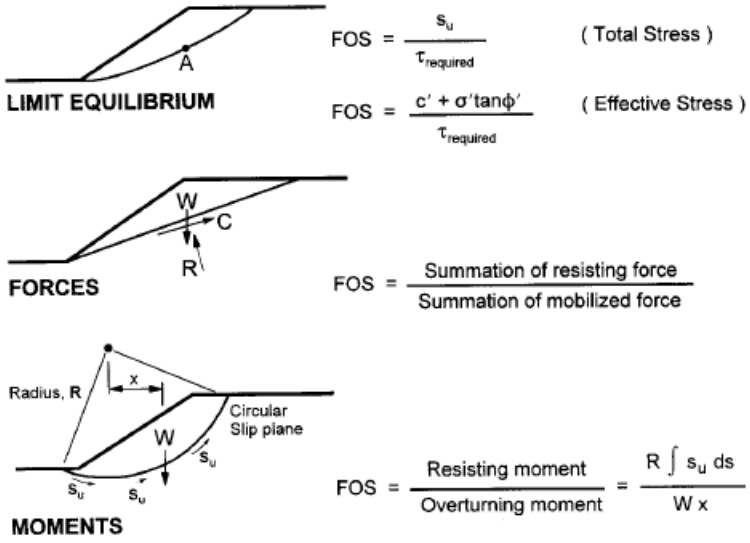

Figure 1-19. Various definitions of the FoS

The limit equilibrium procedures all use at least some static equilibrium equations to compute the factor of safety. Some procedures use and satisfy all of the equilibrium equations, others use and satisfy only some. The Table 1-6 shows the most known limit equilibrium methods developed by many researchers.

1.3.11.2. Method of slices

The methods discussed earlier do not depend on the distribution of the effective normal stresses along the failure surface. Table 1-6 summarize the adopted static equilibrium conditions satisfied by Limit Equilibrium Methods.

Table 1-6. Static equilibrium conditions satisfied by Limit Equilibrium Methods

Method	Force equilibrium		Moment equilibrium
	x	y	
Ordinary method of slices OMS (Fellenius 1927 et 1936)	No	No	Yes
Bishop's simplified (Bishop, 1955)	Yes	No	Yes
Janbu's simplified (Janbu, 1954 et 1973)	Yes	Yes	No
Corps of Engineers (1970)	Yes	Yes	No
Spencer's (Spencer, 1967 et 1973)	Yes	Yes	Yes
Bishop's rigorous (Bishop, 1955)	Yes	Yes	Yes
Janbu's generalized (Janbu, 1954 et 1973)	Yes	Yes	No
Sarma's (Sarma, 1973)	Yes	Ye	Yes
Morgenstern-Price (Morgenstern and Price, 1965)	Yes	Yes	Yes

1.3.12. Infinite Slope Procedure

In nature, one of the most known form of slope failures are the shallow failures where only the surficial layer (few meters) forms the sliding mass along a slip surface typically parallel to the face of the slope. This type of movements is usually triggered by precipitation occurred during the rainy seasons. For such a scenario, the failure mass can be assumed to extend infinitely along the sliding direction due to its very reduced length-to-depth ratio (Zhang et al., 2011b). As shown in the Figure 1-20, Abramson et al (2002) proposed the relationship D/L to distinguish between rotational and translational failures where when it is $<< 0.1$ in the case of translational failures. The FoS of slope in such a scenario can be determined using only one force equilibrium equation in the vertical direction (Qi and Vanapalli, 2015).

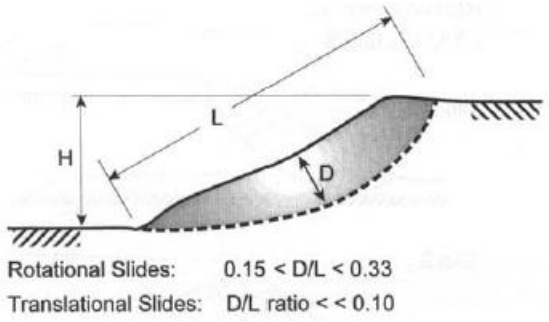

Figure 1-20. Aspects ration of failure mass

To carry out the force equilibrium, the one soil slice with a width of l in the sloping direction (Figure 1-21) is considered, the thickness in the direction perpendicular to the plane is unit, multiplying the surface of the slice by the unit weight γ gives the weight of this soil slice as follow:

$$W = \gamma l Z \cos\beta \qquad \text{Equation 27}$$

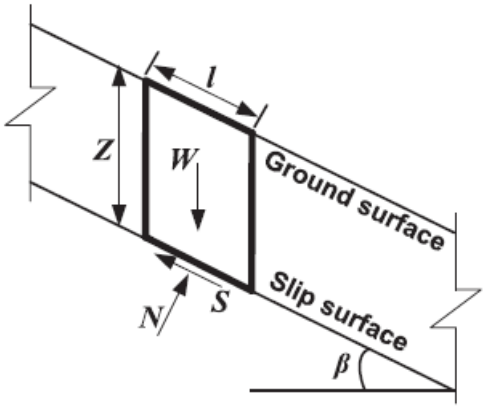

Figure 1-21. Force acting on a slice (Infinite slope formulation)

The normal and shear components of the force vector acting on the slip surface are obtained as follows:

$$N = \gamma l Z \cos^2 \beta \quad \text{Equation 28}$$

$$S = \gamma l Z \cos \beta \sin \beta \quad \text{Equation 29}$$

Therefore, the normal and shear stresses on the slip surface for an infinite slope can be readily obtained by dividing N and S by the area of the plane (i.e. ‘‘l’’), gives:

$$\sigma = \gamma Z \cos^2 \beta \quad \text{Equation 30}$$

$$\tau = \gamma Z \cos \beta \sin \beta \quad \text{Equation 31}$$

As shown in the Equation 25, the FoS is defined as the ratio of magnitude of shear strength to magnitude of mobilized shear stress on the slip surface as many other 2D and 3D traditional limit equilibrium methods. The FoS can be obtained by replacing the Equation 26, Equation 30 and Equation 31 in the Equation 25:

$$FoS = \frac{c}{\gamma Z \cos \beta \sin \beta} + \frac{\tan \varphi}{\tan \beta} \quad \text{Equation 32}$$

The two terms on the right hand side of Equation 32 represent the shear strength contribution due to cohesion and internal friction angle, respectively. As the surficial layer of slopes are generally unsaturated, the infinite slope procedure was developed to consider the unsaturated behavior of soils. Chapter two contains a detailed discussion on this subject.

1.3.13. FEM methods of slope stability SRM

One of the widely used method of calculating the FoS is the Strength Reduction Method (SRM) where the FoS is defined as the shear strength margin, which is also adopted in conventional limit equilibrium method and is widely accepted by engineers for practical applications (Shen et al., 2012). This method is integrated in geotechnical softwares (i.e., FLAC) to calculate the factor of safety of slopes.

First, for the Mohr-Coulomb failure criterion, the shear strength τ_f is given as presented in the Equation 25 The reduced shear strength τ_m along the failure surface is expressed as follows:

$$\tau_m = \tau_f / FoS \quad \text{Equation 33}$$

By substituting the Equation 25 in the Equation 33, the reduced shear strength formula becomes

$$\tau_m = c/FoS + \sigma_n \cdot tan\,\varphi/FoS \quad \text{Equation 34}$$

After a series of adjusting the value of FoS until the slope failure, where the ultimate FoS is the FoS. The bracketing and bisecting procedure (Dawson et al., 1999) is widely used to quickly obtain the reference value of FoS. As an example, the steps used in the FLAC software are explained by Shen et al. (2012).

First, the upper and lower brackets were established. The initial lower bracket was a trial value of FoS for which the solution converged. The initial upper bracket was a trial value of FoS for which the solution did not converge. Next, a middle value between the upper and lower brackets was tested. When the solution converged, the lower bracket was replaced by this new value. On the contrary, it replaced the upper bracket. The process was repeated until the difference between upper and lower brackets was less than 10^{-3}. In the present study the FLAC was used to assess the stability of Aine-Tine slope, a detailed investigation is presented in chapter two.

1.4. Pipeline systems

The term pipe is defined as a closed conduit with different forms of cross section, usually circular. It can be made of any appropriate material such as steel, plastic and concrete. The term **pipeline** refers to a long line of connected segments of pipe, with pumps, valves, control devices, and other equipment/facilities needed for operating the system. It is intended for transporting a fluid (liquid or gas), mixture of fluids, solids, fluid-solid mixture.

The term pipeline also implies a relatively large pipe spanning a long distance (Liu, 2004). Pipelines are the least understood and least appreciated modes of transport. Pipelines are poorly understood by the general public because they are most often buried underground and invisible. Despite the low degree of recognition by the public, pipelines are vitally important to the economic well-being and security of most nations. All modern nations rely almost exclusively on pipelines to transport the following commodities:

- Water from treatment plants to individual homes and other buildings
- Sewage from homes to treatment plants.
- Natural gas all the way from wells to the consumers who may be located more than a thousand miles away — be it a home, a factory, a school, or a power plant.
- Crude oil from oil fields to refineries.
- Refined petroleum products (gasoline, diesel, jet fuel, heating oil, etc.) from refineries to various cities over hundreds of miles.

1.4.1. Advantages of pipelines

In comparison with barges, rails and trucks, the transport of large quantities of fluid (liquid or gas) through pipelines is undoubtedly the most preferred mode of transport (Liu, 2004) for the following reasons:

- Economical
- Low energy consumption
- Friendly to environment
- Safe for humans
- Unaffected by weather
- High degree of automation
- High reliability
- Efficient land use
- High degree of security
- Less susceptible to theft

1.4.2. Components of pipelines:

Pipelines are complex systems of fluid transportation. They include many components such as pipes, fittings (valves, couplings, etc.), inlet and outlet structures, pumps (for liquid) or compressors (for gas), and auxiliary equipment (flowmeters, cathodic protection systems, and automatic control systems including computers and programmable logic controllers) (Liu, 2004).

1.4.3. Types of pipelines

Different applications or operating conditions call for the use of different types of pipes for pipeline projects, consequently, pipelines can be categorized in many different ways. For example, depending on the commodity transported, there are water pipelines, sewer, natural-gas pipelines, oil pipelines (for crude oil), product pipelines (for refined petroleum products). Considering the material of construction of pipeline, two broad classifications are used: metallic and nonmetallic pipes. The discussion below is taken from the pipeline engineering book of Liu (2004).

1.4.3.1. Metallic tube

Most metallic pipes are stronger and harder to break, but they are more conductive to heat and electricity and less corrosive-resistant than nonmetallic pipes.

a) **Ordinary Steel Pipe**: Ordinary steel pipes are made of wrought (carbon) steel. They may be either seamless or seamed (welded).
b) **Corrugated Steel Pipe:** Corrugated steel pipes are thin-wall, large-diameter pipes made of galvanized steel sheets having either helical or annular corrugations. Due to its low cost, the corrugated steel pipe is used extensively in sewer and drainage systems in the USA.

c) **Cast-Iron Pipe:** There are two types of cast-iron pipe: the ordinary or gray cast-iron pipe, and the ductile-iron pipe. The ordinary cast-iron pipe is made of iron containing 3 to 4% of carbon in the form of graphite flakes.

d) **Ductile-Iron Pipe:** The ductile-iron pipe is made of iron containing approximately 3.5% of carbon in spheroidal or nodular form, and a magnesium alloy. It is rather ductile, and does not rupture easily. It combines the advantages of the gray cast-iron pipe, including corrosion-resistance and long life, with the advantage of steel pipe – ductility.

e) **Stainless steel pipes:** They are made of steel that contains chrome-nickel alloys, and they are corrosion resistant. However, due to its high price, stainless steel pipe is used only in special applications such as when the fluid or environment is rather corrosive, or when no rusting of pipe can be tolerated such as in pharmaceutical or food industries.

f) **Aluminum Pipe:** They are corrosion resistant and are used in certain food plants and chemical plants

g) **Copper pipe:** Copper is corrosion-resistant but expensive. It is used only for small pipes such as those used in plumbing.

1.4.3.2. Nonmetallic pipes

Nonmetallic pipes may not be as strong as metallic pipes structurally, they may be lighter in weight, more economical, or may have certain other advantages such as being more corrosion resistant.

a) **Concrete Pipe**:

b) **Plastic pipes**: Three types of plastic pipes used commonly are PVC (polyvinyl chloride), PE (polyethylene), and PP (polypropylene). They are used for water, wastewater, natural gas, and certain other fluids that do not dissolve or chemically interact with the plastic material. Plastic pipes are low cost, lightweight, easy to cut and join, and corrosion resistant.

c) **Clay (ceramic) pipe**: Vitrified clay pipes ("clay pipes" for short) are used for sewers and drain tiles. Their advantages include low cost and high corrosion resistance.

d) Graphite and Carbon Pipes: They are very brittle, and are used only in special applications involving very high temperature.

e) Asbestos Cement Pipe (pipes made of cement mixed with asbestos fiber): In the past, they were widely used for sewers and water lines. Nowadays, they are no longer used because inhaling asbestos has proved to cause lung cancer.

f) Rubber and Elastomer Piping: Natural rubber and synthetic rubbers (elastomers) are used for making flexible hoses. They are needed for small-scale, special applications, such as gardening and hydraulic machineries.

g) Glass Pipe: The disadvantages of glass pipes are that they are extremely brittle, difficult to tap or handle, and expensive. The advantages are that they are inert to corrosive fluids, are clean, and can withstand relatively high temperature. They are

used mainly in food processing plants and pharmaceutical plants for their cleanliness, and in chemical plants for their ability to handle corrosive fluids such as strong acids.

1.4.4. Connections (Joints)

The classification of the pipelines considering the method of assembling of pipelines is summarized in Table 1-7.

Table 1-7. Pipeline classification considering the ways of assembling

Type of pipeline	Description
Segmented pipeline	Segmented pipeline has joints possessing lower strength and stiffness relative to the pipe barrel. For example, cast iron pipes with caulked or rubber gasket joints, ductile iron pipes with rubber gasket joints, concrete or asbestos pipes with mechanical joints, etc., are treated as segmented pipelines. The joints of the segmented pipes are generally referred to as unrestrained joints.
Continuous Pipeline	Continuous pipeline has joints possessing higher strength and stiffness relative to the pipe barrel. For example, a steel pipeline with welded (butt, single lap or double lap welded) joints is treated as continuous pipeline. The joints of the continuous pipelines are often referred to as restrained joint.

Pipes can be joined (connected) in several ways, as follows:

a) **Bonded (welded) joints:** They include welding for steel pipe, brazing or soldering for brass, copper and lead pipes, and fusing of plastic pipes.
b) **Threaded joints**: Used for connecting threaded pipe sections together, or connecting a threaded pipe to a threaded coupling or fitting.
c) **Flanges**: Flanges are the most common way to provide a strong joint without permanently joining the pipe sections together as done in welding. They are used extensively for steel pipes at both the inlet and the outlet of pumps, valves, flowmeters, and other fittings. Use of flanges allows such devices be easily installed in the pipeline and easily disconnected from the pipe.
d) **Mechanical joints**: Various mechanical connectors exist for ease in assembly/disassembly.
e) **Bell-and-spigot joints**: See Figure 1-22 for those used in pressure concrete pipes. Other pipes, including glass pipes and plastic pipes, also use bell-and-spigot joints.

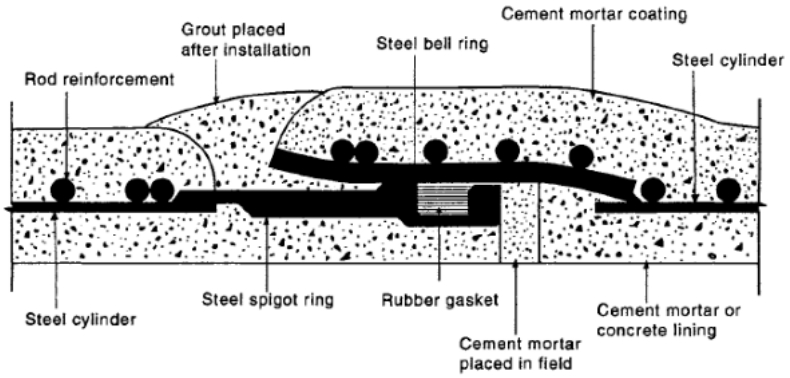

Figure 1-22. Bell-and-spigot joint used in Pretension concrete cylinder pipe

f) **Push-on joints**: Joints that can be connected together simply by pushing two pipe sections (segments) against each other. Likewise, the sections can be disconnected simply by pulling them apart.

In the literature, one of the adopted ways to classify pipelines is the **rigidity** which depends on the material stiffness, which is a function of its modulus of elasticity and section dimensions, the pipelines can be subdivided into two groups which are as follow:

- Rigid.
- Flexible.

Al-Khazaali et al. (2018) used two different values of modulus of elasticity (20 and 2 GPa) to simulate rigid and flexible pipes, respectively. While many researchers used different values of the modulus of elasticity such as 2 GPa (Han et al., 2016), 20 GPa (Potts and Zdravković, 2001) and 200 GPa (Watkins and Anderson, 2000).

1.4.5. Pipeline loadings

Pipelines are usually designed to be buried at a certain depth which is approximately equal to 2 times of the diameter of the pipe which is in accordance with the pipeline engineering practice (Mohitpour et al., 2007). A buried pipeline is typically subjected to a variety of external loads which are mainly due to differential ground displacements (Ng, 1994), which occur during its service. These displacements can be caused by many sources as listed below:

- Adjacent deep excavation
- Trenching and construction works
- Soil Swelling / Shrinking of embedding soil
- Frost Heave
- Traffic loading
- Landslides or unstable grounds
- Earthquake and faults movements of the pipeline.

Considering the 2D cross section, these loads exert shear and normal stresses on the pipeline ring that induce internal forces (i.e., internal axial, F_A, and shear, F_S, force and bending moment, M_B (see Figure 1-23), and deform the pipelines.

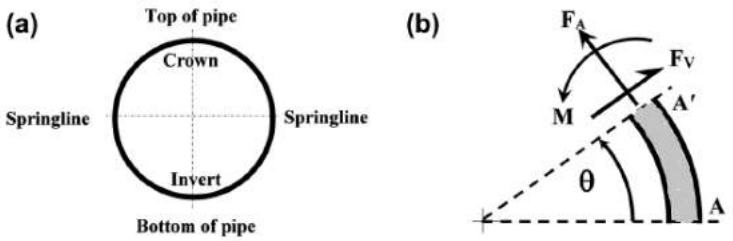

Figure 1-23 Pipeline hoop: (a) terminology; (b) ring internal forces.

The water mains performance are typically expressed in terms of the frequency of breaks per kilometers per years (5breaks/100km/1years is high frequency) (Rajani et al., 1996). Rajani et al. (1996) confirmed that water main failures is influenced by climate change.

1.4.6. Behavior of buried pipelines

Timoshenko and Goodier (1968) and (1970) were among the first who studied the behaviour of pipelines in their books. The rigidity is one of the key parameters of pipeline design. Considering the rigidity, there are two different types of pipelines: namely, rigid pipes (concrete, heavy walled cast iron pipes) and flexible pipes (polyvinyl chloride, polyethylene, and steel pipes) (Moser and Folkman, 2008). There are fundamental differences between the behaviors of both these types of pipelines which are summarized in Table 1-8 which is established by considering two different limit states for pipeline systems that are adopted by many standards and design codes:

Table 1-8. Limit states of pipeline systems

Limit state	Specifications
Ultimate limit state (ULS)	This limit takes into account burst or collapse of pipeline systems leading to safety hazards, which include rupture, yielding caused by primary loads, buckling resulting in collapse or rupture, and fatigue
Serviceability limit state (SLS)	It relates to design and service requirements (i.e., restrict normal operation or affect durability) of pipeline systems without resulting in yielding caused by secondary loads, and buckling not resulting in collapse.

The differences between the behavior of rigid and flexible pipes was highlighted for the first time by Marston and Anderson (1913). ***Zhao et al. (1998)*** reported that the rigid pipelines are designed and installed to resist the applied loads while in the case of flexible pipelines, they carry only a small portion of the applied loads and the major portion of the loads will be carried by the neighboring soil of the pipe. As an example to understand the difference between the behavior of rigid and flexible pipeline, the Figure 1-24 shows the deformation induced in the soil cover or backfill located above and around the ring of the pipeline. In the case of flexible pipelines, the backfill settles and a depression would appear due to pipe deformation especially in the vertical direction, while a hump or soil crack may be seen above an undeformed rigid pipelines.

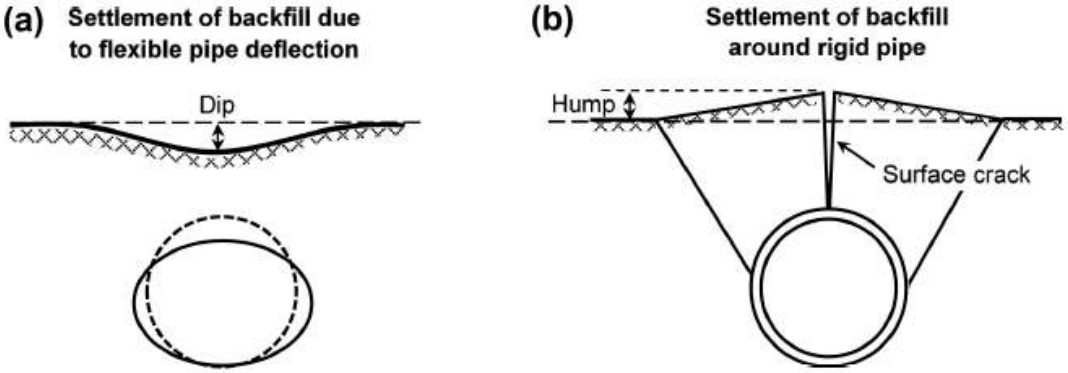

Figure 1-24. Backfill deformation: (a) flexible pipe; (b) rigid pipe (Watkins and Anderson, 2000)

Table 1-9, established by Al-Khazaali et al . (2018), summarizes some key limit state requirements derived from several specifications, standards, and design codes for rigid and flexible pipes.

- The American Petroleum Institute (API)
- International Organization for Standardization (ISO)
- American Standards for Testing Methods (ASTM)
- British Standards Institution (BS)
- Ontario Provincial Standard Specification (OPSS)
- Det Norske Veritas Offshore Standards (DNV).

Table 1-9. Key specifications for rigid and flexible pipes (Al-Khazaali et al., 2018).

Pipe type	Standards specifications, and design codes	Specification and description
Flexible	• API-17J • ISO-13628-2 • API-17K	Flexible pipe body is composed of a composite of layered materials that form a pressure-containing conduit and pipe structure allows large deflection without a significant increase in bending stress. Flexible pipes can be subdivided into: • Unbounded flexible pipes: maximum allowable bending strain for polyethylene (PE) and polyamide (PA) is 7.7%; for polyvinylidene fluoride (PVDF) it is 7% in static applications and for storage in dynamic applications, and 3.5% for operation in dynamic applications. For other polymer materials, allowable strain will be as specified by manufacturer. Refer to Table 6 in API 17 J and ISO 13628-2. • Bonded flexible pipes, maximum allowable strain for elastomer material is 50% of design maximum strain for aged material. Refer to Table 7 in API 17 K.

	• API 17B • ISO 13628-11	This recommendation practice defines flexible pipe as pipe with low bending stiffness and high axial tensile stiffness. These requirements can be achieved by using a composite pipe wall construction of helical armoring layers and polymer sealing. However, flexible pipes are designed to serve particular requirements for different projects and there are no specific or standard products. • Flexible pipe should be designed to prevent failure due to the combined effect of internal pressure, external pressure, torsional forces, axial forces, and bending. • Flexible pipes have internal diameters usually ranging from 0.05 to 0.5 m (2 to 20 in.). However, in some cases internal diameter can reach up to 0.914 m (36 in.) for low-pressure bonded flexible pipes such as oil suction and discharge hoses.
	• ASTM F1668-08	Flexible pipes that are typically designed to rely on stiffness of soil surrounding them for support and transmit load on pipe to soil at the side, such as thermoplastic and fiberglass. • Deflection of buried pipe may be expressed in general terms as “pipe deflection = load on pipe / (pipe stiffness + soil stiffness)”. • Maximum deflection of buried flexible pipe is derived from both structural consideration including pipe cracking, yielding, strength, strain, and local deflection, and practical consideration including such factors as flow requirements, clearance for inspection and cleaning, and maintenance of joint seals.
	• MTO OPSS 401 • MTO OPSS 421	Flexible pipe diameter or span should not vary from manufactured dimensions by more than 5% during cover and backfill placing operations.
Rigid	• BSI EN-1295-1	**.** Pipe types can be specified based on relative pipe and surrounding soil stiffness that is useful in evaluation of backfill load, and type of material from which pipe is made. For example, pipes that are fabricated of material fractured under small deformations are referred to as rigid pipes.
	• MTO OPSS 401	**.** For rigid pipes, 2% deflection is maximum deflection that rigid pipelines can sustain without cracks while flexible pipelines can deflect more than 2% safely.

• DNV DNV-OS-F101 • DNV DNV-RP-F116	. Rigid pipes can be fabricated of carbon steel, stainless steel, clad-pipe. . Maximum accumulated nominal plastic strains should not exceed 2%. . Yield stress, YS, of rigid steel pipe is defined as stress at which total strain is 0.5% (Figure 1-25). . Tensile strains should not increase 0.4%.

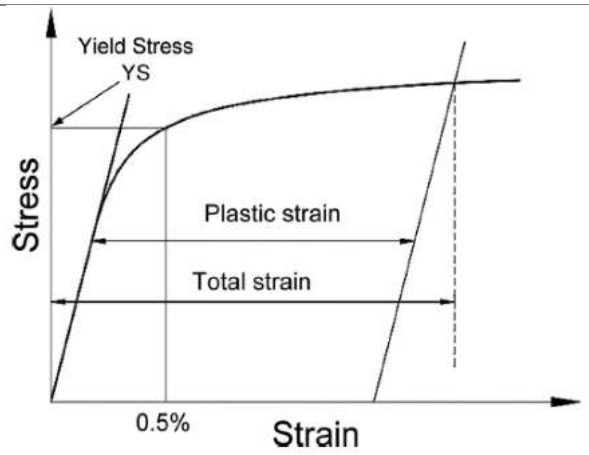

Figure 1-25. Stress–strain curve for steel

1.4.6.1. Pipelines performances

Al-Khazaali (2019) stated that the stresses applied on the wall of rigid pipes due to external and internal loads combination is a critical factor that controls the rigid pipeline behavior where the plastic deformation that occur in this type of pipeline are very small and can be neglected. Moser (2001) reported that the stiffness of **flexible** pipeline is more crucial while studying the behavior of such class of pipelines. The behavior of the pipeline is generally linear elastic and the material characteristics which are the Young's modulus and the Poisson's ratio of steel, aluminum and concrete are generally constant in tension and compression loadings as reported by (Leonards and Roy, 1976). In the same work, they stated that the concrete pipelines develop cracks before the collapse unlike the steel pipelines which yield (see Figure 1-28).

During the period of service of pipelines, the cross section of these structures can be subjected to many scenario of loadings which are summarized by Bickel (2004) which describes the possible deformations that can occur on unconfined (non-buried) (see Figure 1-26) and partially confined pipelines (see Figure 1-27).

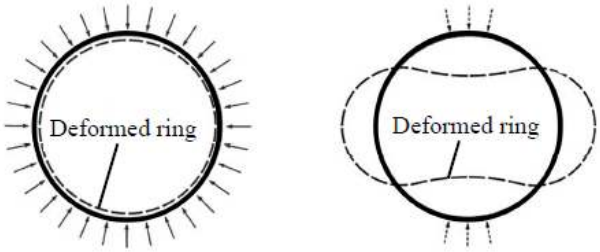

Figure 1-26. Pipeline deformation under (a) uniform radial loads (b) invert and crown punctual loads (in the case of unconfined pipeline)

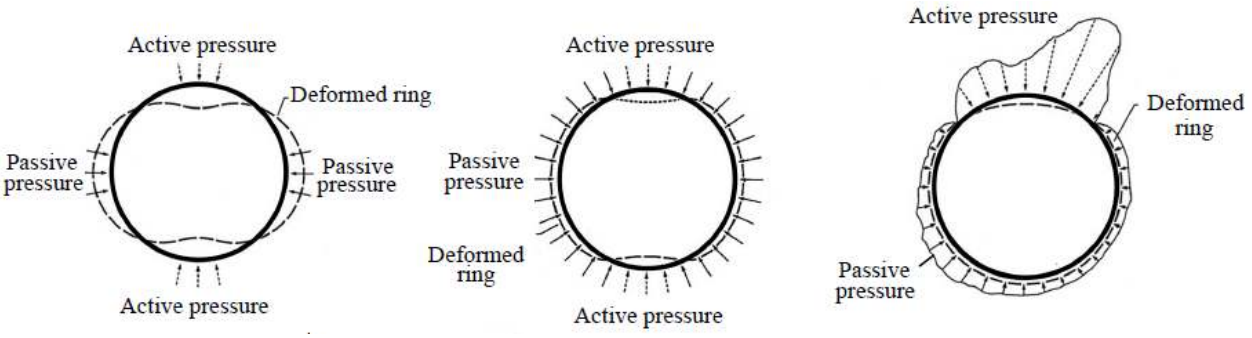

Figure 1-27. Pipeline deformation under (a) uniform radial loads (b) invert and crown punctual loads (in the case of partially confined pipeline)

In the same direction, Watkins and Anderson (2000) defined four main possible performance limits with respect to the flexibility of the ring of the pipeline and the soils consistency as shown in Figure 1-28. The resulted deformation along the pipeline perimeter are summarized in Table 1-10.

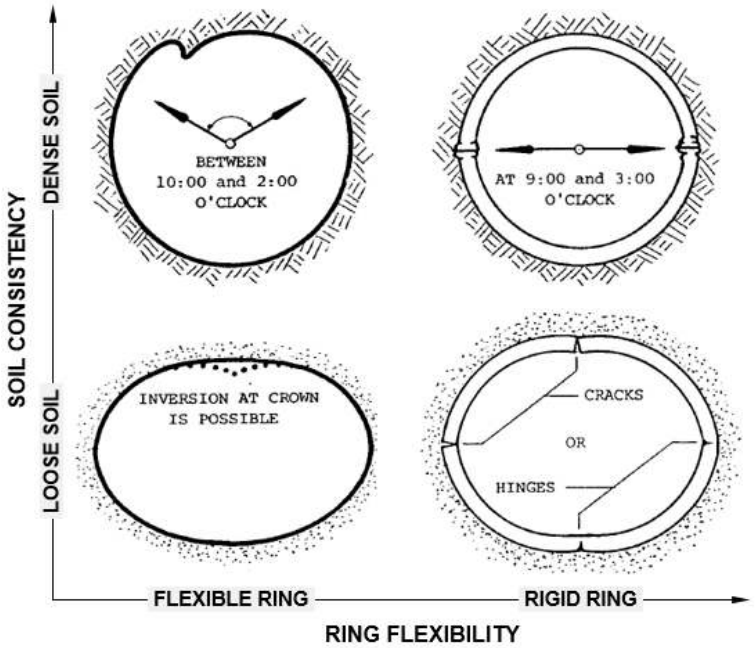

Figure 1-28. Typical examples of performance limits for the pipe and their location

Buried pipeline are usually verified considering two performance limits: yield strength, and ring deflection where, in general, yield strength applies to rigid pipes such as concrete pipes, and ring deflection applies to flexible pipes.

Table 1-10. Description of the resulted deformations

		Pipeline Rigidity	
		Flexible	Rigid
Soil Consistency	Dense	Wall buckling	Wall crushing
	Loose	Ring deflection	Wall cracking or plastic hinging

1.4.6.2. Ovalization of pipelines

In landslide zones, lateral spread as well as fault crossing zones, high lateral soil loading can be produced and consequently they will easily lead to a buried pipeline ovalization where the degree of ovalization is a function of the pipe wall thickness and stiffness which are both the components of the rigidity. The ovalization depends also on the location from where the lateral movement have occurred. At varying locations at and away from the offset (-25, -10, 0, 10, 25 feet) Figure 1-29 shows the effect of high lateral loads due to faulting on the variation of cross sectional distortions occurred on the ring of a 66-inch diameter welded steel pipe. The same observations have been obtained by Vazouras et al. (2010) when studying the effect of strike fault on two different typical grades of pipeline (API 5L X65 steel and (b)API 5L X80 steel) where it was found that the ovalization increases with the magnitude of the fault movement as shown in Figure 1-30 (d represents the faults displacement).

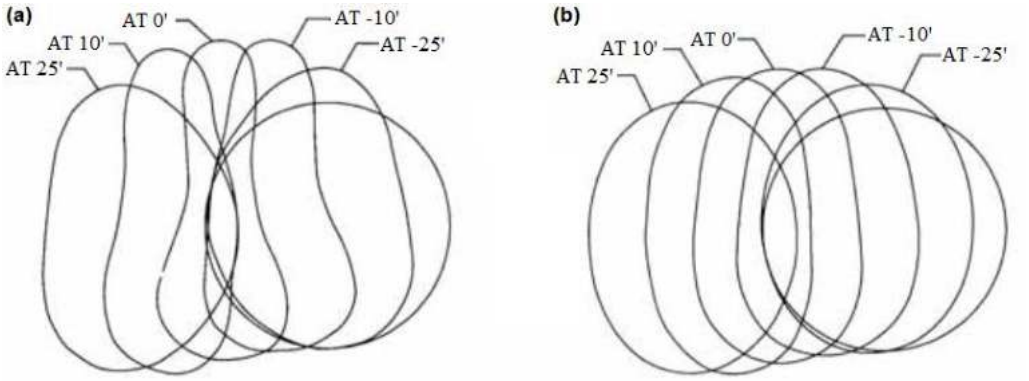

Figure 1-29. Steel pipe ovalization due to fault offset (foot) (a) 0.375-inch (b) 0.75-inch wall thickness (ALA, 2005)

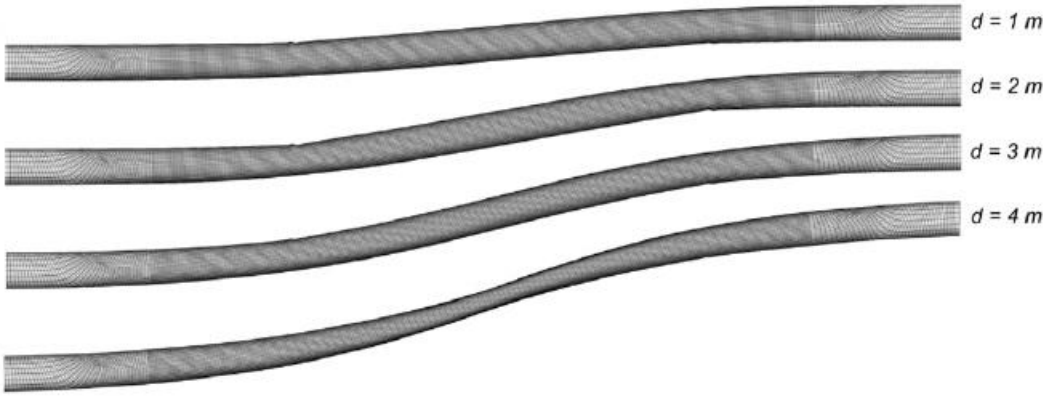

Figure 1-30. Deformed shape of a pipeline for fault displacement d=1-4 m (Vazouras et al., 2010)

As a serviceability limit state, the cross-sectional ovalization of the pipe is one of the relevant conditions that are taken into consideration when designing buried pipelines to keep their normal operations (Bouatia et al., 2020). The ovalization is limited by the design codes such as ALA (2005) where the designer or the owner of the pipeline systems (governments or societies) should limit this type of deformation. This condition can be expressed through the so-called flattering parameter f which can be written as follow:

$$f = \Delta D / D \qquad \text{Equation 35}$$

Where, ΔD is the maximum variation of the pipeline diameter and D is the pipeline diameter as seen in Figure 1-31. The ovalization is limited at 15% as suggested by Gresnigt (1986) and adopted by the Dutch specification NEN 3650 (2006).

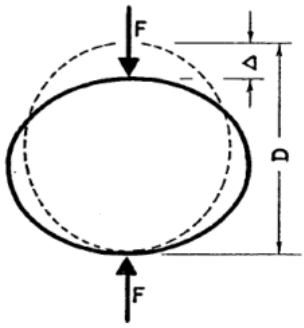

Figure 1-31. Deformation of pipeline ring under vertical concentrated loading

1.4.7. Soil pipeline interaction modelization

The modelization of soil-pipeline interaction in buried pipelines is a complex problem due the existence of two different materials (i.e., Soil, Pipe) with large different elastic characteristics (i.e., young's modulus, Poisson's ratio). The complexity increases due to the nonlinear behaviour of the soil. *Extensive full scale pipe loading experiments under controlled conditions and normal field conditions have been performed in the UK by British Gas, the Water Research Centre and by the Transport and Road Research Laboratory (Needham & Leach, 1987).* The use of the finite element analysis is increasing due the time consuming and the limitation of the controlled parameters during the laboratory testing. Two methods are widely used in the literature to model the soil-pipeline interaction using finite element methods:

- **Soil mesh finite element model**: The complicated nonlinearity of the system is modeled by dividing the soil-pipeline system into finite elements or zones with different geometries (i.e., line, triangle, cubes) and different model behaviour (i.e., elastic, elastoplastic).
- **Beam on Nonlinear Winkler Foundation (BNWF) model**: The soil is represented by independent springs lumped at discrete locations of the pipe. Due to its simplicity expressed under the mathematical convenience and ability to incorporate nonlinearity, this model is extensively used in practice where the soil surrounding the pipe body is simulated using nonlinear springs (ALA, 2005) (IITK-GSDMA, 2007).

As seen in the Figure 1-32 (b), the surrounding soil can be modelled using four types of springs representing the resistance components of the soils to the applied ground deformations as follows:

- Axial soil spring to represent soil resistance over the pipe surface along its length.
- Lateral soil spring to represent the lateral resistance of soil to the pipe movement.
- Vertical bearing spring used to represent the resistance of soil in the vertical direction at the bottom of the pipe.
- Vertical uplift spring to represent the vertical resistance of the soil at the top of the pipe.

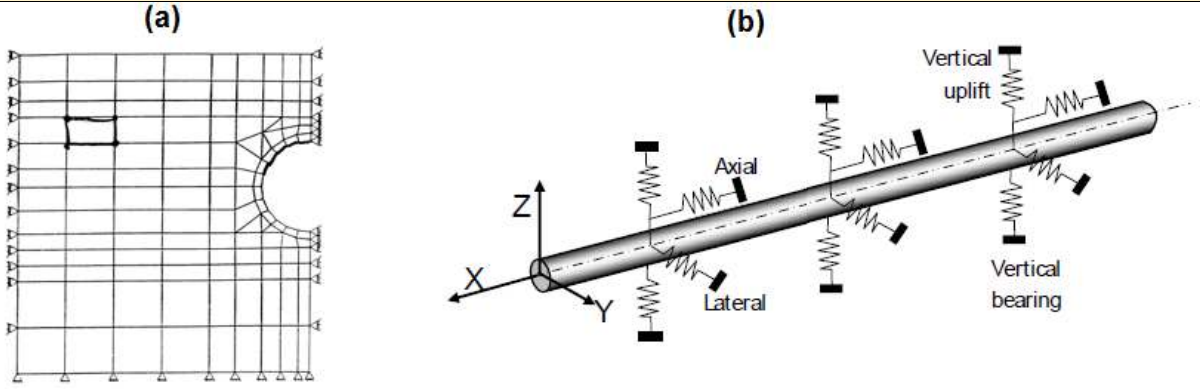

Figure 1-32. (a) Finite element model (b) BNFF model

1.4.7.1. Continuous pipelines

Figure 1-33 represent the schematic configuration of the BNWF model used to simulate continuous pipelines subjected to ground deformation in longitudinal and transverse direction.

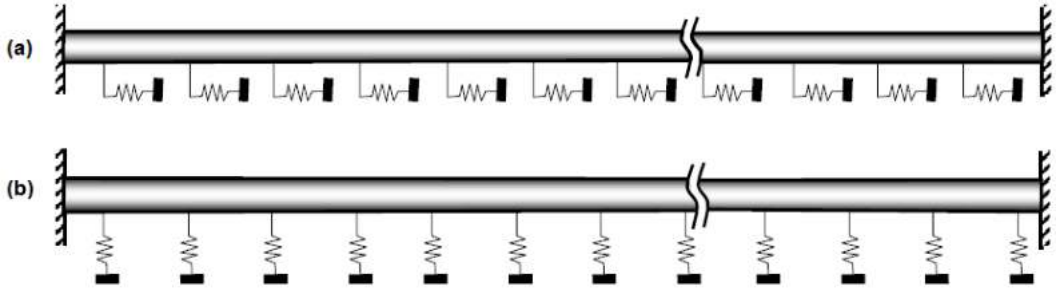

Figure 1-33. Continuous pipe-soil model for (a) longitudinal and (b) transverse ground deformation

Using the model presented in Figure 1-33. (b), A method for estimating the horizontal movement of a long shallow buried pipeline due to the nearby excavation and backfilling of a long deep trench parallel to the pipeline was proposed by Crofts at al. (1977). The research consists of analyzing an elastic model of the problem composed by a beam embedded in an elastic foundation which is locally displaced laterally (Figure 1-34.) and considering the effects of backfill stiffness and end restraint are examined.

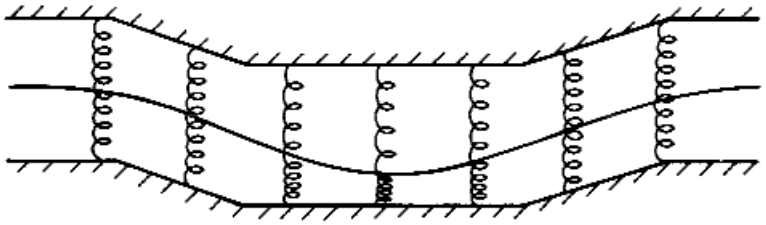

Figure 1-34. Model of beam embedded in an elastic foundation locally displaced laterally.

1.4.7.2. Segmented pipelines

Figure 1-35 represents the schematic configuration of the BNWF model used to simulate segmented pipelines subjected to ground deformation in longitudinal and transverse direction.

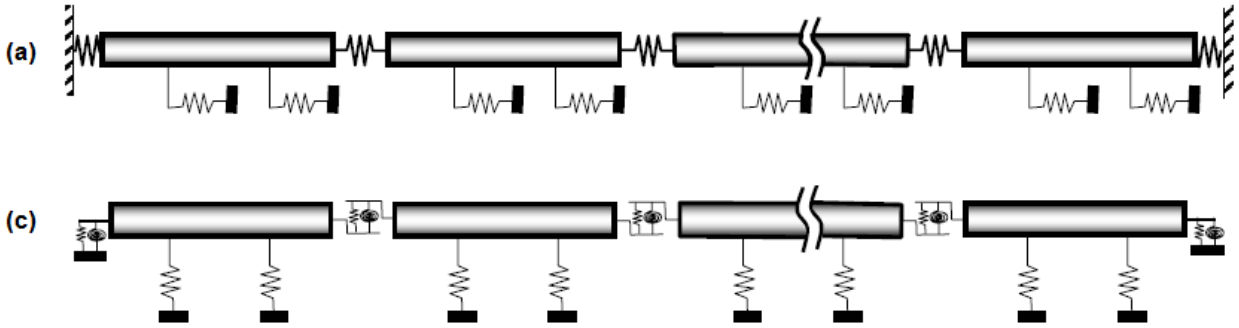

Figure 1-35. Segmented pipe-soil model for (a) longitudinal and (b) transverse ground deformation

1.4.8. Buried pipeline interaction with expansive soils

The saturation of unsaturated soils by filling the pores by the water consequently expressed as the increase of the water content induces two different types of deformation which can be upward in **expansive soils** and downwards in the case of **collapsible soils**. The focus of the present study is on the expansive soil where limited researches have been taken on the behavior of buried pipelines in expansive soils. Some of the undertaken research are summarized below with their main results. Expansive soils can severely damage structures constructed on, or within, them (Clark, 1971). By swelling more than by shrinking. Relatively long wet periods followed by long dry and warm periods are climatic conditions favorable to high volume changes in expansive soils (Gallage et al., 2012) (Clark, 1971). Dry climates having periodically high GWTs, and relatively dry soil conditions having a source of moisture, such as a water leak from the pipe or from other nearby utilities or sources, are also situations that can create problems in expansive soils (Clark, 1971).

1.4.8.1. Ng (1994)

Ng (1994) reported that the induced relative movement which follows shrink/swell movement are considered as important factors that can generate external loadings applied on buried pipeline ring. Expansive soils can severely damage structures constructed on, or within, them (Clark, 1971). In addition, these types of soil are frequently corrosive. Fortunately, it's not the case in the Aine-Tine site as confirmed by the LNHC Batna investigation reports (2016) (2017).

The increase in moisture content results in an increase in soil loading on the pipeline (Robert and Soga, 2013). In this direction, Robert and Soga (2013) highlighted the importance of considering the unsaturated behavior while studying pipeline problems. Gould et al. (2009) reported that the highest rate of pipeline failures occurred between the months: December to May which corresponds to the rainy season in large areas around the world.

During the rainy seasons (i.e., in Algeria=Winter), large amounts of water may enter in the soil and result in excessive soil heave (Saadeldin et al., 2015) (Qi and Vanapalli, 2016). On the contrary, a decrease of degree of saturation during the dry seasons may result in the settlement of soils, as illustrated in Figure 1-36.

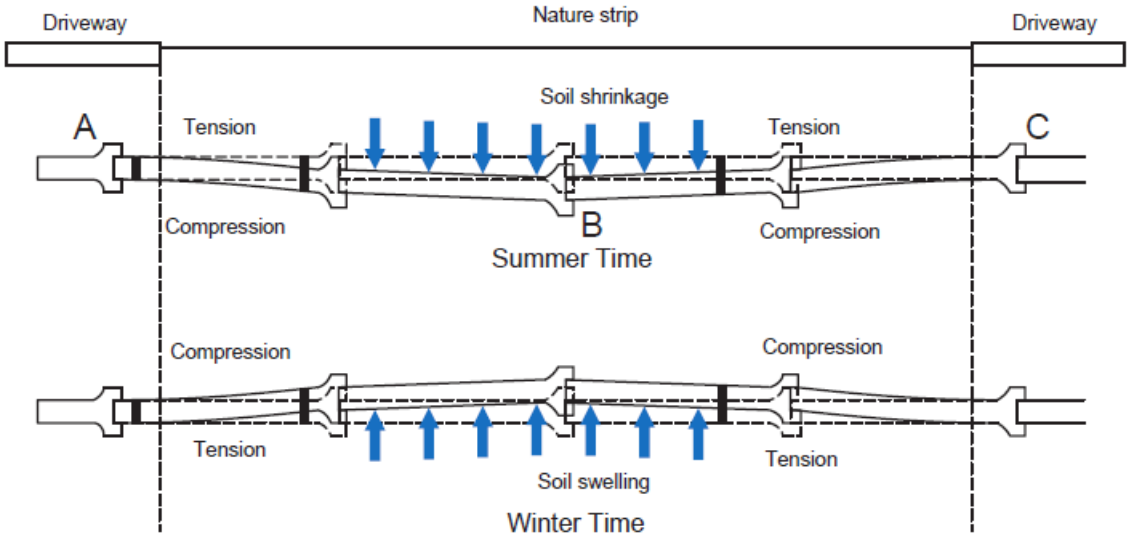

Figure 1-36. Schematic of pipe–soil movement due to moisture change (Rajeev et al., 2012).

In addition to expansion, the fine grained soils are also sensitive to frost heave (i.e., silts and clays) as reported by many researchers (Taber, 1929) (Huang et al., 2004).

1.4.8.2. Rajeev and Kodikara (2011)

Rajeev and Kodikara (2011) studied longitudinally the behavior of buried pipelines subjected to swelling soil movement due to increase in soil suction where a consistent large-scale laboratory experiments have been undertaken on a plastic pipe. Using FLAC3D computer program, a three dimensional numerical model is developed to analyze the pipe response assuming that the pipe will behave as a linearly elastic material, while the soil is modelled using the Mohr–Coulomb failure criterion. The change of moisture content was applied from the base of the model to simulate the rise of the GWT by applying three increment of water level. From the study, reasonably good agreement between the experimental results and model predictions is reported and the developed model can be used to simulate swelling movement on buried pipeline.

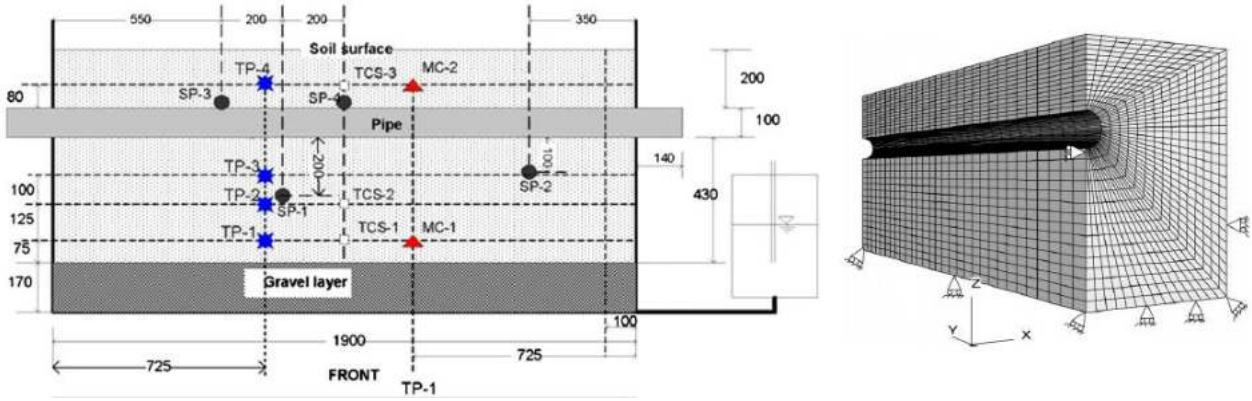

Figure 1-37. Experimental and numerical models (Rajeev and Kodikara, 2011)

1.4.8.3. Gallage et al., 2012

As the pipe asset ages, buried pipe failures or breaks have become a major concern to most water and gas utilities. Failures of these pipes can produce negative social, environmental and

economic impacts on the community due to the surrounding soil movement which closely related to seasonal climatic changes, and particularly to the moisture content of soil (Gallage et al., 2012). Gallage et al., (2012) continued the research started by Rajeev and Kodikara (2011) to deepen the investigations on the effect of density and the burial depth which were found to be proportional to the overburden pressure and the swelling pressure that control the swelling displacements.

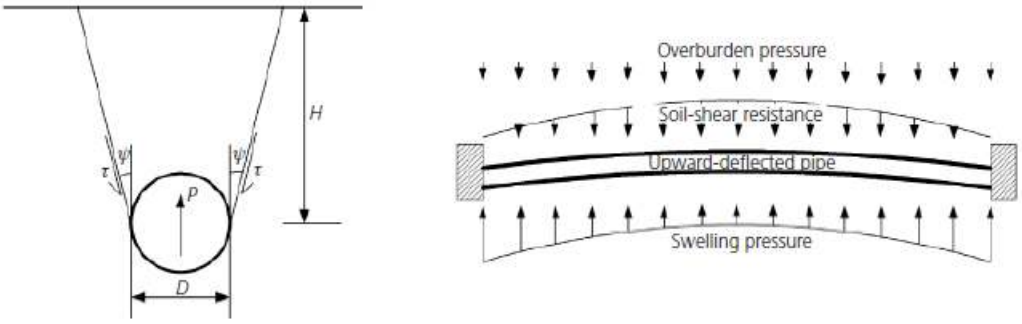

Figure 1-38. External stresses acting on deflected buried pipe (Gallage et al., 2012)

1.4.8.4. Huang et al. (2015)

In the purpose of developing and improving the design criteria for pipeline construction in arctic regions, where soils are subjected to high frost heave, Huang et al. (2015) conducted a full-scale experimental investigation on the effect of the frost heave on the 900 mm pipeline dimeter with 105 m length. The full-scale chilled gas pipeline experiment was conducted in Fairbanks, Alaska, USA. Including both freezing and thawing phases the monitoring data were collected from December 1999 to January 2005 of a one-third of the pipeline which was put in permafrost and the remaining was in non-permafrost which generated vertical movement caused by differential frost heave in the transition zone between frozen and unfrozen soil. It was found that the bending actions were the main factor for the circumferential and longitudinal strain distribution in the pipeline where the maximum tensile and maximum compressive strains along the pipeline were approximately located at the transition zone between the two types of soils.

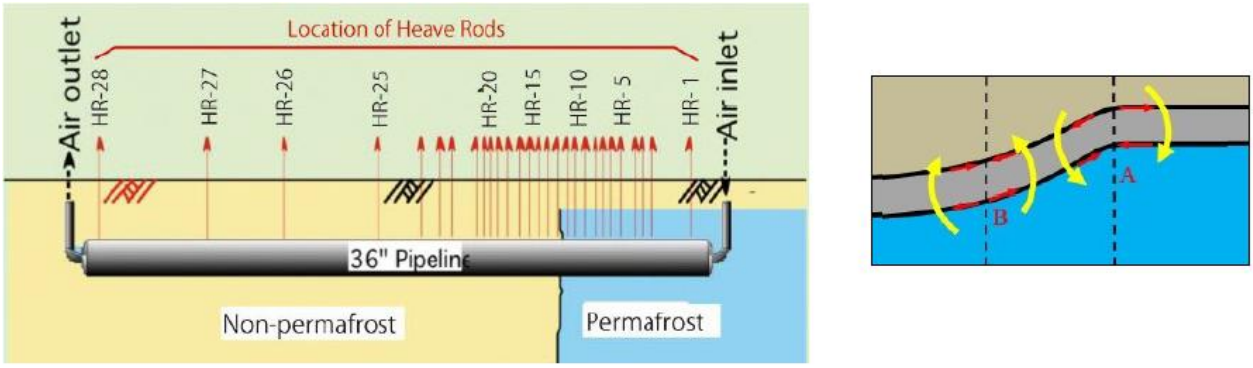

Figure 1-39. Large-scale experimental model (Huang et al., 2015)

1.4.8.5. Kouretzis et al. (2015)

Considering a straight and continuous pipeline whose route crosses an area of finite width where differential settlement or heave of the ground surface may develop, Kouretzis et al. (2015)

developed a simplified analytical method to estimate both the strains and internal forces which can be applied to HPDE, cast iron or concrete pipelines buried in expansive or collapsible soils.

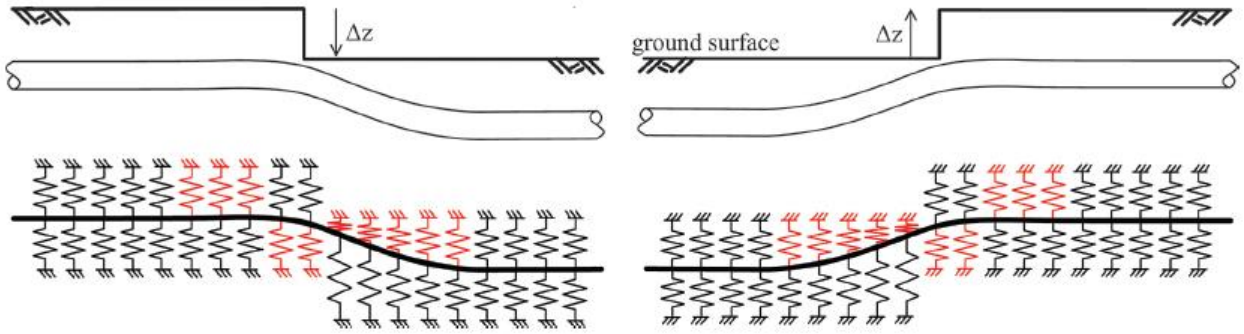

Figure 1-40. Beam spring model used by Kouretzis et al. (2015)

This method constitutes a high potential alternative to elaborate three-dimensional analyses using numerical solutions on the pipelines which cross geotechnical problematic areas and are susceptible to permanent ground surface settlement or heave.

1.4.8.6. Saadeldin et al. (2015)

Through a 2D numerical analysis to study the effect of the (1) reduction of soil suction and (2) the burial depth parameters on the upward displacement of pipeline buried in unsaturated soils, Saadeldin et al. (2015) concluded that the suction has significant influence on the magnitude of vertical displacement at different depths. A pipeline of 6.5 m length and 0.15 m diameter was considered to be buried in Regina expansive clay which supposed to have an initial suction of 2000 kPa and exposed to a rainfall precipitation in order to increase the suction to different values (i.e. 1000, 500, 180, and 38 kPa). The main conclusions of the present study are as follow:

a) Significant increase in upward displacement of the pipeline is associated with reduction of soil suction for different depths of burial.
b) The vertical displacement of the pipeline is highly influenced by burial depth.

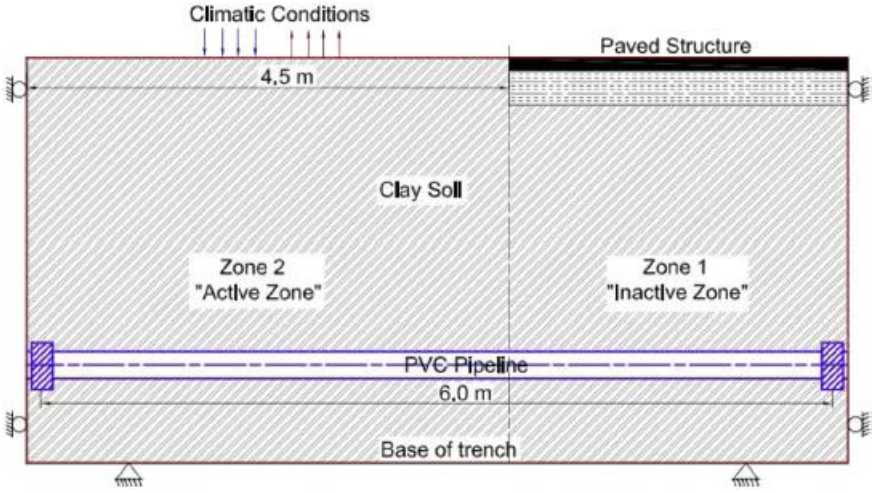

Figure 1-41. Numerical model (Saadeldin et al., 2015)

1.4.9. Buried pipeline subjected to Permanent Ground Deformations (PGD)

Permanent Ground deformations PGD can be seen in the nature as many form such as landslides, soil liquefaction, shrink/swell movements as well as faults and they can be triggered by many possible factors such as earthquakes and precipitations and high temperature gradients. They are seen as large mass movement of soil over an extended area. These can be very damaging to buried pipes as they are dragged along within the soil mass and experience applied relative deformations. The pipe response depends on its orientation relative to the direction of the soil mass permanent ground displacement (PGD), as highlighted in Figure 1-42 which shows typical configurations of PGD due to landslide.

Transverse PGD: The pipe run oriented perpendicular to the soil movement doing an angle 90° with the direction of the movement, where it is mainly subjected to bending at the left and right limits of the movable mass (Figure 1-42 (a)). This was confirmed by Feng et al. (2015) who reported that the developed stresses due to sliding movements along the body of pipeline are concentrated in both sides of the landslides and its distribution can be described using an exponential equation.

Longitudinal PGD: The pipe run oriented parallel to the soil movement doing an angle 0° with the direction of the movement, in this configuration the pipeline is mainly subjected to tension and compression efforts which correspond to the back and the front locations of the moving mass, respectively (Figure 1-42 (b)).

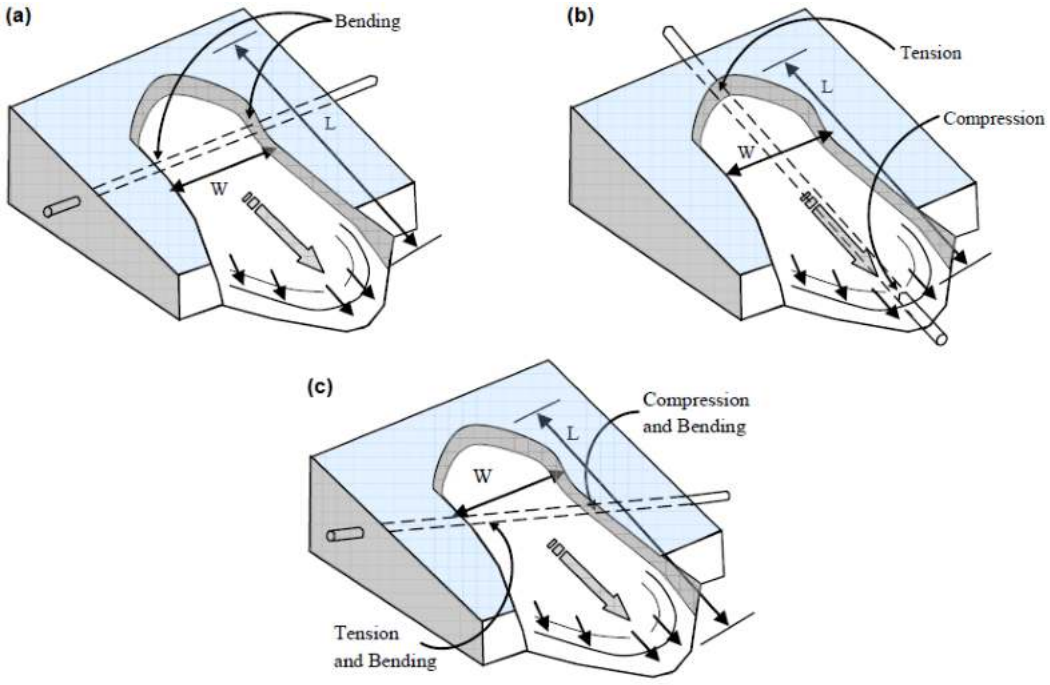

Figure 1-42. Principal PGDs on pipelines considering the orientation (ALA, 2005) (IITK-GSDMA, 2007)

Both the longitudinal and transverse directions: More complicated configuration that can face engineers is seen in the Figure 1-42 (c) where the pipeline crosses the moving mass with an angle different than 0° or 90°. The design codes ALA (2005) and IITK GSDMA (2007) recommend the FEM method to study design pipelines. The FEM can study important pipelines that are

subjected to large PGDs such as the case of landslides or surface fault offset) and considering any orientation. The following section are prepared based on the information provided by one of the most used guidelines to design the pipelines subjected to permanent ground deformations PGD due to but not limited to seismic events, landslides and faults.

1.4.9.1. Rajani and Morgenstern (1993)

The pipeline could undergo substantial straining, leading to wrinkling buckles, especially when the pipeline crosses a transition zone between two soils with different frost susceptibilities or between unfrozen and already frozen soils (Rajani and Morgenstern, 1993). Using the load-displacement curves developed for rigid anchors, Rajani and Morgenstern (1993) developed an approximate 3D solution to examine the uplift behavior of a shallow pipeline embedded in an elastoplastic medium. The comparison results of the developed solution with 3d finite element analysis confirms that it can be a practical alternative for analyzing the uplift behavior of shallow pipelines as well as for the laterally loaded piles. The developed model is based on the famous equation that relates the deformation of the beam $y''(x)$ to the flexural moment $M(x)$ as follow:

$$EIy''(x) = -M(x) \qquad \text{Equation 36}$$

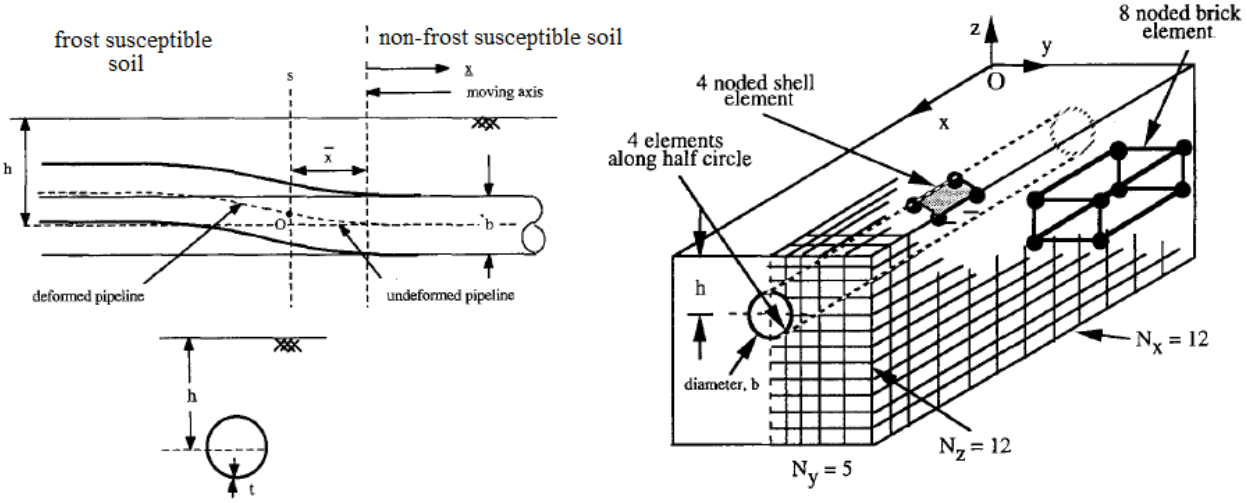

Figure 1-43. Scheme and numerical models (Rajani and Morgenstern, 1993)

1.4.9.1. O'Rourke et al. (2008)

Large scale tests in 2D and 3D were carried out by O'Rourke et al. (2008) to describe the large-scale split-box facilities for testing pipeline response to earthquake-induced ground rupture of the George E. Brown, Jr. Network for Earthquake Engineering Simulation (NEES). A log spiral model was developed to account analytically for maximum horizontal pipe force due to relative soil-pipe displacement as a function of depth to pipe diameter ratio and peak direct shear soil friction angle. Excellent agreement is shown between the log spiral predictions and full-scale test data when maximum horizontal force is expressed in dimensionless terms as a function of depth to pipe diameter ratio and peak direct shear angle of soil friction. Moreover, the ground rupture surface predicted by the log spiral model compares favorably with the location of concentrated soil

strain during large-scale 2-D tests. For more details, the article presents some very interesting details about the different stages of the tests.

1.4.9.1. Palmer et al. (1999)

Pipelines are linear structures constructed to carry fluids for long distances and they may cross steep terrain where for non-buried pipelines the friction between the ground surface soil and the pipelines body is not enough to resist the slipping force from the pipeline weight component along the slope direction (Palmer et al., 1999). Palmer et al. (1999) proposed a graphical method to assess the stability of pipes on an arbitrary slope which considers the effect of the temperature which increases the developed compressive forces along the pipeline (see Figure 1-45).

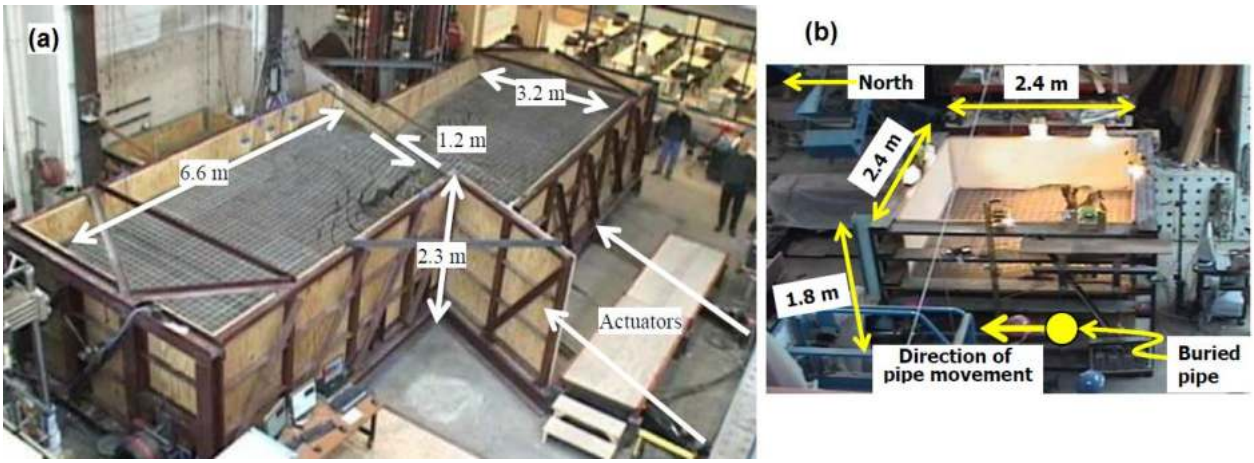

Figure 1-44. (a) 3D and (b) 2D Laboratory testing of pipeline at the Cornell University NEES

1.4.9.1. Rajani et al. (1996)

Water mains form an essential part of the life line systems of modern urban towns and cities (Rajani et al., 1996). An analytical soil-pipeline interaction model has been developed to provide the response of jointed water mains to changes in internal pressure and temperature developing a simplified Winkler model which accounts for axial and radial restraints as seen in Figure 1-46. The study results confirmed that the higher the diameter of pipeline the higher the maximum axial stresses. It was found also that the axial pipe-soil reaction modulus is very sensitive to the temperature and the soils type which need to be carefully taken into accounts. The study reported that for a ratio of modulus of elasticity between pipe and soil higher than 500 the pipe starts to not feel the radial restraints coming from the surrounding soils.

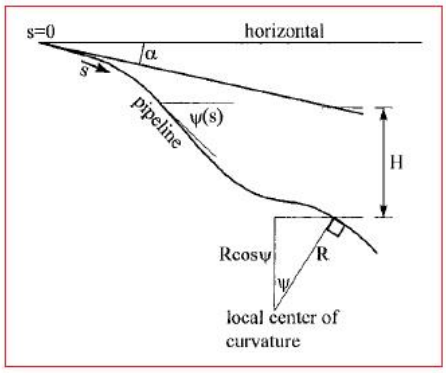

From the equilibrium of an element ds,

$$dP/ds = w \sin \psi - T \quad (1)$$

$$N = w \cos \psi - P d\psi/ds. \quad (2)$$

If the pipeline is on the point of sliding downhill,

$$T = +N\mu = +N \tan \alpha, \quad (3)$$

where μ is a coefficient of friction, equal to tan α where α is an angle of friction. If the pipeline is on the point of sliding uphill, the plus sign in (3) is replaced by a minus sign.

Substituting from (3) into (2) and (1),

$$dP/ds - P\mu d\psi/ds = w(\sin \psi - \mu \cos \psi). \quad (4)$$

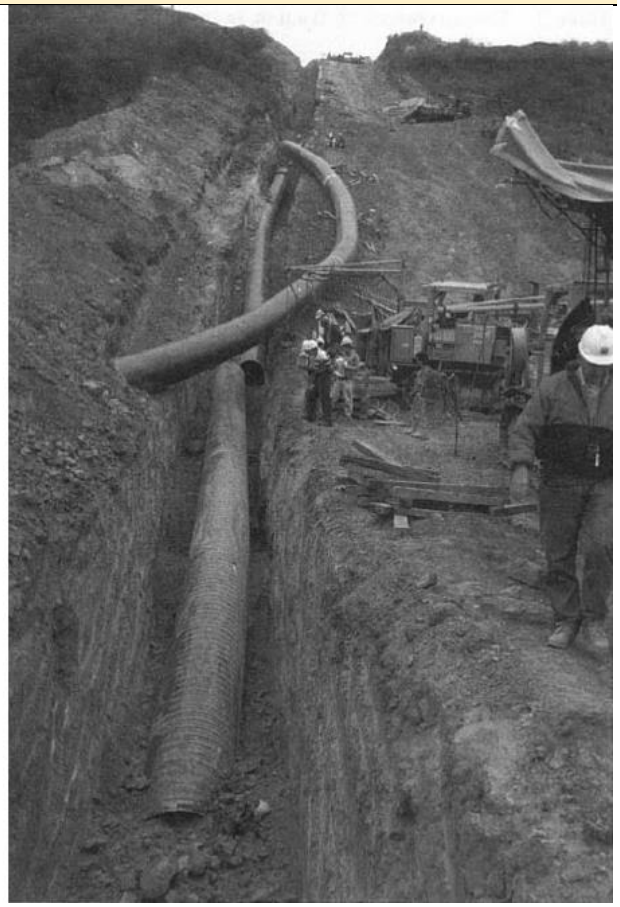

Figure 1-45. The 36-inch pipeline in Colombia subjected to sliding on a steep slope (Palmer et al., 1999)

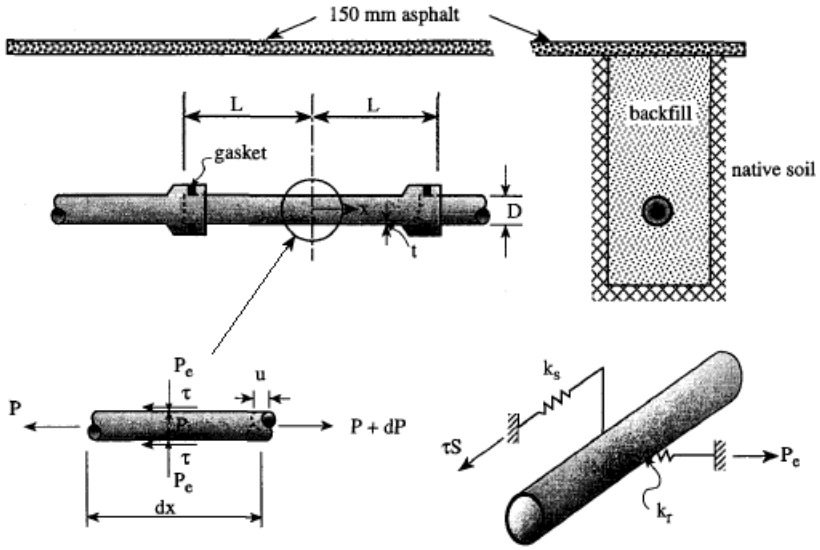

1.4.9.2.

Figure 1-46. Model used by Rajani et al. (1996)

1.4.9.3. Roy et al. (2016)

Using a 2D approach, Roy et al. (2016) simulated lateral pipeline–soil by performing a comprehensive parametric study performed to study the effect of mechanical parameters such as

the friction angle and the dilation angle of a dense sand on the mechanism of failure (Figure 1-47 (b)). The soil was simulated using the MC model.

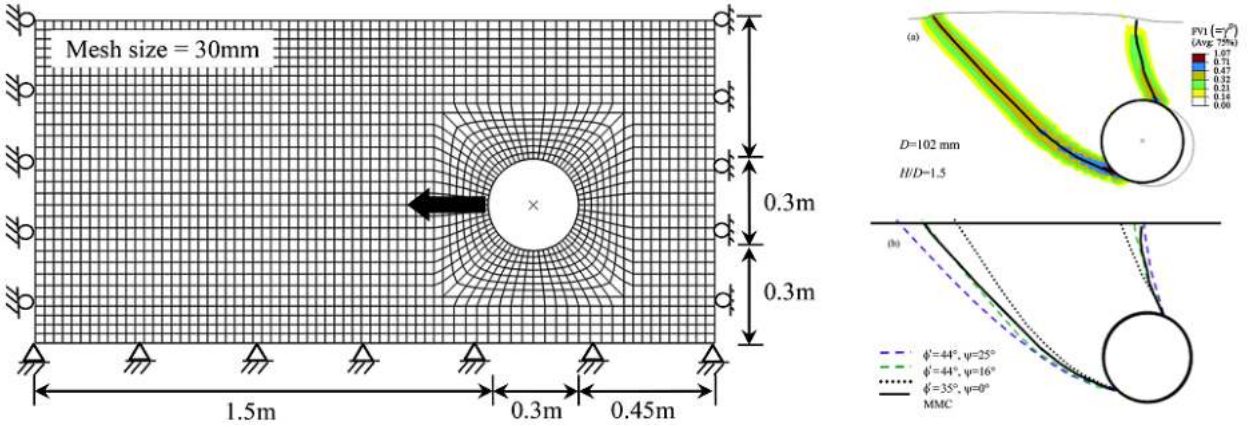

Figure 1-47. Finite element model (Roy et al., 2016)

1.4.9.1. Vazouras et al. (2010, 2012, 2015, 2017)

In 3D simulation, a group of research in Greece published a series of papers Vazouras et al. (2010) (2012) (2015) (2017) which addressed the mechanical behavior of buried steel pipes crossing active strike-slip tectonic faults (Figure 1-48). Several parameters were taken into consideration such as the soil type clay or sand (density, friction angle and cohesion), the pipeline grade (API 5L X65 and API 5L X80), the ratio D/t, the orientation of the faults or the angle between the pipeline and the fault (0° to 45°). The investigation is based on numerical simulation of the nonlinear response of the soil–pipeline system through finite elements, accounting for large strains and displacements, inelastic material behavior of the pipeline and the surrounding soil. The effects of internal pressure on pipeline performance are also investigated.

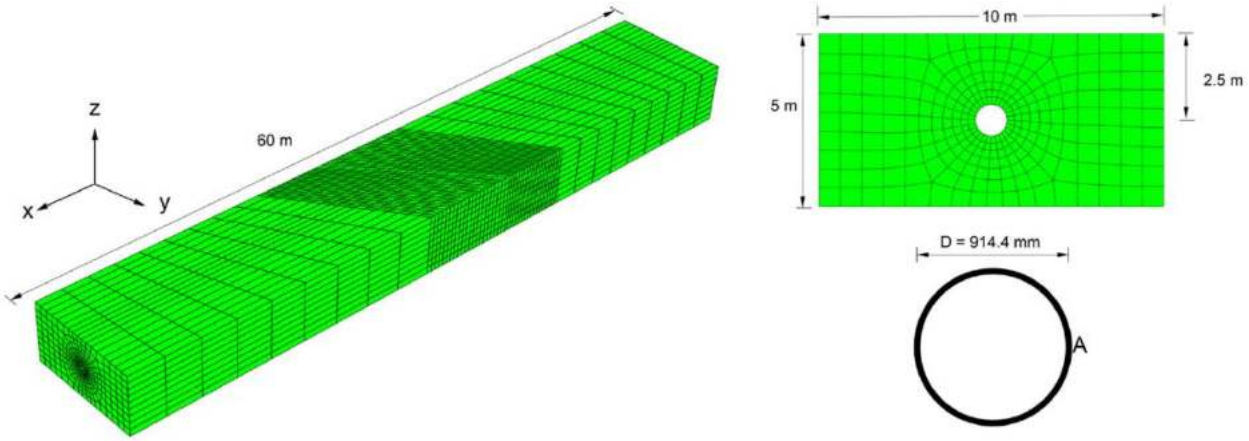

Figure 1-48. Finite element model (Vazouras et al., 2012)

The group of research developed analytical solutions to study the structural behavior of buried pipelines (deformation, internal forces). The obtained results from their interesting researches can be very helpful for the development of performance-based design methodologies for buried steel pipelines.

1.4.9.2. Al-Khazaali et al. (2018)

Al-Khazaali et al. (2018) studied soil deformation associated with excavation on the proximity buried pipelines (Figure 1-49). The induced relative displacement between the pipeline and the surrounding were analyzed and consequently, a methodology to determine the safe depths of unsupported excavations in unsaturated soils without causing excessive strains or internal forces in the ring of rigid and flexible pipes was proposed.

1.4.9.1. Al-Khazaali and Vanapalli (2019, 2020)

Through consistent laboratory investigations (Figure 1-50), Al-Khazaali and Vanapalli (2020) reported that the design of pipeline systems based on conventional approaches underestimates the external, and internal forces demonstrating that the pipeline systems in unsaturated soil experiences higher external axial forces. Due to this reason, design procedures extending the principles of saturated soil mechanics for pipelines buried in unsaturated soils is not conservative; it is unsafe (Vanapalli and Al-Khazaali, 2019). This study highlighted that the rational interpretation of the pipeline systems is possible by extending the principles of unsaturated soil mechanics where it was found that the axial load test results of the prototype pipeline in unsaturated sand were found to be 2–2.5 times greater than saturated condition.

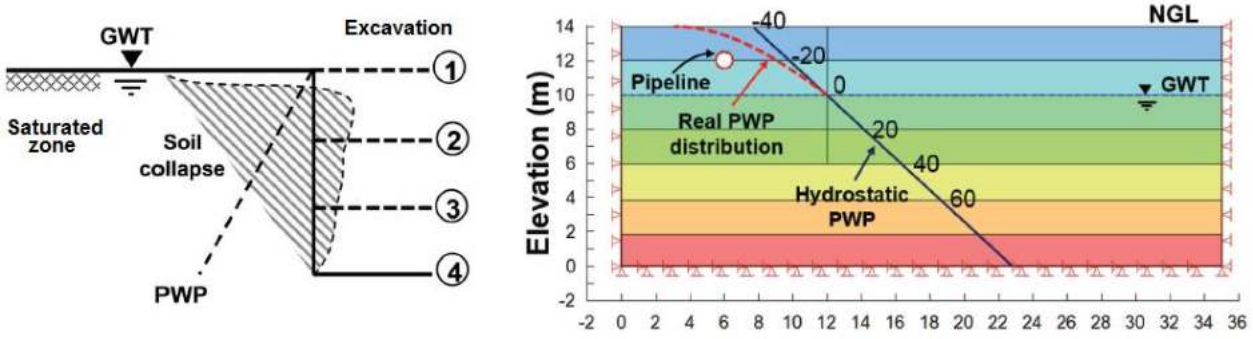

Figure 1-49. Numerical model used Al-Khazaali et al. (2018)

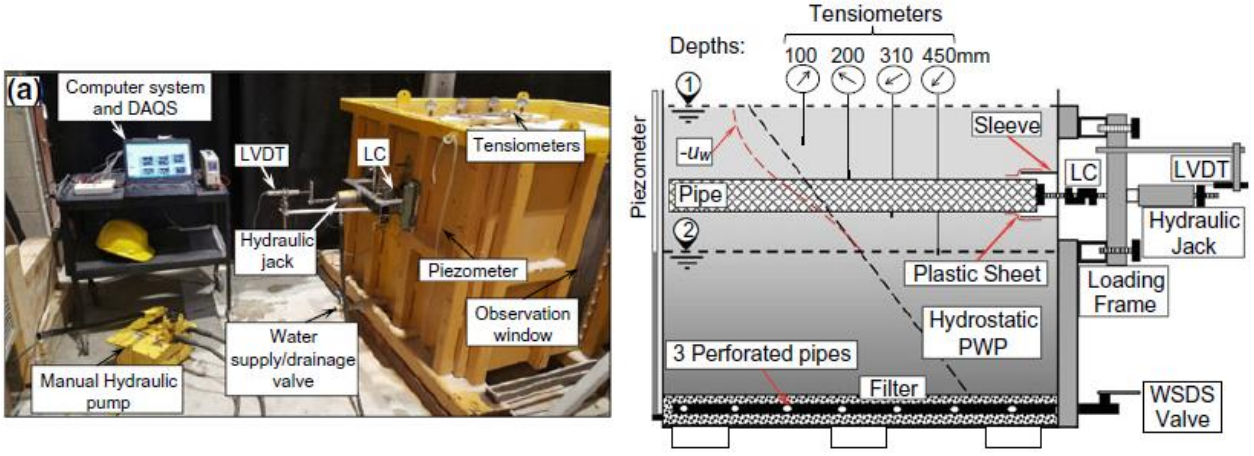

Figure 1-50. The full test setup and a graphical illustration of the test setup (Vanapalli and Al-Khazaali, 2019).

1.5. Conclusion

In this chapter a literature review was done where the main aspects needed to understand the problem of Aine-Tine pipeline which is related to three different axes unsaturated soil, slope stability and pipeline systems. We have tried to check the recent and main findings and used methods and tools around the world without neglecting the basic points of each of the three axes. Based on the discussion of the previous studies and researches the main conclusion that can be derived is the following:

a) The safe design of the pipeline systems around the world is an active subject.
b) It is mandatory to consider the unsaturated behavior of soils to design the buried network of pipelines in the Mila basin which will help to limit the costly and repetitive damages that occurred on the Aine-Tine pipeline.

This chapter is intended to serve a scientific contribution, that presents a coherent support to reinforce the limited studies that addressed the interaction of buried pipelines with unsaturated slopes.

1.6. References

Abramson, L.W., Lee, T.S., Sharma, S., Boyce, G.M., 2002. Slope stability and stabilization methods, 2nd ed. ed. Wiley, New York.

Adem, H.H., Vanapalli, S.K., 2014a. Elasticity moduli of expansive soils from dimensional analysis. Geotech. Res. 1, 60–72. https://doi.org/10.1680/gr.14.00006

Adem, H.H., Vanapalli, S.K., 2014b. Prediction of the modulus of elasticity of compacted unsaturated expansive soils. Int. J. Geotech. Eng. 9, 163–175. https://doi.org/10.1179/1939787914Y.0000000050

Adem, H.H., Vanapalli, S.K., 2013. Constitutive modeling approach for estimating 1-D heave with respect to time for expansive soils. Int. J. Geotech. Eng. 7, 199–204. https://doi.org/10.1179/1938636213Z.00000000024

Akin, I.D., Likos, W.J., 2020. Suction Stress of Clay Over a Wide Range of Saturation. Geotech. Geol. Eng. 38, 283–296. https://doi.org/10.1007/s10706-019-01016-7

ALA, 2005. Seismic Guidelines for Water Pipelines. American Lifelines Alliance, Federal Emergency Management Agency (FEMA).

Al-Khazaali, M., 2019. Soil-Pile, Pile Group Foundations and Pipeline Systems Interaction Behavior Extending Saturated and Unsaturated Soil Mechanics (Thesis). Université d'Ottawa / University of Ottawa. https://doi.org/10.20381/ruor-23095

Al-Khazaali, M., Vanapalli, S.K., 2020. A Novel Experimental Technique to Investigate Soil–Pipeline Interaction under Axial Loading in Saturated and Unsaturated Sands. Geotech. Test. J. 43, 70–93. https://doi.org/10.1520/GTJ20180059

Al-Khazaali, M., Vanapalli, S.K., Oh, W.T., 2018. Numerical investigation of soil–pipeline system behavior nearby unsupported excavation in saturated and unsaturated glacial till. Can. Geotech. J. 56, 69–88. https://doi.org/10.1139/cgj-2017-0411

Anand, V., Satish Kumar, S.R., 2018. Seismic Soil-structure Interaction: A State-of-the-Art Review. Structures 16, 317–326. https://doi.org/10.1016/j.istruc.2018.10.009

Athmania, D., Benaissa, A., Hammadi, A., Bouassida, M., 2010. Clay and Marl Formation Susceptibility in Mila Province, Algeria. Geotech. Geol. Eng. 28, 805–813. https://doi.org/10.1007/s10706-010-9341-5

Aung, K.K., Rahardjo, H., Leong, E.C., Toll, D.G., 2001. Relationship between porosimetry measurement and soil—water characteristic curve for an unsaturated residual soil, in: Unsaturated Soil Concepts and Their Application in Geotechnical Practice. Springer, pp. 401–416.

Biot, M.A., 1941. General theory of three-dimensional consolidation. J. Appl. Phys. 12, 155–164.

Bishop, A.W., 1959. The principles of effective stress. Tech. Ukebl. 106(9), 859–863.

Bishop, A.W., Blight, G.E., 1963. Some Aspects of Effective Stress in Saturated and Partly Saturated Soils. Géotechnique 13, 177–197. https://doi.org/10.1680/geot.1963.13.3.177

Bouatia, M., Demagh, R., Derriche, Z., 2020. Structural Behavior of Pipelines Buried in Expansive Soils under Rainfall Infiltration (Part I: Transverse Behavior). Civ. Eng. J. 6, 1822–1838. https://doi.org/10.28991/cej-2020-03091585

Brackley, I.J., 1971. Partial collapse in unsaturated expansive clay. CSIR.

Brooks, R.H., Corey, A.T., 1964. Hydraulic Properties of Porous Media and Their Relation to Drainage Design. Trans. ASAE 7, 0026–0028. https://doi.org/10.13031/2013.40684

Burland, J.B., 1964. Correspondence. Géotechnique 14, 64–68. https://doi.org/10.1680/geot.1964.14.1.64

Clark, C.M., 1971. Expansive-Soil Effect on Buried Pipe. J. - AWWA 63, 424–427. https://doi.org/10.1002/j.1551-8833.1971.tb04116.x

Cooper, R.G., Ballantyne, C.K., Jarman, D., 2007. Mass movements in Great Britain, Geological conservation review series. Joint Nature Conservation Committee, Peterborough.

Crofts, J.E., Menzies, B.K., Tarzi, A.I., 1977. Lateral displacement of shallow buried pipelines due to adjacent deep trench excavations. Géotechnique 27, 161–179. https://doi.org/10.1680/geot.1977.27.2.161

Cruden, D.M., 1991. A simple definition of a landslide. Bull. Int. Assoc. Eng. Geol. 43, 27–29. https://doi.org/10.1007/BF02590167

Dawson, E.M., Roth, W.H., Drescher, A., 1999. Slope stability analysis by strength reduction. Géotechnique 49, 835–840. https://doi.org/10.1680/geot.1999.49.6.835

de Blasio, F.V., 2011. Introduction to the Physics of Landslides. Springer Netherlands, Dordrecht. https://doi.org/10.1007/978-94-007-1122-8

Dikau, R., Brunsden, D., Schrott, L., Ibsen, M.-L., 1996. Landslide recognition: identification, movement, and causes, Publication / International Association of Geomorphologists. Wiley, Chichester ; New York.

Duncan, J.M., Wright, S.G., Brandon, T.L., 2014. Soil strength and slope stability, Second edition. ed. John Wiley & Sons Inc, Hoboken, New Jersey.

Feng, W., Huang, R., Liu, J., Xu, X., Luo, M., 2015. Large-scale field trial to explore landslide and pipeline interaction. Soils Found. 55, 1466–1473. https://doi.org/10.1016/j.sandf.2015.10.011

Fredlund, D.G., Morgenstern, N.R., 1976. Constitutive relations for volume change in unsaturated soils. Can. Geotech. J. 13, 261–276. https://doi.org/10.1139/t76-029

Fredlund, D.G., Morgenstern, N.R., Widger, R.A., 1978. The shear strength of unsaturated soils. Can. Geotech. J. 15, 313–321. https://doi.org/10.1139/t78-029

Fredlund, D.G., Rahardjo, H., 1993. Soil mechanics for unsaturated soils. John Wiley & Sons.

Fredlund, D.G., Xing, A., 1994. Equations for the soil-water characteristic curve. Can. Geotech. J. 31, 521–532. https://doi.org/10.1139/t94-061

Fredlund, D.G., Xing, A., Fredlund, M.D., Barbour, S.L., 1996. The relationship of the unsaturated soil shear strength to the soil-water characteristic curve. Can. Geotech. J. 33, 440–448. https://doi.org/10.1139/t96-065

Fredlund, D.G., Xing, A., Huang, S., 1994. Predicting the permeability function for unsaturated soils using the soil-water characteristic curve. Can. Geotech. J. 31, 533–546. https://doi.org/10.1139/t94-062

Fredlund, M.D., Wilson, G.W., Fredlund, D.G., 2002. Use of the grain-size distribution for estimation of the soil-water characteristic curve. Can. Geotech. J. 39, 1103–1117.

Gallage, C.P.K., Chan, D., Kodikara, J., 2012. Response of a plastic pipe buried in expansive clay. Proc. Inst. Civ. Eng. - Geotech. Eng. 165, 45–57. https://doi.org/10.1680/geng.9.00037

Gardner, W.R., 1958. SOME STEADY-STATE SOLUTIONS OF THE UNSATURATED MOISTURE FLOW EQUATION WITH APPLICATION TO EVAPORATION FROM A WATER TABLE: Soil Sci. 85, 228–232. https://doi.org/10.1097/00010694-195804000-00006

GeoSlope International Ltd, 2007. SIGMA/W user's guide for stress-deformation analysis. GEO-SLOPE International Ltd. Calgary, AB, Canada.

Gresnigt, A.M., 1986. Plastic design of buried steel pipelines in settlement areas. Heron Delft 31, 1–113.

Han, Z., Vanapalli, S.K., Kutlu, Z.N., 2016. Modeling Behavior of Friction Pile in Compacted Glacial Till. Int. J. Geomech. 16. https://doi.org/10.1061/(ASCE)GM.1943-5622.0000659

Highland, L., 2004. Landslide types and processes. Fact Sheet. https://doi.org/10.3133/fs20043072

Holtz, R.D., Kovacs, W.D., 1981. An Introduction to Geotechnical Engineering. Prentice-Hall.

Huang, S., Barbour, S.L., Fredlund, D.G., 1998. Development and verification of a coefficient of permeability function for a deformable unsaturated soil. Can. Geotech. J. 35, 411–425. https://doi.org/10.1139/t98-010

Huang, S.L., Bray, M.T., Akagawa, S., Fukuda, M., 2004. Field Investigation of Soil Heave by a Large Diameter Chilled Gas Pipeline Experiment, Fairbanks, Alaska. J. Cold Reg. Eng. 18, 2–34. https://doi.org/10.1061/(ASCE)0887-381X(2004)18:1(2)

Huang, S.L., Yang, K., Akagawa, S., Fukuda, M., Kanie, S., 2015. Frost Heave Induced Pipe Strain of an Experimental Chilled Gas Pipeline, in: Innovative Materials and Design for Sustainable Transportation Infrastructure. Presented at the International Symposium on Systematic Approaches to Environmental Sustainability in Transportation, American Society of Civil Engineers, Fairbanks, Alaska, pp. 405–416. https://doi.org/10.1061/9780784479278.037

Hungr, O., Leroueil, S., Picarelli, L., 2014. The Varnes classification of landslide types, an update. Landslides 11, 167–194. https://doi.org/10.1007/s10346-013-0436-y

IITK-GSDMA, 2007. GUIDELINES for SEISMIC DESIGN of BURIED PIPELINES. Indian Institute of Technology Kanpur - Gujarat State Disaster Management Authority, National Information Center of Earthquake Engineering, Kanpur, India.

Karube, D., Kawai, K., 2001. The role of pore water in the mechanical behavior of unsaturated soils. Geotech. Geol. Eng. 19, 211–241. https://doi.org/10.1023/A:1013188200053

Kausel, E., 2010. Early history of soil–structure interaction. Soil Dyn. Earthq. Eng. 30, 822–832. https://doi.org/10.1016/j.soildyn.2009.11.001

Khalili, N., Khabbaz, M.H., 1998. A unique relationship for χ for the determination of the shear strength of unsaturated soils. Géotechnique 48, 681–687. https://doi.org/10.1680/geot.1998.48.5.681

Kouretzis, G.P., Karamitros, D.K., Sloan, S.W., 2015. Analysis of buried pipelines subjected to ground surface settlement and heave. Can. Geotech. J. 52, 1058–1071.

Leonards, G., Roy, M., 1976. Predicting Performance of Pipe Culverts Buried in Soil, Phase 1 : Interim Report (No. FHWA/IN/JHRP-76/15, 1(12) Pt 2). Purdue University, West Lafayette, IN. https://doi.org/10.5703/1288284313924

Leong, E.-C., Rahardjo, H., 1997. Permeability Functions for Unsaturated Soils. J. Geotech. Geoenvironmental Eng. 123, 1118–1126. https://doi.org/10.1061/(ASCE)1090-0241(1997)123:12(1118)

Liu, H., 2004. Pipeline Engineering. CRC Press.

Liu, Y., Cai, Y., Huang, S., Guo, Y., Liu, G., 2019. Effect of water saturation on uniaxial compressive strength and damage degree of clay-bearing sandstone under freeze-thaw. Bull. Eng. Geol. Environ. https://doi.org/10.1007/s10064-019-01686-w

LNHC Batna, 2017. Rapport d'etude de sol (2017).

LNHC Batna, 2016. Rapport d'etude de sol (2015) (Rapport d'etude de sol No. 127/2015). GENEST, Batna, Algérie.

Lu, N., Kaya, M., 2014. Power Law for Elastic Moduli of Unsaturated Soil. J. Geotech. Geoenvironmental Eng. 140, 46–56. https://doi.org/10.1061/(ASCE)GT.1943-5606.0000990

Marston, Anderson, 1913. The Theory of Loads on Pipes in Ditches and Tests of Cement and Clay Drain Tile and Sewer Pipes.

Matyas, E.L., Radhakrishna, H.S., 1968. Volume Change Characteristics of Partially Saturated Soils. Géotechnique 18, 432–448. https://doi.org/10.1680/geot.1968.18.4.432

McKee, C.R., Bumb, A.C., 1987. Flow-Testing Coalbed Methane Production Wells in the Presence of Water and Gas. SPE Form. Eval. 2, 599–608. https://doi.org/10.2118/14447-PA

Meilani, I., Rahardjo, H., Leong, E.-C., 2005. Pore-water pressure and water volume change of an unsaturated soil under infiltration conditions. Can. Geotech. J. 42, 1509–1531. https://doi.org/10.1139/t05-066

Mohitpour, M., Golshan, H., Murray, A., 2007. Pipeline design & construction: a practical approach, 3rd ed. ed. ASME Press, New York.

Moser, A.P., Folkman, S., 2008. Buried Pipe Design, Third Edition, 3rd ed. McGraw-Hill Education.

Murray, E.J., Sivakumar, V., 2010. Unsaturated Soils: A fundamental interpretation of soil behaviour. John Wiley & Sons, New York.

Ng, P.C.F., 1994. Behaviour of buried pipelines subjected to external loading. (phd). University of Sheffield.

Oh, W.T., Vanapalli, S.K., Puppala, A.J., 2009. Semi-empirical model for the prediction of modulus of elasticity for unsaturated soils. Can. Geotech. J. 46, 903–914. https://doi.org/10.1139/T09-030

O'Rourke, T.D., Jezerski, J.M., Olson, N.A., Bonneau, A.L., Palmer, M.C., Stewart, H.E., O'Rourke, M.J., Abdoun, T., 2008. Geotechnics of Pipeline System Response to Earthquakes, in: Geotechnical Earthquake Engineering and Soil Dynamics IV. Presented at the Geotechnical Earthquake Engineering and Soil Dynamics Congress IV, American Society of Civil Engineers, Sacramento, California, United States, pp. 1–38. https://doi.org/10.1061/40975(318)193

Palmer, A.C., Tebboth, L., Miles, D., Calladine, C.R., 1999. Instability of Pipelines on Slopes. J. Appl. Mech. 66, 794–799. https://doi.org/10.1115/1.2791757

Potts, D.M., Zdravković, L., 2001. Finite Element Analysis in Geotechnical Engineering: Volume two - Application. Thomas Telford Publishing. https://doi.org/10.1680/feaigea.27831

Qi, S., Vanapalli, S.K., 2016. Influence of swelling behavior on the stability of an infinite unsaturated expansive soil slope. Comput. Geotech. 76, 154–169. https://doi.org/10.1016/j.compgeo.2016.02.018

Qi, S., Vanapalli, S.K., 2015. Hydro-mechanical coupling effect on surficial layer stability of unsaturated expansive soil slopes. Comput. Geotech. 70, 68–82. https://doi.org/10.1016/j.compgeo.2015.07.006

Rahardjo, H., Melinda, F., Leong, E.C., Rezaur, R.B., 2011. Stiffness of a compacted residual soil. Eng. Geol. 120, 60–67. https://doi.org/10.1016/j.enggeo.2011.04.006

Rajani, B., Morgenstern, N., 1993. Pipelines and Laterally Loaded Piles in Elastoplastic Medium. J. Geotech. Eng. 119, 1431–1448. https://doi.org/10.1061/(ASCE)0733-9410(1993)119:9(1431)

Rajani, B., Zhan, C., Kuraoka, S., 1996. Pipe-soil interaction analysis of jointed water mains. Can. Geotech. J. 33, 393–404. https://doi.org/10.1139/t96-061

Rajeev, P., Chan, D., Kodikara, J., 2012. Ground–atmosphere interaction modelling for long-term prediction of soil moisture and temperature. Can. Geotech. J. 49, 1059–1073. https://doi.org/10.1139/t2012-068

Rajeev, P., Kodikara, J., 2011. Numerical analysis of an experimental pipe buried in swelling soil. Comput. Geotech. 38, 897–904. https://doi.org/10.1016/j.compgeo.2011.06.005

Rampino, C., Mancuso, C., Vinale, F., 2000. Experimental behaviour and modelling of an unsaturated compacted soil. Can. Geotech. J. 37, 748–763. https://doi.org/10.1139/t00-004

Robert, D., Soga, K., 2013. Soil-Pipeline Interaction in Unsaturated Soils, in: Mechanics of Unsaturated Geomaterials. John Wiley & Sons, Inc., Hoboken, NJ USA, pp. 303–325. https://doi.org/10.1002/9781118616871.ch13

Roy, K., Hawlader, B., Kenny, S., Moore, I., 2016. Finite element modeling of lateral pipeline–soil interactions in dense sand. Can. Geotech. J. 53, 490–504. https://doi.org/10.1139/cgj-2015-0171

Saadeldin, R., Hu, Y., Henni, A., 2015. Numerical analysis of buried pipes under field geo-environmental conditions. Int. J. Geo-Eng. 6, 6. https://doi.org/10.1186/s40703-015-0005-4

Satyanaga, A., Rahardjo, H., Leong, E.-C., Wang, J.-Y., 2013. Water characteristic curve of soil with bimodal grain-size distribution. Comput. Geotech. 48, 51–61. https://doi.org/10.1016/j.compgeo.2012.09.008

Sawangsuriya A., Edil T. B., Bosscher P. J., 2009. Modulus-Suction-Moisture Relationship for Compacted Soils in Postcompaction State. J. Geotech. Geoenvironmental Eng. 135, 1390–1403. https://doi.org/10.1061/(ASCE)GT.1943-5606.0000108

Shen, H., Klapperich, H., Abbas, S.M., Ibrahim, A., 2012. Slope stability analysis based on the integration of GIS and numerical simulation. Autom. Constr. 26, 46–53. https://doi.org/10.1016/j.autcon.2012.04.016

Taber, S., 1929. Frost Heaving. J. Geol. 37, 428–461. https://doi.org/10.1086/623637

Timošenko, S.P., Goodier, J.N., 1970. Theory of elasticity, 3rd ed, Engineering societies monographs. McGraw-Hill, Auckland.

Timoshenko, S., 1968. Résistance des matériaux. Dunod, Paris.

UNESCO Working Party On World Landslide Inventory, 1993. A suggested method for describing the activity of a landslide. Bull. Int. Assoc. Eng. Geol. 47, 53–57. https://doi.org/10.1007/BF02639593

van Genuchten, M.Th., 1980. A Closed-form Equation for Predicting the Hydraulic Conductivity of Unsaturated Soils. Soil Sci. Soc. Am. J. 44, 892–898. https://doi.org/10.2136/sssaj1980.03615995004400050002x

Van Terzaghi, K., 1936. The shearing resistance of saturated soils, in: Proc. 1st. Int. Conf. Soil Mech. Found. Eng., Cambridge, Mass. pp. 54–56.

Vanapalli, S., Oh, W., 2010. A model for predicting the modulus of elasticity of unsaturated soils using the soil-water characteristic curve. Int. J. Geotech. Eng. 4, 425–433. https://doi.org/10.3328/IJGE.2010.04.04.425-433

Vanapalli, S.K., Al-Khazaali, M., 2019. Axial Load-Displacement Behavior of Energy Pipeline Systems in Sand, in: Latha G., M. (Ed.), Frontiers in Geotechnical Engineering, Developments in Geotechnical Engineering. Springer Singapore, Singapore, pp. 121–138. https://doi.org/10.1007/978-981-13-5871-5_7

Vanapalli, S.K., Fredlund, D.G., Pufahl, D.E., Clifton, A.W., 1996. Model for the prediction of shear strength with respect to soil suction. Can. Geotech. J. 33, 379–392. https://doi.org/10.1139/t96-060

Vazouras, P., Dakoulas, P., Karamanos, S.A., 2015. Pipe–soil interaction and pipeline performance under strike–slip fault movements. Soil Dyn. Earthq. Eng. 72, 48–65. https://doi.org/10.1016/j.soildyn.2015.01.014

Vazouras, P., Karamanos, S.A., 2017. Structural behavior of buried pipe bends and their effect on pipeline response in fault crossing areas. Bull. Earthq. Eng. 15, 4999–5024. https://doi.org/10.1007/s10518-017-0148-0

Vazouras, P., Karamanos, S.A., Dakoulas, P., 2012. Mechanical behavior of buried steel pipes crossing active strike-slip faults. Soil Dyn. Earthq. Eng. 41, 164–180. https://doi.org/10.1016/j.soildyn.2012.05.012

Vazouras, P., Karamanos, S.A., Dakoulas, P., 2010. Finite element analysis of buried steel pipelines under strike-slip fault displacements. Soil Dyn. Earthq. Eng. 30, 1361–1376. https://doi.org/10.1016/j.soildyn.2010.06.011

Vu, H.Q., Fredlund, D.G., 2011. Challenges to modelling heave in expansive soils. Can. Geotech. J. https://doi.org/10.1139/t06-073

Vu, H.Q., Fredlund, D.G., 2004. The prediction of one-, two-, and three-dimensional heave in expansive soils. Can. Geotech. J. 41, 713–737. https://doi.org/10.1139/t04-023

Watkins, R.K., Anderson, L.R., 2000. Structural mechanics of buried pipes. CRC Press, Boca Raton, FL.

Williams, 1982. The surface of the Earth, an introduction to geotechnical science. Longman Inc, New York.

Zeng, L., Xiao, L.-Y., Zhang, J.-H., Gao, Q.-F., 2020. Effect of the characteristics of surface cracks on the transient saturated zones in colluvial soil slopes during rainfall. Bull. Eng. Geol. Environ. 79, 699–709. https://doi.org/10.1007/s10064-019-01584-1

Zhang, J., Peng, J., Li, J., Zheng, J., 2018. Variation of Resilient Modulus with Soil Suction for Cohesive Soils in South China. Int. J. Civ. Eng. 16, 1655–1667. https://doi.org/10.1007/s40999-018-0315-y

Zhang, L.L., Zhang, J., Zhang, L.M., Tang, W.H., 2011a. Stability analysis of rainfall-induced slope failure: a review. Proc. Inst. Civ. Eng. - Geotech. Eng. 164, 299–316. https://doi.org/10.1680/geng.2011.164.5.299

Zhang, L.L., Zhang, J., Zhang, L.M., Tang, W.H., 2011b. Stability analysis of rainfall-induced slope failure: a review. Proc. Inst. Civ. Eng. - Geotech. Eng. 164, 299–316. https://doi.org/10.1680/geng.2011.164.5.299

Chapter 02

AINE-TINE SLOPE STABILITY INVESTIGATION

2. Aine-Tine slope investigations

2.1. Information background

The content presented in this chapter was used to prepare the following contributions entitled:

Bouatia, M., Demagh, R., 2019. ***Numerical Assessment of Slope Stability of Ain-Tinn Mila Province (Algeria),*** in: Shehata, H., Desai, C.S. (Eds.), Advances in Numerical Methods in Geotechnical Engineering, Sustainable Civil Infrastructures. Springer International Publishing, Cham, pp. 133–143. https://doi.org/10.1007/978-3-030-01926-6_10

Bouatia, M., Demagh, R., 2018. ***2D and 3D Numerical Investigation of Slope Stability - Case of Mila (Algeria)***, in: ACEM18/Structures18. Presented at the 2018 World Congress on Advances in Civil, Environment, & Materials research, Techno-Press, Songdo Convensia, Incheon, Korea.

Bouatia, M., Demagh, R., Derriche, Z., Azman, K., Aminaton, M. (----) **Shallow Layer Stability Analysis of Unsaturated Slopes**. (to be submitted in an international journal)

2.2. Aine-Tine slope description

2.2.1. Introduction

The study of a geotechnical problem requires a thorough understanding of the site conditions and the soil characterization in order to simulate correctly the behavior of the system infrastructure and the soil system. In this part of the chapter, the site is described in many aspects geographic, topographic, geologic and climatic which were done using different sources of data such as google earth, maps and regional climatic station recordings. As for as the soil is concerned, soil site investigation results as presented by the LNHC (Laboratoire Nationale de l'Habitat et de la Construction) were collected.

2.2.2. Geographic situation

The study area is located in Mila province, situated in the North-East of Algeria (Figure 2-1). It is situated at 490 km from Algiers (i.e., the capital of the country) and at about 60 km from the city of Constantine. Mila covers an area of 3,550 km^2. It comprises composed by five districts with 32 municipalities. The Aine-Tine site can be bracketed by latitudes 06°18'30" and 06°19'00" and longitudes 36°25'30" and 36°25'45" (Figure 2-2).The Mila province belongs to the eastern Alpine chain in the north of Algeria. It is north bordered by Skikda and Jijel Provinces (Mediterranean Sea), south bordered by the Batna Province, at the West by the Sétif province and Constantine province in the East.

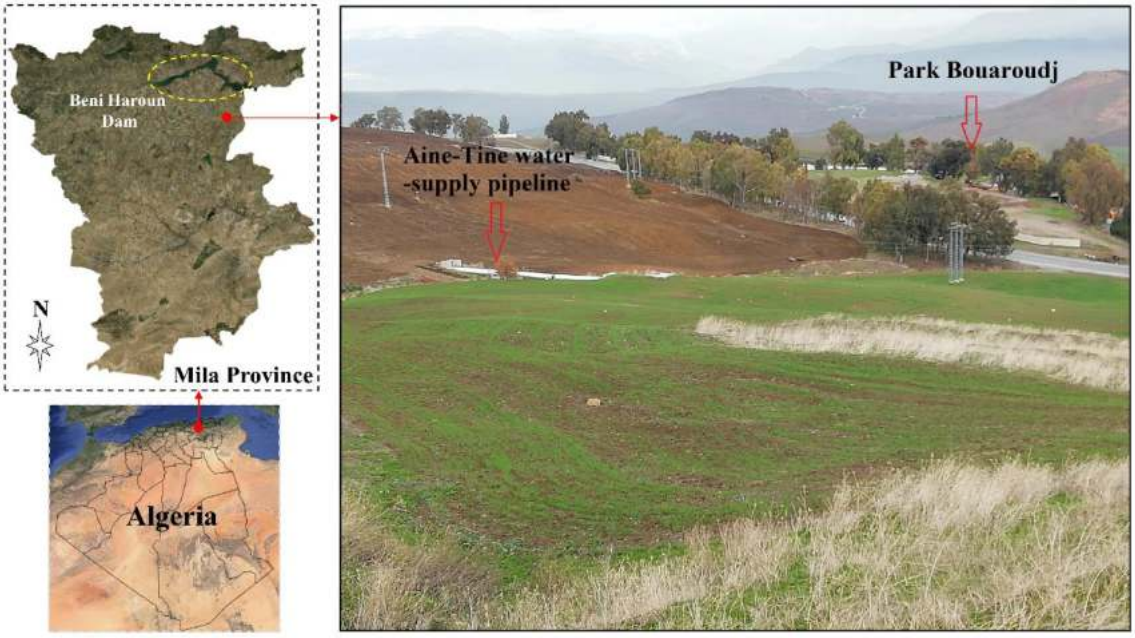

Figure 2-1 a photograph of Aine-Tine area

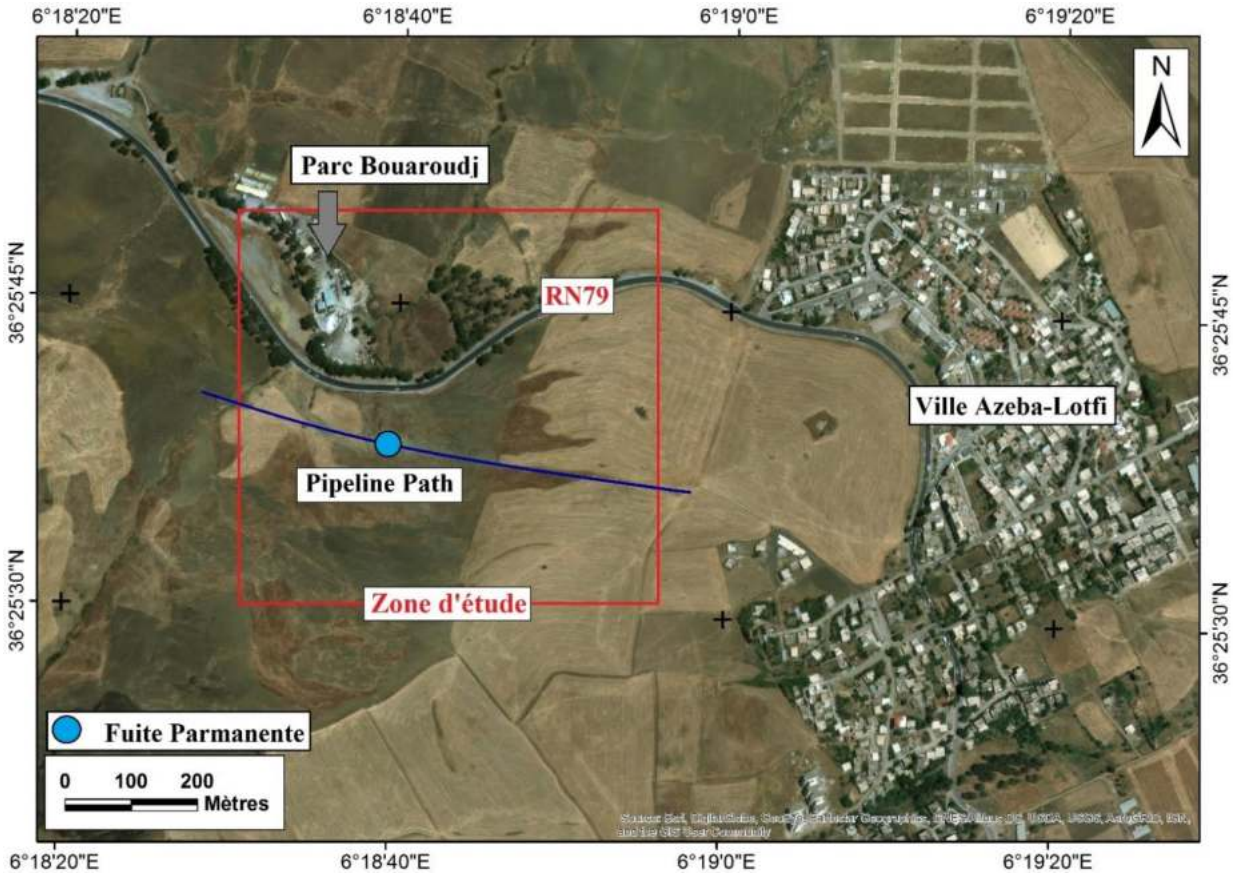

Figure 2-2 The Aine-Tine Slope details

2.2.3. Topographic conditions

Generally, the elevation on the site vary between 610 and 690 m. The geometry of Aine-Tine area is complex where many slopes can be observed with slope angles varying from 0° to 45°

according to several on-site visits. As shown in Figure 2-3 the area is crossed by the National highway RN79 which is a two lane road relating Mila province with primarily Constantine province and several other eastern provinces. The connecting pathway of Aine-Tine water transport pipeline is also crossing the area. It must be mentioned that the blue circle that appear in Figure 2-2 indicate leakage points recorded during the service life of the pipeline. It was notably observed during the site visit that the leakage points of Aine-Tine slope are located at an approximately flat area (slope 0°) this prompts us to think twice before deciding on the main causes of several leak points observed on the route of the pipeline. Where slope instabilities or soil expansion in these regions are the main causes that can disrupt the proper functioning of the Aine-Tine pipeline.

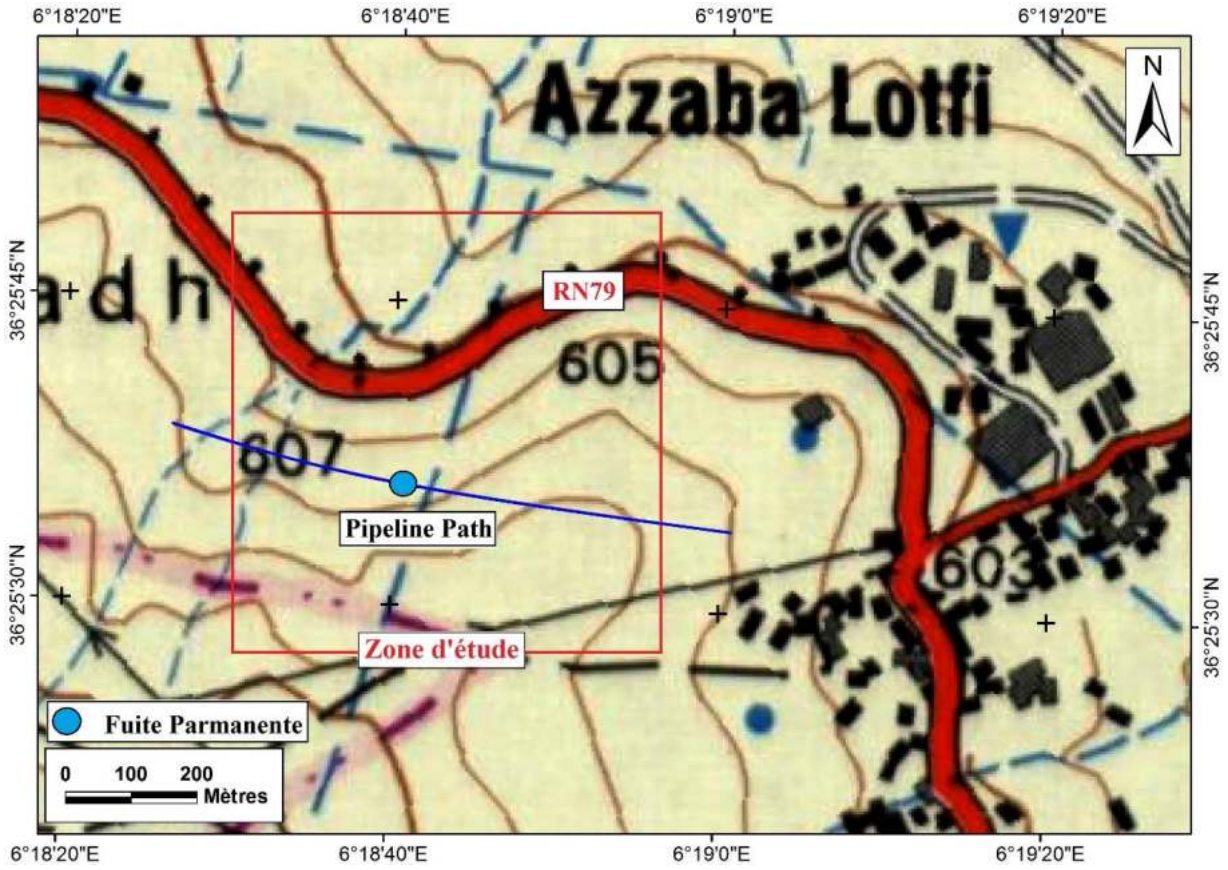

Figure 2-3 Aine-Tine area Topographic background

2.2.4. Geological conditions

Geologically, the site is part of the Constantinian basin where Mila's exposure soil consists of Mio-Pliocene and Quaternary continental deposits which cover a set of carbonate, bedrock, of the Cretaceous to Eocene ages (Figure 2-4). From the Figure 2-5, it can be concluded that more than 70% of geological formations distribution inside Mila province are Alluviums and clays, where they occupy 50.14% and 21.83% of the total area, respectively (Athmania et al., 2010). It is also notable the existence of marl around the Aine-Tine area (Figure 2-6). The layering composition of Aine-Tine slope was determined based on the Standard Penetration Test (SPT) results, the bedrock indicated by the refusal, was obtained to be at 20 m depth. Additionally, the shallow layer of Aine-Tine slope is assumed to have 4 to 5 m depth characterized by a low number

of blows oscillating around 10, which signify a weak layer performance. In the chapter of slope stability, the residual shear strength parameters will be used to conduct the calculation because of the weathered nature of the soils in the Aine-Tine shallow layer.

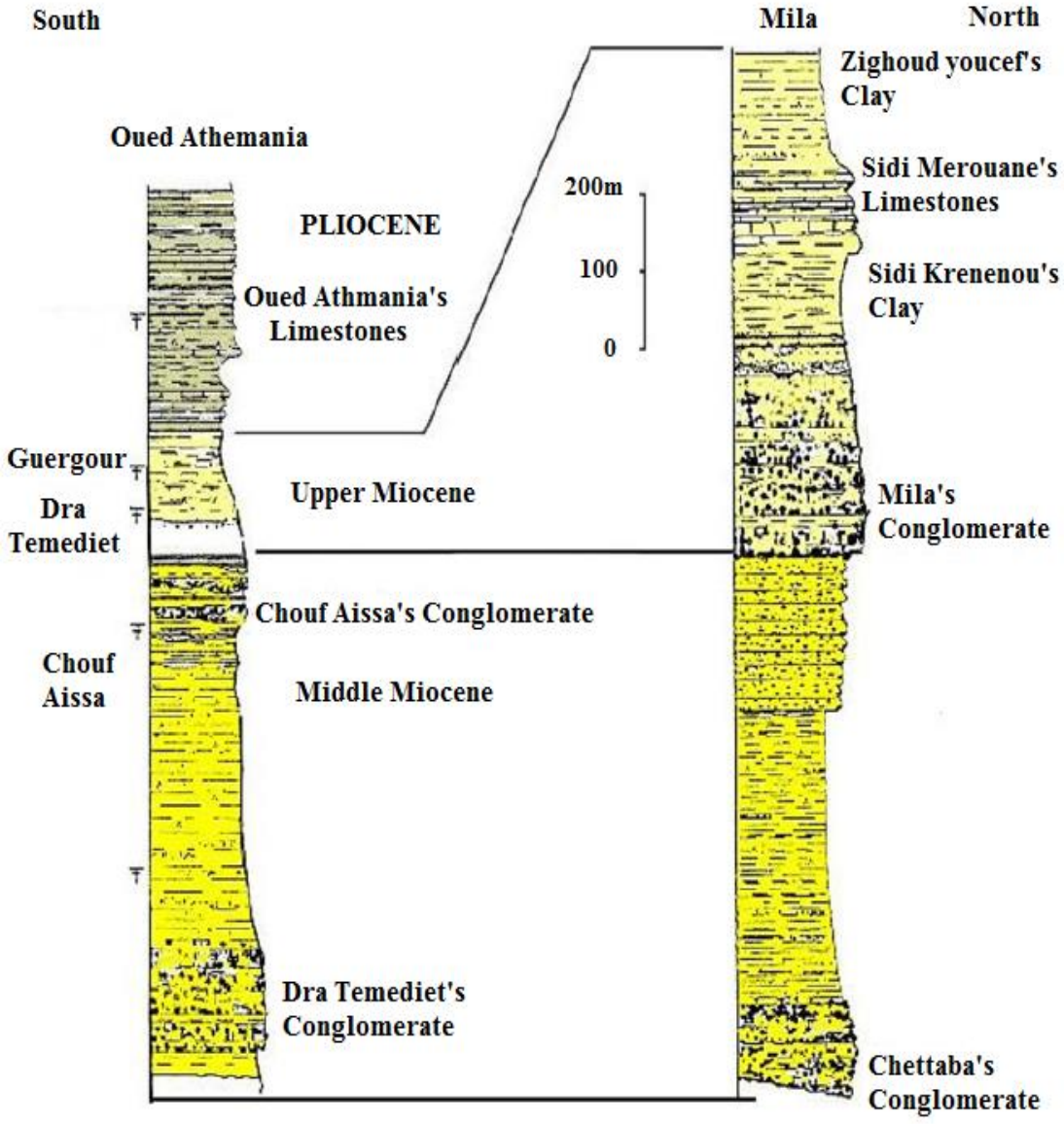

Figure 2-4. Mila's basin lithology (Athmania et al., 2010)

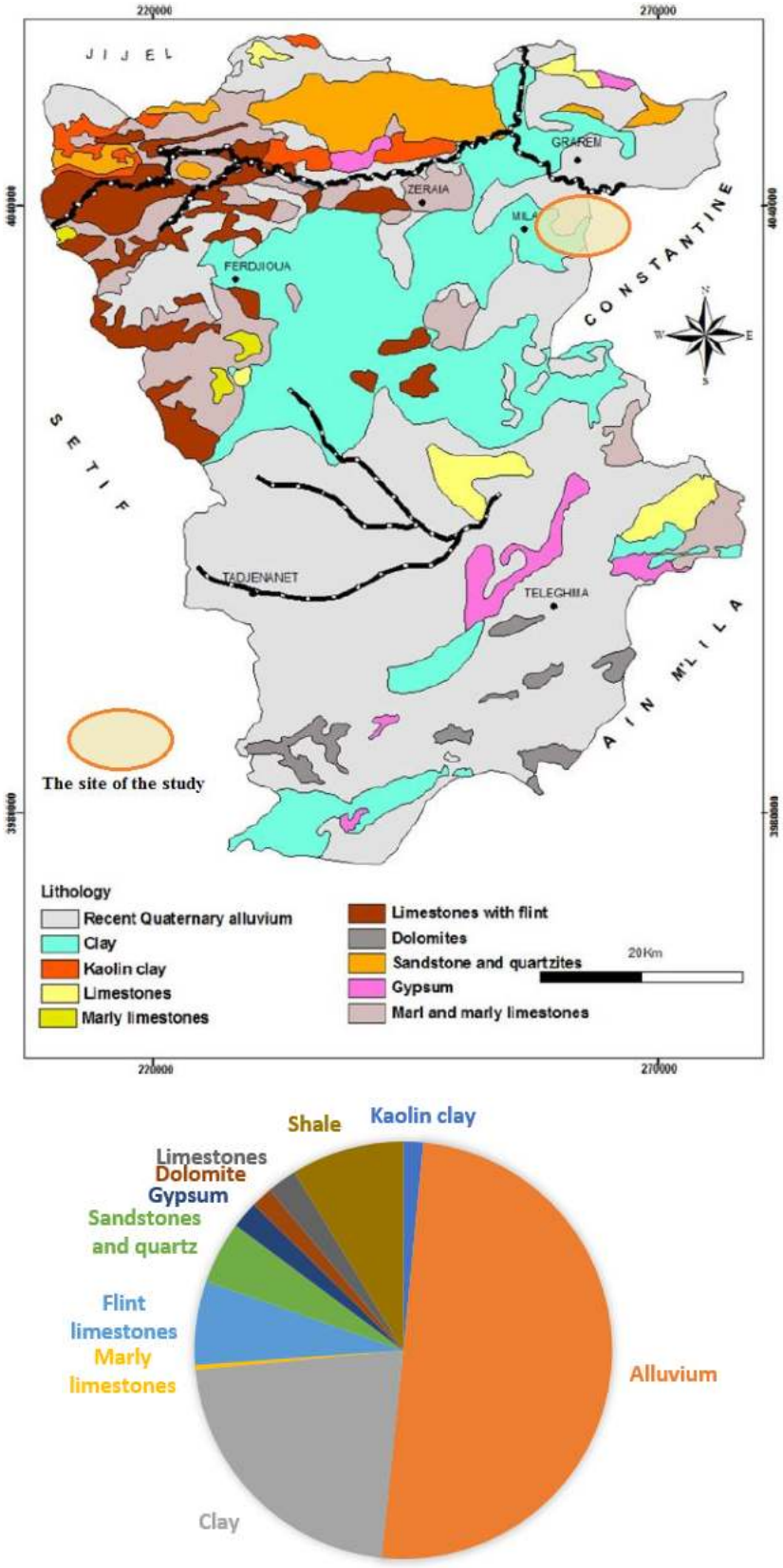

Figure 2-5. Principal geological formations Outcrop Inside Mila Province (Athmania et al., 2010)

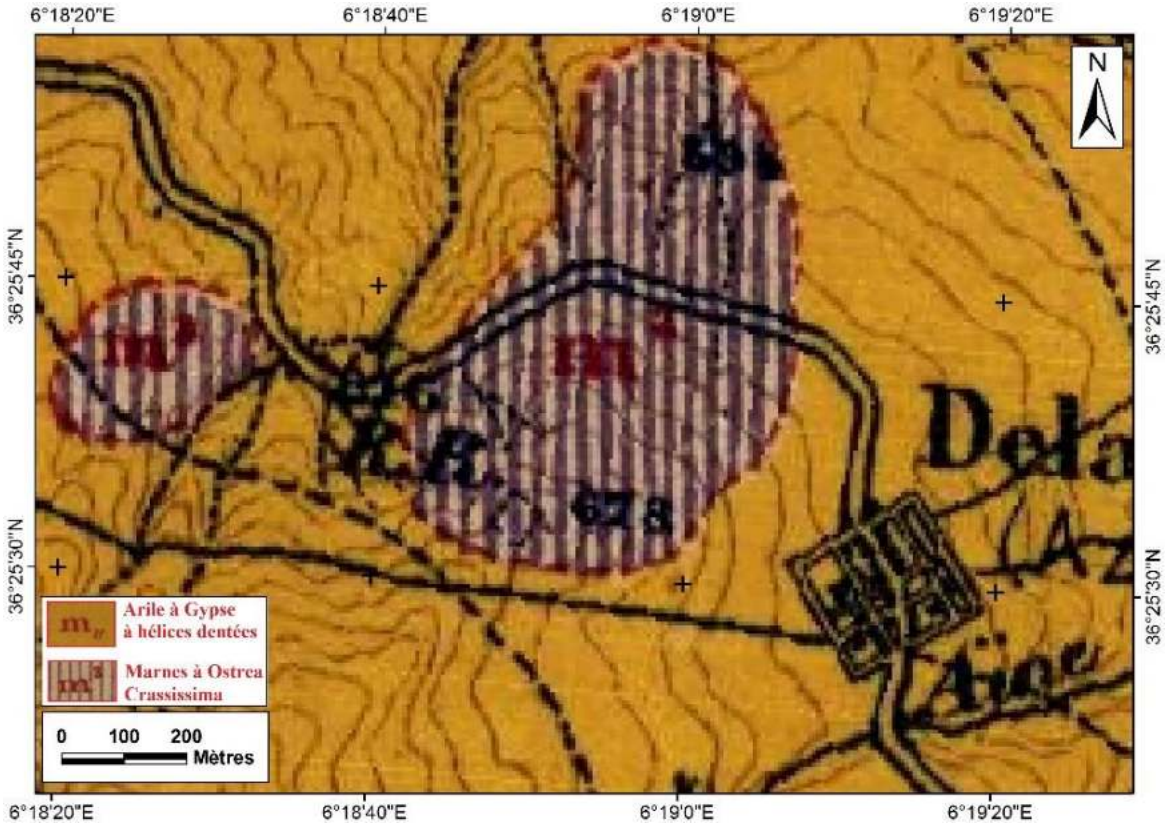

Figure 2-6. Aine-Tine Area Geologic background

2.2.5. Geotechnical background

2.2.5.1. Geotechnical characteristics

The content of this section is based on the results of two different geotechnical surveys performed by the LNHC laboratory (Laboratoire Nationale de L'Habitat et de la Construction). The first campaign was carried out in 2016 and the second in summer of 2017. The campaign comprises on site (Figure 2-8) and laboratory investigations.

2.2.5.1. Site bore hole analysis

Thirty (30) recognition wells of 4m deep were conducted to determine the depth of soil at the site, to identify any variation in soil type with increasing depth and to provide samples for further testing. Figure 2-7 shows the observed vertical soil profile at the field study site. It can be seen that the first 0.2 – 0.5 m is surface soil containing organic material, including plant (grass) roots. Below 0.4 m to 4.0 m the soil is inorganic brownish clay and greenish to greyish marl.

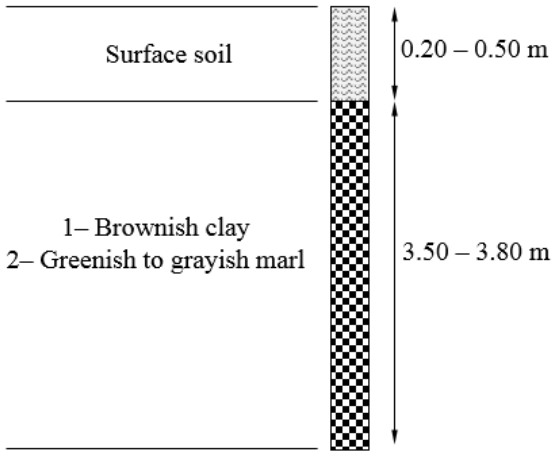

Figure 2-7. Shallow layer soil constitution

Figure 2-8 visit on the site

- Particle size analysis:

The particle size analysis for particle sizes down to 80 μm was conducted by dry sieving following NF P 94-056. The particle size analysis for particle smaller than 80 μm was then conducted in accordance with NF P 94-057. The results of the sieve analysis are shown in Figure 2-9 where 29 samples were taken from 4 m deep wells and 8 samples have been taken from 6 bore holes.

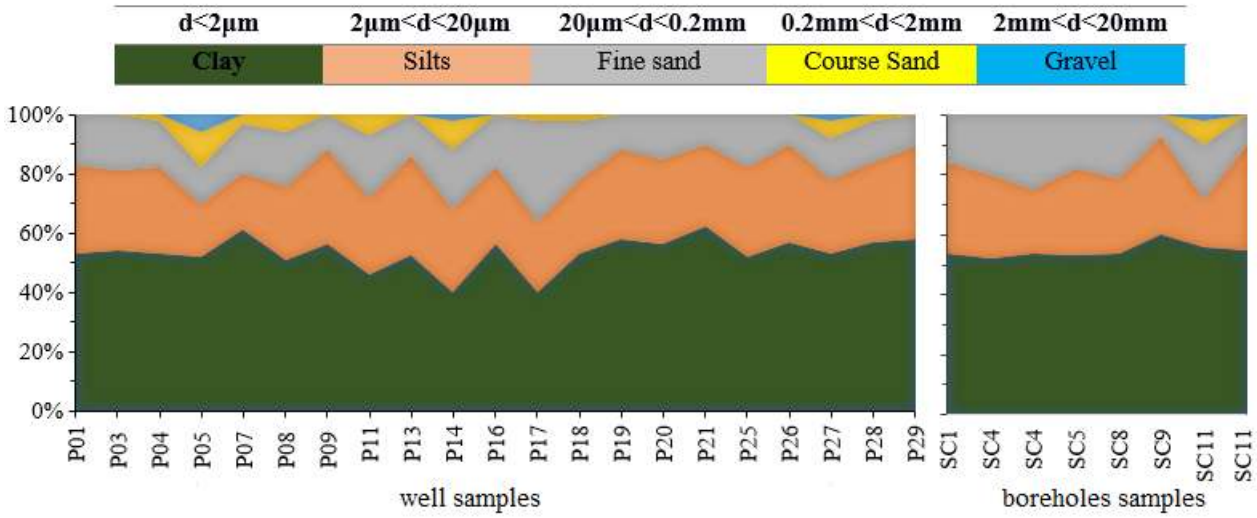

Figure 2-9 Sieve analysis

- Plasticity:

The plastic and liquid limits were determined in accordance with NF P 94-051. Figure 2-10 shows the projection of the results of the plasticity indices on the Casagrande chart. The clays of Aine-Tine slope totally located above the **line A**. Therefore, they can be classified as **medium plastic** material for values where the liquid limit is between 30% and 50% and as **very plastic** for those where the liquid limit is greater than 50%.

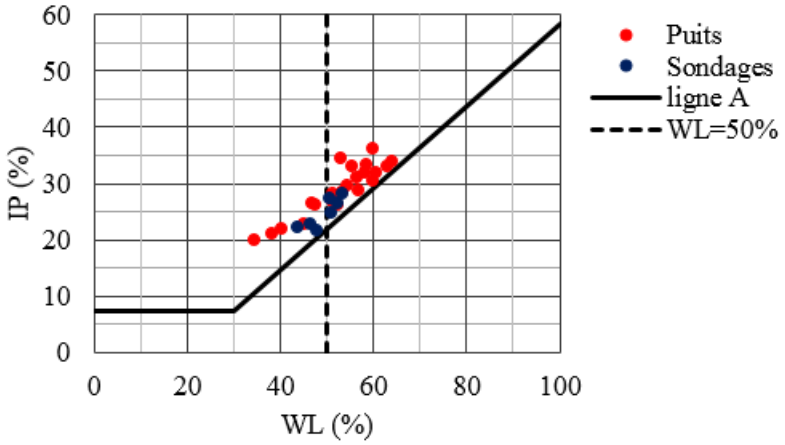

Figure 2-10 Plasticity index on Casagrande chart

The Unified Soil Classification System (USCS) is a soil classification system used in engineering and geology to describe the texture and grain size of a soil. Where the suitable part for the present study is resented in Table 2-1.

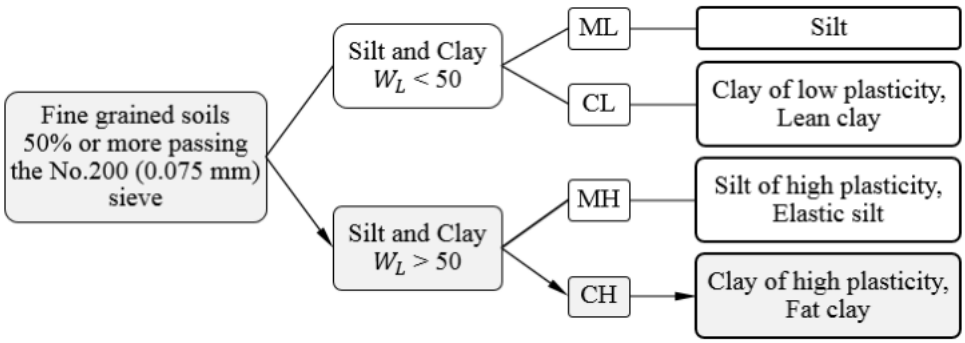

Table 2-1 Capture of the Unified Soil Classification System (USCS)

Based on the results above and the Table 2-1, the soils of Aine-Tine area are classified according to USCS classification system as CL and CH, which are inorganic clays of low and high plasticity, respectively where the clay content is more than 52% except in two samples where the sand percentile is much higher. The water of the samples was obtained following NF P 94-050. The results of the water content confirm that the soils of the Aine-Tine site are wet to very wet.

- Shear strength parameters:

As the pipeline is buried in the shallow layer which has undergone repetitive movements, it was decided to measure the peak and residual values of the parameters of shear strength. The results of the friction angle and cohesion of five different samples taken on the shallow layer in different locations of Aine-Tine site are presented in the Figure 2-11 and Figure 2-12. These values are used to verify the residual stability of Aine-Tine. The peak cohesion of Aine-Tine site ranges from 10 to 34 kPa while the residual is ranged between 4 and 9 kPa. On the other hand, the peak values of friction angle range from 15° to 22°. Besides, the residual values range from 8° to 11°.

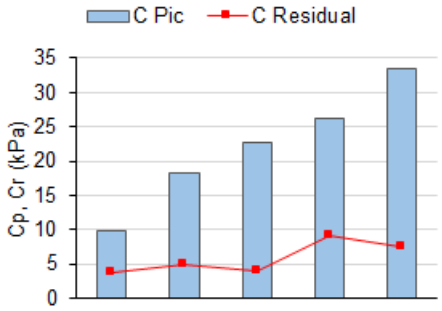

Figure 2-11 Peak and Residual cohesion

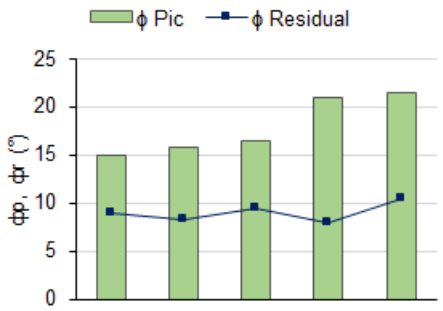

Figure 2-12 Peak and Residual friction angle

- Aine-Tine underground water table:

In Aine-Tine area, the GWT was found to be static and located at 13 to 15 m from the ground surface (LNHC Batna, 2016). The location of the GWT plays an important role solving of geotechnical problems. It controls the magnitudes of positive and negative water pressures that the soil develops. In the present study, the depth of 15 m is adopted to conduct the analyses.

- Negative and positive soil pore water pressure

The pores below the GWT are approximately filled with water this will generate a positive water pressure which is proportional with the distance from the GWT. In the contrary, the pores located above the GWT surface are partially filled with water where the filling rate is related to the distance from the GWT which is the main factor that controls the capillary rising and consequently the water content of soil. The partially saturated soils develop a new component of stress which is called by the geotechnical community the negative water pressure which attracted the attention of many researchers and practitioner on recent decades (Biot, 1941).

- Standard Penetration Test SPT

In order to have an idea about the underground constitution (layer, consistence, …), the second geotechnical campaign was planned to include SPT boreholes. The method of SPT consists in getting the idea about the consistency of a soil in depth by calculating the number of blows required to drive the SPT cone for 30 cm deep. The SPT boreholes were carried out where for each 1.5m depth for 25 m depth which appears to be sufficient to describe the layering constitution using the geological criterion. The results of the SPT are shown in Figure 2-14.

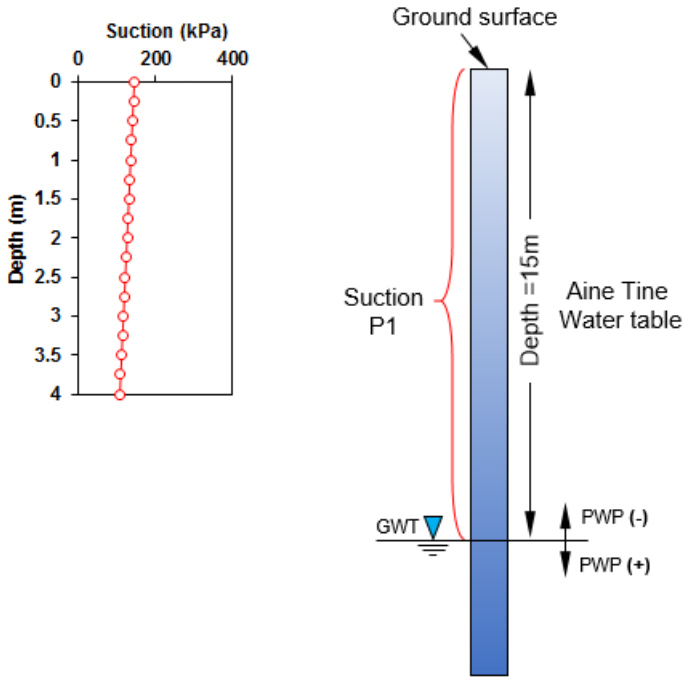

Figure 2-13. The GWT of Aine-Tine site and its suction profile

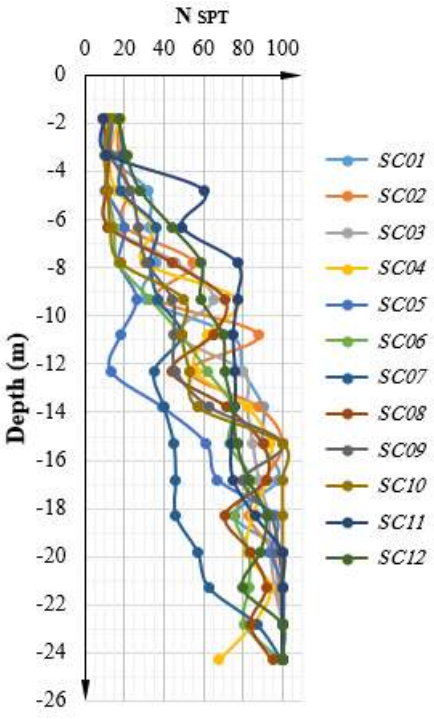

Figure 2-14. SPT Results

Figure 2-15. SPT location on the site of Aine-Tine.

According to the Engineering Manual EM 1110-2-2504 of the US Army Corps of Engineers published in 1994 (Table 2-2), the obtained values of the SPT (N_{SPT}<20) indicate that the surficial layer (0m<z<6-8m) of the Aine-Tine site present weak relative densities which range from very loose to medium where the bulk density (M_s/V_t) range from 1600 to 2100 kg/m^3.

Table 2-2. Correlation between relative density NSPT and Bulk density (Teng, 1962)

Compactness	Relative density (%)	N_{SPT} value	Bulk density (kg/m³)
Very loose	0 - 15	0 - 4	< 1600
Loose	16 - 35	5 - 10	1530 - 2000
Medium	36 - 65	11 - 30	1750 - 2100
Dense	66 - 85	31 - 50	1750 - 2245
Very dense	86 - 100	> 50	> 2100

2.2.6. Climatic conditions

Aine-Tine slope is located in the Mila province which bears a semi-arid climate to mild winter surrounded on both sides by a cool sub-humid climate characteristic of mountainous terrain. The study area belongs to the semi-arid climate that receives precipitation below potential evapotranspiration, but not as low as a desert climate. The semi-arid climate is characterized by two seasons: Hot dry in summer and cold rainy in winter. the Mila province is marked by fairly large temperature variations; the temperatures in summer are quite high and are around 40 °C. In winter, they are generally low and can sometimes drop below zero degrees. Detailed investigations of the hydrological properties of the eastern side of Algeria. Mebarki (2005) indicated that the annual average precipitation in Mila province is 678.5 mm/years. In 1984 the maximum annual precipitation reached 1058 mm. The maximum monthly average is between 120 and 145 mm/month (i.e. December). During the period from October to April, each year, the precipitation

in Mila primarily occurs where December in the rainiest month. Mila is geotechnical problems prone area (i.e., landslides and a shrink/swell movements) in which the precipitation is the principle trigger of these phenomena especially during wet seasons. The great instabilities are due to the high sensitivity of the clayey soils, mainly related to the decrease in suction following precipitations. Based on the in-situ investigations results, the GWT level has been found to be located at about 15 m depth.

Based on a consistent work about landslides in Mila municipality, Chettah (2009) reported that the rainfall map for Algeria shows a geographical distribution of precipitations characterized by a general decrease from north to south and from east to west. The average precipitation ranges between 2000 mm/year at high altitudes at the edge of the Mediterranean Sea and falls to less than 600 mm/year in October on the high plains, and then decreases until it reaches a value of 100 mm/year in the Central Sahara region. It can be noticed from the Ombrothermal curve of Figure 2-16 that the dry season spans from November to mid-April.

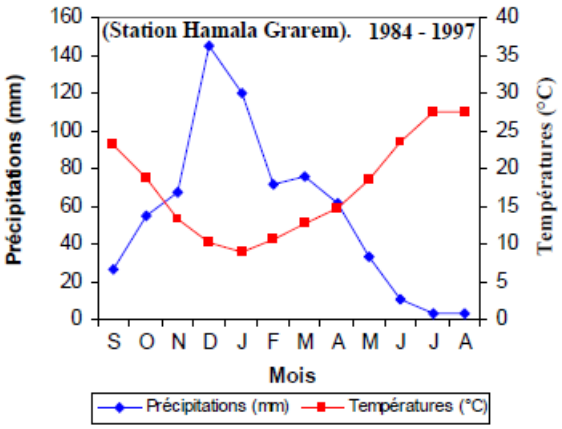

Figure 2-16. Ombrothermal curve of the Hamala-Grarem station (1984-1997) (Chettah, 2009)

2.2.7. Conclusion

The Aine-Tine site conditions have been presented in this part where the geotechnical characteristics of Aine-Tine site are not sufficient for the analysis of soil structure interaction where the unsaturated behavior is needed. For this reasons we have used several published results on similar soils to determine the unsaturated soil characteristics such as the curve of water retention or the SWCC which is mainly related to the size of pores.

2.3. Aine-Tine Slope Stability Verification (PART I)

2.3.1. Introduction

In many part of the world, landslides cause important human lives and economic losses caused by landslides are very important (Conforth, 2005). The stability of natural slopes is an issue to both the geotechnical community as well as to researchers (Khemissa, 2006). There is an increasing recognition of the need for assessment of landslide susceptibility and hazard and for landslide risk management (Chowdhury, 2010) of urban regions. The Aine-Tine pipeline suffers from the movements that occur in the sloping soil of Mila basin. This chapter is devoted to study the susceptibility of the slope to landside occurrence.

2.3.2. Geometry

In slope stability study, the geometry and layering of the slope are the main factors that govern the stability of the slope. Unlike man made slopes, the natural slopes have complicated geometries which need more caring about this important parameter. To overcome this topographic problems, many researchers have integrated the Geographic Information System (GIS) (Xie et al., 2004) (Xie et al., 2006) (Dahal et al., 2008) to get more realistic topographic data of the analysed lands and consequently more reliable results about the stability of slopes. The Aine-Tine slope is a natural slope with a complex geometry which requires the integration of the GIS technology to build a realistic geometry.

In the present part of thesis, we have used a GIS technique called the **Photogrammetry** which consists of a series of coherent steps to obtain the component of the coordinates of the terrain in abscissa, ordinate and elevation from the processing of satellite images. The first part of the processing which is the generation of the global topographic survey was carried out in the engineering office Cabinet du Géometre Expert Foncier SIDHOUM Sebti". The second part was carried out in the engineering office of technical studies SETS which includes the generation of the elevation profiles Y_i as shown Figure 2-17 using CIVIL3D software. The same procedures was used by Shen et al. (2012) to verify the stability of the Xuecheng slope which is a natural slope modified by human activity located in the province of Sichuan at the southwest of China.

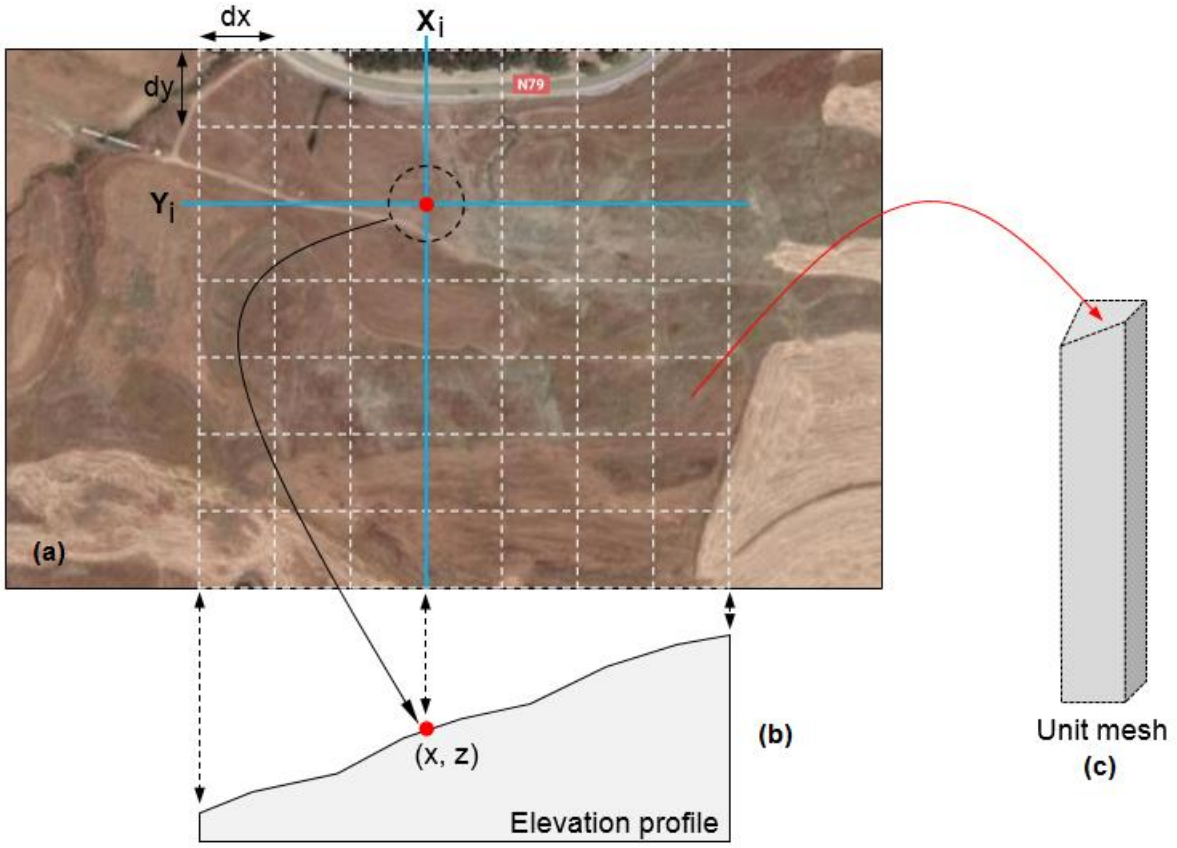

Figure 2-17. The scheme of the geometry construction

The satellite image used in the obtaining of the topographic data in the present study area were bought from the Institut National de Cartographie et de Télédetection (INCT). It was found that the most updated image of the Mila basin is the one produced in 1984.

Figure 2-18 shows the elevation data profile obtained at fixed ordinate Y_i and for different values of X_i which is sufficient to build the 2D cross section for the numerical model as shown in Figure 2-22. With an offset of **dy** or **dx** fixed by the user, based on the required precision, the creation of the next profiles Y_{i+1} allow the software to generate the elementary units of the geometry. The used offset in the present study is 5m which is consistent with the density of the topographic data offered by the photogrammetry technique.

TOPOTAB - Notepad

File Edit Format View Help

```
; Tables of interpolated data from contour map
;  Table number corresponds to constant y = 5
;  with each x,z pair at point where the line intersects a contour level
;
;  Table 1 => y = 0
table 1 0 950
table 1 20 925
table 1 64 900
table 1 130 875
table 1 160 875
table 1 315 900
table 1 353 875
table 1 425 870

;  Table 2 => y = 5
table 2 0 910
table 2 20 925
table 2 50 925
table 2 110 900
table 2 180 900
table 2 215 925
table 2 276 950
table 2 306 925
table 2 425 900

;  Table 3 @ y = 10
table 3 0 890
table 3 122 875
```

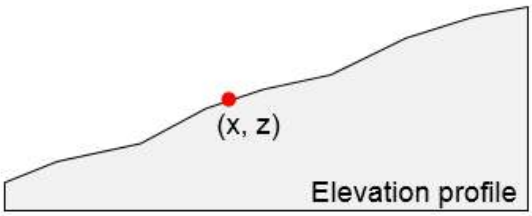

Figure 2-18. Topographic data of the cross section elevations

2.3.1. FISH language

FISH is a programming language embedded within FLAC3D that enables the user to define new variables and functions. These functions may be used to extend FLAC3D's usefulness or add user defined features. For example, new variables may be plotted or printed, special grid generators may be implemented, servo-control may be applied to a numerical test, unusual distributions of properties may be specified and parameter studies may be automated (ITASCA, 2005a).

The FISH program developed and used to build the geometry of the 2D and 3D models is shown in the Figure 2-19 which can be called by writing the command line: [call topo] which allow the software to generate the elementary element used in this analyis which is the element **brick** in the case of the 2D models and the element **wedge** for the 3D model as shown in Figure 2-22 and Figure 2-23, respectively.

TOPO - Notepad

File Edit Format View Help

```
; Fish function to generate a model surface from a topographic map
; FISH variables:
;    dx_size     :  element size in x-direction
;    dy_size     :  element size in y-direction
;    n_zon_col   :  number of elements in x-direction
;    n_zon_row   :  number of elements in y-direction
;    z_base      :  elevation (in z-direction) of base of brick primitive
;    z_size      :  number of elements in z-direction
;    xor         :  minimum x-coordinate
;    yor         :  minimum y-coordinate
; Enter the command TOPO to invoke this function
;
def topo
loop i (1,n_zon_col)
  loop j(1,n_zon_row)
     x1=xor+dx_size*(i-1)
     x2=x1+dx_size
     y1=yor+dy_size*(j-1)
     y2=y1+dy_size
     z1=table(j,x1)
     z2=table(j+1,x1)
     z3=table(j+1,x2)
     z4=table(j,x2)
     zb=z_base
     zs=z_size
     command
       gen zon brick p0 x1 y1 zb p1 x2 y1 zb p2 x1 y2 zb p3 x1 y1 z1 &
                     p4 x2 y2 zb p5 x1 y2 z2 p6 x2 y1 z4 p7 x2 y2 z3 &
                     size 1 1 zs
     end_command
   end_loop
end_loop
end
```

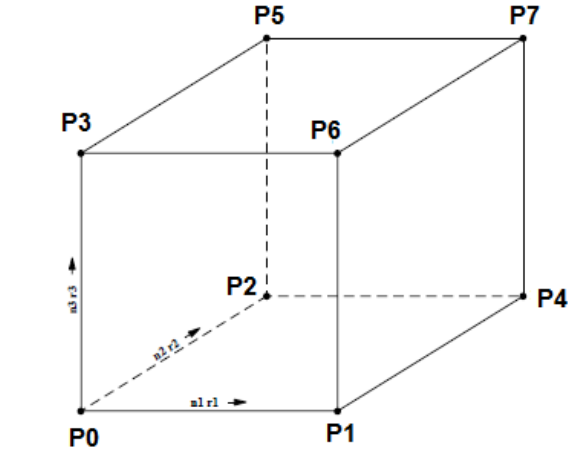

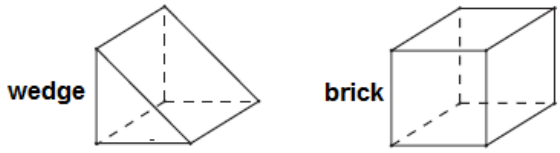

Figure 2-19. The FISH function to built the geometry

In addition to the sizes of the elementary units (brick and wedge) in the x and y direction and knowing the number of columns (**n_zon_col)** and lines (**n_zon_row)** fixed previously and shown as the grid shown in Figure 2-17, by calling the function shown in Figure 2-20 allow the generation of geometries using the **topotab.dat** and **topo.fis** which contain the elevation data and the way of reading these data, respectively.

TOPO-1 - Notepad

File Edit Format View Help

```
; Geometry creation
ca topotab.dat
ca topo.fis
set n_zon_col=10 n_zon_row=10 z_base=500 z_size=5 dx_size=40. dy_size=40.
set xor=0 yor=0
topo

plot set rot 45 45 45
plot show
```

Figure 2-20. Function of the geometry creation

2.3.2. FISH language with FLAC 2D and 3D

- 2D verification of the FoS

In order to simplify simulations and obtain quick results by choosing the most vulnerable cross sections, which requires certain conditions to be applied (symmetry and homogeneity). In 2D numerical simulation only the safety factor and the potential failure line for some particular cross section which is selected in advance can be obtained (Shen et al., 2012).

The Digital Elevation Model (DEM) shown in Figure 2-21 is obtained from the topographic data on the site of the slope, then a treatment of a 5mx5m grid mapping is done using a treatment process to model the topography of slope in its 3D shape. This process also allows to choose the cross sections in any position, and to install a non-uniform distribution of the characteristics according to the depth (i.e. the cohesion).

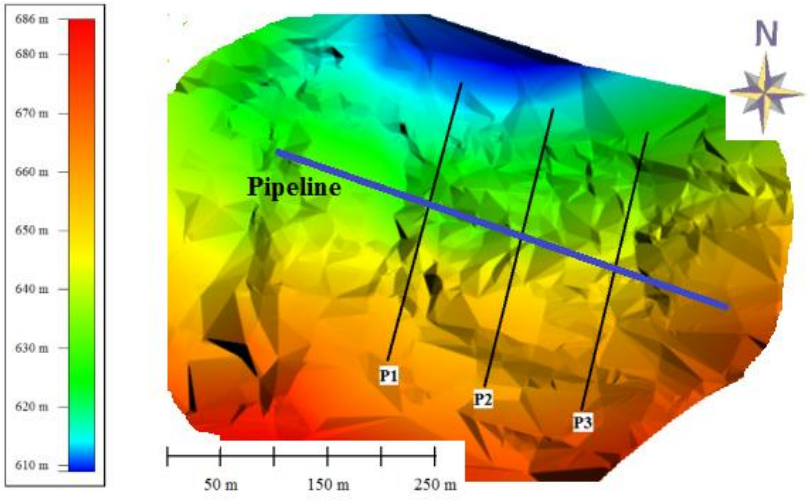

Figure 2-21. DEM of the Aine-Tine Slope

The three cross sections which are subjected to this analysis are located in Middle (P2: Cross-Section-02), West (P1: Cross-Section-01) and East (P3: Cross-Section-03) of the slope as shown

in Figure 2-21. Natural slopes and their corresponding 2D grid geometries are presented in Figure 2-22.

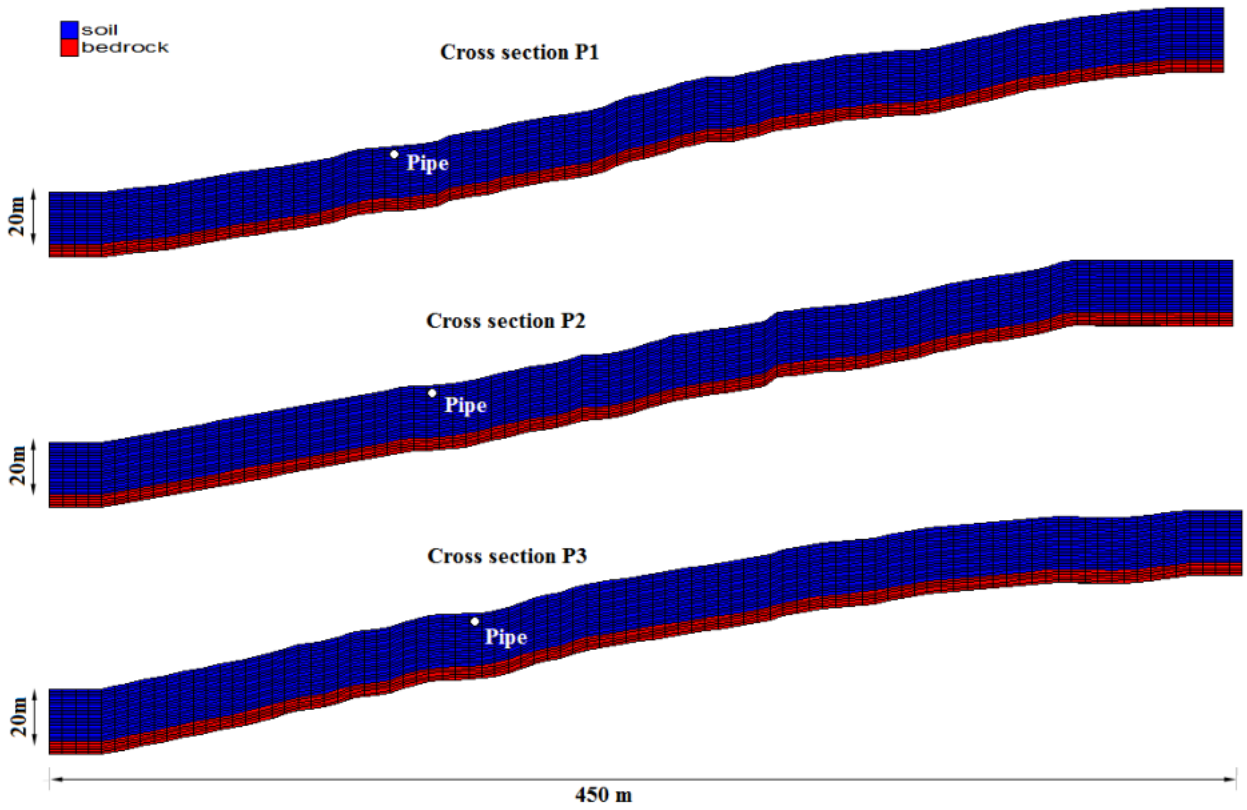

Figure 2-22. Cross section profiles P1, P2 and P3 (Bouatia and Demagh, 2019)

- 3D verification of the FoS

  For complex and heterogeneous slopes, 2D stability analysis is inappropriate and leads to an underestimate of the safety factors with inaccurate results (Shen et al., 2012). Ain-Tine slope is a heterogeneous slope because of the complex topography and morphology of the site. 3D numerical analysis was carried out for more accuracy results but it will be take a significant resolution time because of the high number of nodes and zones comparing with the 2D model. A treatment of a 5mx5m grid mapping is done using a treatment process to model the topography of slope in its 3D shape. This process also offers the same possibilities as the one developed in 2D.

  The 3D model in finite difference is constructed by assembling a wedge element of 5mx5m matrix in (x, y) direction and variable in z direction as shown in Figure 2-23 to obtain 160.720 zones and 87.150 nodes as numerical size of the 3D model, divided in two layers. The first denser mesh layer is the soil of 20 m thick, the second is the bedrock with less mesh density.

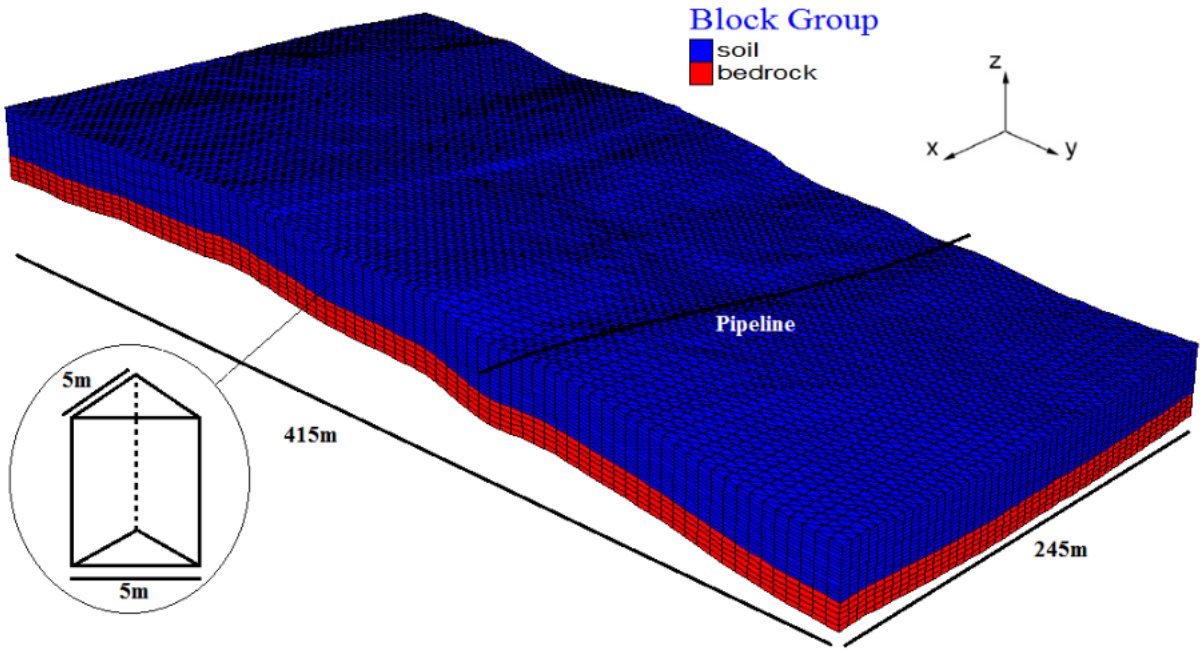

Figure 2-23. 3D numerical model of Ain-Tine slope.

The numerical model used in this analyses is composed of two-layer soil and rock. The geotechnical parameters of the slope are presented in the Table 2-3, they were obtained from the report of geotechnical investigations performed by LNHC during the year 2016 and which include in-situ and laboratory tests. The geotechnical report indicates the existence of a uniform gradient of the cohesion with the depth which begin from 20 kPa at surface with a gradient equal to 1 kPa/m. During the Standard Penetration Tests (SPT), the refusal was reached at approximately 20-meter depth. The latter is the reason to choose the interface between soil and rock as parallel to the ground surface of the slope and having constant depth of 20 m (Figure 2-24).

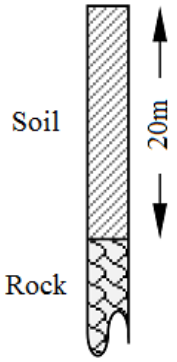

Figure 2-24. Geotechnical models

Table 2-3. Slope Mechanical Parameters (LNHC-Batna, 2016)

Layer	γ(kN/m3)	C (kPa)	φ (°)	Tension (kPa)	Bulk (GPa)	Shear (GPa)
Soil	20.0	20	12	5	2.80	0.80
Rock	21.7	100	40	50	25	15

The elastic constants K and G, rather than Young's modulus E, and Poisson's ratio ν, are used in FLAC because it is believed that bulk and shear moduli correspond to more fundamental aspects of material behavior than do Young's modulus and Poisson's ratio. The equations to convert (E, ϑ) to (K, G) are as follow:

$$K = E/3(1 - 2\vartheta) \quad \text{Equation 1}$$

$$G = E/2(1 + \vartheta) \quad \text{Equation 2}$$

The pair (K, G) makes sense for all elastic materials. The pair (E, ϑ) does not make sense for certain admissible materials. At one extreme, we have materials that resist volumetric change but not shear; at the other extreme, materials that resist shear but not volumetric change. The first type of material corresponds to finite K and zero G, and the second to zero K and finite G. However, the pair (E, ϑ) is not able to characterize either the first or the second type of material (ITASCA, 2005b).

2.3.3. Results and discussion

2.3.3.1. The factor of safety 2D

The results of the factor of safety of the three cross sections are presented in Table 2-4. The cross section P1 presents the weakest factor of safety (i.e., 1.08). Generally, a slope is considered as stable when it has a factor of safety higher than 1.5 which is not the case in the Aine tine slope. Using the weighted average procedure defined by Lambe and Whitman (1969) to have an idea about the global safety of slopes, the overall factor of safety (3D) can be calculated as follow:

$$FoS = (\sum_{i=1}^{n} FoS_i * A_i)/\sum_{i=1}^{n} A_i \quad \text{Equation 3}$$

Where, FoS_i is the factor of safety for each cross section, A_i is the area concerned by the movement for the same cross section i and n is the number of the cross sections chosen for the analysis. the area A_i can be obtained by plotting the component of the displacement in the direction of the sliding movement or by plotting the shear strain contour which show clearly the shear surface and then the land in movement becomes possible which is simply the area above the shear plane. The results of the 2D simulations are summarized in Table 2-4.

Table 2-4 FoS with 2D simulations

Cross section	P1	P2	P3	Weighted Average (3D)
Safety Factor	1.08	1.10	1.12	1.10

Figure 2-25 shows the vector of displacements along the three cross sections of Aine-Tine slope. With this representation, the slip surface can be easily drawn whereas, considering the cross section P1 and P2, the pipeline is located approximately at the toe of the sliding masses where in the case of P3, it is located at the center of the sliding mass. The Figure 2-26 show the contour of displacements along the slope. The pipe is subjected to a horizontal displacement which reaches 1 cm in the case of sections P1 and P2 where in the case of P3 the displacement is measured with millimeters reaching from 5 to 6 mm.

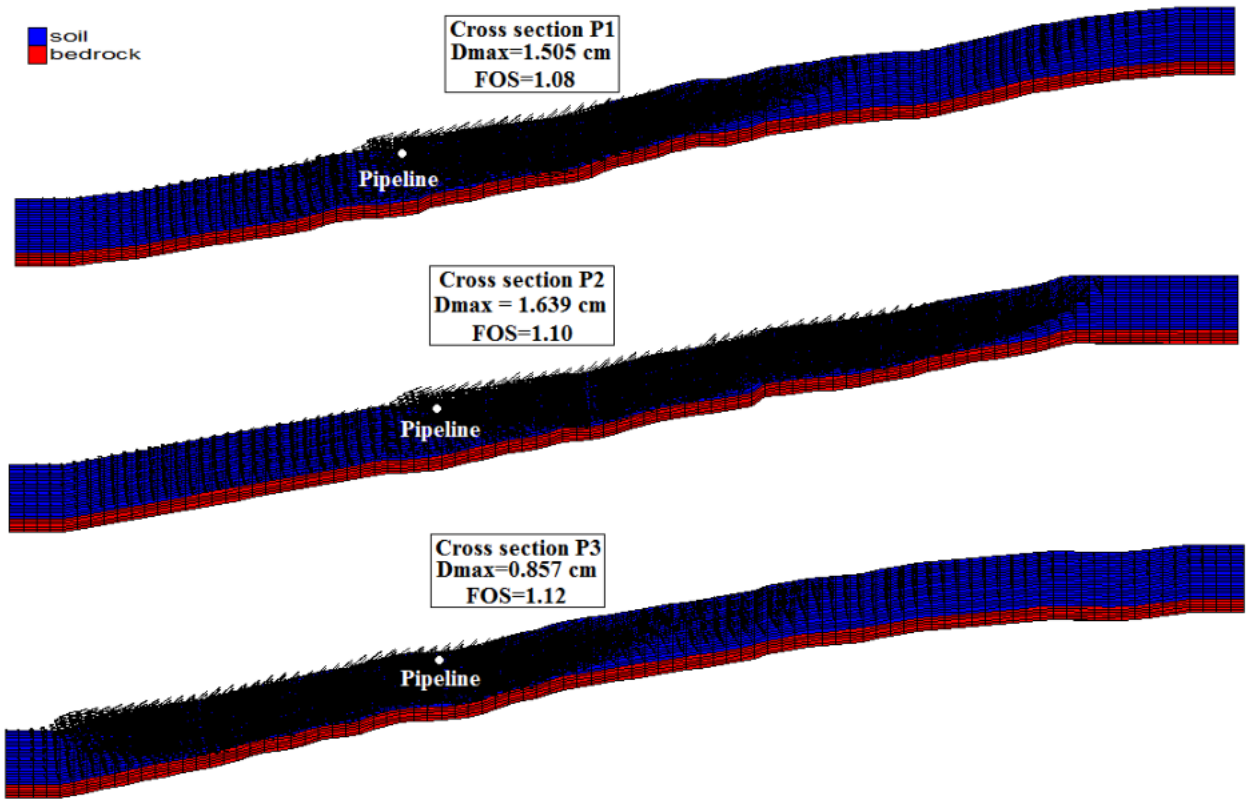

Figure 2-25. Vector of displacements in 2D cross sections

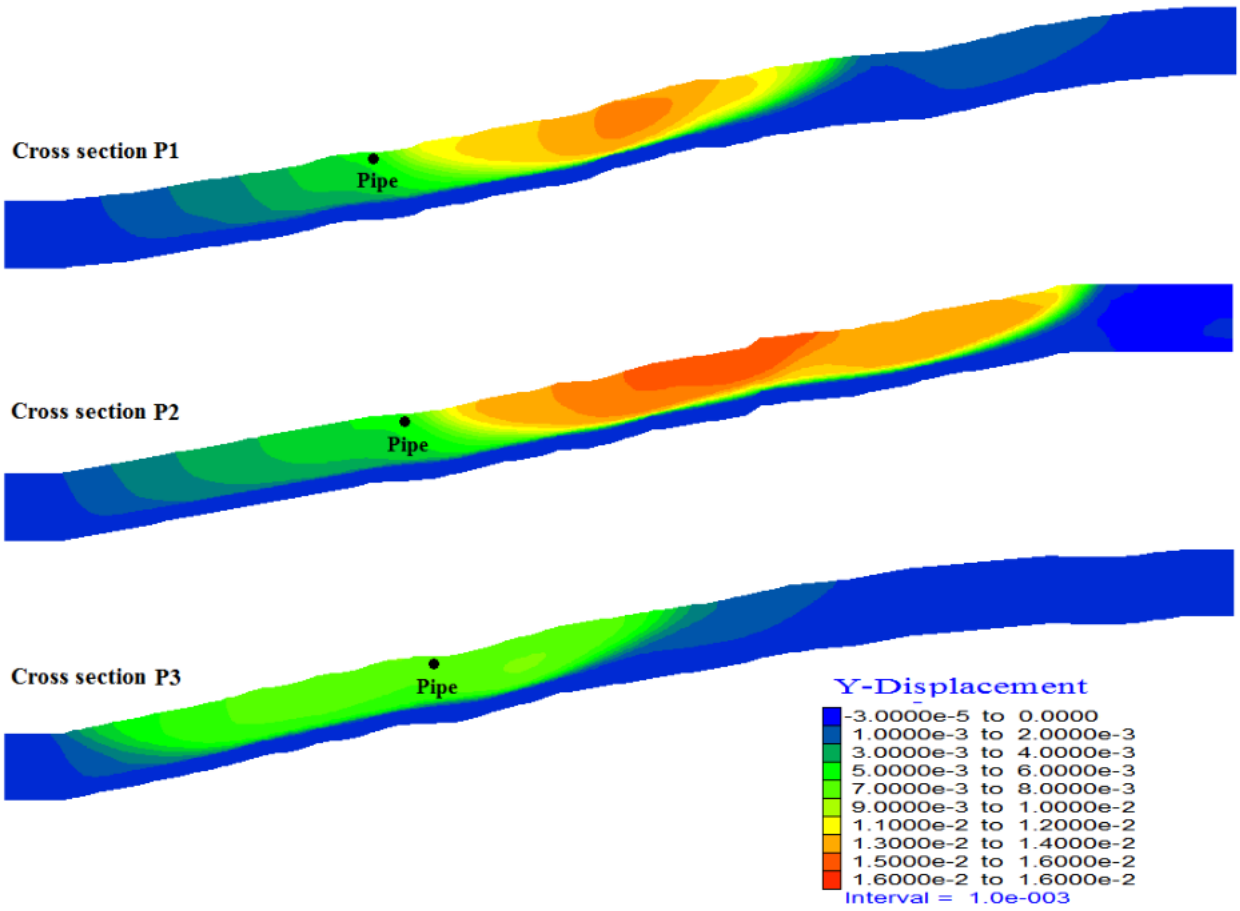

Figure 2-26. Y-Displacements magnitudes in 2D cross sections

2.3.3.1. The factor of safety 3D

The 3D safety factor calculated using FLAC3D strength reduction method is equal to 1.14, which is higher by 5.5% than the minimum 2D safety factor (i.e. 1.08), higher by 3.6% than the average 2D weighted factor of safety (i.e. 1.10) which confirm that 2D slope stability analysis always provides a more conservative estimate of the 3D slope stability problem (Fredlund et al., 2018). After the shear strength has been reduced by a coefficient of 1.14, the displacements in x, y and z directions and the slope state are shown Figure 2-27.

The major displacements on Y direction are concentrated in the eastern side of slope (represented by cross section 3). The major displacements on x direction are concentrated in the eastern side of slope (represented by cross section 3).

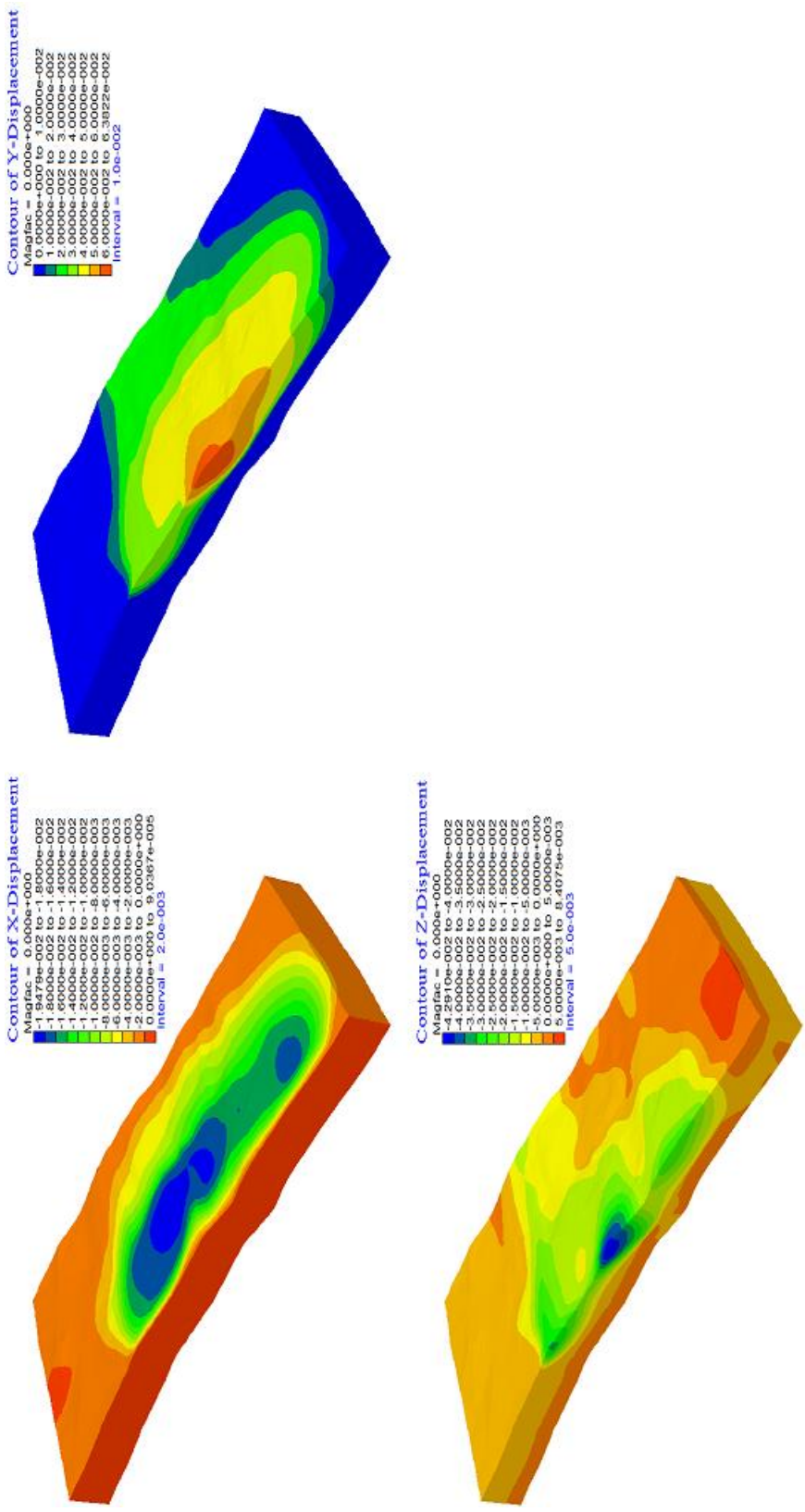

Figure 2-27. XYZ Displacements in 3D

2.3.4. Location of the slip surface using Shear Strain Increment

While doing the research we have developed a FISH program to locate the slip surface in 3D. The location of the slip surface in 3D depth, in extension and in shape is very helpful for engineers to guide and control their solutions while designing infrastructures. The obtained results are shown in Figure 2-28 – 30. The FISH program developed is based on the determination of the zone subjected to high values of shear strain increment SSI which is a helpful way that can give information about the critical depth within the layers of the site and consequently they can be taken into consideration during the treatment of the slope.

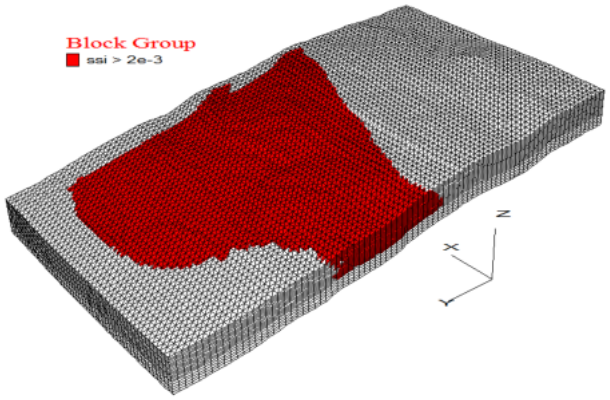

Figure 2-28. Location of the slip surface with SSI=2e-3

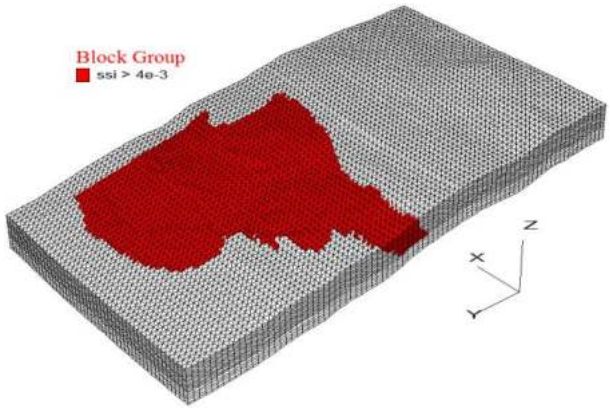

Figure 2-29. Location of the slip surface with SSI=4e-3

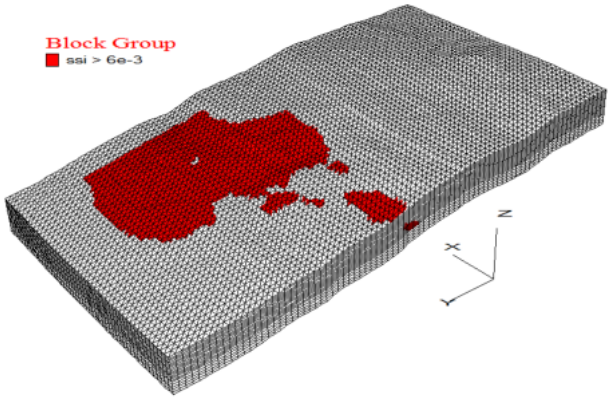

Figure 2-30. Location of the slip surface with SSI=6e-3

Figure 2-28 shows the zones where the shear strain increment is higher than 2.10^{-3}. Figure 2-30 shows the same parameters but with shear strain increment higher than 6.10^{-3}. Based on the comparison of the three figures, it can be seen that the higher the value of the shear strain increment, the smaller the red area indicating the areas most exposed to high shear strain.

2.3.5. Interaction of our site with other infrastructures

Under the high demand for transport, the government decided to duplicate the national highway RN79 which connects the city of Constantine to Mila. Unfortunately, the corridor of the road crosses the slope site, for this reason we thought necessary to consider the effect of this project development on the pipeline. The geometry of the model is shown in Figure 2-31. At this thesis we developed the model which can be very helpful for engineers and future researchers.

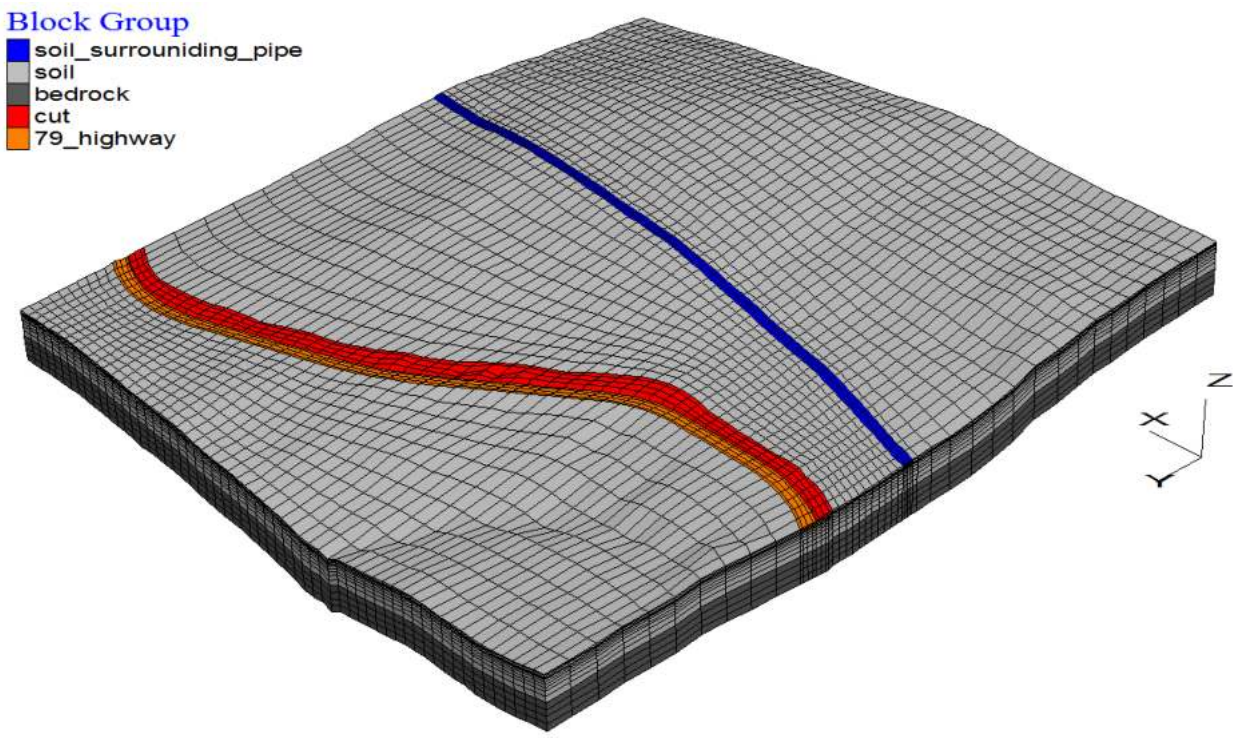

Figure 2-31. Interaction of the Aine Tine pipeline with the duplication of the RN79.

The model shown in Figure 2-34 has been constructed using FISH program developed to build the geometry of the model using volumetric brick elements (Figure 2-32) for the soil zones and structural shell elements for the pipeline. The blue zones of the surrounding soil of the pipeline have been built using the volumetric radial cylinder elements (Figure 2-32). The brick element is an eight noded element while the radial cylinder is twelve noded element.

Figure 2-32. Primitive mesh shapes of the 3D model

The structural shell elements used to construct the pipeline are three noded, flat finite elements joined to each other (Figure 2-33) to construct the pipeline body.

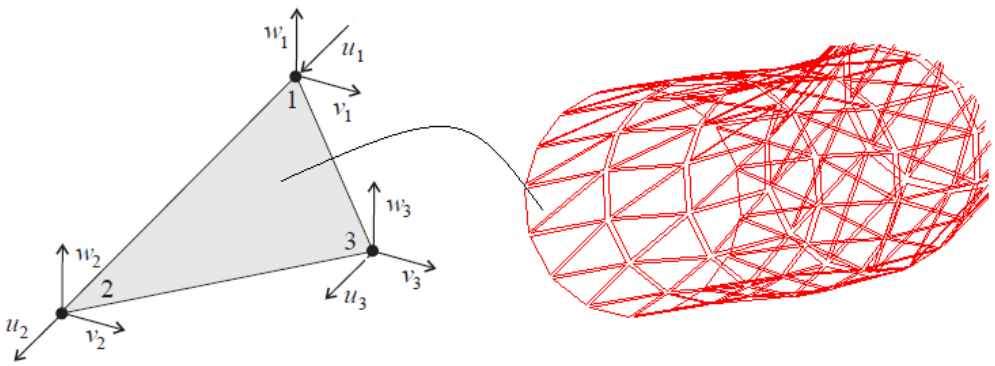

Figure 2-33. Shell structural element to build the pipeline geometry

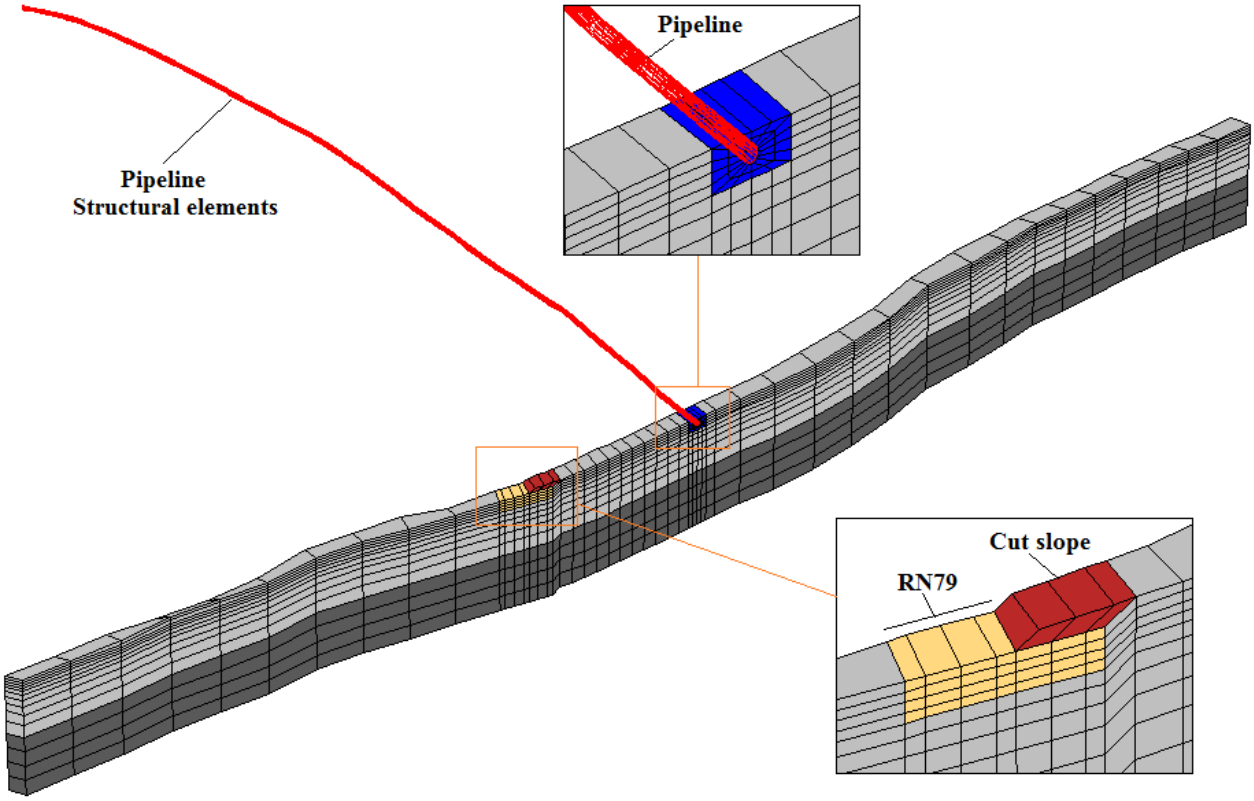

Figure 2-34. Details of the 3D model of the duplication of the RN79 highway

2.3.6. Conclusion

In this part of the chapter, 2D and 3D numerical simulation of Aine-Tine slope stability sliding susceptibility which shall contain a buried pipeline of water transfer was carried out. The potential of stability is evaluated in terms of safety factor and displacements field. The simulations were carried out using the finite difference code FLAC and FLAC3D. This study is started by preparing the 2D in plane strain model and the 3D model (global stability) of the slope.

The results obtained have shown that the Aine-Tine slope gives very low safety factors under natural conditions. These safety factor of Aine-Tine slope would be revised in the next section case of a rapid saturation of the soil mass (natural saturation due to high rainfall or an accidental break of the water pipeline for example). The results of the 3D simulations show that the maximum

displacements are concentrated in the middle of the slope, so the risk is all the greater as the buried pipe is close to the middle of the natural slope. In anyway, these results are comforted by the 2D simulations also.

This study allowed us to confirm that the safety factors calculated using 2D methods are more conservative than those estimated using the 3D model, the latter was more realistic by taking into account the overall slope of the massif with all its topography conditions. Moreover, a poorly justified choice of any cross-section can lead us to make decisions that are too hasty and risky, as is the case with the cross-section 01 if it had been taken alone as reference to estimate the stability of the slope of Ain-Tine. 3D slope stability analysis can be used to achieve more realistic design and be a good decision-making tool to provide the best solutions to more effectively stabilize the expected high displacements.

2.4. Shallow Layer Stability Analysis of Unsaturated Slopes (PART II)

2.4.1. Introduction

Hydraulic and geometric factors control the stability of slopes. This paper discusses the sensitivity of the Factor of safety (FoS) of the shallow layers of unsaturated slopes to the Soil Water Characteristic Curve (SWCC) as a hydraulic factor and the sloping angle as a geometric factor. The obtained results highlighted the importance of the hydraulic (i.e., SWCC) and geometric (i.e., sloping angle) factors while evaluating the stability of unsaturated slopes.

Unsaturated soils are problematic soil formations that are generally located in arid and semi-arid regions, including some tropical areas around the world. The unsaturated soils are an active subject to the research and professional community due to the sensitivity of their behaviours to the moisture content changes, which is associated with many factors such as rainfall, evapotranspiration and GWT depths. The negative pore water pressure (PWP) (suction) present in the unsaturated soils considerably contributes towards the mechanical behavior of such soils as well as to the shear strength and, in turn, the performances of an unsaturated soil above the GWT will be improved (Biot, 1941) (Gerard, 1965) (Fredlund and Rahardjo, 1993) (Karube and Kawai, 2001) (Sheng et al., 2011) (Patil et al., 2018) (Akin and Likos, 2020).

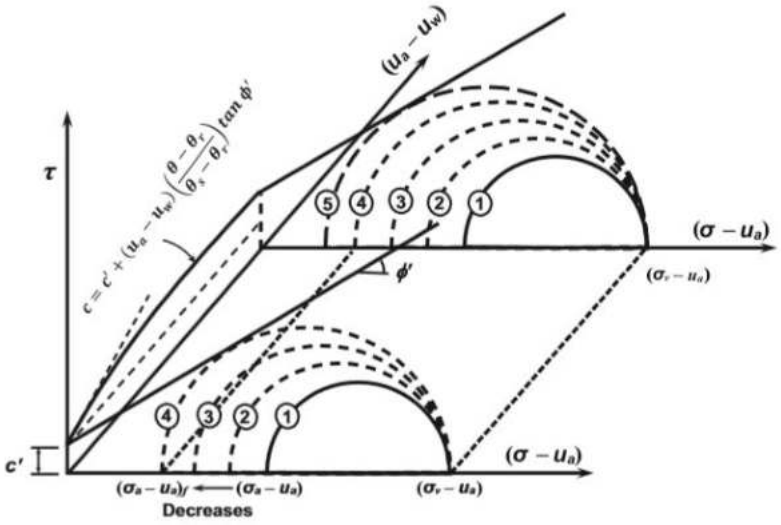

Figure 2-35. Relationship of shear strength and suction

Han et al. (2016) described the suction as a potential energy which holds the soil particles and their packets together by providing tension stress leading to the improvement of unsaturated soils resistance to elastic and plastic deformations. In the slopes of semi-arid and arid regions, the shallow unsaturated layers are prone to failures which causes costly and repetitive damages to the linear infrastructures constructed within or on such slopes (i.e., pipelines, roads). Infinite slope formulation is one of the simplest and widely used methods to calculate the shear strength and consequently, to evaluate the factor of safety (FoS) of infinite slopes. In saturated soils, the Terzaghi's (1943) effective stress relation $(\sigma' = \sigma - u_w)$ is used to study geotechnical problems as well as the slope stability. Mohr-Coulomb (MC) is the widely used failure criterion for slope failure calculations in saturated soils. The application of the MC criterion within unsaturated soils

requires the information about the suction present within the soil skeleton and the definition of the way of its contribution towards the shear strength of such soils (Figure 2-35).

The information about the suction is defined within the soil-water characteristic curve ($SWCC$), which expresses the relationship between the volumetric water content (VWC) and the suction (Agus et al., 2001). Within the unsaturated soils, the water content increases as its suction decreases following wetting processes (i.e., rainfall or irrigation) and vice versa in the case of drying processes (i.e., evapotranspiration). The $SWCC$ is mainly related to the grain size distribution. For example, the relationship between the fine particle content and $SWCC$ shape has been discussed by Jiang et al. (2020). Based on the experimental results, a closed-form expression of the SWCC was established by van Genuchten (1980) (Equation 4). Fourteen years later, Fredlund and Xing (1994) proposed a semi-empirical model to estimate the *SWCC* based on laboratory investigations. The developed model has three fitting parameters a, n and m, which control the shape of the *SWCC*.

$$S = S_r + \frac{1-S_r}{\left[1+\left(\frac{u_a-u_w}{a}\right)^n\right]^m} \qquad \text{Equation 4}$$

Where S is the degree of saturation, (u_a-u_w) is the suction, S_r is the residual saturation and a, n, and m are fitting parameters where $n = 1/(1-m)$. The $SWCC$ is largely used in geo-environmental studies related with unsaturated soils such as:

- The prediction of shear strength of such soils (Fredlund et al., 1978) (Fredlund et al., 1996) (Vanapalli et al., 1996),
- The evaluation of the changes in moisture content inducing slope failures (i.e., Rainfall and GWT raising) (Kristo et al., 2017) (Qi and Vanapalli, 2015) (Lin and Zhong, 2019) (Doumbouya et al., 2020),
- The estimation of the volume changes (i.e., shrink and swelling) (Vu and Fredlund, 2004) (Vu and Fredlund, 2006) (Adem and Vanapalli, 2013) (Fredlund and Morgenstern, 1976)) and
- The calculation of the new values of the mechanical properties of these unsaturated mediums ((Karube and Kawai, 2001) (Oh et al., 2009) (Adem and Vanapalli, 2014) (Zhang et al., 2018).

In the direction of the definition of the way how the suction contributes towards the performances of unsaturated soils, the soil was considered as a three-phase medium, including the soil particles, pore air and pore water phases. Based on this three-phase distribution, Fredlund and Morgenstern (1978) proposed an extension of the Mohr-Coulomb failure criterion to predict the shear strength of the unsaturated soils by using two-state variables which are the net normal stress ($\sigma - u_a$) and the suction ($u_a - u_w$), where σ is the total stress, u_a is the pore-air pressure and u_w is the pore-water pressure (PWP). As an outcome of the new stress states description, Fredlund et al. (1996) developed a model to predict the shear strength of unsaturated soils using the $SWCC$ and the effective shear strength parameters (i.e., Cohesion and Friction angle). In the same year, Vanapalli et al. (1996) established a new expression to predict the shear strength of such soils with

respect to moisture content and suction values present in the unsaturated soil. These two models have been widely used to describe the unsaturated soil behavior in experimental and numerical published researches and also integrated in many software tools (i.e., GeoStudio)

Many studies have been directed to evaluate the effect of the $SWCC$ on the variation of the PWP within unsaturated soils. Zhang et al. (2004) studied the change of several suction profiles within unsaturated slopes, have different SWCCs under different ratios of rainfall-intensity to soil-permeability. For sand, Nguyen and Likitlersuang (2019) conducted a probabilistic analysis of the effect of spatial variability of the effective friction angle, saturated hydraulic conductivity, and the SWCC on the PWP variations in unsaturated soils where they found that the random field of the $SWCC$ produces a significant variation of the negative PWP (suction). The idea concluded based on the previously published works is the importance of the $SWCC$ role in the unsaturated soil mechanics as well as slope stability analysis expressed by its considerable effect on the PWP within such soils. However, studies of the influence of the $SWCC$ fitting parameters on the unsaturated slope stability analysis are limited.

The aim of this part of the chapter is to highlight the importance of considering the unsaturated behavior into consideration to evaluate slope stability. The natural slope of Aine-Tine from Mila province in Algeria was considered. The sensitivity of the safety of the Aine-Tine slope shallow layer to the SWCC's fitting parameters were assessed. The residual effective shear strength properties measured on Aine-Tine clayey soil are utilized as the input parameters in the FoS calculations. The one-dimensional infinite slope stability procedure, which is assumed to be appropriate in the case of Aine-Tine slope was used to evaluate the shear strength of this unsaturated slope. The values of the FoS at two depths (representing the top and bottom of the shallow layer) are calculated considering different sloping angles β to investigate the geometry effect on the safety factor. The suction values (negative PWP above the WT) of the Aine-Tine slope are obtained from the hydrostatic projection of the PWP profile present on the site. The results of the FoS are presented and commented where it was found that the combination, $SWCC$ (represented by the three fitting parameters a, n and m) and the sloping angle β, has a significant influence on the safety factor of unsaturated slopes.

2.4.2. Infinite slope procedure:

Infinite slope formulation is the appropriate procedure to estimate the shearing safety in the case of shallow failures in unsaturated slopes. Such a procedure was used by numerous researchers to carry out the slope stability of unsaturated soils (i.e., (Li et al., 2013) (Qi and Vanapalli, 2015)). Shallow failures are known by a very reduced depth-to-length ratio where the soils of the surficial unsaturated layer are highly sensitive to the hydraulic functions (i.e., $SWCC$, Permeability function). The estimation of the shear strength in such a procedure is based on the determination of the force equilibrium equation of a single vertical slice within the sliding mass in which the slip plane is assumed to be parallel to the ground surface. Figure 2-36 shows the force equilibrium scheme within a single slice having an angle of inclination β.

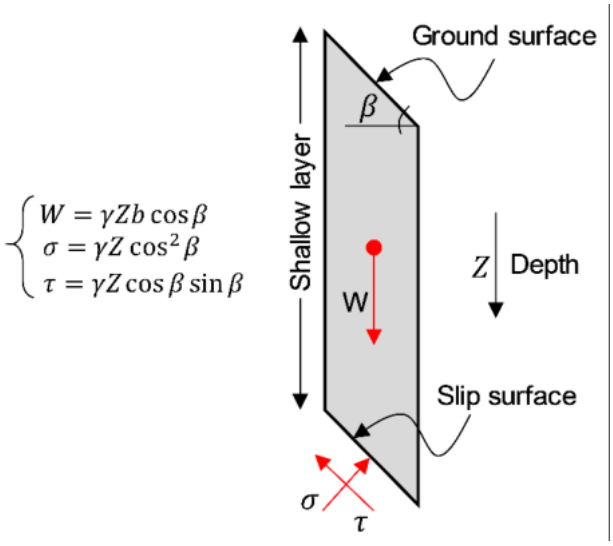

Figure 2-36 Force equilibrium scheme in infinite slope procedure

The FoS is defined as the shearing stress margin between the shear strength provided by the analysed soil and the mobilized shear stress developed at the slip surface; the same definition is also applied in limit equilibrium methods and accepted by the professional community:

$$FoS = \tau_f / \tau \qquad \text{Equation 5}$$

Where τ_f is the shear strength at the slip surface and τ is the mobilized shear stress. The estimation of the shear strength of unsaturated soils in the laboratory is a time-consuming procedure due to its dependency on the water content present in such soils (Lian et al., 2020). For this reason, many researchers developed semi-empirical models to predict the shear strength of such soils (i.e., Fredlund et al. (1978); Vanapalli et al. (1996)). The extension of the world over the years caused an increasing need to construct on and in the unsaturated soils and as a consequence, appeared the necessity to describe the behaviour of these soils. The expansion of the Mohr-Coulomb failure criterion to be applicable in unsaturated soils becomes possible. The Vanapalli et al. (1996) model to predict the shear strength of unsaturated soils which is based on the expansion of Mohr-Coulomb criterion is one of the most acceptable models, is used in this study:

$$\tau_f = c' + (\sigma - u_a)\tan\varphi' + (u_a - u_w)\left(\frac{\theta_w - \theta_r}{\theta_s - \theta_r}\right)\tan\varphi' \qquad \text{Equation 6}$$

Where, c' is the effective cohesion, φ' is the effective internal friction angle, $(\sigma - u_a)$ is the net normal stress, $(u_a - u_w)$ is the suction, θ_w is the volumetric water content, θ_r is the volumetric water content at residual state, θ_s is the volumetric water content at saturated state. The contribution of suction towards the unsaturated shear strength was defined by Vanapalli et al. (1996) as an additional cohesion proportionally related to the suction present in the unsaturated soil and its corresponding water content as shown in the third term of Equation 6. The unsaturated soil will have an apparent cohesion as follows:

$$c = c' + (u_a - u_w)\left(\frac{\theta_w - \theta_r}{\theta_s - \theta_r}\right)\tan\varphi' \qquad \text{Equation 7}$$

By the application of the force equilibrium scheme and considering the infinite slope formulation, the mobilised shear stress at the slip surface located at Z depth is written as follow:

$$\tau = \gamma Z \cos\beta \sin\beta \qquad \text{Equation 8}$$

Where γ is the total unit weight of the unsaturated soil. The FoS expression is obtained by substituting the Equation 6 and Equation 8 in the Equation 5:

$$FoS = \frac{c'}{\gamma Z \cos\beta \sin\beta} + \frac{\tan\varphi'}{\tan\beta} + \frac{(u_a - u_w)[(\theta_w - \theta_r)/(\theta_s - \theta_r)]\tan\varphi'}{\gamma Z \cos\beta \sin\beta} \qquad \text{Equation 9}$$

Looking at the FoS equation (Equation 9), it is clear that it is a summation of three terms which reflect the contributions of the (1) the effective cohesion c', (2) the effective friction angle φ' and (3) the suction $(u_a - u_w)$ (i.e., hydraulic term) towards the FoS, respectively. The information about the suction and the volumetric water content (VWC) needed in the third term are obtained from the $SWCC$.

2.4.1. Soil Water Characteristic Curve SWCC

The soil-water characteristic curve $SWCC$ or the soil retention curve is the characteristic function of unsaturated soils which relates the suction present in soil to the water content represented by the volumetric water content θ_w, degree of saturation S or by, usually, the normalized water content θ_w/θ_s (Figure 2-37). The $SWCC$ is generally composed of three zones of saturation state determined by three suction range zones which are:

- The saturated
- The transition
- The residual zone

One of the commonly used equation to build the SWCC curve for fine and coarse-grained soils over large suction range fluctuating from 0 to 10^6 kPa is the form developed by Fredlund and Xing (1994) as written in Equation 10, which will be used in the present paper to describe the shear strength variations within unsaturated soils.

$$\theta_w/\theta_s = \left\{\frac{1}{\ln\left[e+\left(\frac{u_a - u_w}{a}\right)^n\right]}\right\}^m \qquad \text{Equation 10}$$

Where a, n and m are fitting parameters and $(u_a - u_w)$ is the soil suction. The parameter a is the matric suction value at the inflection point (Figure 2-37). It is closely related to the air-entry value (AEV) of the soil. The AEV is the suction beyond which the soil begins the desaturation and indicates the end of the saturation zone and the beginning of the transition suction range between the saturated and residual zones. n is the slope of the SWCC at the inflection point, and m is associated with the residual water content. As shown in Equation 10, the SWCC is expressed as the variation of the normalized water content with respect to suction. The general shape of the SWCC is presented in Figure 2-37, where the normalized water content varies from 0 to 1. The normalized water content is equal to 1 for low values of suction (i.e., saturated conditions) where the soil pores are filled with water and goes to residual values for high values of suction (i.e.,

unsaturated conditions). The residual value of the normalized water content is mainly related to the type of soil.

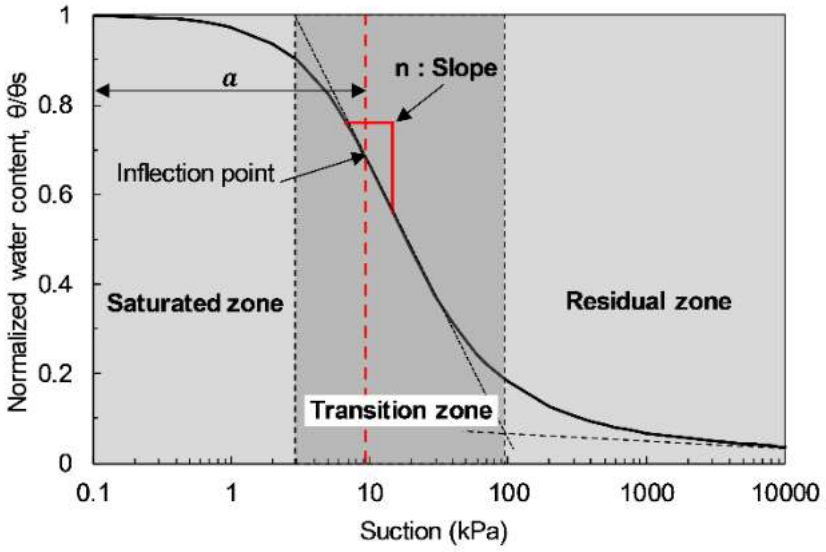

Figure 2-37 Soil Water Characteristic Curve SWCC.

In this study, the Fredlund and Xing (1994) general form of the SWCC to describe the suction and the volumetric water content relationship is assumed to be used instead the term $[(\theta_w - \theta_r)/(\theta_s - \theta_r)]$, because with the Fredlund and Xing's form, there is no need for the definition of the residual and saturated water contents. Following this assumption, The FoS expression becomes as follow:

$$FoS = \frac{c'}{\gamma Z \cos\beta \sin\beta} + \frac{\tan\varphi'}{\tan\beta} + \frac{(u_a - u_w)\left\{\frac{1}{\ln\left[e+\left(\frac{u_a-u_w}{a}\right)^n\right]}\right\}^m \tan\varphi'}{\gamma Z \cos\beta \sin\beta} \qquad \text{Equation 11}$$

With the new equation of the FoS presented in Equation 11, the third term of the FoS expression becomes a function of the fitting parameters a, n and m. At the saturation condition, where the pores of the soil are filled with water, the suction will be zero and the shear strength formula will take the form of the classic Terzaghi's (1943) effective shear strength form used in saturated conditions, this means that the developed semi-empirical model to predict the shear strength ensure the progressive transition between saturated and unsaturated conditions.

In this study, the infinite slope formulation is used to evaluate the sensitivity of the shallow layer FoS to (1) the SWCC by varying the three fitting parameters a, n and m in order to understand the effect of each constitutive parameter on the safety of unsaturated slopes and to (2) the sloping angle β values, through the use of four different values ranging from 10° to 45°, in order to assess the geometry factor effect. The necessary parameters to make calculations are the effective shear strength parameters (i.e., cohesion c' and friction angle φ') and the total unit weight of the soil and the information about the suction and the volumetric water content as well as the sloping angle. The suction and the volumetric water content within the unsaturated slopes vary with depth and they are mainly related to the GWT depth. For these reasons, and to understand the influence of

the depth on the safety of the unsaturated slopes, the FoS calculation will be carried out at two different depths, which represent the top and the bottom of the shallow layer. Aine-Tine slope from Mila province in Algeria is considered to carry out the present study.

2.4.2. The Aine Tine slope:

Aine-Tine slope is a natural unsaturated slope which takes the name of the municipality where it is located. It is very close to Azeba locality. Aine-Tine slope has an average length of 500 m, while the sloping angle is ranging between 15° and 25°, and can be lower or higher in some locations of the slope. Therefore, the assessment of the geometry effect on the FoS is required that's why the calculation of the FoS in this study were conducted using four sloping angles equal to 10°, 20°, 30°, and 45°.

Mila province where the slope is located is classified under a semi-arid climate which is characterized by seasonal rainfall deficits with high variations in water content of the soil in significant proportions between dry and wet seasons (i.e., summer and winter). Over time, the surficial layer of unsaturated regions has been altered by natural agents (i.e., previous slope failures), which weakened the mechanical performances of these soils, including the shear strength parameters. Through Aine-Tine slope area passes the 800 mm diameter buried water transport pipeline coming from Beni-Haroun dam (i.e., the largest dam in Algeria) to supply 12 municipalities by water. This pipeline suffered repetitive breaks expressed by permanent water leakages on the ground surface during the wet seasons (i.e., winter). This is mainly ascribed to the losses of the shear strength associated with the decrease of the soil suction following rainy events resulting in infiltration of the water within the shallow layer where the pipeline is buried.

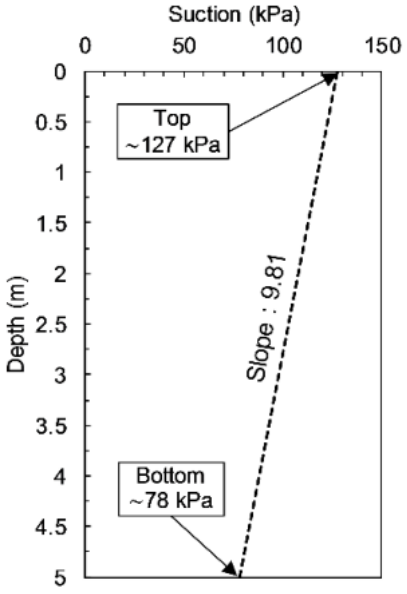

Figure 2-38 Suction profile within Aine-Tine shallow layer

The water suction which develops within the shallow layer is an essential parameter to predict the additional cohesion at the desired depth and to calculate the FoS; it is mainly related to the distance from the GWT level. A static GWT level is detected at 13 m depth in the study area. Using

the simplified hydrostatic projection of the positive PWP profile below the GWT, the negative PWP profile (suction) above the GWT was obtained, while the soil suction at the top and the bottom of the shallow layer can be found by multiplying their distances from the GWT by the gravity g (i.e., 9.81 N/kg). Figure 2-38 shows the suction profile along the Aine-Tine shallow layer. Therefore, the top and bottom suction values are equal to 127 kPa and 78 kPa, respectively.

The SWCC is the hydraulic characteristic of unsaturated soils used in this study to evaluate the influence of its constitutive fitting parameters a, n and m on the FoS. To understand the effect of each parameter on the shape of the SWCC the Figure 2-39 – 41 were plotted. The effect of the parameter a which has a stress unity and associated with the AEV can be highlighted from Figure 2-39, where four values of a are used which are 1, 10, 100, 1000 kPa while the values of n and m are set to 2 and 1, respectively. It is clear that the higher the value of a the higher the suction range of the saturated zone and consequently the transition suction zone will be moved to the right side in proportion with a value and still with the same range size because of the parameter n and m are constant. Generally, the AEV value is lesser than the parameters a.

It is very clear from Figure 2-40 that the parameter n controls the slope of the SWCC where the slope of the SWCC increases proportionally with this parameter resulting in the reduction of the transition suction range size between the saturated and residual conditions associated with an increase in the AEV. Looking at Figure 2-40 and Figure 2-41 simultaneously, it can be concluded that for small values of m, a moderate slope in the high suction range will be obtained associated with increasing of the AEV and the widening of the suction range relative to the transition zone, and for large values of n a sharp corner close to the AEV will be obtained.

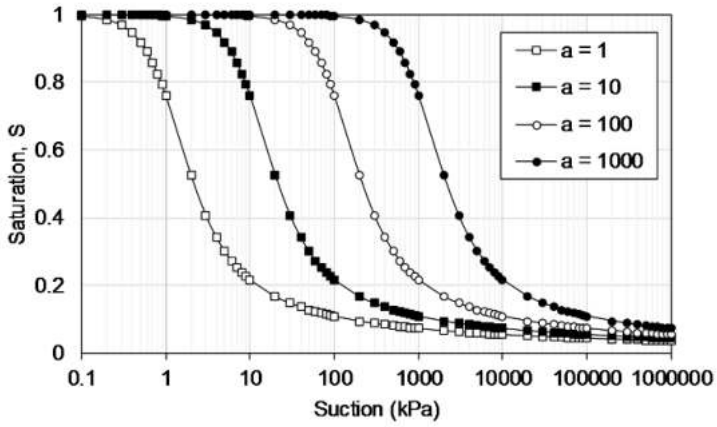

Figure 2-39 Effect of parameter a on the SWCC (n=2, m=1)

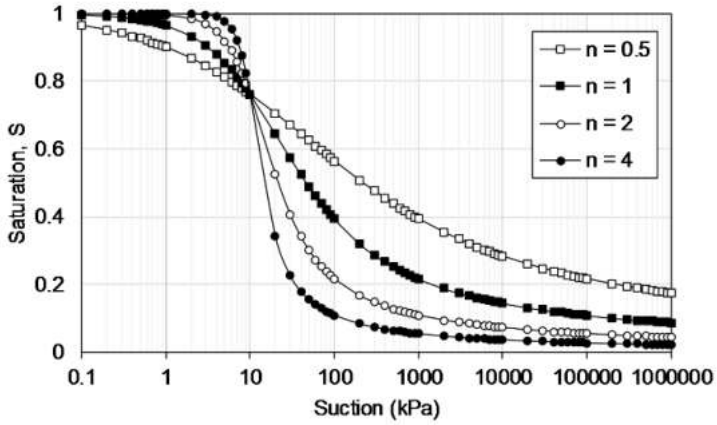

Figure 2-40 Effect of parameter n on the SWCC (a=10, m=1)

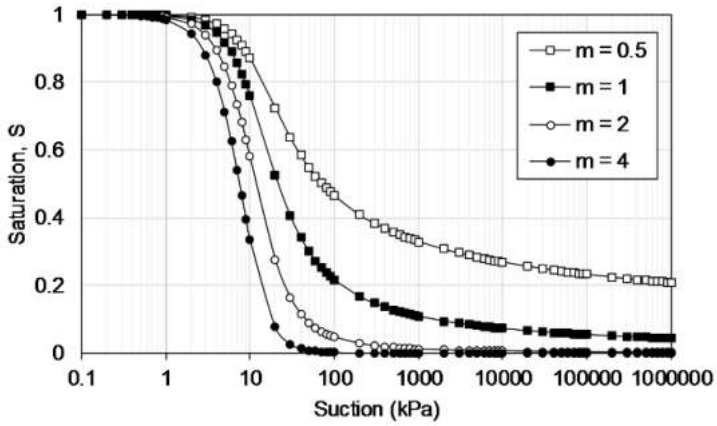

Figure 2-41 Effect of parameter m on the SWCC (a=10, n=2)

Table 2-5 Geotechnical parameters.

Parameter		**Value**
Density γ		18 kN/m3
Cohesion c'		7 kPa
Friction angle φ'		9°
Suction	Top	118 kPa
	Bottom	78 kPa
SWCC	a (n=2, m=1)	1 – 1000
	n (a=10, m=1)	0 – 5
	m (a=10, n=2)	0 – 5
Sloping angle β		10°, 20°, 30°, 45°

Based on the projection of the suction range present within the Aine-Tine shallow layer, it can be concluded that the higher the parameter a, the higher the obtained corresponding VWC, and consequently, the increase of the third term which is related to the resulting additional cohesion. In the case of the parameters n and m, it is the contrary, the higher the values of these two parameters the lower the corresponding VWC which will decrease the third term of the shear strength parameter. The geotechnical parameters used in this study are summarized in Table 2-5.

2.4.3. Results and discussion

In this study, the sensitivity of the slope stability in the surficial layer of the unsaturated slopes was assessed using the widely recognized infinite slope formulation. The assessment was conducted considering both the hydraulic and geometrical factors represented by the $SWCC$ and the sloping angle β, respectively. The effect of $SWCC$ was taken into consideration by studying the variation effect on the shear strength of the three constitutive fitting parameters (1) a ranging from 1 kPa to 1000 kPa, (2) n and m which ranged from 0 to 5. Four different sloping angles of the unsaturated slope are utilized to consider the effect of the slope geometry. Aine-Tine slope from Mila province in Algeria was considered to conduct the FoS calculation. To study the depth influence which is associated with the suction values and the overburden stresses, the calculations of the FoS were carried out at two different locations which represent the top and the bottom of the Aine-Tine shallow layer which is assumed to have 5 m thick based on the SPT investigations. Due to the weathered situation of the surficial soils in the Aine-Tine slope, the residual shear strength parameters were used. The suction present in the surficial layer was assumed to be the results of the hydrostatic projection of the PWP profile below the GWT. In the present study, the shear strength was estimated by using the combination of the semi-empirical model of the unsaturated shear strength prediction developed by Vanapalli et al. (1996) and the general form of the $SWCC$ established by Fredlund and Xing (1994) to obtain the soil suction and the volumetric water content values within the unsaturated soils which are essential parameters to predict the additional component of the apparent cohesion coming from the potential tension forces due to the unsaturated nature of such soils. The results of FoS corresponding to different combinations are presented in Figure 2-42 – 30 where each figure represents the variations of the FoS with respect to one of the SWCC parameters (i.e., a, n or m) at one depth of calculation (i.e., Top or Bottom) considering different sloping angles β (i.e., 10°, 20°, 30°, 45°).

Figure 2-42 – 43 show the variation of the FoS with respect to the parameter a for different values of the sloping angle β at the top and the bottom of the Aine-Tine surficial layer, respectively. The parameters n and m are set equal to 2 and 1, respectively which will results a group of SWCCs with the same size of the transition suction range but with different AEVs proportionally increased with the increase of the parameter a.

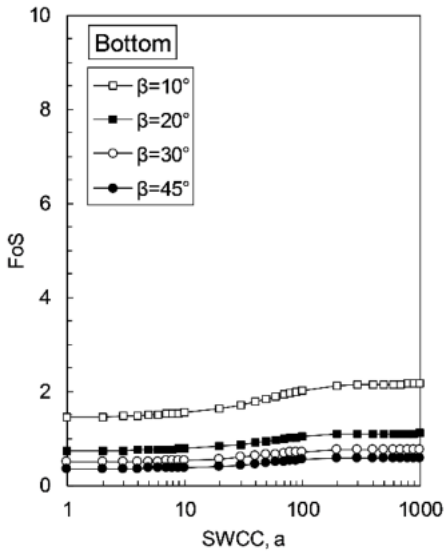

Figure 2-42 FoS variations with respect to the parameter a at the top of the shallow layer

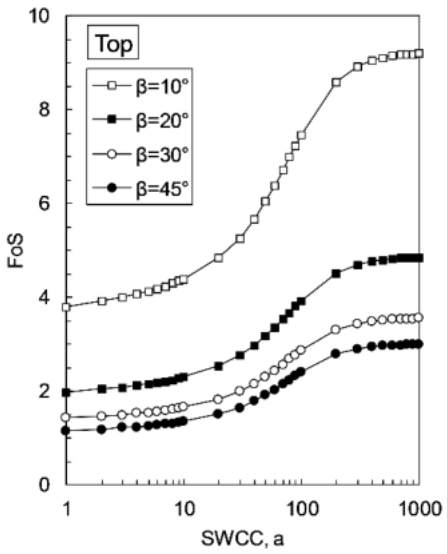

Figure 2-43 FoS variations with respect to the parameter a at the bottom of the shallow layer

The effect of the parameter a on the FoS can be divided into three zones which are primarily controlled by the two fitting parameters n and m. The three zones are as follow: (1) the first zone corresponds to low values of the parameter a where the suction values present within the Aine-Tine surficial layer are located in the residual suction range of the obtained SWCCs (a = variable, n=2, m=1) which is expressed by small variations of the normalized VWC values following the increasing of the parameter a and consequently a negligible influence on the shear strength and the FoS in this range of a values represented by an almost horizontal curve reflecting a slight increase of the FoS. (2) the second zone corresponds to a range of a values where a considerable increasing of the FoS was observed with the increase of the parameter a; this can be ascribed to the correspondence of the suction present within Aine-Tine shallow layer in the transition suction zone of the obtained SWCCs which gives high values of the normalized VWC and consequently a remarkable increase of the third term of the shear strength expression which considerably heightened the FoS. (3) Third zone: This zone comes after a certain value of a, in this zone, the suctions present within the Aine-Tine shallow layer are lesser than the AEV or in another way they are located in the saturated suction zone of the obtained SWCCs. This will lead to the obtaining of a constant value of the normalized VWC which is approximately equal to 1 and consequently, the FoS values will not be influenced by the increase of the parameter a, where an almost horizontality of the FoS curves with respect to the parameter a was obtained.

The parameter n is the second fitting constitutive parameter of the SWCC; it controls the slope of this hydraulic function. The assessment of the effect of this parameter has been conducted by adopting the values of 10 and 1 for a and m parameters, respectively. The results are presented in Figure 2-44 – 45 for the top and the bottom of the shallow layer, respectively. It was found that n is inversely related with the FoS while the higher the value of n the lower the FoS until achieving a certain value of n after which this parameter will have no influence on the FoS expressed by a horizontal profile of the FoS curves. This can be attributed to the effect of n on the SWCC, as

shown in Figure 2-40 where for high values of n the transition suction range of the SWCC will be shortened leading to an almost horizontal curve in the residual suction range located after the inflection point (i.e., 10 kPa in this study) which means that the corresponded normalized VWC to the suctions present within the Aine-Tine shallow layer will tend towards a constant value beyond a certain value of this parameter n leading to the attenuation of the influence of the third term of the FoS expression.

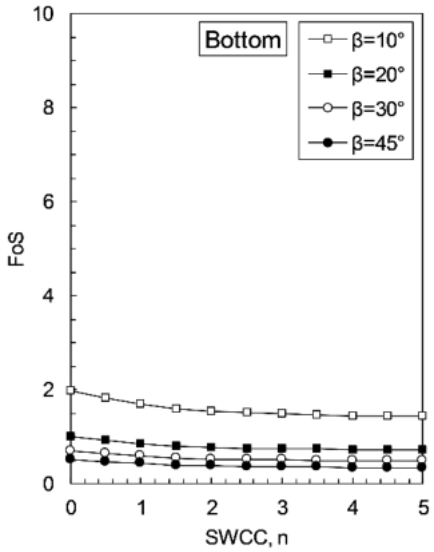

Figure 2-44 FoS variations with respect to the parameter n at the top of the shallow layer

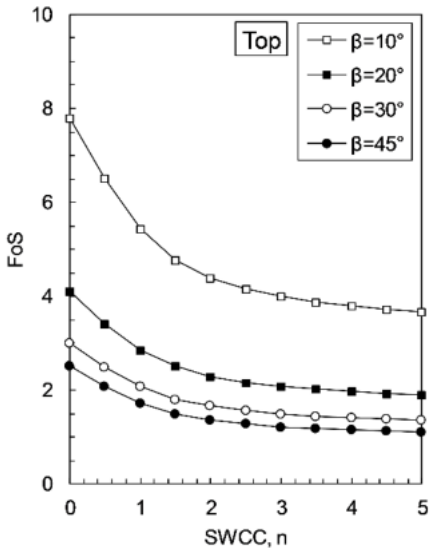

Figure 2-45 FoS variations with respect to the parameter n at the bottom of the shallow layer

The evaluation of the parameter m influence on the FoS is presented in Figure 2-46 – 47 where the same observations were obtained as for the parameter n. This can be ascribed to the reduction of the residual VWC value while increasing of m associated with the shortness of the transition suction range as shown in Figure 2-41 which results in that the corresponded normalized VWC to the suction values present within the Aine-Tine shallow layer will tend towards a zero value beyond a certain value of this parameter m leading to the cancellation of the third term of the FoS expression. In this part of the analysis, the parameter a and n are set equal to 10 and 2, respectively. Based on the comparison between Figure 2-44 and Figure 2-46 and between Figure 2-45 and Figure 2-47, it was found that for low values of n and m, the parameter n has a higher increasing effect on the FoS than the parameter m and vice-versa for high values.

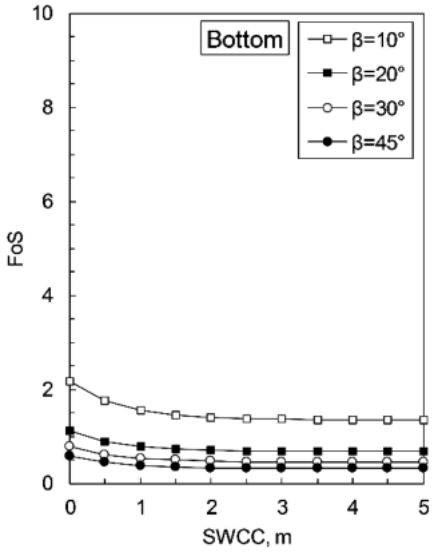

Figure 2-46 FoS variations with respect to the parameter m at the top of the shallow layer

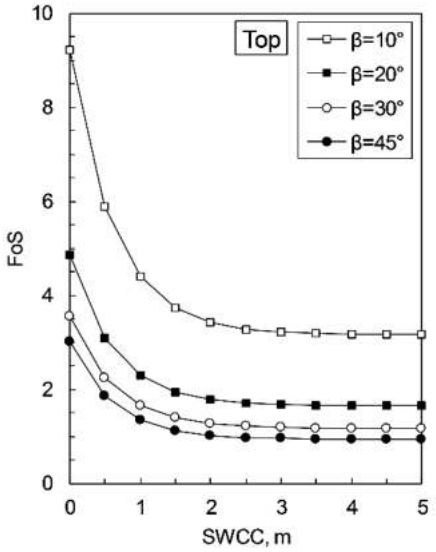

Figure 2-47 FoS variations with respect to the parameter m at the bottom of the shallow layer

In which concern the effect of the sloping angle β. Based on the comparison between the obtained sloping angle curves in all the figures, it is clear that the FoS is inversely proportional with the sloping angle. Moreover, the decrease of the distance between the curves in each figure while increasing the slope angle β indicates that the lower the sloping angle, the higher the contribution of the suction towards the shear strength of the unsaturated soils.

In the current study, the effect of the depth was studied by considering two different depths of the FoS calculation which corresponds to the top and the bottom of the shallow layer where it was found that the higher the depth, the lower the FoS. This can be attributed to the following reasons (1) the decrease in the shear strength associated with the decrease of the suction which is inversely related the depth and (2) the increase of the mobilized shear stress, which is proportional with the overburden stress.

2.4.4. Conclusion

The shear strength of unsaturated soils is related to the unsaturated behavior of such soils. This paper discussed the effect of (1) the hydraulic and (2) the geometric factors on the safety of the shallow layer of unsaturated slopes using the infinite slope formulation. The hydraulic factor was considered by studying the effect of the three SWCC's fitting parameters a, n and m on the FoS. Four sloping angles were adopted to consider the geometric factor. The 5 m thick shallow layer of Aine Tine natural slope was considered to conduct the calculations of the FoS at the top and the bottom of this layer. The following conclusions are obtained:

1. The suction present in unsaturated soils provides an additional cohesion and consequently increases the FoS of the unsaturated slopes in arid and semi-arid area.
2. The provided additional cohesion is related to the SWCC's fitting parameters.
3. The parameter a has an increasing effect on the FoS in a determined range which is controlled by the parameters n and m.

4. The higher the parameter n and m, the lower the obtained additional cohesion and, consequently, the decrease of the FoS.
5. For low values of n and m, The parameter n has a higher increasing effect on the FoS than the parameter m and vice-versa for high values.
6. The FoS is inversely proportional to the sloping angle.
7. The higher the depth of calculation the lower the obtained additional cohesion and consequently, the FoS due to (1) the decrease of the suction which inversely related the distance from the GWT and (2) the increase of the mobilized shear stress which is proportional with the overburden stress.

2.5. References

Adem, H.H., Vanapalli, S.K., 2014. Elasticity moduli of expansive soils from dimensional analysis. Geotech. Res. 1, 60–72. https://doi.org/10.1680/gr.14.00006

Adem, H.H., Vanapalli, S.K., 2013. Constitutive modeling approach for estimating 1-D heave with respect to time for expansive soils. Int. J. Geotech. Eng. 7, 199–204. https://doi.org/10.1179/1938636213Z.00000000024

Agus, S.S., Leong, E.C., Rahardjo, H., 2001. Soil–water characteristic curves of Singapore residual soils. Geotech. Geol. Eng. 19, 285–309. https://doi.org/10.1023/A:1013175913679

Akin, I.D., Likos, W.J., 2020. Suction Stress of Clay Over a Wide Range of Saturation. Geotech. Geol. Eng. 38, 283–296. https://doi.org/10.1007/s10706-019-01016-7

Athmania, D., Benaissa, A., Hammadi, A., Bouassida, M., 2010. Clay and Marl Formation Susceptibility in Mila Province, Algeria. Geotech. Geol. Eng. 28, 805–813. https://doi.org/10.1007/s10706-010-9341-5

Biot, M.A., 1941. General theory of three-dimensional consolidation. J. Appl. Phys. 12, 155–164.

Bouatia, M., Demagh, R., 2019. Numerical Assessment of Slope Stability of Ain-Tinn Mila Province (Algeria), in: Shehata, H., Desai, C.S. (Eds.), Advances in Numerical Methods in Geotechnical Engineering, Sustainable Civil Infrastructures. Springer International Publishing, Cham, pp. 133–143. https://doi.org/10.1007/978-3-030-01926-6_10

Chettah, W., 2009. Investigation des propriétés minéralogiques et géomécaniques des terrains en mouvement dans la ville de Mila « Nord-Est d'Algérie » (Thèse de Magistère). University of Batna 1 Hadj Lakhdhar, Batna, Algérie.

Chowdhury, R., 2010. Geotechnical Slope Analysis.

Dahal, R.K., Hasegawa, S., Nonomura, A., Yamanaka, M., Dhakal, S., 2008. DEM-based deterministic landslide hazard analysis in the Lesser Himalaya of Nepal. Georisk Assess. Manag. Risk Eng. Syst. Geohazards 2, 161–178. https://doi.org/10.1080/17499510802285379

Doumbouya, L., Guan, C.S., Bowa, V.M., 2020. Influence of Rainfall Patterns on the Slope Stability of the Lumwana (the Malundwe) Open Pit. Geotech. Geol. Eng. 38, 1337–1346. https://doi.org/10.1007/s10706-019-01094-7

Fredlund, D.G., Morgenstern, N.R., 1976. Constitutive relations for volume change in unsaturated soils. Can. Geotech. J. 13, 261–276. https://doi.org/10.1139/t76-029

Fredlund, D.G., Morgenstern, N.R., Widger, R.A., 1978. The shear strength of unsaturated soils. Can. Geotech. J. 15, 313–321. https://doi.org/10.1139/t78-029

Fredlund, D.G., Rahardjo, H., 1993. Soil mechanics for unsaturated soils. John Wiley & Sons.

Fredlund, D.G., Xing, A., 1994. Equations for the soil-water characteristic curve. Can. Geotech. J. 31, 521–532. https://doi.org/10.1139/t94-061

Fredlund, D.G., Xing, A., Fredlund, M.D., Barbour, S.L., 1996. The relationship of the unsaturated soil shear strength to the soil-water characteristic curve. Can. Geotech. J. 33, 440–448. https://doi.org/10.1139/t96-065

Fredlund, M.D., Fredlund, D.G., Zhang, L., 2018. Moving from 2D to a 3D Unsaturated Slope Stability Analysis, in: PanAm Unsaturated Soils 2017. Presented at the Second Pan-

American Conference on Unsaturated Soils, American Society of Civil Engineers, Dallas, Texas, pp. 136–145. https://doi.org/10.1061/9780784481691.014

Gerard, C.J., 1965. The Influence of Soil Moisture, Soil Texture, Drying Conditions, and Exchangeable Cations on Soil Strength 1. Soil Sci. Soc. Am. J. 29, 641–645. https://doi.org/10.2136/sssaj1965.03615995002900060017x

Han, Z., Vanapalli, S.K., Kutlu, Z.N., 2016. Modeling Behavior of Friction Pile in Compacted Glacial Till. Int. J. Geomech. 16. https://doi.org/10.1061/(ASCE)GM.1943-5622.0000659

ITASCA, 2005a. User's manuel, FLAC3D (Fast Lagrangian Analysis of Continua).

ITASCA, 2005b. User's manuel, FLAC3D (Fast Lagrangian Analysis of Continua).

Jiang, X., Wu, L., Wei, Y., 2020. Influence of Fine Content on the Soil–Water Characteristic Curve of Unsaturated Soils. Geotech. Geol. Eng. 38, 1371–1378. https://doi.org/10.1007/s10706-019-01096-5

Karube, D., Kawai, K., 2001. The role of pore water in the mechanical behavior of unsaturated soils. Geotech. Geol. Eng. 19, 211–241. https://doi.org/10.1023/A:1013188200053

Khemissa, M., 2006. Méthodes d'analyse de la stabilité et techniques de stabilisation des pentes. Actes JNGG.

Kristo, C., Rahardjo, H., Satyanaga, A., 2017. Effect of variations in rainfall intensity on slope stability in Singapore. Int. Soil Water Conserv. Res. 5, 258–264. https://doi.org/10.1016/j.iswcr.2017.07.001

Lambe, T.W., Whitman, R.V., 1969. Soil mechanics, Series in soil engineering. Wiley, New York.

Li, W.C., Lee, L.M., Cai, H., Li, H.J., Dai, F.C., Wang, M.L., 2013. Combined roles of saturated permeability and rainfall characteristics on surficial failure of homogeneous soil slope. Eng. Geol. 153, 105–113. https://doi.org/10.1016/j.enggeo.2012.11.017

Lian, B., Peng, J., Wang, X., Huang, Q., 2020. Moisture content effect on the ring shear characteristics of slip zone loess at high shearing rates. Bull. Eng. Geol. Environ. 79, 999–1008. https://doi.org/10.1007/s10064-019-01597-w

Lin, H., Zhong, W., 2019. Influence of Rainfall Intensity and Its Pattern on the Stability of Unsaturated Soil Slope. Geotech. Geol. Eng. 37, 615–623. https://doi.org/10.1007/s10706-018-0631-7

LNHC Batna, 2016. Rapport d'Etude de Sol (No. 01). LNHC Batna, Ain Tinn, Mila, Algeria.

Mebarki, A., 2005. HYDROLOGIE DES BASSINS DE L'EST ALGERIEN : RESSOURCES EN EAU, AMENAGEMENT, ET ENVIRONNEMENT (thèse de doctorat d'etat). University of Mentouri, Constantine.

Nguyen, T.S., Likitlersuang, S., 2019. Reliability analysis of unsaturated soil slope stability under infiltration considering hydraulic and shear strength parameters. Bull. Eng. Geol. Environ. 78, 5727–5743. https://doi.org/10.1007/s10064-019-01513-2

Oh, W.T., Vanapalli, S.K., Puppala, A.J., 2009. Semi-empirical model for the prediction of modulus of elasticity for unsaturated soils. Can. Geotech. J. 46, 903–914. https://doi.org/10.1139/T09-030

Patil, U.D., Puppala, A.J., Hoyos, L.R., Banerjee, A., 2018. Strength, Stiffness and Radial Anisotropy of Compacted Silty Sand Under Suction-Controlled Axisymmetric Shearing. Geotech. Geol. Eng. 36, 3945–3960. https://doi.org/10.1007/s10706-018-0590-z

Qi, S., Vanapalli, S.K., 2015. Hydro-mechanical coupling effect on surficial layer stability of unsaturated expansive soil slopes. Comput. Geotech. 70, 68–82. https://doi.org/10.1016/j.compgeo.2015.07.006

Shen, H., Klapperich, H., Abbas, S.M., Ibrahim, A., 2012. Slope stability analysis based on the integration of GIS and numerical simulation. Autom. Constr. 26, 46–53. https://doi.org/10.1016/j.autcon.2012.04.016

Sheng, D., Zhou, A., Fredlund, D.G., 2011. Shear Strength Criteria for Unsaturated Soils. Geotech. Geol. Eng. 29, 145–159. https://doi.org/10.1007/s10706-009-9276-x

van Genuchten, M.Th., 1980. A Closed-form Equation for Predicting the Hydraulic Conductivity of Unsaturated Soils. Soil Sci. Soc. Am. J. 44, 892–898. https://doi.org/10.2136/sssaj1980.03615995004400050002x

Vanapalli, S.K., Fredlund, D.G., Pufahl, D.E., Clifton, A.W., 1996. Model for the prediction of shear strength with respect to soil suction. Can. Geotech. J. 33, 379–392. https://doi.org/10.1139/t96-060

Vu, H.Q., Fredlund, D.G., 2006. Challenges to modelling heave in expansive soils. Can. Geotech. J. 43, 1249–1272. https://doi.org/10.1139/t06-073

Vu, H.Q., Fredlund, D.G., 2004. The prediction of one-, two-, and three-dimensional heave in expansive soils. Can. Geotech. J. 41, 713–737. https://doi.org/10.1139/t04-023

Xie, M., Esaki, T., Cai, M., 2004. A GIS-based method for locating the critical 3D slip surface in a slope. Comput. Geotech. 31, 267–277. https://doi.org/10.1016/j.compgeo.2004.03.003

Xie, M., Esaki, T., Qiu, C., Wang, C., 2006. Geographical information system-based computational implementation and application of spatial three-dimensional slope stability analysis. Comput. Geotech. 33, 260–274. https://doi.org/10.1016/j.compgeo.2006.07.003

Zhang, J., Peng, J., Li, J., Zheng, J., 2018. Variation of Resilient Modulus with Soil Suction for Cohesive Soils in South China. Int. J. Civ. Eng. 16, 1655–1667. https://doi.org/10.1007/s40999-018-0315-y

Zhang, L.L., Fredlund, D.G., Zhang, L.M., Tang, W.H., 2004. Numerical study of soil conditions under which matric suction can be maintained. Can. Geotech. J. 41, 569–582. https://doi.org/10.1139/t04-006

Chapter 03

STRUCTURAL BEHAVIOR OF PIPELINES BURIED IN EXPANSIVE SOILS UNDER RAINFALL INFILTRATION

3. Structural Behavior of Pipelines Buried in Expansive Soils under Rainfall Infiltration

3.1. Background information

The content presented in this chapter was used to prepare the following manuscripts entitled:

a) Bouatia, M., Demagh, R., Derriche, Z., 2020. Structural Behavior of Pipelines Buried in Expansive Soils under Rainfall Infiltration (Part I: Transverse Behavior). Civ. Eng. J. 6, 1822–1838. *https://doi.org/10.28991/cej-2020-03091585*
b) Bouatia, M., & Demagh, R. 2019. Effect of the initial soil suction on Structures Buried in an Expansive Soil during a Rainfall Infiltration Case of Aine-Tine pipeline. In 1st International Congress on Advances in Geotechnical Engineering and Construction Management ICAGECM'19 (p. 122), Skikda, Algeria.

3.2. Introduction

Buried pipelines are important lifeline infrastructures used by many countries and companies to transport fluids (i.e., water or gas) to remediate to the strong hydraulic and energy resources inequalities over the world. The geotechnical and structural engineers faced many challenges to safely and durably design and build these budget-consuming projects. Landslides, fault movements as well as shrink/swell soil displacements can exert important additional loadings on structures especially for pipelines buried within expansive soils. These loadings may damage these structures or disturb their normal operations whenever their magnitudes reach the strength limits of the structure material.

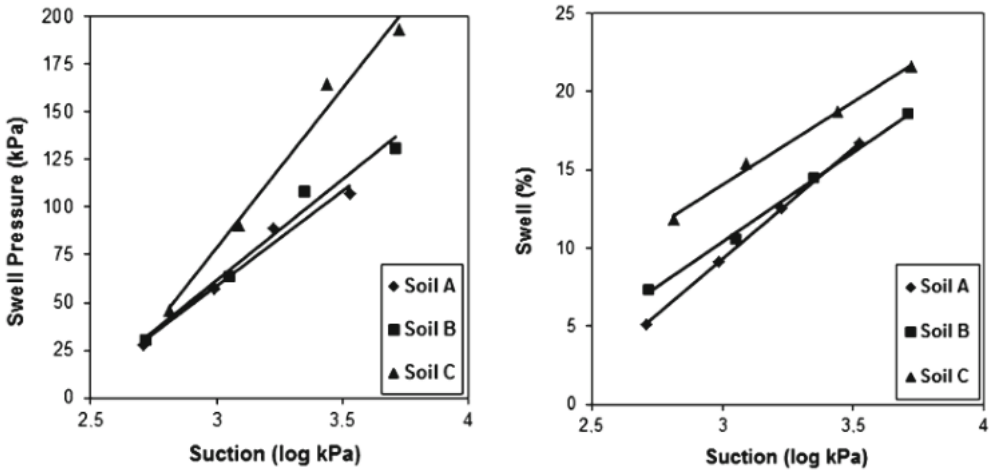

Figure 3-1. Relationship of swelling pressure and percent swell with soil suction (Uzundurukan et al., 2014)

In recent decades, professional and academic forensic surveys have revealed that the unsaturated behavior of expansive soils is the main cause of the reported damages that occurred on many types of structures such as lightweight structures and buildings (Zhang and Briaud, 2015) (Ozer et al., 2012), water transport canals used in agriculture activities (Yilmaz, 2007). Severe damages were reported also on buried pipelines (Clark, 1971) (Robert et al., 2016a) in many parts of the world such as arid and semi-arid regions, as a result of deformations induced by volume changes that characterize expansive soils (Uzundurukan et al., 2014) (Ito et al., 2014). Figure 3-1

shows the results of the investigation carried out by Uzundurukan et al. (2014) on the study of the relationship between suction and swell characteristics of three clayey soils classified as CH following the USCS classification where the color are respectively for Soil1, soil2 and soil 3: gray, green and dark gray. It was found that there are linear relationships between percent swell (%) and suction (in log kPa term); also the results of testing indicate that the relationships between swelling pressure and suction depend on the nature of the three different clayey soils.

It is known that arid and semi-arid areas, are usually characterized, by a deep GWT and by extremely dry surface soils which bear negative PWPs (suction) (Fredlund and Rahardjo, 1993a) and which are extremely sensitive to wetting and drying. When these soils are expansive, the supply of a tiny quantity of water may develop within these soils important swelling deformations as well as important swelling pressures when the deformations are blocked. The mechanical characteristics (i.e., shear strength and deformation parameters) of the soils located above the GWT are inversely related to the moisture content which increases the sensitivity of these soils to the climate conditions such as rainfall (Biot, 1941) (Fredlund and Morgenstern, 1976) (Kumar et al., 2020). Figure 3-2 gives the variation in soil suction at different depths with respect to time (1 year) considering exposed and unexposed grounds to climate conditions where it is very clear that the suction changes correlate well with the seasonal weather conditions.

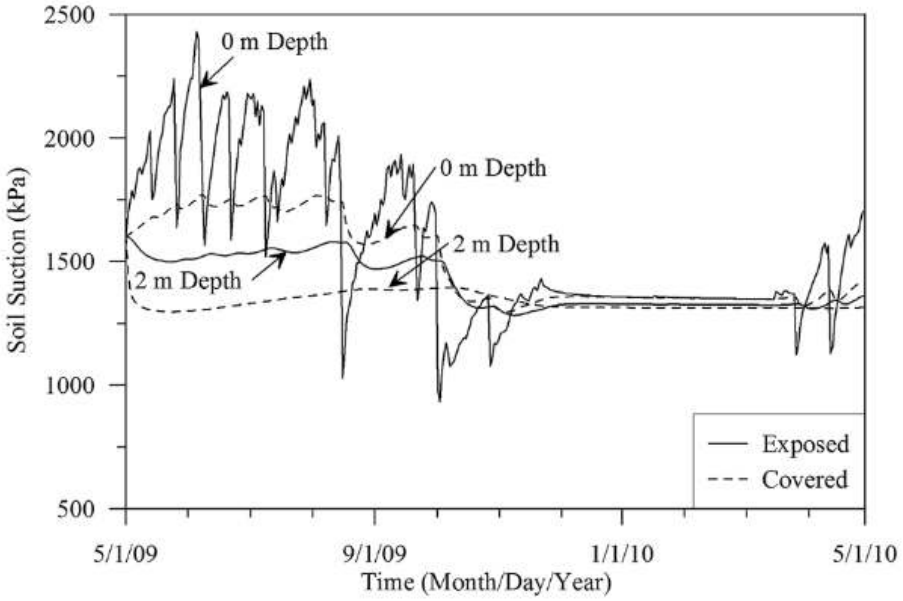

Figure 3-2. Suction variation versus time (Ito et al., 2014)

Han et al. (2016) describe the suction as an energy potential that takes the form of a tension stress which is exerted on the soil skeleton, this potential keeps, together, the soil particles in packets, offering more resistance of the soil against deformations. Figure 3-3 presents the results of measured and predicted values of peak shear strength τ_p and elastic modulus E with respect to suction performed on the Bukit Timah Granite soil. Rainfall precipitation or irrigation activities provide a downward water flow in the expansive soil increasing its moisture content and reducing its suction simultaneously, and consequently provoke volume changes which are measured as vertical displacements on the ground surface of such types of soil (Fredlund and Morgenstern, 1976) (Adem and Vanapalli, 2013) (Vu and Fredlund, 2006).

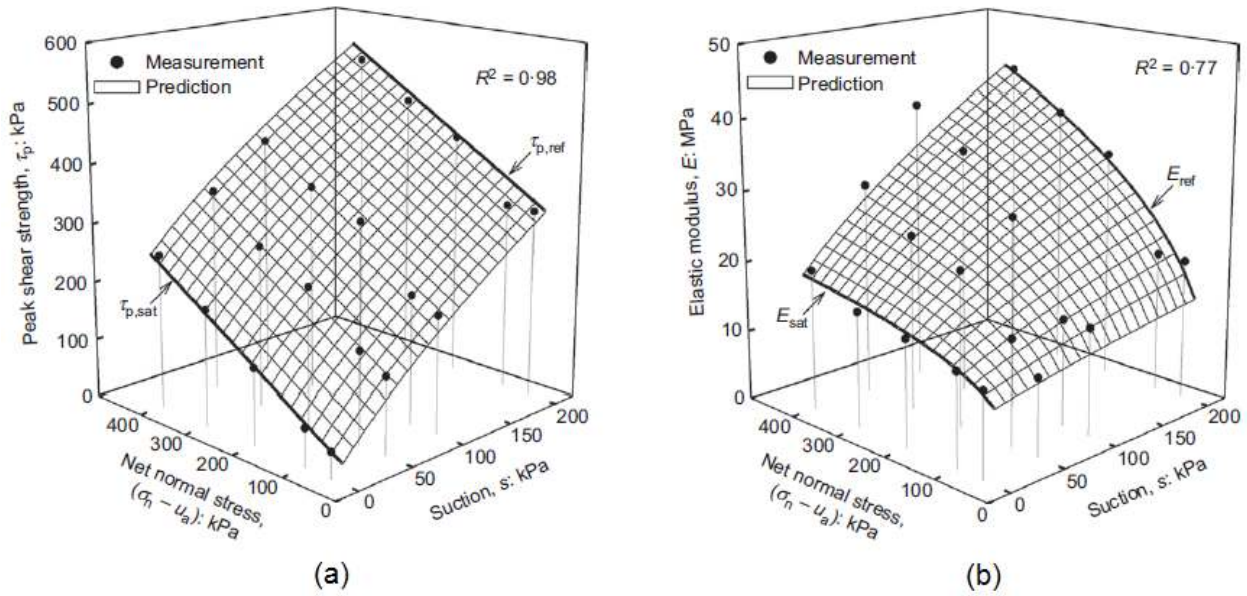

Figure 3-3. Measured and predicted values of (a) τ_p–s relationships; (b) E–s relationships of Bukit Timah Granite (Han and Vanapalli, 2016)

Figure 3-4 presents a typical void ratio constitutive surface plotted in semi logarithmic scale with respect to the net normal stress and suction. Where C_m is the volume change index with respect to changes in matric suction and C_s is the swelling index with respect to changes in net normal stress. It is very clear that for low net normal stresses the slope of the increase in volume is higher. The lower net normal stresses are mainly located at shallow depth where generally surficial foundations, road and pipelines are constructed. The volume changes that occur in the pipeline embedding soil provoke loading forces on the structure of the pipeline that can endanger the stability of the lifeline infrastructure. The unsaturated behavior effects on pipeline response have been analyzed both experimentally and numerically as well as under different loading conditions (i.e., landslides, faults movements, ...).

Experimental large scale tests have been conducted by Randeniya et al. (2019) to investigate deformations of a steel pipeline buried in an unsaturated clayey soil under different saturation conditions; they found that the backfill soil's degree of saturation can considerably control pipeline deformations. Full-scale tests and finite element simulations were carried out by Robert et al. (2016b). They found that the unsaturated soil strength and stiffness increase with soil suction and externally imposed ground movements that increase lateral loads on pipelines. Huang et al. (2015) have conducted a full scale analysis of the effect of the frost heave on a 105m long and 0.9m diameter 35m long chilled gas pipeline buried in permafrost in Alaska. They found that the pipelines buried in the arctic region suffer damages due the induced soil vertical movements which principally take the form of bending actions causing strains on the pipeline bodies.

In which concern numerical studies, a finite element analysis has been conducted by Rajeev and Kodikara (2011) and Robert and Soga (2013). The obtained results showed that the reduction in suction due to the increase in moisture content provokes an increase of the soil loading on the buried structures such as pipelines. In this direction, an interesting study about the background of pipelines have been undertaken by Al-Khazaali et al. (2018) that can be used as a good platform to

undertake pipeline-soil interaction researches in unsaturated mediums. Moreover, the response of buried pipelines under strike-slip fault movements have been studied by Vazouras et al. (2015) and Oghabi et al. (2017). Saadeldin et al. (2015) have investigated through a parametric study the influence of the moisture content variations on the longitudinal movements of a hypothetical pipeline of 6 m length and 0.15 m diameter that occurred due to change in suction by considering different boundary conditions. The transverse soil-pipeline system deformations associated with trenching was studied by Al-Khazaali et al. (2018) considering the effect of the GWT level and that of the depth of excavation. This study helps to define the safe combination (GWT, Depth) when trenching near to buried pipeline in unsaturated soils. All the previous studies highlighted the importance of taking into consideration the unsaturated behaviour of the expansive embedding soils which can cause important additional loadings on the buried structures considering the longitudinal response of the pipelines.

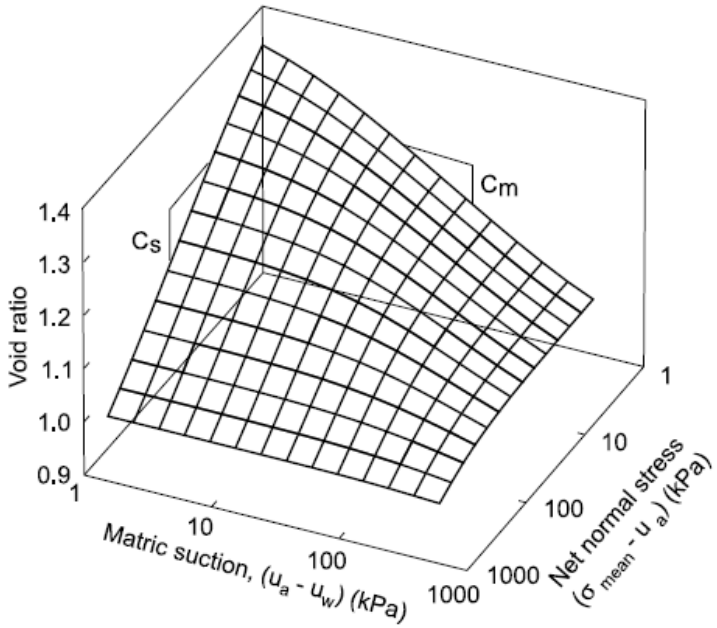

Figure 3-4. A typical void ratio constitutive surface plotted in semi logarithmic scale (Vu and Fredlund, 2004)

To address the substantial hydrological shortage that characterize the eastern side of Algeria, more than 600 km of water supply pipelines supplying water from the Beni-Haroun dam, were buried in the Mila basin (Mila province, Algeria), a region known by its semi-arid climate (Chettah, 2009) and famous as a highly sensitive region to shrink/swell movements (Athmania et al., 2010) (Figure 3-5). In recent years, many of the water transport pipelines have suffered repetitive damages in north of Algeria taking the form of leakage points along the pipeline route (Figure 3-6). During the rainy season the problem worsens and the leakage rate recorded increases. Unfortunately, after the construction of the Beni-Haroun dam in 2006 (i.e., the largest dam in Algeria, Mila province), the Algerian Ministry of Water Resources received several investigation reports on the damages that occurred on the water supply pipelines which are experiencing many leakage points along their routes. The site named Aine-Tine is one of the reported cases. Forensic studies indicated that the cause is mainly related to the interaction between these buried structures with the expansion of the clayey embedding soils of Mila basin where large areas have been

classified by Athmania et al. (2010) as highly sensitive to the shrink/swell phenomena. The classification performed is done adopting a French method developed by the Bureau of Geological and Mining Research (BRGM). The BRGM's method takes into account lithological, mineralogical and geotechnical characteristics of the clayey formations that identified in the Mila province territory. The Aine-Tine site located in Aine-Tine municipality is crossed by an 800 mm diameter water supply pipeline which carries water to more than 12 municipalities of the Mila province. The susceptibility map is established using three classes as follow: low, medium, high. The Aine Tine site is located in the highly sensitive seen with red color (Figure 3-5)

The serious economic and environment effects of these damages highlight the importance of taking into consideration the unsaturated behavior of such soils during the design and the construction of pipelines in Algeria. The safety and durability of buried pipeline-systems necessitate careful design studies which need to take into account all of the probable contributing factors related to the materials (i.e., soil and pipeline), environment (i.e., freezing, drying and wetting cycles) and loading (i.e., overburden stresses, traffic) to study the behavior of pipelines usually buried in the vadose zone (i.e., above the GWT) at 2 to 3 m from the ground surface in order to predict and reduce the possible damage of these structures.

In this study, a Finite Element Analysis has been conducted using the commercial software SIGMA/W software tool to assess the pipeline structural response expressed in terms of radial induced axial force F_A, shear force F_S and bending moment M_B that are exerted on the pipeline perimeter following the expansive soil volume change provoked by a 4 mm/day rainfall infiltration event lasting for 30 days (i.e., 1 month). The present study aims to understand the effect of soil wetting on the unsaturated-soil/pipeline interaction by considering (1) different rainfall time durations and (2) the initial soil suction conditions. The water supply 800 mm diameter pipeline coming from the Beni-Haroun dam buried at 2 m depth in Aine-Tine (Mila, Algeria) expansive soil was used in this numerical analysis. First, the chapter begins with an introduction which presents a summary of the literature on previous pipeline-soil interaction studies and the background and goals of the present study followed by a presentation of the methodology used to perform the analysis and then an overview of the SIGMA/W software tool finite element software used in this investigation. Following a detailed description of the main features of the Aine-Tine area the numerical model adopted (geometry and boundary conditions) the material characteristics used to simulate Aine-Tine expansive soil and the pipeline structure are exposed. The results obtained are presented and discussed where finally conclusions and future works are proposed at the end of this study.

3.3. Methodology

Pipelines are linear structures used for transporting fluids such as gas and liquids. They are usually buried in various types of soils over long distances and can go through areas with high sensitivity to expansion. In the present work, a two-dimensional numerical simulation is performed to analyze the transverse structural behaviour of a buried pipeline following expansion movements due to rainfall precipitation. The paper is a contribution to help engineers to predict reasonably what are the probable reasons that cause several water leakage points and which constitute

continuous disturbance of the water supply process. The main steps of the numerical analysis are summarized in the flowchart below (see Figure 3-7):

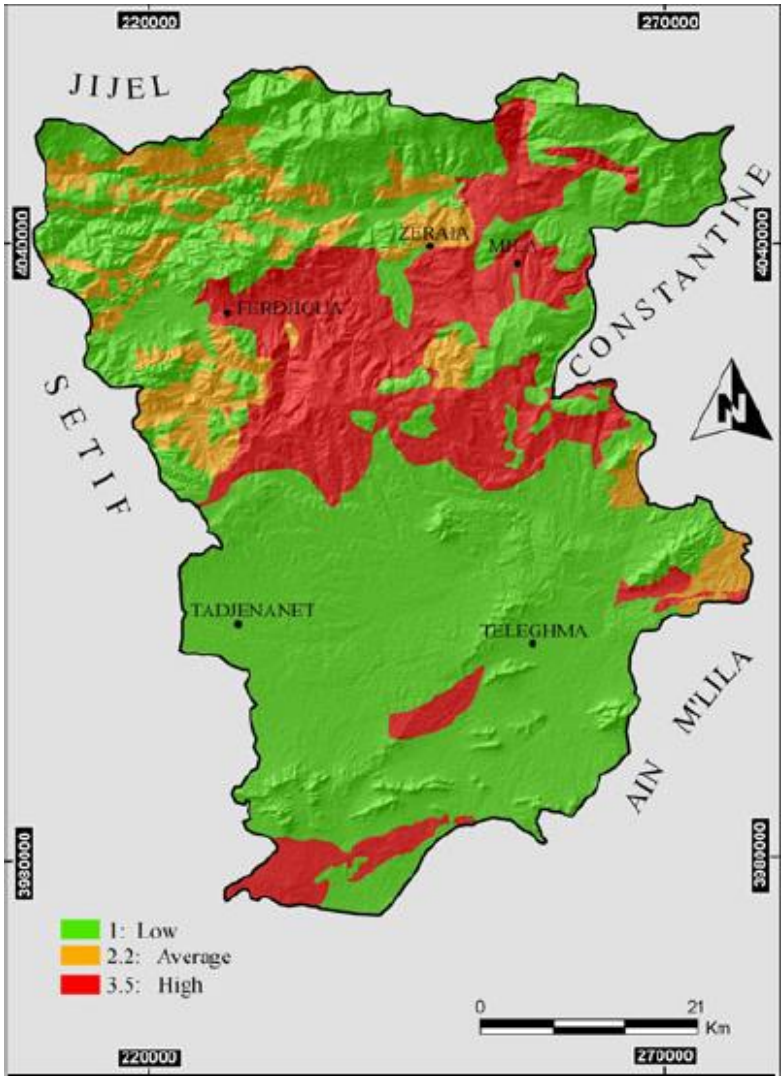

Figure 3-5. Mila Province «swelling-shrinkage» susceptibility map (Athmania et al., 2010)

Figure 3-6 Water leakage point at Aine-Tine site

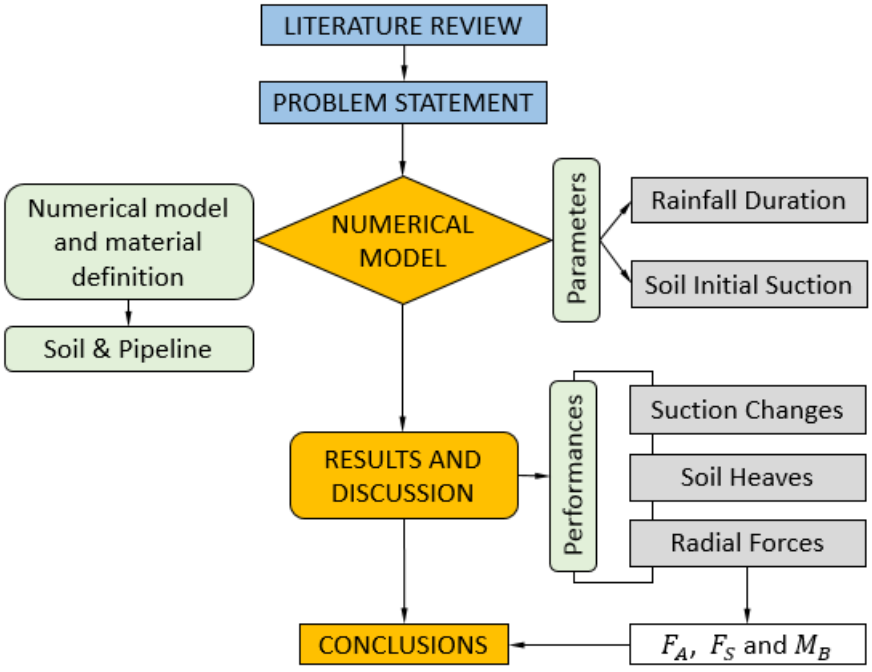

Figure 3-7 Research flowchart of the present paper

3.4. The study area

The study area is located in the Mila province in the North-East of Algeria (see Figure 3-9) which belongs to the eastern Alpine chain of the north of Algeria. It is north bordered by the Skikda and Jijel Provinces, south by the Batna Province, west by the Setif province and by the Constantine

province in the East. It is situated at 490 km from Algiers (i.e., the capital of the country) and at about 60 km from the city of Constantine. Mila covers an area of 3,550 km^2, composed by five districts and a number of 32 municipalities. The Aine-Tine site can be bracketed by latitudes 06°18'30" and 06°19'00 and longitudes 36°25'30" and 36°25'45". Geologically, Mila's exposure soil consists of Mio-Pliocene and Quaternary continental deposits which cover a set of carbonate, bedrock, of Cretaceous to Eocene ages. As seen in Figure 3-8, more than 70% of the geological formations are Alluviums and clays, where these occupy 50.14% and 21.83%, respectively (Athmania et al., 2010).

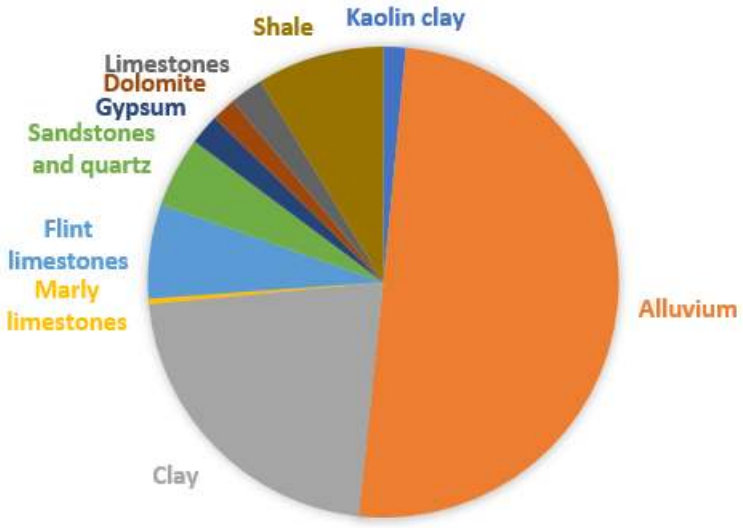

Figure 3-8 Geological formations outcrop statistical distribution inside Mila Province

The study area belongs to the semi-arid climate region of the country that receives precipitation below potential evapotranspiration, but not as low as the desert climate. The semi-arid climate is characterized by only two seasons: a hot dry season in summer and a cold rainy season in winter. Detailed investigations of the hydrological properties of the eastern side of Algeria have been presented by Mebarki (2005). The annual average precipitation in Mila province is 678.5 mm/year, even though in 1984 the maximum annual precipitation reached 1058 mm. The maximum monthly average is between 120 and 145 mm/month (i.e. December). During the period October to April, December is the rainiest month of the Mila region. It must be stressed that Mila is a geotechnical problem prone area (i.e., landslides and a shrink/swell movements). Rainfall precipitation is the principal trigger of these instability phenomena which occur especially during the wet season. This is due to the high sensitivity of clayey soils related to the decrease in suction following precipitations. Site investigation results indicated the GWT level has been found to be located at about 15 m depth which is consistent with the data reported in the thesis of Mebarki (2005).

3.5. Finite element analysis using SIGMA/W

The present study is a two-dimensional plane-strain numerical simulation of the soil-pipeline-environment interaction. The powerful 2D finite element SIGMA/W software tool was used. SIGMA/W is one of the modules of GEOSTUDIO software suite proposed by GeoSlope (2007). The suite is usually used for modeling stresses and deformations in ground and structural

materials. The SIGMA/W module is widely used for geotechnical research and practice by civil and mining communities to carry out slope stability, consolidation, shrinkage/swelling and structural analysis in both saturated and unsaturated conditions (Al-Khazaali and Vanapalli, 2020) (Qi and Vanapalli, 2015) (Teimouri and Khalkhali, 2018). In our case, it is used here to investigate the transverse structural behavior of a steel pipeline buried in a high expansive soil considering the unsaturated behavior of the soil.

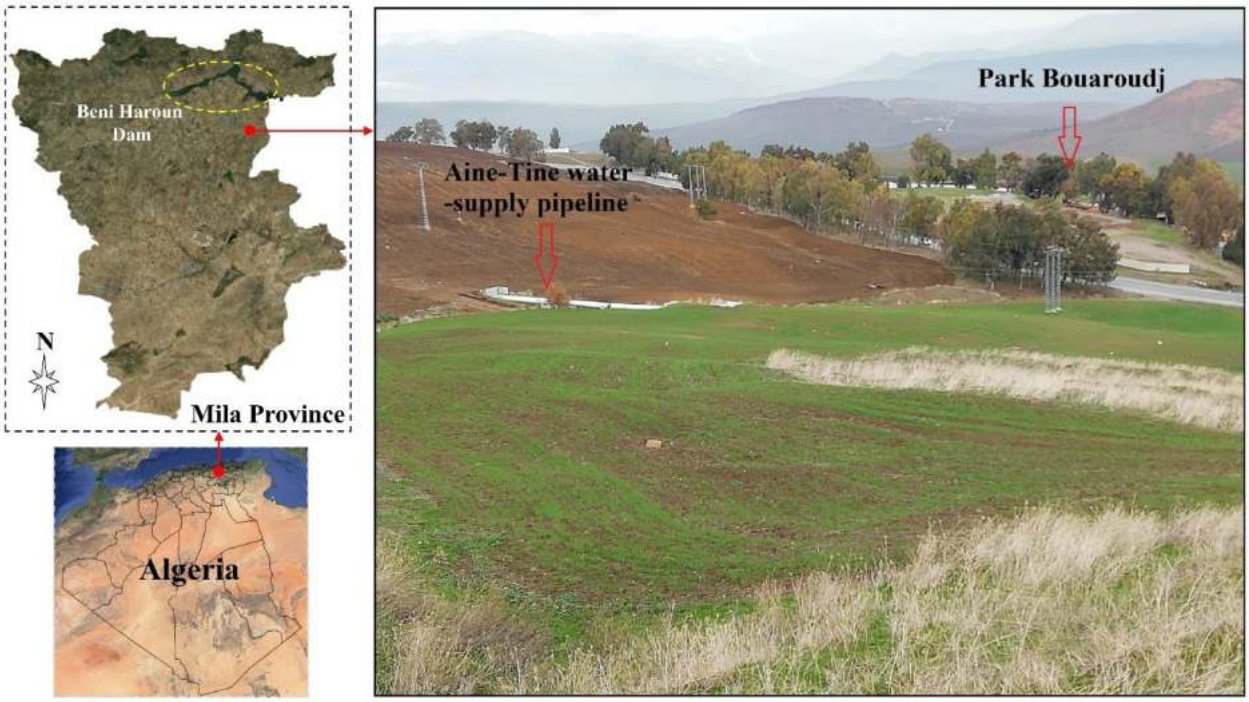

Figure 3-9. Aine-Tine area location

Similar 2D software programs (Plaxis 2D, FLAC 2D) can equally be used to carry out the present study. When comparing SIGMA/W and Plaxis 2D, it must be indicated that both give similar and conservative results due to the assumption of plane strain modeling. SIGMA/W is more flexible and faster than Plaxis 2D. Its software library contains linear, nonlinear, elastic and elastoplastic soil constitutive models to simulate soils with different meshing options controlling the form (i.e., triangle, square or combination between both) and the global size with possibility of refining. Plaxis 2D on the other hand, provides five mesh resolutions which can be applied (very coarse, coarse, medium, fine and very fine). As for the boundary conditions and loading options SIGMA/W makes it possible to consider constant values as for the usual x, y fixities or functions (i.e., spline, linear or step function) of time to simulate environment conditions such as precipitation or seismic actions. SIGMA/W gives also the possibility to model structures such as pipelines and retaining walls using bar and beam elements. The partial differential force equilibrium and water continuity equations are the two fundamental equations which govern the mechanical behavior of soil and flow behavior of the water phase in unsaturated soils, respectively (Qi and Vanapalli, 2015). These two equations are incorporated into SIGMA/W, which simplifies the two-dimensional saturated and unsaturated hydromechanical analyses. The unsaturated behavior of soils is governed by an incremental stress-strain relationship developed by Fredlund and Rahardjo (1993b) where it is a function of the net normal stress (σ-u_a) and the suction (u_a-u_w) as stress

state variables. Shear strength and stiffness of unsaturated soil are functions of these two stress state variables. The two-dimensional matrix formulation of the stress-strain relationship incorporated in SIGMA/W is as follows:

$$\begin{Bmatrix} \Delta\boldsymbol{\varepsilon_x} \\ \Delta\boldsymbol{\varepsilon_y} \\ \Delta\boldsymbol{\gamma_{xy}} \end{Bmatrix} = \frac{\mathbf{1}}{\boldsymbol{E}} \begin{bmatrix} \mathbf{1} & -\boldsymbol{\vartheta} & \mathbf{0} \\ -\boldsymbol{\vartheta} & \mathbf{1} & \mathbf{0} \\ \mathbf{0} & \mathbf{0} & \mathbf{2(1+\vartheta)} \end{bmatrix} \begin{Bmatrix} \Delta(\boldsymbol{\sigma_x - u_a}) \\ \Delta(\boldsymbol{\sigma_y - u_a}) \\ \Delta(\boldsymbol{\tau_{xy}}) \end{Bmatrix} + \frac{\mathbf{1}}{\boldsymbol{H}} \begin{bmatrix} \mathbf{1} & \mathbf{0} & \mathbf{0} \\ \mathbf{0} & \mathbf{1} & \mathbf{0} \\ \mathbf{0} & \mathbf{0} & \mathbf{1} \end{bmatrix} \begin{Bmatrix} \Delta(\boldsymbol{u_a - u_w}) \\ \Delta(\boldsymbol{u_a - u_w}) \\ \Delta(\boldsymbol{u_a - u_w}) \end{Bmatrix} \quad \text{Equation 1}$$

Where ε_x, ε_y and γ_{xy} are the normal and shear strain components, σ_x, σ_y and τ_{xy} are the normal and shear stress components, E is the Young's modulus of the soil structure. H is the elasticity modulus with respect to a change in suction and μ is the Poisson's ratio. H is estimated adopting the relationship $H = E/(1-2\vartheta)$ according to Vu and Fredlund (2004) (2013) published works. SIGMA/W helps users to consider automatically the additional shear strength of unsaturated soils evolving from the suction by extending the Mohr-Coulomb failure criterion as shown in Equation 2.

$$\boldsymbol{\tau_f = c' + (\sigma - u_a)\tan\varphi' + (u_a - u_w)\,\Theta\,\tan\varphi'} \quad \text{Equation 2}$$

Where Θ is the normalized volumetric water content (VWC) or $(\theta_w - \theta_r)/(\theta_s - \theta_r)$ where θ_r is the VWC at residual state, θ_s is the VWC at saturated state. Modeling of the unsaturated behavior requires the definition of the hydraulic property functions of the soil, which are the SWCC and the permeability function K which relates the VWC and the hydraulic conductivity to the soil suction. The calculation of the variation of unsaturated modulus of elasticity (E_{unsat}) due to the change in saturation state of the soil is possible using the incorporated function which defines the modulus of elasticity as a function of effective stress or suction (see Section 6.3) which takes into account changes in PWPs under precipitation, irrigation activities or rising of GWT. In addition to the van Genuchten (1980) model of the SWCC included in Plaxis 2D, the used software includes the Fredlund and Xing (1994) model and allows users to define their own SWCC. Additionally, unlike others similar 2D geotechnical software's (i.e., Plaxis2D or FLAC2D), SIGMA/W allows practitioners to define and combine geometries and analyze multiple geotechnical problems in a single modeling project and to solve analyses in parallel which considerably reduces simulation times.

3.6. Transverse behavior

3.7. Numerical Model

3.7.1. Model geometry

A uniform soil profile is assumed to extend down to 4 m depth under the ground level with a length of 8 m horizontally, as shown in Figure 3-10. The horizontal and vertical dimensions of the model are set to avoid the effects of boundary conditions. These dimensions are related directly to the pipeline diameter where according to the recommendations presented in many published researches (Vazouras et al., 2010) (Vazouras et al., 2015) (Oghabi et al., 2017), it was found after simulations that it is sufficient to numerically evaluate induced large displacements on pipeline transverse cross section by having a cross-section model with 10 and 5 times the pipe diameter for

horizontal and vertical dimensions, respectively. On the basis of these recommendations the present study was carried out adopting the model dimensions shown in Figure 3-10.

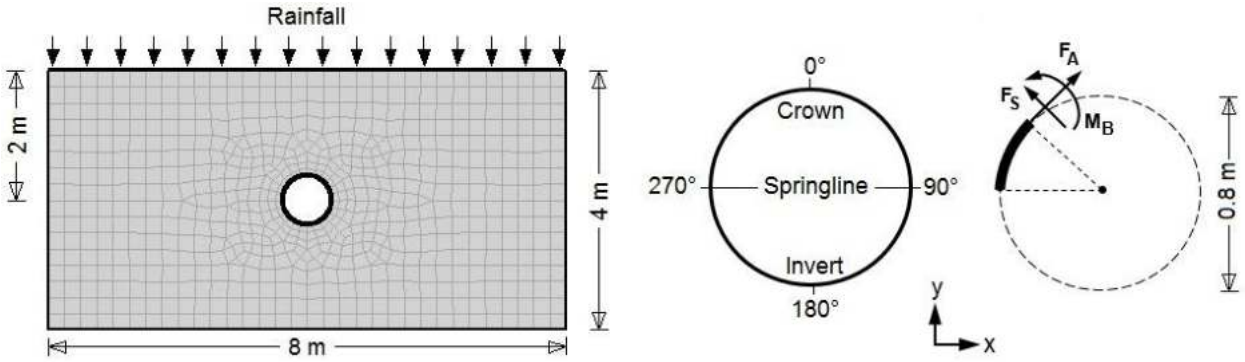

Figure 3-10. Finite element model and pipeline cross-section detail

The meshes were generated automatically using the available option in SIGMA/W quadrilateral and triangles elements where a unified mesh size of 0.25 m was applied for the soil region. For the pipe, the beam element perimeter is divided into 24 equal segments, which gives an angle increment of 15° for each segment. The length s of each segment can be obtained by applying the following equation $s = r.\theta$ (i.e. 0.104m) where r is the radius of the pipeline and θ is the angle. The total number of elements in the model is equal to 690 elements.

3.7.2. Boundary conditions

The boundary conditions of the model are: left and right boundaries are fixed only in the x-direction and the bottom boundary is fixed both in the x and y directions. To model the rainfall effect, a 4 mm/day constant rainfall unit flux q (mm/day) lasting for 30 days, which corresponds to the minimum daily average occurring in the rainiest month in the Mila basin (i.e., December) was assigned to the top surface of the model. As for the suction, the boundary conditions are given in Figure 3-11. To study the effect of suction, four initial profiles of suction P1, P2, P3 and P4 are imposed on the model based on the assumption of a hydrostatic linear distribution of the suction above the GWT to simplify the study. The imposed suction profiles may correspond to different GWT levels or reflect different degrees of surface evapotranspiration that characterize arid and semi-arid climate regions such as Mila province. The theoretical GWT levels corresponding to the suction profiles P1, P2, P3 and P4 are equal to 15, 30, 60 and 120 m, respectively. The first profile corresponds to the Aine-Tine area GWT depth which gives a suction value at the top surface of the model equal to 147 kPa (see Figure 3-11). The other profiles are obtained by a double increment way (P1=1/2 P2, P2=1/2 P3 and P3=1/2 P4). Therefore, four pressure head values equal to -11, -26, -56 and -116 m are, respectively, maintained along the bottom boundary nodes of the model for each suction profile during the rainfall simulation.

3.8. The Aine-Tine Clay

The pipeline is buried in the vadose zone of the Aine-Tine area which is classified according to USCS classification system as CH, which is an inorganic clay of high plasticity with a clay content equal to 52%. The geotechnical parameters of Aine-Tine clay are presented in Table 3-1. They were summarized from in situ and laboratory investigation reports of soil studies carried out

on the Aine-Tine site between the years 2016 and 2017. The integrated extended elastic-perfectly plastic Mohr-Coulomb (MC) constitutive model was used to model the clayey soil. It is successfully used to analyze soil-pipeline interaction problems considering the unsaturated behavior of the soil (Robert et al., 2016b) (Robert and Soga, 2013) (Vazouras et al., 2015). The gravity is set to 9.81 m/s^2.

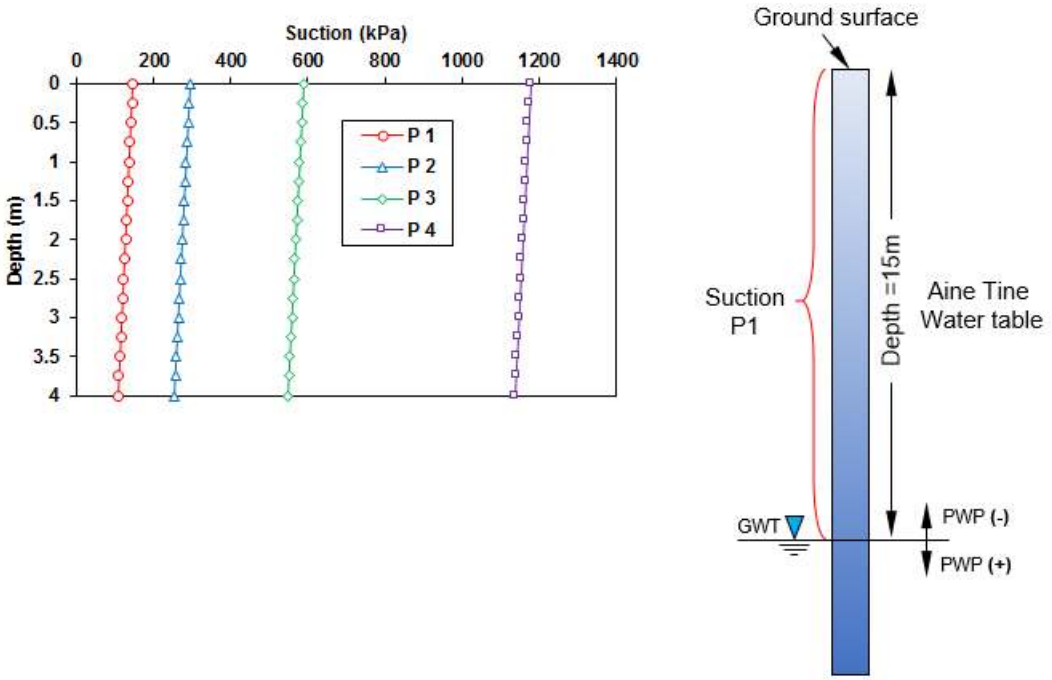

Figure 3-11. The profiles of initial suction conditions P1, P2, P3 and P4 and Aine-Tine GWT details

3.8.1. Hydraulic property functions, SWCC and K

Physical parameters such as particle size distribution and plasticity indices are the main factors that determine the shape of the SWCC. An estimation of the SWCC function was carried out based on literature reviews where the similarity of the index properties was considered as the criterion of selection amongst many published soil results around the world. The estimated SWCC has been found to be close to that of the Regina clay presented in Adem and Vanapalli (2013), Qi and Vanapalli (2015) and Azam et al. (2013) papers (Figure 3-12).

Using Pedo-Transfer prediction options available in SIGMA/W software such as the van Genuchten (1980) and Fredlund and Xing's (1994) methods, the SWCC can be estimated. In the present study, the van Genuchten model shown in Equation 3 was used to estimate the SWCC using the particle size distribution data and the plasticity index results shown in Table 3-1.

$$\boldsymbol{S = S_r + \frac{1-S_r}{\left[1+\left(\frac{u_a-u_w}{a}\right)^n\right]^m}} \qquad \text{Equation 3}$$

Where S is the degree of saturation, (u_a-u_w) is the suction, S_r is the residual saturation and a, n, and m are fitting parameters where n=1/(1-m). The corresponding van Genuchten (1980) values of these parameters used in this study are as follow: a=0.5, n=1.08. The pore water movement is governed by the soil permeability function K.

Table 3-1. Aine-Tine clay geotechnical parameters

Material	Soil property	Value
Aine-Tine Clay	Particle size distribution (%)	Sand=26, Silt=22, Clay=52
	Atterberg limits (%)	w_L=65.32, w_P=27.87, I_P=37.45
	Void ratio e	0.69
	Total unit weight γ_t (KN/m3)	19.1
	Dry unit weight γ_d(KN/m3)	15.7
	Natural moisture content w_{nat} (%)	22
	Elastic modulus E_{sat} (kPa)	1000
	Poisson's ratio μ	0.4
	Angle of internal friction φ (°)	15
	Cohesion C (kPa)	22
	Saturated permeability K_{sat}(m/day)	5.10^{-3}
	USCS Classification	CH, Inorganic clay of high plasticity

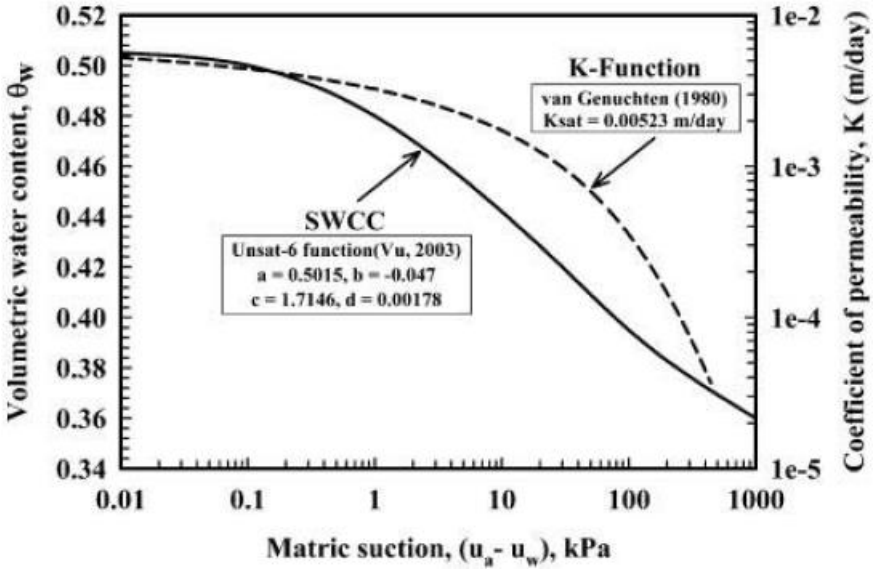

Figure 3-12 Hydraulic characteristics of unsaturated Regina expansive clay (Adem and Vanapalli, 2013)

Using the SWCC and the saturated permeability K_{sat}, the permeability function K was generated based on the van Genuchten method which is integrated in the GeoStudio software suite library. K_{sat} is assumed to be 5.10^{-3} m/day. Figure 3-13 presents the SWCC and K functions used to perform the present study.

3.8.1. Modulus of elasticity variation with respect to suction

Many researchers have reported the dependency between soil stiffness and the suction value (Randeniya et al., 2019) (Oh et al., 2009) (Zhang et al., 2018). Oh et al. (2009) proposed a semi-empirical model to predict the unsaturated Young's modulus E_{unsat} of unsaturated cohesionless soils as shown in Equation 4 using the saturated elastic modulus E_{sat} and two fitting parameters.

The extended model by Adem and Vanapalli (2014a) to cover all types of soils, was utilized in this study.

$$E_{unsat} = E_{sat}\left[1 + \alpha \frac{(u_a - u_w)}{(P_a/101.3)}(S)^{\beta}\right] \quad \text{Equation 4}$$

Where P_a is the atmospheric air pressure and α and β are fitting parameters. In this analysis, the fitting parameters α and β, are taken equal to 2 and 0.1, respectively. The chosen values of α and β are appropriate for fine-grained expansive soils (i.e., clay) as confirmed by Adem and Vanapalli (2014a) (2014b).

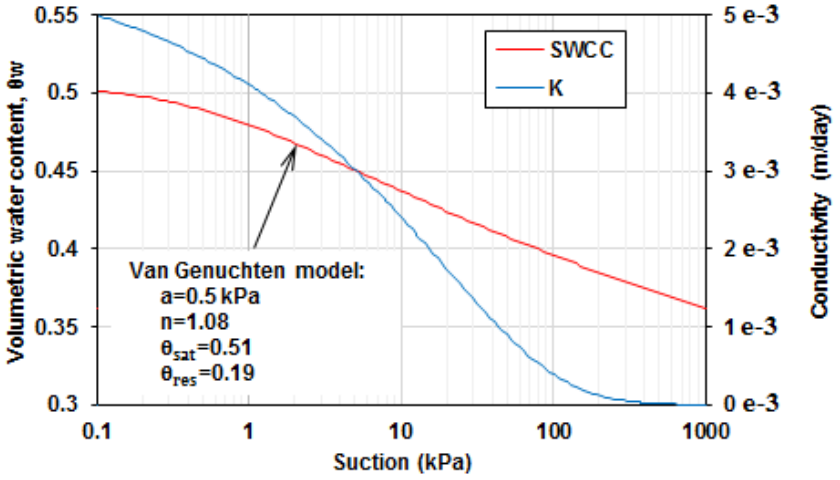

Figure 3-13 Hydraulic characteristics of Aine Tine soil

3.9. The pipeline

Different diameter sizes of water transport pipelines are buried in the Mila Basin. The analyzed section of pipeline buried in Aine-Tine site is 800 mm diameter and has a diameter-to-thickness ratio equal to 40 and assumed to be covered by 2 m deep clayey soil. The pipeline ring was modeled as a beam element using the linear elastic model. The behavior of the steel pipeline is governed by its rigidity, which is a function of its geometry dimensions and elastic modulus. The elastic modulus is assumed to be 2 GPa which corresponds to a flexible pipeline classification. The Aine-Tine pipeline characteristics are summarized in Table 3-2. Figure 3-10 shows the cross section used to calculate the moment of inertia that is essential for transverse pipeline simulations in the case of 2D plane-strain analysis.

Table 3-2. Aine-Tine pipeline parameters

Material	Soil property	Value
Aine-Tine Pipeline	External diameter Q_{ext} (mm)	800
	Thickness t (mm)	20
	D/t	40
	Young's modulus E (GPa)	2

3.9.1. Interface between the soil and the pipeline

There are several cases in Geomechanics in which it is necessary to represent planes on which ***sliding*** or ***separation*** can occur, for example

1. Joint, fault or bedding planes in a geologic medium;
2. Interface between a foundation and the soil;
3. A contact plane between a bin or chute and the material that it contains;
4. A contact between two colliding objects.

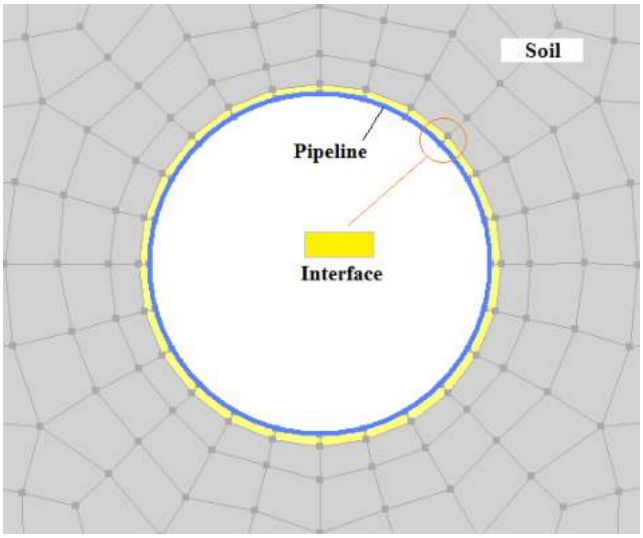

Figure 3-14 Detail of the interface

Generally, softwares provides interfaces that are characterized by Coulomb sliding and/or tensile and shear bonding. Interfaces have the properties of friction, cohesion, dilation, normal and shear stiffnesses, and tensile and shear bond strength. In the present study, the SIGMA software tool was used to generate the interface between the pipeline and the soil using line area option. The interface was modeled using the same characteristics of the surrounding clayey soil

3.9.2. The Moment of inertia of the pipeline

The cross section is a critical geometric parameter to perform correct analysis and get sure results about the structural response of structures. Figure 3-15 shows the details that explain the procedure for choosing the appropriate cross section for each part of calculation (i.e., longitudinal and transverse) where the section AA' with rectangular form having 1m length and the thickness t as the width is appropriate for the transverse assessment while the section BB' with annular form of thickness t and having D_{ext} and D_{int} as external and internal diameters is appropriate for the longitudinal analysis.

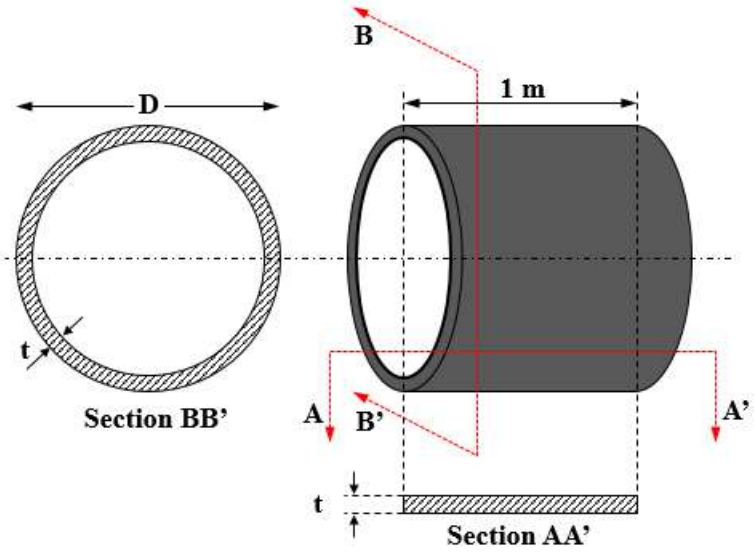

Figure 3-15. Cross sections adopted in longitudinal and transverse calculation

The formula used to calculate the moment of inertia which are required for both longitudinal and transverse calculations are shown in Equation 5 and Equation 6 respectively.

$$I = \frac{bh^3}{3} \qquad \text{Equation 5}$$

$$I = \frac{\pi}{64}\left(D_{ext}^4 - D_{int}^4\right) \qquad \text{Equation 6}$$

In the equation 5, the parameter b is equal to 1m length and the parameter h represent the thickness t of the pipeline.

3.10. Results and discussion

The numerical analyses were conducted to simulate the effect of the volume changes that occur in the expansive soil subjected to a saturation process acting as an external hydraulic loading (i.e., rainfall precipitation) on the buried pipeline. The results are presented in terms of induced (1) heave and deformations and (2) internal forces that apply along the ring of the pipeline following the decrease of soil suction. The rainfall time duration is taken into account by considering the results of four chosen time durations equal to 4, 8, 15 and 30 days of simulation and four initial suction profiles were studied to consider the effect of the initial suction (i.e., P1, P2, P3 and P4).

3.10.1. Suction variations

Rainfall infiltration provides a downward flux which increases the water content of the soil and decreases consequently the suction (i.e. negative PWP) of the soil. In this study, the effect on the suction of the rainfall that occurs during the rainiest month (December) in Mila basin is modelled. For the four initial suction profile conditions P1, P2, P3 and P4, the suction variations were evaluated as a transient seepage analysis under 4 mm/day rainfall infiltration using SIGMA/W software where the hydraulic response is governed by the SWCC and the permeability function K.

Figure 3-16 presents the variation of the suction profiles at the outer edges of the model in response to the wetting process throughout the simulation periods. It can be noticed that the soil

suction decreases gradually starting from the top surface going to the bottom of the soil depth. and proportionally with time as shown for each chosen time duration of simulation 0, 4, 8, 15 and 30 days. Figure 3-16 (a), (b), (c) and (d) are presented to provide a comparison where it is obvious that the higher the initial suction profile (P1, P2, P3 and P4), the higher the range of suction fluctuations. Similarities of the hydraulic response were obtained in many published studies (Qi and Vanapalli, 2016).

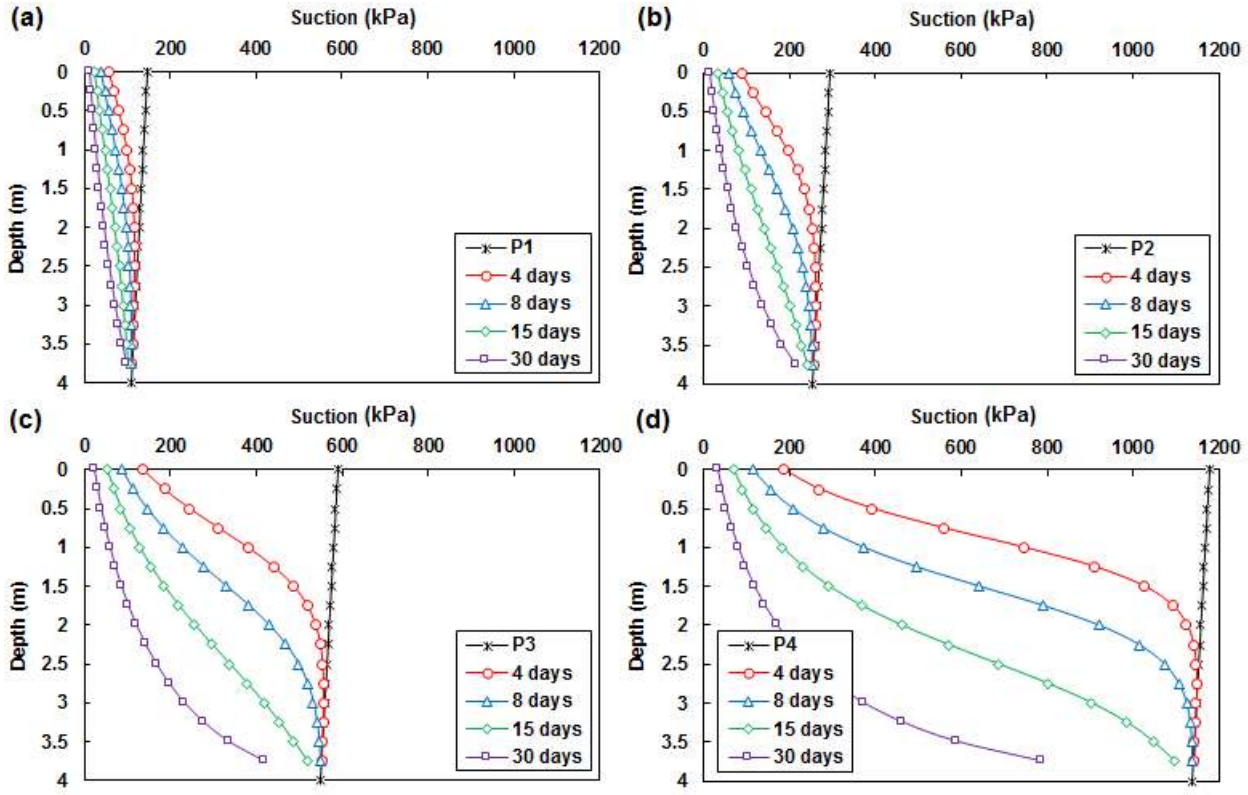

Figure 3-16. Evolution of soil suction with rainfall time for the suction profiles P1, P2, P3 and P4

3.10.2. Soil volume changes (Heave)

The induced decrease of suction discussed in the above section leads to volume changes associated with deformations within the soil. Figure 3-17 depicts the contours of vertical displacements, for the whole model, after 30 days of 4mm/days rainfall intensity for different initial suction profile conditions P1, P2, P3 and P4 presented, respectively, in Figure 3-16. The direction and magnitude of soil deformations can be viewed by the red arrow vectors for which the ascending vertical direction dominates the movements. The final calculated displacements at the top surface of the model, crown and invert of the pipeline are illustrated in Figure 3-17 where those obtained at the top surface are equal to 1.54, 2.01, 3.81 and 8.51 cm which correspond to the suction profiles P1, P2, P3 and P4, respectively, while those calculated at the crown of the pipeline are as follow 0.54, 0.82, 1.80 and 4.24 cm. Besides, matching proportionality between heave and decrease of soil suction have been obtained by Rajeev and Kodikara (2011) during their experimental and numerical investigations on the effect of swell movements on buried pipelines following the moisture content increase to saturation level within the soil due to a succession of capillary rises. Figure 3-18 is presented to provide a comparison at the end of the simulation (30 days) where it

can be observed that the higher the initial suction the higher the induced heave at the upper surface of the model. The magnitudes of heave decrease with depth where the ratios of the vertical displacements at the crown of the pipeline with those at the top surface of the model are equal to 35, 41, 47 and 50% which correspond to P1, P2, P3 and P4, respectively.

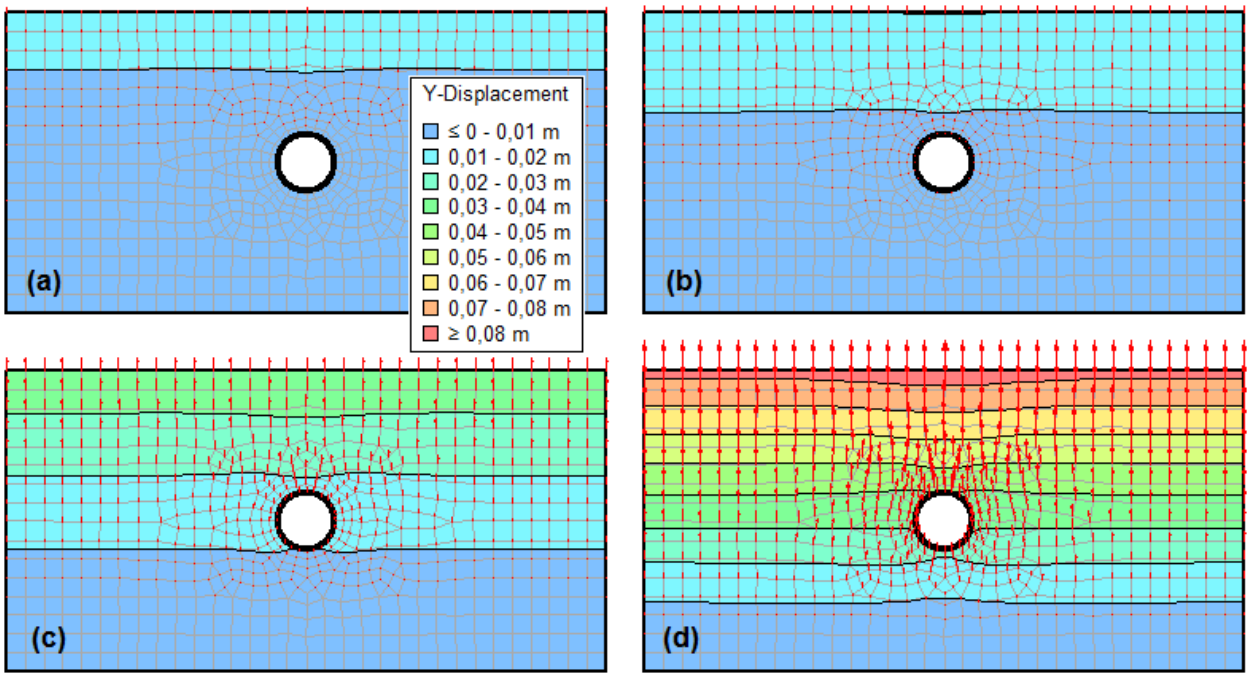

Figure 3-17. Vector and maximum displacements for different initial suction after 30 days of rainfall infiltration

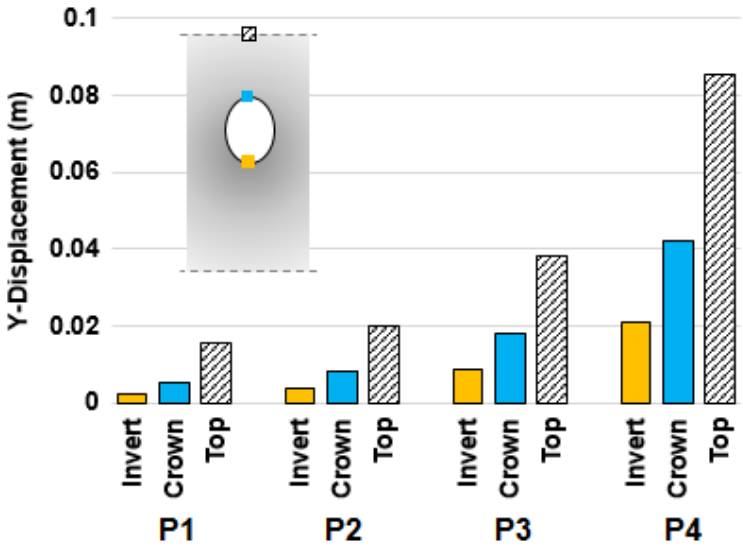

Figure 3-18. Y-Displacement values at the Invert, Crown and Top surface for P1, P2, P3 and P4

Figure 3-19 shows the distortions in the soil regions (with 5 x times magnification) around the pipeline area when the simulation period has reached the 30^{th} day of rainfall infiltration for each initial soil suction profile. The deformed meshes indicate the magnitude and direction of the ground movements while the black ring indicates the original location of the pipe. Based on the comparison between the four deformed meshes (from P1 to P4), it is clear that deformations around

the pipeline perimeter increase as the initial suction increases because of the increasing role of the soil suction that acts like a hydraulic stress that produce soil deformations which can be clearly seen in Equation 1 which correspond to the second member of the right hand side of the stress-strain relationship presented in Equation 7.

$$\begin{Bmatrix} \Delta\boldsymbol{\varepsilon}_{x\,(suction)} \\ \Delta\boldsymbol{\varepsilon}_{y(suction)} \\ \Delta\boldsymbol{\gamma}_{xy(suction)} \end{Bmatrix} = \frac{1}{H}\begin{bmatrix} \mathbf{1} & \mathbf{0} & \mathbf{0} \\ \mathbf{0} & \mathbf{1} & \mathbf{0} \\ \mathbf{0} & \mathbf{0} & \mathbf{1} \end{bmatrix}\begin{Bmatrix} \Delta(\boldsymbol{u_a} - \boldsymbol{u_w}) \\ \Delta(\boldsymbol{u_a} - \boldsymbol{u_w}) \\ \Delta(\boldsymbol{u_a} - \boldsymbol{u_w}) \end{Bmatrix} \qquad \text{Equation 7}$$

Where, $\Delta\varepsilon_x$, $\Delta\varepsilon_y$ and $\Delta\gamma_{xy}$ are the normal and shear strain components with respect to the soil suction. Figure 3-19c and d showed that the soil at the pipeline crown and invert deformed significantly due to the high state of unsaturation in the suction P3 and P4, respectively, which induces a vertical displacement of the pipe. In the case of P1 and P2 the deformed meshes are presented in Figures 3-19a and b, respectively, for which the observed deformations mainly concern the crown of the pipeline due the limited expansion that can occur at the pipeline invert mainly due to the low state of unsaturation of these two initial conditions.

A cross-section ovalization of the pipeline can be clearly observed in Figures 3-19b, c and d because the final vertical displacements (obtained at the 30th days) at the crown of pipeline are higher than those of the invert which leads to an increase of the pipeline diameter in the vertical direction as can be observed from Figure 3-18 where the increase of the diameter in the vertical direction reaches 1 and 2.1 cm taking into account the profile P3 and P4, respectively (GWT= 60 and 120m). This is obviously associated with a decrease in diameter at the springline reaching a value of 2.04 cm in the case of the profile P4 (GWT=120m). Such behavior which is consistent with the findings of Rajeev and Kodikara (2011) and Oghabi et al. (2017) can be attributed firstly to (1) the vertical direction of seepage as the upper zones saturate before the lower zones which is principally linked to the magnitude of suction with depth, SWCC and K of the soil and secondly to (2) the volume change magnitudes which is proportional to the range of suction fluctuations. The same observations were made by Adem and Vanapalli (2013) and Vu and Fredlund (2006). The profile P1, P2, P3 and P4 can represent different degrees of evapotranspiration during a dry season. As a result of this, it can be concluded from here that the higher the evapotranspiration or the depth of the GWT the higher the induced distortions within the expansive soil mass and consequently the induced loading on the pipeline ring.

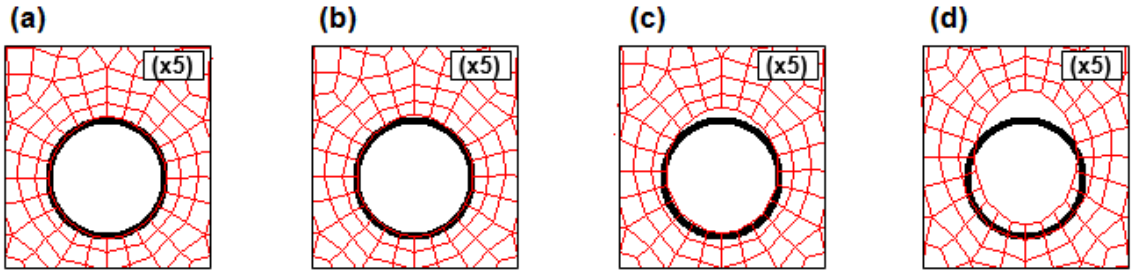

Figure 3-19. Deformed mesh around the pipeline perimeter (x5 magnitude)

3.10.3. Radial forces

The obtained radial forces in the present analysis will be discussed considering those obtained in some previous studies carried out under other external loading such as unsupported excavation and frost heave in cold regions.

- Al-Khazaali et al. (2018) used successfully SIGMA/W to investigate numerically the effect of a succession of unsupported excavations on nearby buried water transport pipeline considering of the effect of suction.
- Huang et al. (2015) studied experimentally the circumferential induced strains and bending following vertical displacement due to frost heave in a permafrost.

a) Axial forces F_A

The volume changes that occur in the expansive soil mass associated with heave at the top surface will result in stresses and strains on the pipeline ring and this will consequently lead to additional loads expressed in this study as pipeline internal forces.

The result of the axial forces F_A along the perimeter of the Aine-Tine pipeline under different rainfall infiltration time durations at the chosen time steps 4, 8, 15, and 30 days considered for the four initial suction profiles P1, P2, P3 and P4 are shown in Figure 3-20. It can be seen that positive values are obtained at the crown and invert (at angles 0° and 180°) positions of the pipeline perimeter which means the development of axial compression forces for all the initial suction profiles while negative values appeared in the springline (right, 90° and left, 270°) which means axial tension forces were developed in this location of the perimeter. Figure 3-20d shows the developed axial forces after 30 days of rainfall for the suction profile P4 which corresponds to the deepest GWT used in this study. The tension forces reached 67.26 kN and 66.03 kN at the crown and invert, respectively. The obtained values are 38% higher than those obtained after 15 days of simulation (Figure 3-20 c) while the increase reaches 104% between 8 days (Figure 3-20 b) and 15 days. Regarding the compressive axial forces, the magnitudes are slightly lower and the ratios are equal to 14% and 139% from 8 days to 15 days and from 15 days to 30 days, respectively. Due to the downward vertical direction of infiltration flow, the obtained values at the crown location are a slightly higher than those obtained in the invert while they are identical at the left and right springline locations. The axial compression and tension forces proportionally increased with both the duration of the infiltration from 4 to 30 days and the initial soil suction profiles from P1 to P4. From the results of Figure 3-20, it can be concluded that for a shallow GWT which corresponds to the results indicated by the red contours and a short period of rainfall, as in the case of 4 days (Figure 3-20 a), the pipe ring will receive negligible axial forces.

The presented results reflect the behavior of the soil-pipeline system with respect to the rain time duration and the initial suction conditions. This can be ascribed to the soil suction contribution to the unsaturated behavior of the Aine-Tine soil which is expressed as volume expansion. Following the rainfall infiltration, the decrease of the suction around the pipeline ring will produce stresses and strains at all nodes of the model. This will consequently, lead to an increase in tension axial forces at the crown and invert location. In contrast, the decrease of the soil suction with rainfall for all the cases P1, P2, P3 and P4 will also cause an increase in compression axial forces

at the springline location. Similar observations have been reported by Alkhazaali et al. (2018). However, the axial compressive forces were obtained at the springline location (i.e., 90° and 270°) while tensile forces were obtained at the crown and invert locations (i.e., 0° and 180°). This is due to the dominance of the horizontal displacements induced by a succession of unsupported vertical excavation operations unlike in the present study, the vertical displacements are dominant due to the expansion of the Aine-Tine soil upwards.

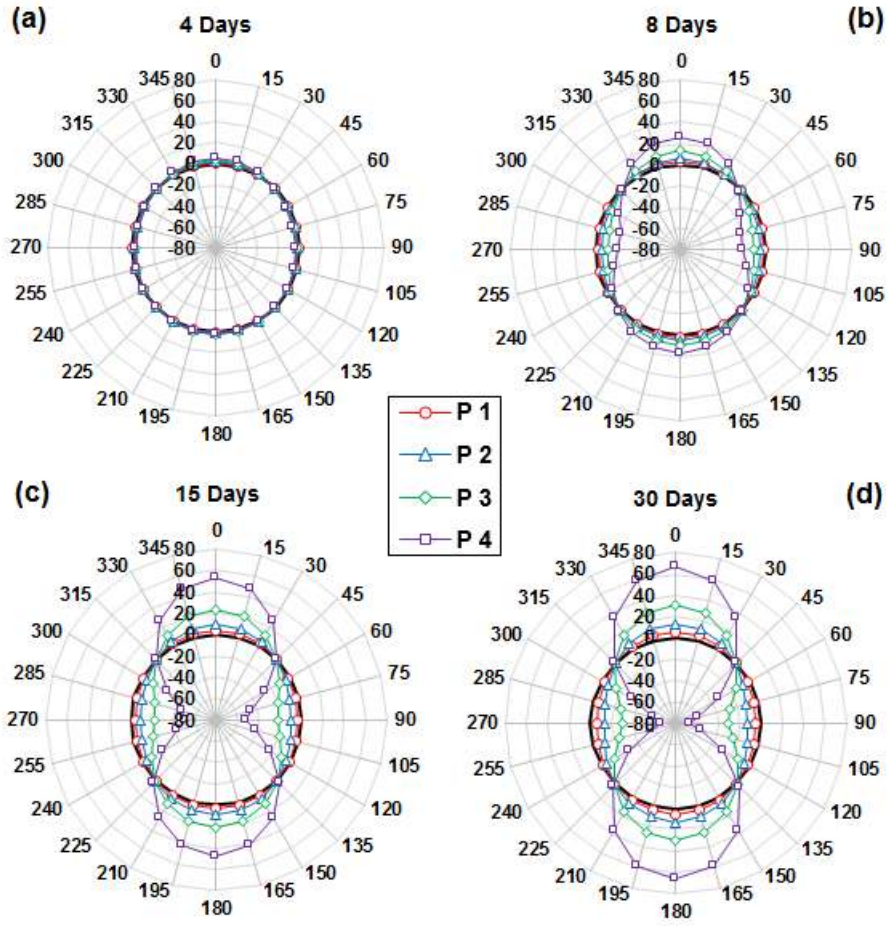

Figure 3-20. Axial force F_A distribution along pipeline perimeter (kN) with time

b) Shear forces F_S

Figure 3-21 presents the variation of the circumferential shear forces along the cross section pipeline wall. The shear forces developed on the pipeline wall increase with the rainfall time duration. Where the maximum peak (Positive) values were calculated approximately at angles 30° and 225° while the minimum peak (Negative) values were calculated at angles 135° and 330° while those obtained in Al-Khazaali et al. (2018) are located approximately in the same locations (Approximately ± 5°) with opposite signs and increase with the depth of excavation which has the same role as the downward flux which induces the vertical movements in the present analysis. Furthermore, the obtained shear forces have symmetrical distribution whereas those obtained by Al-Khazaali et al. (2018) are higher in magnitude and much higher at the side close to the front of the excavation. This is due to the horizontal direction of the large sliding movements as discussed above.

It can be noticed from each of the plotted curves, that obviously the induced shear forces increase with respect to the initial suction profile conditions P1, P2, P3 and P4, which corresponds to different theoretical GWT levels or may reflect different degrees of evapotranspiration which are very probable in arid and semi-arid climate such as the site of the present study. The magnitudes of the calculated shear forces are lower than those of the axial forces where the positive peak values for P4 (with purple color) calculated at the location 30° are equal to 0.25, 1.11, 1.92 and 2.32 kN and those calculated at 225° reached 0.04, 0.41, 1.4 and 1.95 kN. The same observation about the change of magnitudes can be drawn regarding the influence of the duration and the depth of the GWT as for the axial forces.

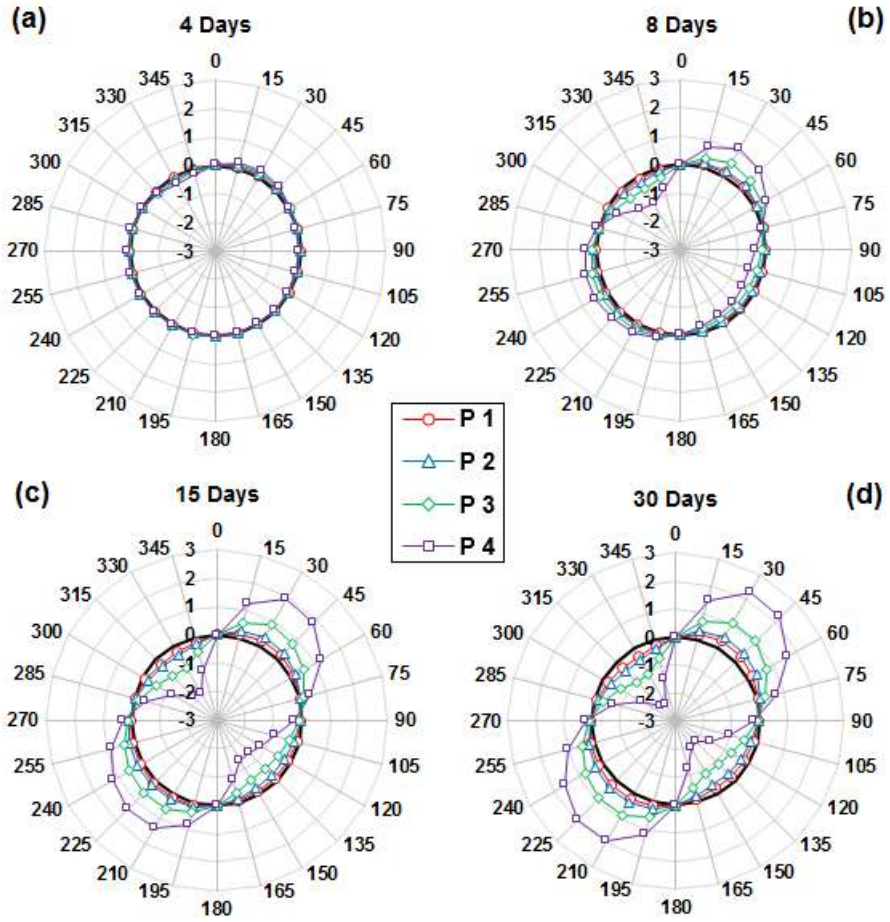

Figure 3-21. Shear force F_S distribution along pipeline perimeter (kN) with time

a) Bending moment M_B

The bending moment results M_B calculated along the pipeline perimeter are shown in Figure 3-22 using the color red, blue, green and purple to represent the results of P1, P2, P3 and P4, respectively. It is clear that they present a similar trend and present a consistent response as for the previous internal forces (axial and shear forces). The peak positive values were found at angles 90° and 270° while, for the peak negative values, they were found at angles 0° and 180° which are the similar location for the peak axial force values but with different signs.

Regardless of the time duration chosen it can be observed that peak values of calculated bending moment increased almost twice between each two subsequent initial suction condition from P1 to P4 and have dissymmetric distribution. Similar results in terms of trends but with different magnitudes are reported in Huang et al. (2015) for buried gas pipelines in cold regions which experienced vertical movements caused by differential frost heaves leading to the generation of circumferential strains as well as bending moments which are worse in the transition zone between frozen and unfrozen soil. Based on the comparison between the results of the peak values plotted in Figure 3-22, it was found that regardless of the duration of the simulation or the depth of the GWT, the order with respect to the magnitudes is as follows: the crown (0 °), springline (90 ° and 270 °) and the invert (180 °) while the maximum values of bending moment are calculated using the profile P4 after 30 days of rainfall and they reach values, respectively, 0.51, 0.41 and 0.38 kN.m. Reading attentively the Figure 3-21 and Figure 3-22, it can be seen that at zero shear stresses location, the peak values (positive and negative) of bending moments were obtained. From the obtained results, it obvious that the internal forces are sensitive to the variation of the soil suction following a rainfall event on high expansive soil such as the clay of Aine-Tine site.

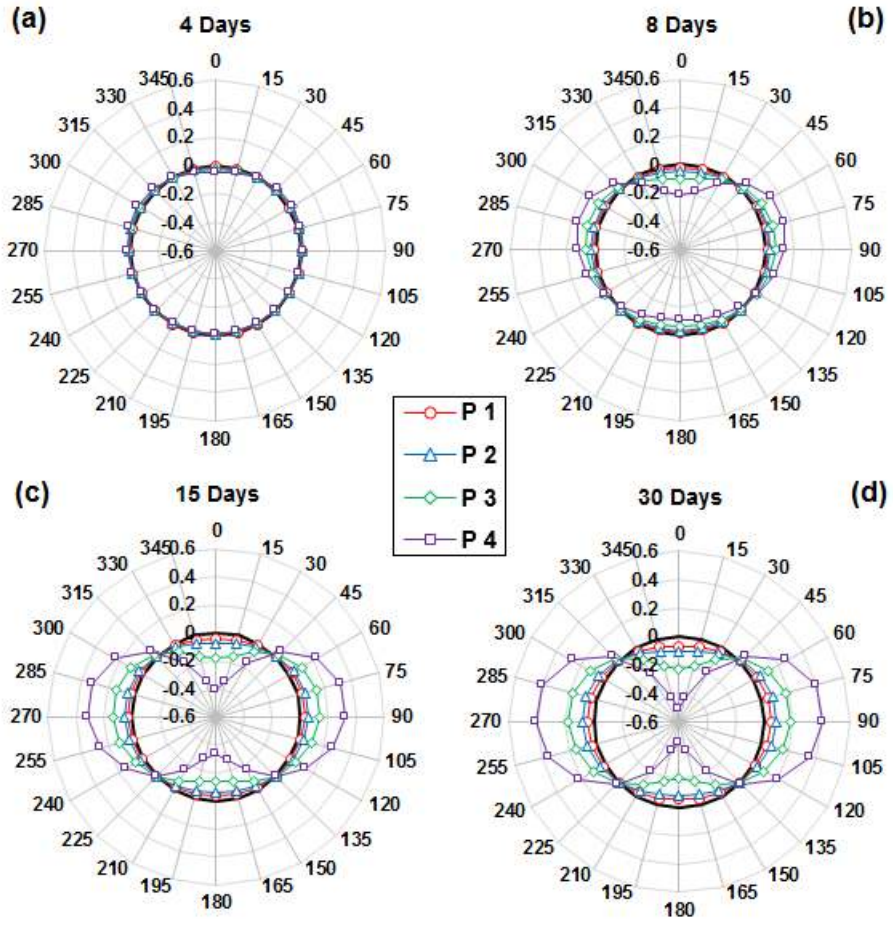

Figure 3-22. Transverse bending Moment distribution along pipeline perimeter (kN) with time

3.11. Longitudinal behavior

3.11.1. Numerical model

As for the transverse model, a uniform soil profile is assumed to extend down to 4 m depth under the ground level with a length of 60 m horizontally (Figure 3-23). The vertical and horizontal dimensions of the model are set to avoid the effects of geometric and hydraulic boundary conditions, respectively. These vertical dimension of the model geometry is related directly to the pipeline diameter where according to the recommendations presented in many published researches ((Vazouras et al., 2015) (Oghabi et al., 2017) (Azam et al., 2013)). It was found after simulations that it is sufficient to numerically evaluate induced large displacements on pipeline transverse cross section by having a cross-section model with a minimum of 5 times the pipe diameter for the vertical dimension of surrounding soil. Furthermore, the longitudinal dimension is mainly depending to the values of the highest value of the initial suction where, in our case, it was found that a model with 60 m length is sufficient to avoid the effect of the geometry boundaries on the stability of results when the maximum suction is equal to 1200 kPa at the top of the model.

The meshing of the model is chosen to be homogeneous where the unit zone is 1x0.25 m in horizontal and vertical directions, respectively. In which concern the boundary conditions, the same fixities and initial suction profiles were applied as in the transverse model while for the rainfall precipitation the same duration and flux were applied just on the half of the top surface of the model (Figure 3-23).

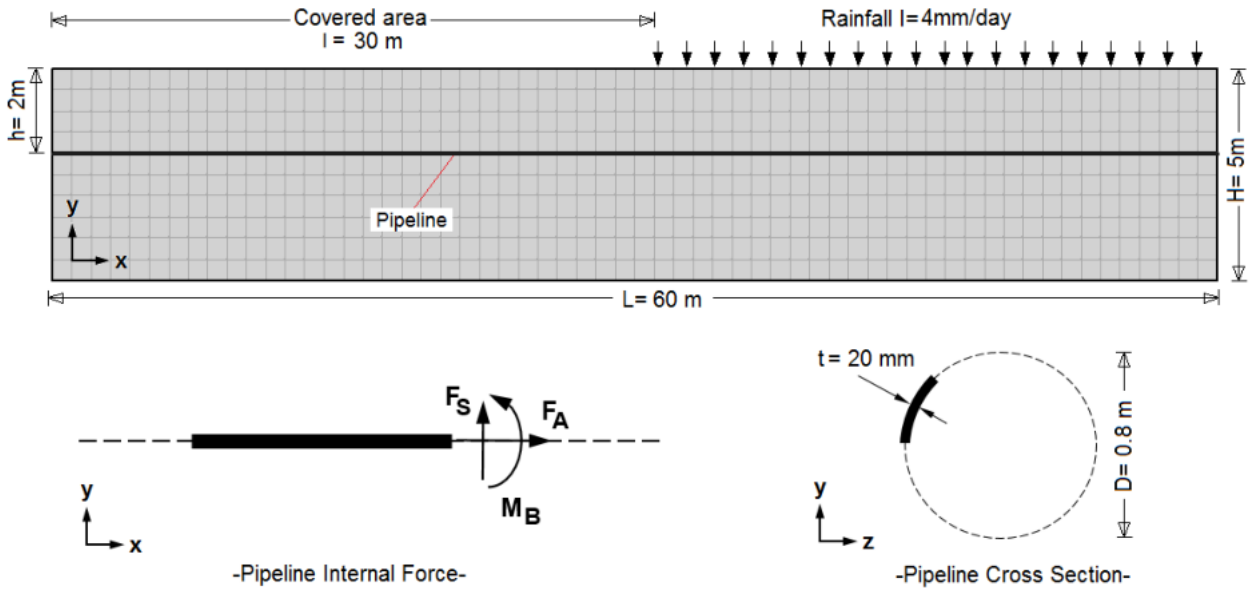

Figure 3-23. Longitudinal finite element model

3.12. Results and discussion (Longitudinal forces)

3.12.1. Heave

Following the decrease of suction, positive volume changes associated with deformations in the soil were obtained due to the expansion of clayey soil of Aine Tine slope (Figure 3-24). Figure 3-25 shows the profile of the induced vertical displacements at the exposed part to the rain of the top surface and for different initial suction profile conditions P1, P2, P3 and P4 shown with colors

yellow, green, red and blue after 4, 8, 15 and 30 days of 4mm/days rainfall intensity as shown in Figure 3-25 (a) (b) (c) (d), respectively.

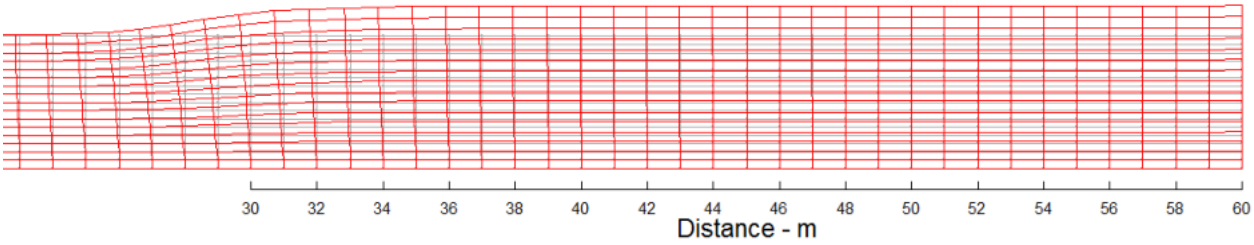

Figure 3-24. Expansion of clayey soil of Aine Tine slope

Considering the amplitudes of the vertical displacement, the obtained profiles of heaves can be divided into three regions as follow:

a) Unexposed part to the rain: located in the left side of each illustration where null values of heave were obtained due the non-variation of the water content.
b) Exposed part to the rain: located on the right side of the model (x>30) where upwards movements were resulted where the magnitude is proportionally related to the initial suction values and the duration of the simulation.
c) Central part: it is a transition zone which becomes larger and larger with respect to the initial values of suction and the duration of the rainfall precipitation.

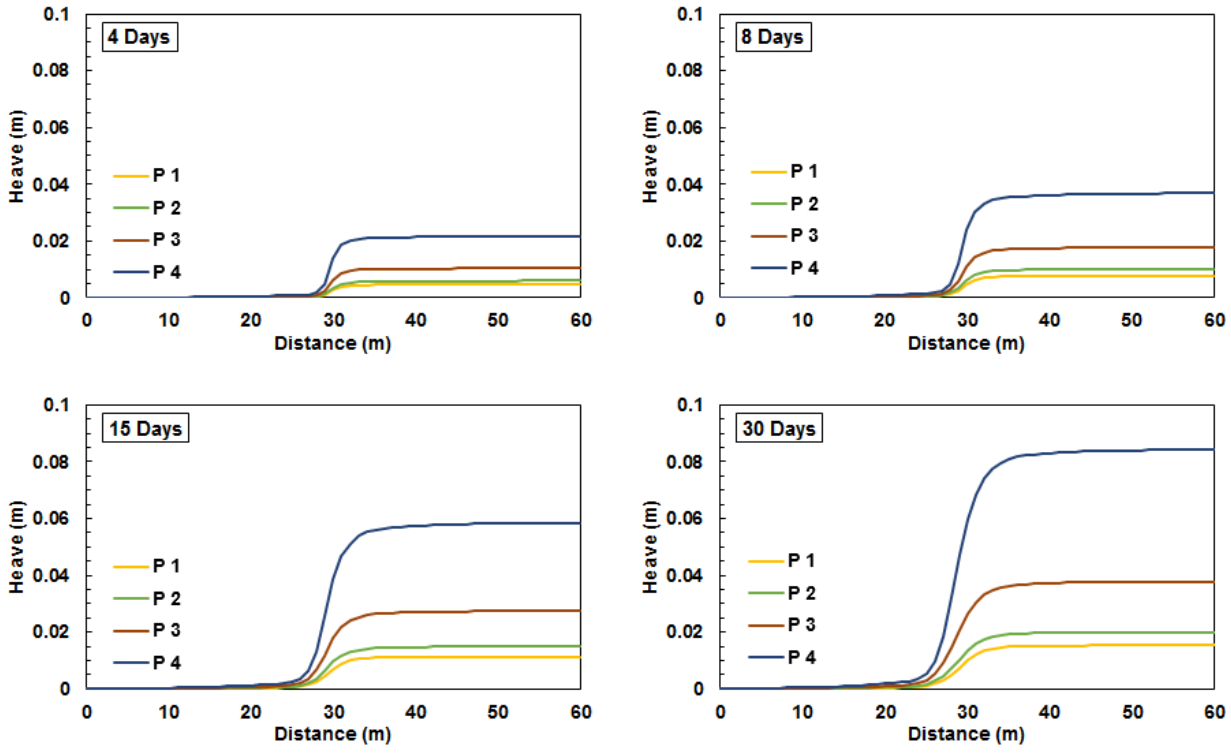

Figure 3-25. Vertical heave distribution on Top surface (m) with time

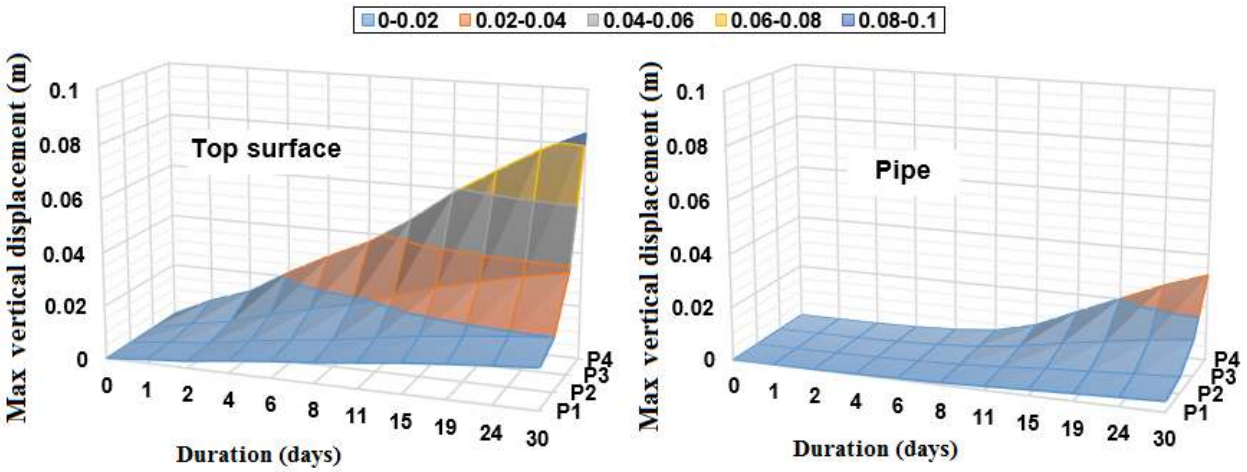

Figure 3-26. The maximum vertical displacement at the exposed part to the rain

The maximum induced vertical displacement located at the top surface of the exposed part to the rain are summarized in the Figure 3-26. After 4 days of simulation, they reached 0.46, 0.6, 1.04 and 2.18cm for the suction conditions P1, P2, P3 and P4, respectively, while they reached 1.54, 2, 3.78 and 8.42cm after 30 days of rainfall. The vertical displacement at the pipeline location start to appear after approximately 8 days of rainfall (Figure 3-26) they reached 1.37 and 3.23 cm after 30 days of rainfall for suction conditions P2 and P4, respectively.

3.12.2. Longitudinal forces

As for the transverse analysis, in the longitudinal modelization, stresses and strains on the pipeline body will be generated following the swelling movements that occur in the expansive soil. The curves with yellow, green, red and blue colors represent the results of each depth of GWT and in other words to the profile of the initial soil suction P1, P2, P3 and P4, respectively.

a) Axial forces F_A

Figure 3-27 shows the variations of the axial forces that followed the expansion of the Aine-Tine clayey soil under the rainfall precipitation which correspond to different chosen duration of simulation equals to 4, 8, 15 and 30 days. The first remark is about the shape of the resulted profiles where they take dissymmetric shape where the center is the point between the exposed and the unexposed parts to the rainfall infiltration with positive values representing compression forces at the left side (i.e., unexposed part) and with negative values at the right side (i.e., exposed part) indicating tension forces. Two peak values with opposite values were obtained which are located at the following abscissa 25m <x< 26m for the compressive forces and at the abscissa 32m <x< 34m for the tension forces. The second remark is about the relationship between the rainfall duration and the initial suction with the magnitudes of the obtained components of internal forces which are proportionally related.

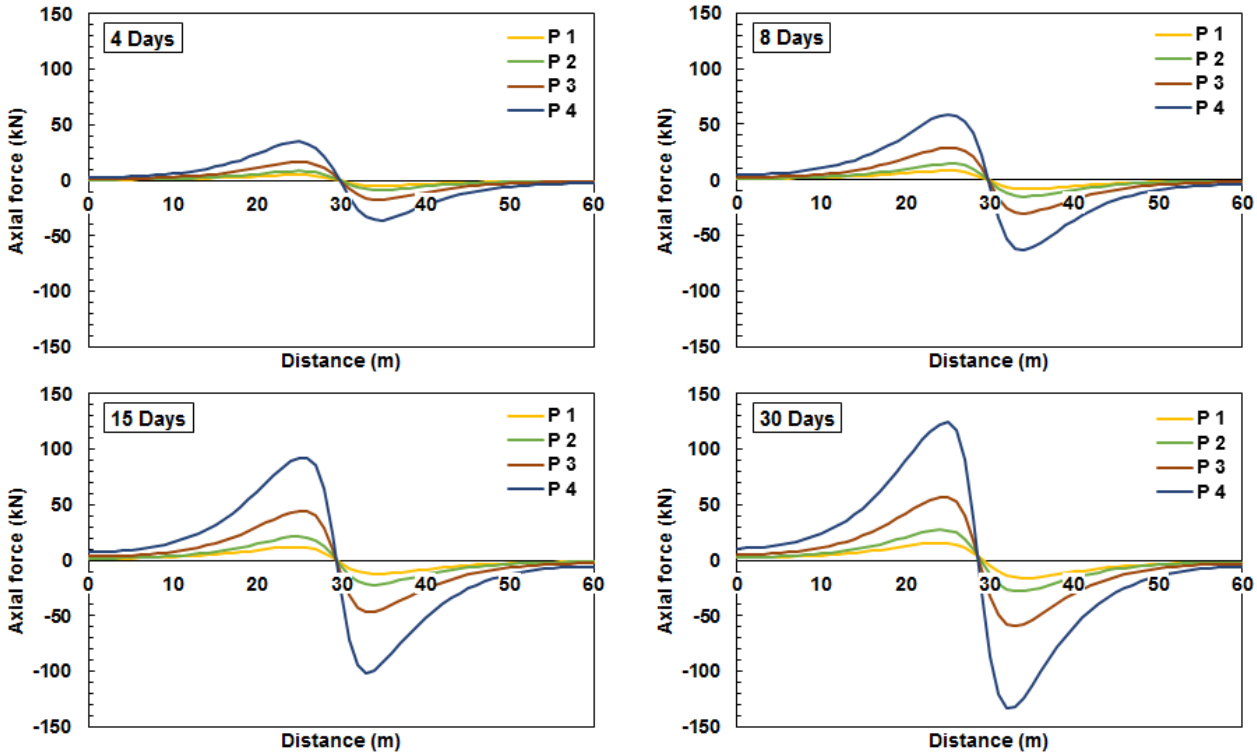

Figure 3-27. Longitudinal axial forces distribution along pipeline (kN) with time

The tension forces touched 133.58 kN at the end of simulation in the case of initial suction profile P4 while tension forces reached 124.07 kN. Considering the annular cross section of Aine-Tine pipeline, These forces generated tension and compression stresses summarized below (Table 3-3). The developed stresses can be much higher in other scenarios with longer duration of rainfall and suction profile where suction values can reach 10000 kPa in expansive soils as the one used by Zhang and Briaud (2015).

Figure 3-28 shows the displacement in the horizontal direction induced at the central part of the model after 30 days of simulations considering the conditions of suction profile P4 which correspond to the deepest GWT in the present study. The orientation of the displacement vectors shows that the central part becomes more influenced by the horizontal component of the displacements where they are oriented from the part exposed to rain to the unexposed part.

Table 3-3. Longitudinal tension and compression stresses developed at the end of simulation

Suction profile	Area (m^2)	Tension stresses (kPa)	Compression stresses (kPa)
P1	0.0248	3.32	3.08
P2		1.47	1.42
P3		0.69	0.68
P4		0.40	0.38

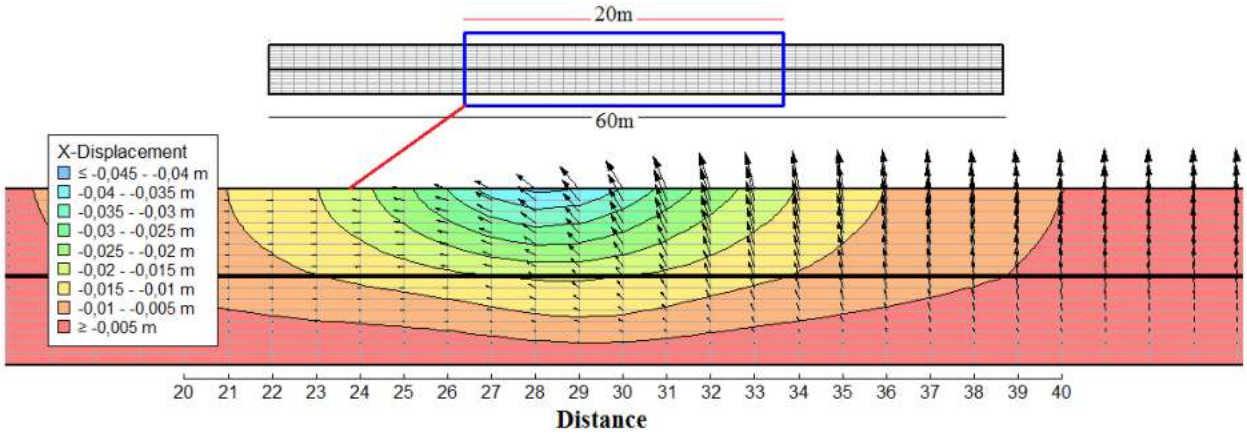

Figure 3-28. X-displacement at the central part of the model

Figure 3-29 presents the final profiles of horizontal displacement at the center of the model obtained after 30 days of rainfall. Considering the suction profile P4, the horizontal displacement exceeded 3 cm at the top of the model where the displacement reached 1.5cm at the pipeline depth (Z=2m) while those calculated considering the suction profile P1, are equal to 0.72cm and 0.23cm at Z=4m and Z=2m, respectively. The obtained results (Figure 3-29) are very useful to justify the results of the axial forces shown in Figure 3-27, where the curves of axial forces depict two zones, the first zone is a zone of compression, located at the part not exposed to rain, which is attributed to the negative component of the horizontal displacement mainly oriented on the left side of the model. On the other hand, a tension zone where the tensile forces can be attributed to the elongation of the pipeline under the vertical direction of soil expansion and to the horizontal direction of the clay expansion.

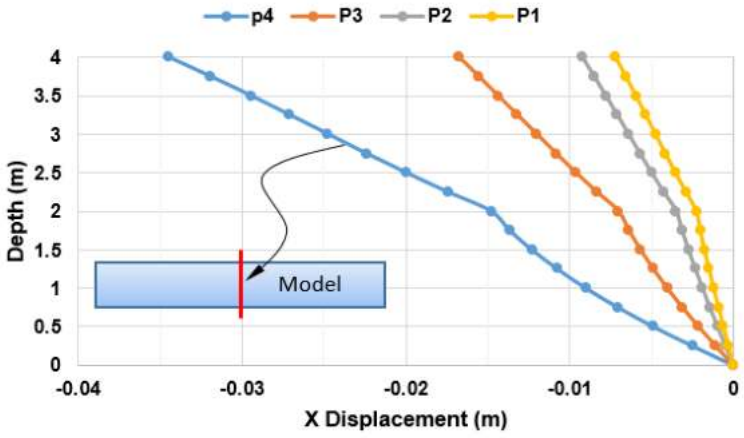

Figure 3-29. Final X-displacement at the central part of the model after 30 days of rainfall

b) Shear force F_S

The variation of the shear forces on the pipeline are shown in the Figure 3-30. Taking an approximately symmetric distribution around the center of the model, the shear forces curves presents three peaks of values one negative located at the center and two positive located at the left and right sides from the central point. The central peak values are higher than those of the two other peaks. The magnitudes of this force components increase with respect to both the duration and the

initial suction. As for the axial stresses, considering the annular cross section of Aine-Tine pipeline, the developed shear forces generated shear stresses summarized below (Table 3-4).

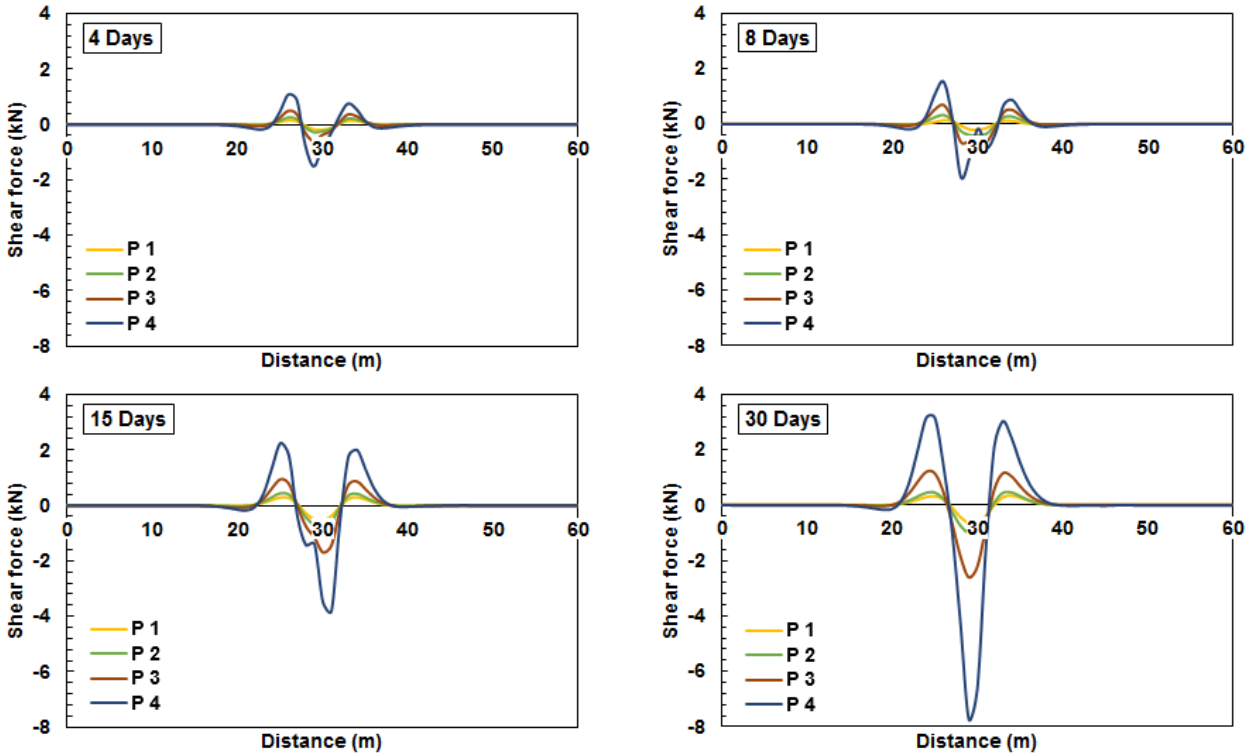

Figure 3-30. Longitudinal Shear forces distribution along pipeline (kN) with time

Table 3-4. Longitudinal shear stresses developed at the end of simulation

Suction profile	Area (m^2)	Peak 1 (kPa)	Peak 2 (kPa)	Peak 3 (kPa)
P1	0.0248	128.13	311.06	122.49
P2		47.55	104.76	41.50
P3		18.94	40.70	19.34
P4		12.49	26.19	13.70

a) Bending moment M_B

Figure 3-31 shows the variation of the bending moment developed on the pipeline body where as for the axial and shear forces the duration of the rainfall and the initial suction have the same effects on the magnitudes of bending moment. The shape of the bending moment curves takes the same form as for the axial internal forces with different magnitudes and signs.

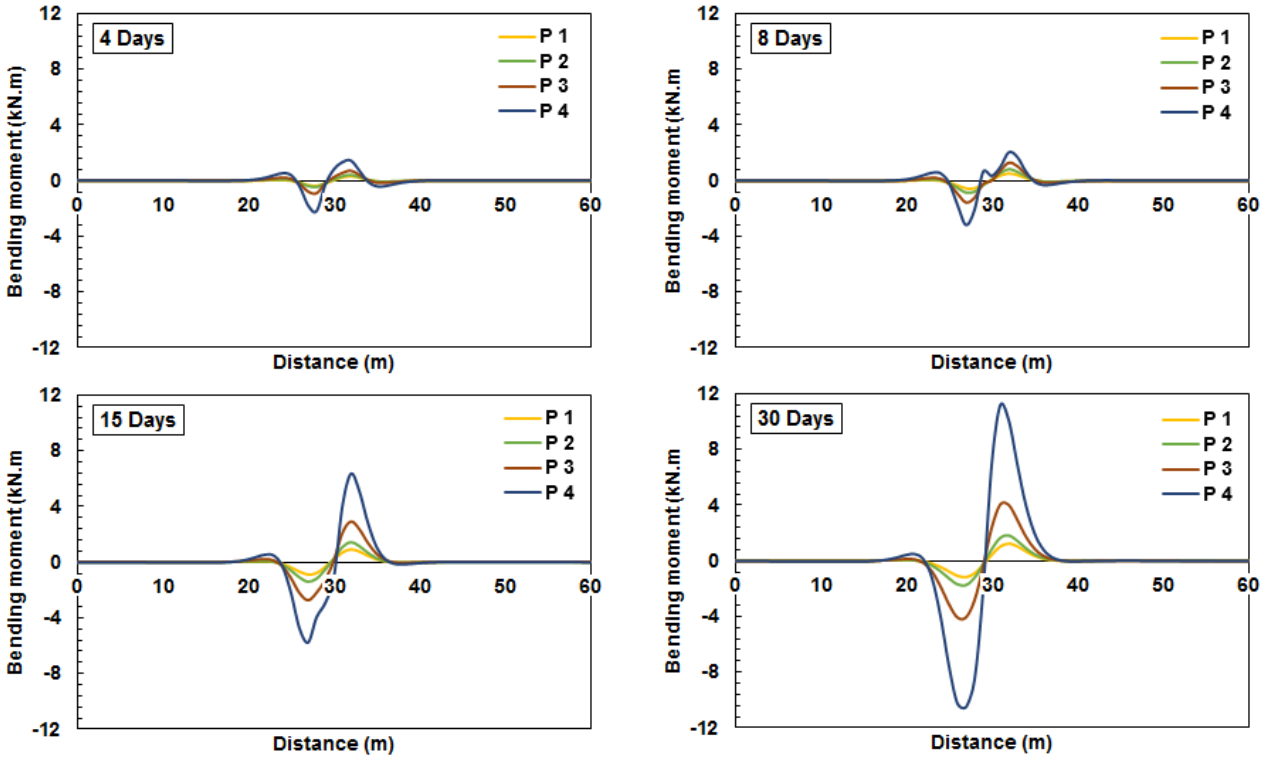

Figure 3-31. Longitudinal bending moment distribution along pipeline (kN) with time

3.13. Conclusion

In the present chapter, numerical analyses were performed to investigate the transverse and longitudinal structural behavior of buried pipelines in expansive soils considering the unsaturated behavior of soil under the effect of 4mm/day rainfall precipitation lasting for 30 days as an external hydraulic loading. Considering the 800 mm water supply pipeline coming from the Beni-Haroun Dam and buried at 2 m depth in Aine-Tine (Mila, Algeria) high expansive soil, four simulations were performed to demonstrate the effect of the initial suction profiles P1, P2, P3 and P4 which may represent different degrees of aridity that characterize regions with arid and semi-arid climate.

A simplified two dimensional models was proposed using the finite element software SIGMA/W. The results obtained were expressed in terms of (1) changes in soil suction, (2) heave and deformations and (3) radial and longitudinal forces (Axial F_A, Shear F_S forces and Bending moment M_B) that are developed on the pipeline. Analysis of the results allowed to reach the following conclusions:

— Rainfall events can cause additional loads on buried pipelines in expansive soils because of the important role of the unsaturated behavior of such soils especially in arid and semi-arid regions where the surficial soils present high values of suction.

— Due to the soil saturation process caused by the progressive rainfall infiltration of water within the soil, the expansive soil exhibits volume changes associated with heave at the ground surfaces following decrease in suction indicating that the effect

of the soil suction must be taken carefully into consideration, especially where the seasonal variation of moisture content is very high.

— The induced soil heave and the radial and longitudinal forces exerted on the pipeline wall increase with the initial soil suction (P1, P2, P3 and P4) and also with the rainfall duration (4, 8, 15 and 30 days).

— The initial suction values worked out from the GWT depth or from the degree of evapotranspiration and the importance of the rainfall precipitation are important factors that impact seriously the unsaturated behavior of the soil behavior as well as the response of the pipeline structure.

— The pipeline cross-section ovalization can be a logic reason to many water leakage points along the paths of the Mila water supply pipelines including the one located in Aine-Tine site especially near the pipeline joints. Figure 3-32 shows the values of ovalization obtained after different duration of simulation. It is very clear that the values of ovalization obtained are lower than the value of 15% adopted by the Dutch specification NEN 3650 as a criterion of performance of ovalization, however, these values can be the trigger for damage during certain scenarios of large displacement as the area of Aine-Tine is landslides prone area.

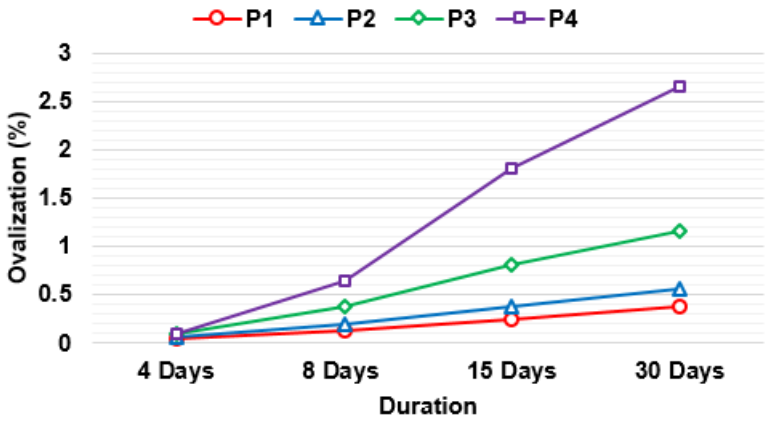

Figure 3-32. Cross section ovalization

The results of the present study are very useful to understand and predict one of the possible origin of the damages reported on the Ain-Tine water supply pipeline. They made clear that in order to achieve a realistic design of buried lifeline infrastructures, the unsaturated behavior of the embedding expansive soil should be taken into consideration under realistic climatic conditions of the region. Moreover, this study analyzed only the transverse behavior of the pipeline structure under simplified hypotheses. In order to achieve more realistic results, a representative daily precipitation data (i.e., intensity, duration and frequency) would be used instead. In addition, many types of the pipelines such as rigid, flexible, welded and jointed and with different diameter are buried to transport fluids and which need to be considered in the future studies. It is also strongly recommended to include the investigation of the expansion behavior of soils located in arid and semiarid regions.

3.14. References

Adem, H.H., Vanapalli, S.K., 2014a. Prediction of the modulus of elasticity of compacted unsaturated expansive soils. Int. J. Geotech. Eng. 9, 163–175. https://doi.org/10.1179/1939787914Y.0000000050

Adem, H.H., Vanapalli, S.K., 2014b. Elasticity moduli of expansive soils from dimensional analysis. Geotech. Res. 1, 60–72. https://doi.org/10.1680/gr.14.00006

Adem, H.H., Vanapalli, S.K., 2013. Constitutive modeling approach for estimating 1-D heave with respect to time for expansive soils. Int. J. Geotech. Eng. 7, 199–204. https://doi.org/10.1179/1938636213Z.00000000024

Al-Khazaali, M., Vanapalli, S.K., 2020. A Novel Experimental Technique to Investigate Soil–Pipeline Interaction under Axial Loading in Saturated and Unsaturated Sands. Geotech. Test. J. 43, 70–93. https://doi.org/10.1520/GTJ20180059

Al-Khazaali, M., Vanapalli, S.K., Oh, W.T., 2018. Numerical investigation of soil–pipeline system behavior nearby unsupported excavation in saturated and unsaturated glacial till. Can. Geotech. J. 56, 69–88. https://doi.org/10.1139/cgj-2017-0411

Athmania, D., Benaissa, A., Hammadi, A., Bouassida, M., 2010. Clay and Marl Formation Susceptibility in Mila Province, Algeria. Geotech. Geol. Eng. 28, 805–813. https://doi.org/10.1007/s10706-010-9341-5

Azam, S., Shah, I., Raghunandan, M.E., Ito, M., 2013. Study on swelling properties of an expansive soil deposit in Saskatchewan, Canada. Bull. Eng. Geol. Environ. 72, 25–35. https://doi.org/10.1007/s10064-012-0457-0

Biot, M.A., 1941. General theory of three-dimensional consolidation. J. Appl. Phys. 12, 155–164.

Chettah, W., 2009. Investigation des propriétés minéralogiques et géomécaniques des terrains en mouvement dans la ville de Mila « Nord-Est d'Algérie » (Thèse de Magistère). University of Batna 1 Hadj Lakhdhar, Batna, Algérie.

Clark, C.M., 1971. Expansive-Soil Effect on Buried Pipe. J. - AWWA 63, 424–427. https://doi.org/10.1002/j.1551-8833.1971.tb04116.x

Fredlund, D.G., Morgenstern, N.R., 1976. Constitutive relations for volume change in unsaturated soils. Can. Geotech. J. 13, 261–276. https://doi.org/10.1139/t76-029

Fredlund, D.G., Rahardjo, H., 1993a. Soil mechanics for unsaturated soils. John Wiley & Sons.

Fredlund, D.G., Rahardjo, H., 1993b. Soil mechanics for unsaturated soils. John Wiley & Sons.

Fredlund, D.G., Xing, A., 1994. Equations for the soil-water characteristic curve. Can. Geotech. J. 31, 521–532. https://doi.org/10.1139/t94-061

GeoSlope International Ltd, 2007. SIGMA/W user's guide for stress-deformation analysis. GEO-SLOPE International Ltd. Calgary, AB, Canada.

Han, Z., Vanapalli, S.K., 2016. Stiffness and shear strength of unsaturated soils in relation to soil-water characteristic curve. Géotechnique 66, 627–647. https://doi.org/10.1680/jgeot.15.P.104

Han, Z., Vanapalli, S.K., Kutlu, Z.N., 2016. Modeling Behavior of Friction Pile in Compacted Glacial Till. Int. J. Geomech. 16. https://doi.org/10.1061/(ASCE)GM.1943-5622.0000659

Huang, S.L., Yang, K., Akagawa, S., Fukuda, M., Kanie, S., 2015. Frost Heave Induced Pipe Strain of an Experimental Chilled Gas Pipeline, in: Innovative Materials and Design for

Sustainable Transportation Infrastructure. Presented at the International Symposium on Systematic Approaches to Environmental Sustainability in Transportation, American Society of Civil Engineers, Fairbanks, Alaska, pp. 405–416. https://doi.org/10.1061/9780784479278.037

Ito, M., Azam, S., Hu, Y., 2014. A two stage model for moisture-induced deformations in expansive soils. Environ. Syst. Res. 3, 19. https://doi.org/10.1186/s40068-014-0019-5

Kumar, S., Sahu, A.K., Naval, S., 2020. Influence of Jute Fibre on CBR Value of Expansive Soil. Civ. Eng. J. 6, 1180–1194. https://doi.org/10.28991/cej-2020-03091539

Mebarki, A., 2005. HYDROLOGIE DES BASSINS DE L'EST ALGERIEN : RESSOURCES EN EAU, AMENAGEMENT, ET ENVIRONNEMENT (thèse de doctorat d'etat). University of Mentouri, Constantine.

Oghabi, M., Khoshvatan, M., Marto, A., 2017. Evaluation of the Response of Buried Steel Pipelines Subjected to the Strike-slip Fault Displacement. Civ. Eng. J. 3, 661–671. https://doi.org/10.21859/cej-03093

Oh, W.T., Vanapalli, S.K., Puppala, A.J., 2009. Semi-empirical model for the prediction of modulus of elasticity for unsaturated soils. Can. Geotech. J. 46, 903–914. https://doi.org/10.1139/T09-030

Ozer, M., Ulusay, R., Isik, N.S., 2012. Evaluation of damage to light structures erected on a fill material rich in expansive soil. Bull. Eng. Geol. Environ. 71, 21–36. https://doi.org/10.1007/s10064-011-0395-2

Qi, S., Vanapalli, S.K., 2016. Influence of swelling behavior on the stability of an infinite unsaturated expansive soil slope. Comput. Geotech. 76, 154–169. https://doi.org/10.1016/j.compgeo.2016.02.018

Qi, S., Vanapalli, S.K., 2015. Hydro-mechanical coupling effect on surficial layer stability of unsaturated expansive soil slopes. Comput. Geotech. 70, 68–82. https://doi.org/10.1016/j.compgeo.2015.07.006

Rajeev, P., Kodikara, J., 2011. Numerical analysis of an experimental pipe buried in swelling soil. Comput. Geotech. 38, 897–904. https://doi.org/10.1016/j.compgeo.2011.06.005

Randeniya, C., Robert, D. j., Li, C.-Q., Kodikara, J., 2019. Large-scale experimental evaluation of soil saturation effect on behaviour of buried pipes under operational loads. Can. Geotech. J. 57, 205–220. https://doi.org/10.1139/cgj-2018-0544

Robert, D., Soga, K., 2013. Soil-Pipeline Interaction in Unsaturated Soils, in: Mechanics of Unsaturated Geomaterials. John Wiley & Sons, Inc., Hoboken, NJ USA, pp. 303–325. https://doi.org/10.1002/9781118616871.ch13

Robert, D.J., Soga, K., O'Rourke, T.D., 2016a. Pipelines Subjected to Fault Movement in Dry and Unsaturated Soils. Int. J. Geomech. 16. https://doi.org/10.1061/(ASCE)GM.1943-5622.0000548

Robert, D.J., Soga, K., O'Rourke, T.D., Sakanoue, T., 2016b. Lateral Load-Displacement Behavior of Pipelines in Unsaturated Sands. J. Geotech. Geoenvironmental Eng. 142, 04016060. https://doi.org/10.1061/(ASCE)GT.1943-5606.0001504

Saadeldin, R., Hu, Y., Henni, A., 2015. Numerical analysis of buried pipes under field geo-environmental conditions. Int. J. Geo-Eng. 6, 6. https://doi.org/10.1186/s40703-015-0005-4

Teimouri, A.B.B., Khalkhali, A.B., 2018. Stability Control of Narmab Dam and Sensitivity Analysis of Reliability Coefficients. Civ. Eng. J. 4, 2197-2209–2209. https://doi.org/10.28991/cej-03091150

Uzundurukan, S., Keskin, S.N., Yıldırım, H., Göksan, T.S., Çimen, Ö., 2014. Suction and Swell Characteristics of Compacted Clayey Soils. Arab. J. Sci. Eng. 39, 747–752. https://doi.org/10.1007/s13369-013-0852-2

van Genuchten, M.Th., 1980. A Closed-form Equation for Predicting the Hydraulic Conductivity of Unsaturated Soils. Soil Sci. Soc. Am. J. 44, 892–898. https://doi.org/10.2136/sssaj1980.03615995004400050002x

Vazouras, P., Dakoulas, P., Karamanos, S.A., 2015. Pipe–soil interaction and pipeline performance under strike–slip fault movements. Soil Dyn. Earthq. Eng. 72, 48–65. https://doi.org/10.1016/j.soildyn.2015.01.014

Vazouras, P., Karamanos, S.A., Dakoulas, P., 2010. Finite element analysis of buried steel pipelines under strike-slip fault displacements. Soil Dyn. Earthq. Eng. 30, 1361–1376. https://doi.org/10.1016/j.soildyn.2010.06.011

Vu, H.Q., Fredlund, D.G., 2006. Challenges to modelling heave in expansive soils. Can. Geotech. J. 43, 1249–1272. https://doi.org/10.1139/t06-073

Vu, H.Q., Fredlund, D.G., 2004. The prediction of one-, two-, and three-dimensional heave in expansive soils. Can. Geotech. J. 41, 713–737. https://doi.org/10.1139/t04-023

Yilmaz, I., 2007. The effect of swelling clays on a water transport canal between Köklüce HPP and Erbaa HPP (Turkey). Bull. Eng. Geol. Environ. 66, 467–472. https://doi.org/10.1007/s10064-007-0086-1

Zhang, J., Peng, J., Li, J., Zheng, J., 2018. Variation of Resilient Modulus with Soil Suction for Cohesive Soils in South China. Int. J. Civ. Eng. 16, 1655–1667. https://doi.org/10.1007/s40999-018-0315-y

Zhang, X., Briaud, J.-L., 2015. Three dimensional numerical simulation of residential building on shrink–swell soils in response to climatic conditions. Int. J. Numer. Anal. Methods Geomech. 39, 1369–1409. https://doi.org/10.1002/nag.2360

Chapter 04

NUMERICAL ANALYSIS OF BURIED WATER SUPPLY PIPELINES SUBJECTED TO SHALLOW PGD

4. Numerical Analysis of Buried Water Supply Pipelines Subjected to Shallow PGD

4.1. Background information

The content presented in this chapter was used to prepare the following contribution entitled:

Bouatia, M., Demagh, R., Derriche, Z., 2021. Numerical Analysis of Buried Pipelines Subjected to permanent Ground Deformations due to Shallow Landslides. Jordan Journal of Civil Engineering

4.2. Introduction

Permanent Ground Deformations (PGD) are happen usually happened following lateral spreading, fault movements as well as landslides that, mainly, triggered by naturals hazards such as earthquakes and intense precipitations. In Europe, it was found that ground movement, such as slope instability, was the cause of 13% of gas pipeline incidents during the period from 2004 to 2013 (Wu et al., 2017). The present study will help the engineers and planners to understand the effective causes of many recorded water leakage cases and pipelines breaks leading to hard disruptions of the normal operations of water supplying in the eastern side of Algeria.

Pipelines networks are widely used to transport liquids such as water and gas over long distances and often, they can go throughout a variety of geological and topographical conditions, where in many cases, it is imperative to bury these very important lifelines on sloping grounds. The stability of these slopes is sensitive to many failure causing factors such as precipitation, faults as well as seismic movements. The induced relative movements of the soil and the buried pipelines due to slope failures can result in catastrophic environment and economic losses following pipeline ovalization and breaks as a result of the additional external loads acting on these linear structures.

Pipelines are usually buried at shallow depths to protect them against external loads coming from upward and downward movements including, but not limited to wheels, expansion of soil as well as frost heaves. However, there are still other sources of damages that cannot be avoided and which lead to large PGD, which are known to be non-reversible deformations. These sources usually follow natural hazards like landslides, faulting or liquefaction induced lateral spreading (Ariman and Muleski, 1981) (Ng, 1994). The main causes of these phenomena are the earthquakes and intense precipitations that reduce the shear strength and consequently destroy the buried pipelines within these slopes.

In the literature, the soil-structure interaction is an active subject where the soil-pipeline systems occupy a considerable part because of the interaction of two different materials (i.e., pipe and soil) and their complex relationships. A large published works analyzed and discussed numerically and experimentally the behavior of buried pipelines under different natural and manmade loading conditions (Rajani and Morgenstern, 1993) (Li et al., 2013) (Randeniya et al., 2019) (Al-Khazaali and Vanapalli, 2020).

Vazouras et al. (2010) conducted rigorous three-dimensional numerical investigations on the mechanical response of buried pipelines subjected to the movement of strike-slip seismic faults. The fault was normal to the pipeline longitudinal direction with a diameter equal to 914.4 mm.

Through an extensive parametric study, the obtained results suggest the safe combinations of fault displacement and diameter-to-thickness parameters of two typical pipelines considering the developed strains of the pipeline structures, and taking into account two different cohesive soils (soft and stiff clays) and two cohesionless soils (loose and dense sands). In the same direction, the effect of the fault angle was investigated by Vazouras et al. (2012). Later, Vazouras and Karamanos (2017) studied the behavior of a 36-inch-diameter pipeline elbows of 90°, 60° and 30° bend angles subjected to pull-out forces due strike-slip fault movements; the obtained results confirm that appropriate placed elbows can be used as mitigating devices to reduce the induced action at the fault locations.

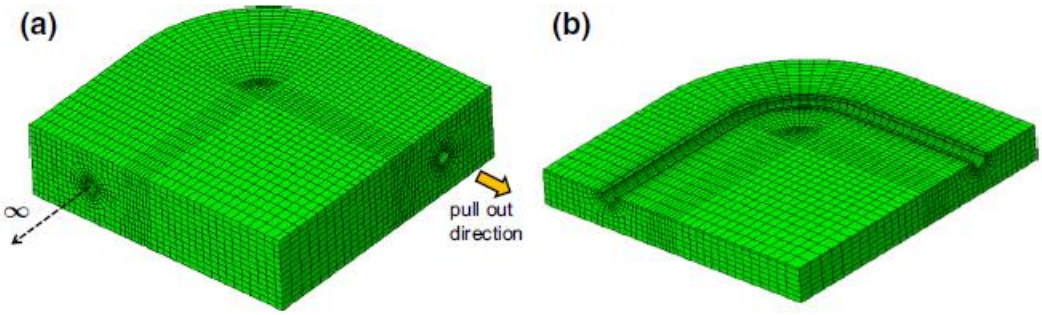

Figure 4-1. pipeline elbows subjected to pull-out forces (Vazouras and Karamanos, 2017)

More recently, Bouatia et al. (2020a) used SIGMA/W to study the transverse structural response of an 800 mm water transport pipeline buried in Mila basin (Mila, Algeria) expansive soils under rainfall precipitations. They found that the upward expansion movements induce internal forces on buried pipelines ring that are proportionally related to the rainfall duration and to the water table depth as well as the degree of evapotranspiration.

Many experimental investigations were carried out to explore the interaction between landslides and buried pipelines. Zhang and Askarinejad (2019) performed a small-scale centrifuge tests to assess the effect of slope failures, induced by surcharge loading applied on the crest of a sandy slope with an inclination of 18.4°, on the external forces acting on buried pipes at various locations. The analysis considered two types of sand and different embedment depths (Figure 4-2). The study proposed a method which allows the prediction of the maximum external loadings exerted on the pipe whatever the circular failure mechanism of the slope. For more details, the reader can read the paper to understand the methodology of the experimental work which is very intersecting.

In addition, it was highlighted that the location of the pipe plays an important role to minimize the effects of the induced movements. O'Rourke et al. (2008) conducted large-scale parametric investigations of the effect of rapid large deformations similar to sudden ground deformations that follow the natural hazards such as landslides, faults and earthquakes on pipelines buried in unsaturated compacted sands. The analyzed pipeline is 407 mm diameter and a diameter-to-thickness ratio equal to 17 subjected to 1.22 m fault displacement at 65° crossing angle. The study highlighted the similarity of the lateral forces that are developed between dry and partially saturated sand.

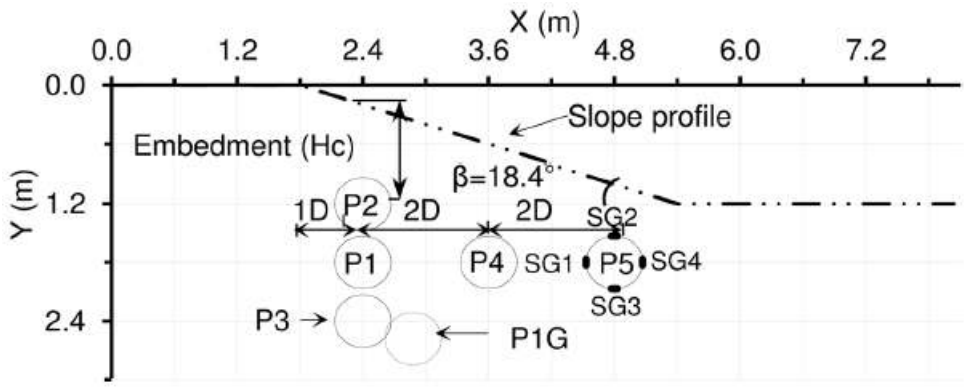

Figure 4-2. Five pipe locations for DC Sand tests (P1 to P5) and one pipe location for Geba Sand test (P1G) (Zhang and Askarinejad, 2019)

Feng et al. (2015) studied the case of a large-scale landslide crossed by a gas pipeline prototype. After a series of excavations, the induced lateral movements brought the pipeline towards the toe of the slope and it was found that the most affected locations on the pipeline body are on both sides of the movable ground (i.e., landslide) limits and in the central part of the landslide (Figure 4-3). It was found that the induced stress distribution and deformation along the pipeline is in the form of a saddle in both vertical and horizontal directions (Figure 4-4).

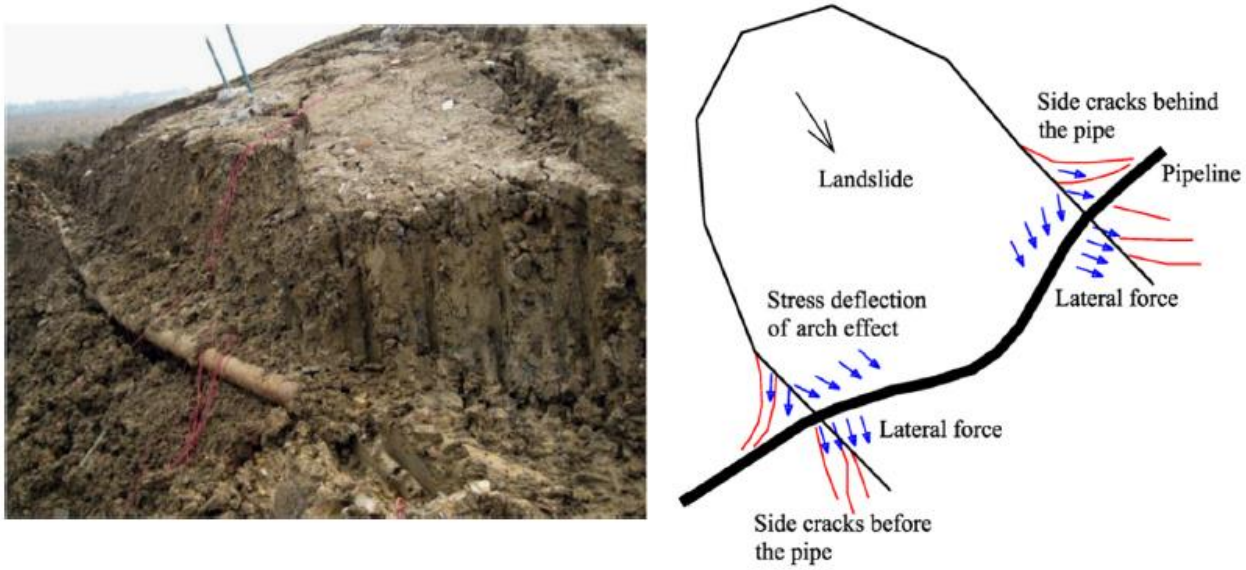

Figure 4-3. (a) Strong down warping of the pipeline (b) Schematic diagram of the generation of forces and cracks at the boundary of the landslide induced by the deformation of the pipeline (Feng et al., 2015)

On the other hand, Shi et al. (2019) conducted a consistent physical modelling to investigate the axial behavior of the pipeline subsea continental slopes. Using a small-scale laboratory testing procedure, Al-Khazaali and Vanapalli (2020) defined a new experimental technique to study the axial behavior of buried pipeline in unsaturated sands and subjected to longitudinal axial forces.

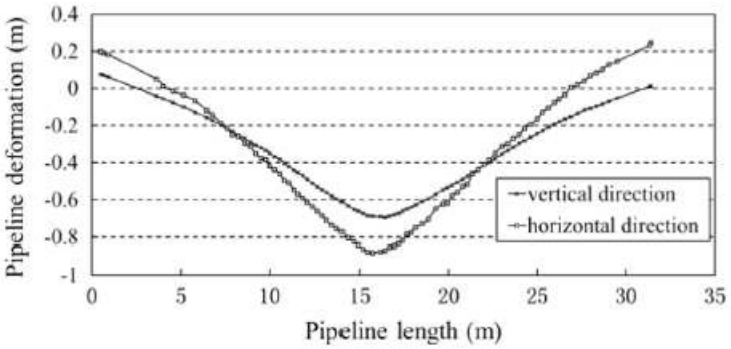

Figure 4-4. The final deformation of the pipeline (Feng et al., 2015)

Recently, in July and August 2020, the province of Mila located in the north of Algeria suffered repetitive earthquake events which caused catastrophic damages on the infrastructures including the pipeline networks of Beni-Haroun Dam as a consequence of large shallow PGD that occurred on the pipelines routes. Many water leakage points causing intense disruption of water supply towards the eastern provinces of the country were recorded. The majority of the recorded cases are mainly related to shallow slope failures and where the slip planes pass through the pipeline diameter unlike the deep slip surfaces where the pipelines are totally carried away with the sliding mass. The main conclusion drawn from the previous discussion is that the literature is rich of longitudinal investigation of pipeline under different loading conditions unlike the transverse behavior. However, research efforts to account for shallow permanent soil deformations on buried pipelines are very limited in the literature, even though they occur frequently with hard economic and environment losses.

This chapter presents the details of a numerical investigation of the effect of very shallow permanent ground deformation that can be triggered by natural hazards such as landslides on the structural transverse behavior of buried pipelines. Using the commercial software SIGMA/W, the evaluation of (1) the pipeline deformation and (2) the radial internal efforts (i.e., axial forces F_A, shear forces F_S and bending moment M_B) that are developed on the pipeline perimeter have been performed. The main objective is to understand the effect of permanent ground deformations (PGD) on the transverse soil-pipeline interaction by considering (1) two different rigidities of pipeline (i.e., rigid and flexible) and (2) different magnitude of the ground deformation, ranging from 0.1 m to 2 m. The water supply pipeline coming from Beni-Haroun Dam of 0.8 m diameter D assumed to be buried at 2 m depth in Aine-Tine (Mila, Algeria) soil was used to perform this finite element analysis.

4.3. Permanent ground deformations PGD

The PGD are defined as non-reversible movement of the ground surface. Many PGDs that followed landslides or earthquake shakings generate quasi-static worst loadings for no-seismically designed buried structures (i.e., pipelines). Seismic design of buried pipelines has great importance in the field of lifeline engineering (IITK-GSDMA, 2007) (ALA, 2005). Unfortunately, it was not considered in many cases with the pipeline networks. Table 4-1 provides the most common natural hazards that can cause PGDs on buried pipelines.

Table 4-1. Common natural hazards causing PGD (IITK-GSDMA, 2007) (ALA, 2005)

Hazard type	Definition
Faulting	Faulting are PGDs that are characterized by abrupt permanent ground deformations.
Liquefaction	Liquefaction is a phenomenon that occurs in loose to medium dense sandy saturated soil during seismic shaking. During liquefaction, the soil loses a substantial amount of its shear strength and acts like a viscous fluid.
Lateral spread and flow failure	Lateral spreading is a phenomenon which occurs in a gently sloping ground when the soil deposit liquefies due to seismic shaking. The soil loses its shear strength during liquefaction, which in turn results in lateral movement of liquefied soil and any overlaying soil layer.
Slope movement, landslides	Landslides are the mass movements of the ground which may be triggered by an earthquake or some other causes.
Settlement	Settlement are vertical movement which results from the densification of relatively loose, partially saturated or dry granular soils (manifestation of volumetric strains). Settlement increases with decreasing relative density and soil fines content.

Wu et al. (2014) reported that the most hazardous relationship is when the pipeline traverses landslide. According to the strike of the pipeline and the sliding direction of the landslide, the relationship between the pipeline and landslide can be divided into three situations as follow:

a) The strike of the pipeline is perpendicular to the sliding direction of the landslide that is pipeline traverse landslide Figure 4-2(a).

b) The direction of the pipeline is parallel to the landslide direction, that is, the pipeline crosses the landslide lengthwise Figure 4-2(b).

c) The strike of the pipeline is skew to the sliding direction of the landslide, that pipeline goes obliquely across landslide. The development status of pipeline geohazard and the positional relationship with the pipeline determines the magnitude of damage risk.

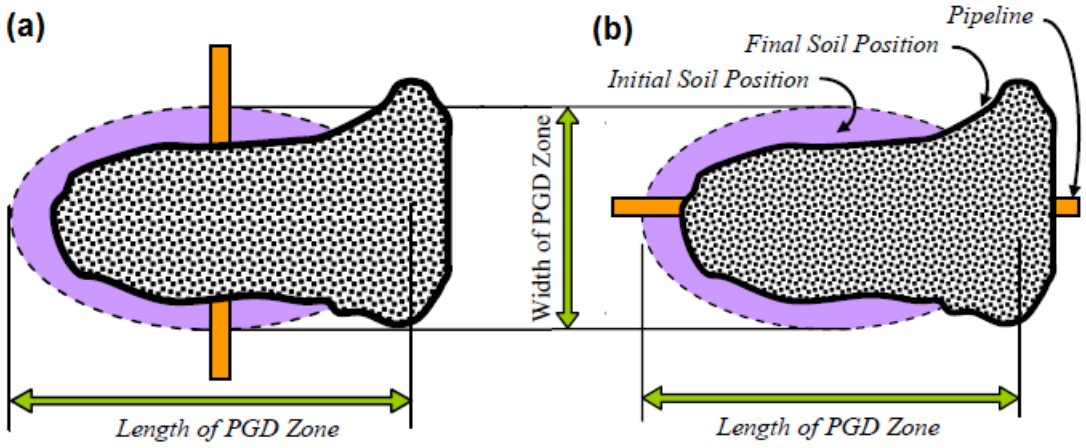

Figure 4-5. Pattern of transverse and longitudinal permanent ground deformation (IITK-GSDMA, 2007)

Figure 4-6 shows the idealized scheme of buried pipelines subjected to PGD taking the form of a slope failure displacement in transverse situation. Therefore, the location of pipeline in the landslide can be divided into five conditions (Wu et al., 2014) as follow:

- The pipelines are installed in the front of the landslide mass (Figure 4-7 (a)). When the land sliding occurs, the down-sliding force acts perpendicularly on the pipes, which deforms the pipe simultaneously. And the down-sliding force will bend or even rupture the pipe, which reduces the transmission capacity and service life of the pipes.
- The pipelines are installed in the rear part of the landslide mass (Figure 4-7 (b)). When the land sliding occurs, the down-sliding force has less effect on the pipes while the upper soil mass, the self-weigh of the pipes and the friction of soil are the main strength lead to the pipeline damage.
- The pipelines are installed near the sliding surface (Figure 4-7(c)). The partial down-sliding force of landslide causes bending deformation of the pipe.
- The gas pipelines are installed under the sliding surface (Figure 4-7(d)). In this situation, the sliding deformation of the landslide does not damage the pipes directly. However, when the land sliding occurs, it may trigger a new secondary landslide even expose the pipe. Therefore, in practical engineering, these circumstances also need to be treated with engineering treatments.
- The gas pipelines are installed in the front of shear outlets (Figure 4-7(e)). When land sliding occurs, the pipeline will be squeezed even located in the front of the landslide mass because of the shallow burial depth, which have negative effect on the maintenance of the pipeline and increase the unsafe factors

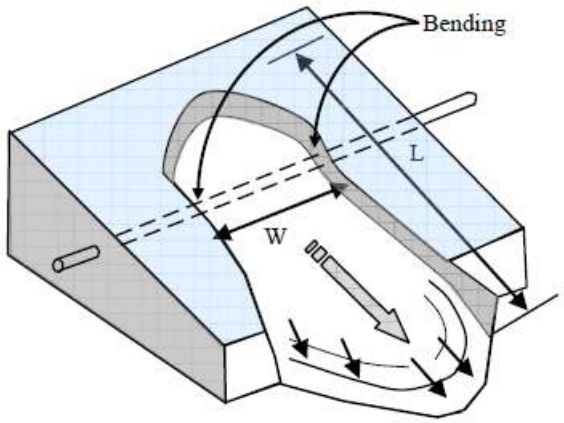

Figure 4-6. Pipeline subjected to transverse PGD (IITK-GSDMA, 2007)

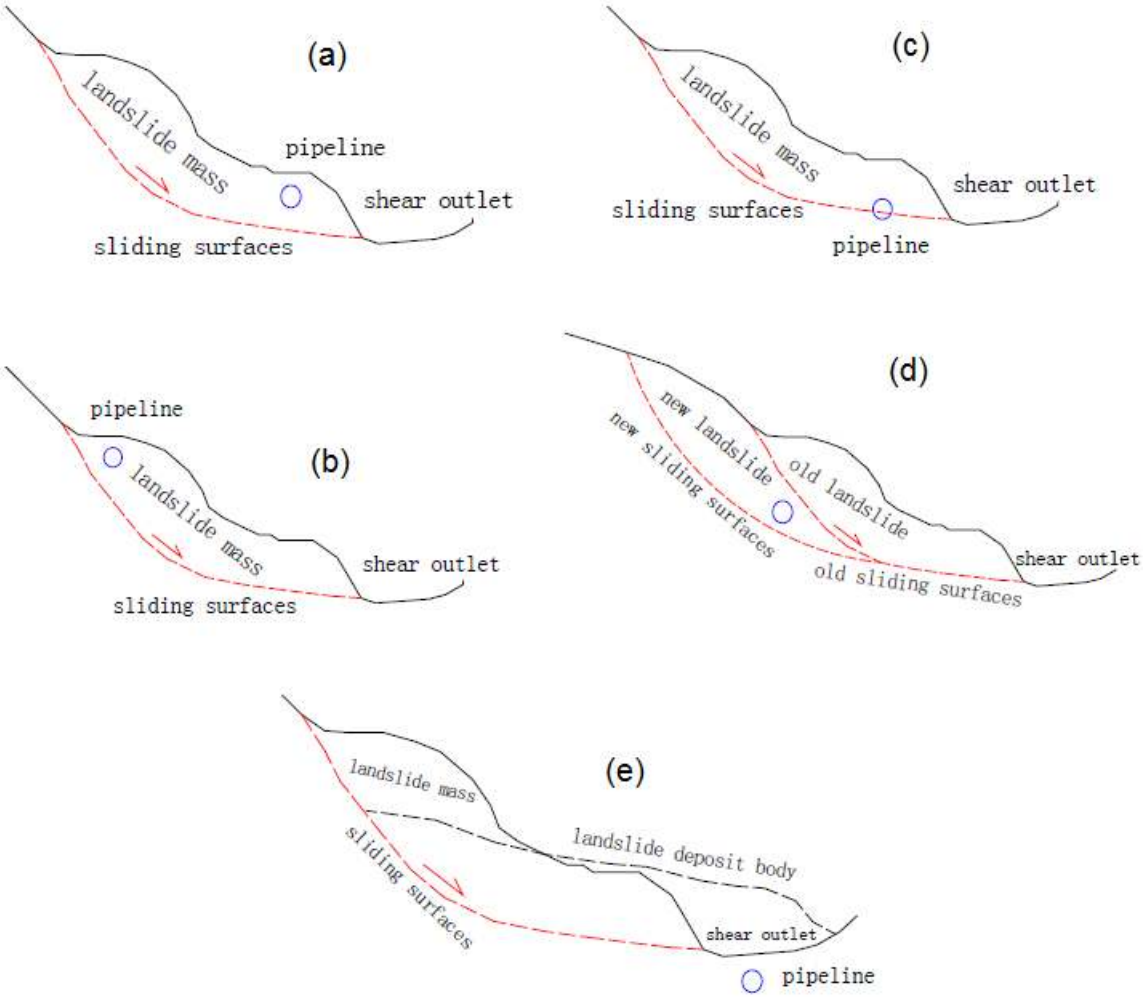

Figure 4-7. Positional relationship between pipeline and landslide and hazard analysis (Wu et al., 2014)

4.4. Recent Seismic Activity in the Mila province

In Algeria, the seismic activity is mainly concentrated in the northern part of the country due to the rapprochement of the Eurasian and African plates. The most important and damaging earthquakes have been recorded in the region named The Tell, which designate a band of few tens of kilometers, parallel to the Mediterranean Sea. The seismicity in northern Algeria occurs permanently; the seismic observation stations records approximately 50 shakes per month where almost 90% of this activity is low in magnitude and occurs far from urban centers (CRAAG, 2020). Prior to 2007, the county of Mila was rated as having low sensitivity towards damaging earthquakes, but since December 2017, the county received a swarm of earthquakes with a magnitude M ranging between 0.9 and 3.9. The earthquakes were attributed to manmade activities due to the construction of the Beni-Haroun Dam (Semmane et al., 2012). Figure 4-8 presents the recent earthquakes recorded by the Algerian Center of Research in Astronomy, Astrophysics and Geophysics (CRAAG) where 78% (i.e., 14/18) of the recent seismic activity happened in the territory of Mila province.

The percentile of 78% reflects the high sensitivity of Mila basin to the permanent ground deformations that can follow seismic movement in this province such as shallow slope failures that

are characterized by very surficial failure plans. Very recently, in the 7th August 2020 two sequential earthquakes of magnitudes M= 4.5 and M= 4.9 were happened in the Mila province at 2 and 3 kilometers, respectively, towards the south of the Hamala district. Due to the catastrophic material losses to the buildings and pipeline networks. The Algerian government has classified El-Kherba village as a ruined village and it was decided that citizens must be entirely moved away from the village. As can be seen in Figure 4-8, the earthquakes of the Hamala municipality were preceded by a series of shaking movements recorded in the 17th July 2020 at Sidi-Marouane municipality, close to Beni-Haroun Dam and the maximum observed magnitude M reached 4.5.

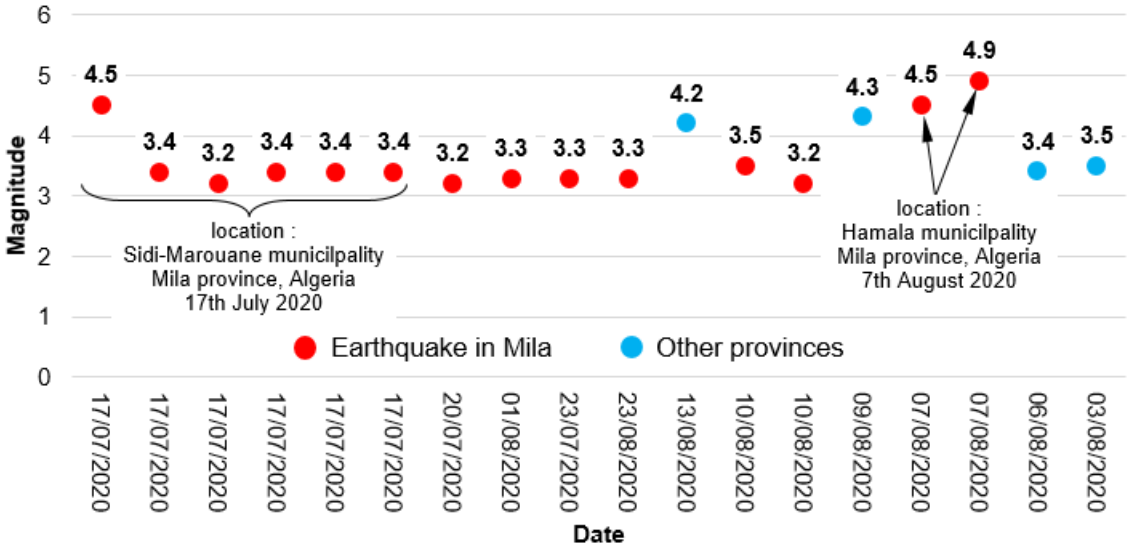

Figure 4-8. Recent Seismic Activity in the Mila province (CRAAG, 2020)

Following this sudden natural earthquakes, many on-site interventions have been done by the authorities to repair the pipeline networks damaged as a consequence of the large induced PGDs due to slope movements. The resulting water pipe breaks affected a large number of districts, including Mila, Aine-Tine, Grarem-Gouga, Sidi-Marouane, Zeghaia, Oued-Nedja, Ahmed-Rachedi, Rouached and Ferdjioua, in addition to the eastern provinces. Based on the first investigations carried out on the pipeline networks buried in the Mila basin, the identified cases of damaged pipes are of different diameters equal to 500 mm, 700 mm and 800 mm. The pipeline of water supply of 800 mm diameter D buried in Aine-Tine slope is the subject of our research program where the objective is to analyze the behavior of this lifeline buried in a high sloping area. The Aine-Tine site is one of the most famous cases of pipeline breaks which suffered repetitive damages that hugely disrupt the normal operations of the water supplying. The majority of the pipelines are buried at shallow depth including Aine-Tine pipeline and this study constitute a contribution in the numerical analysis of buried steel pipeline subjected to PGDs that follow natural hazards (i.e., earthquakes and intense precipitation).

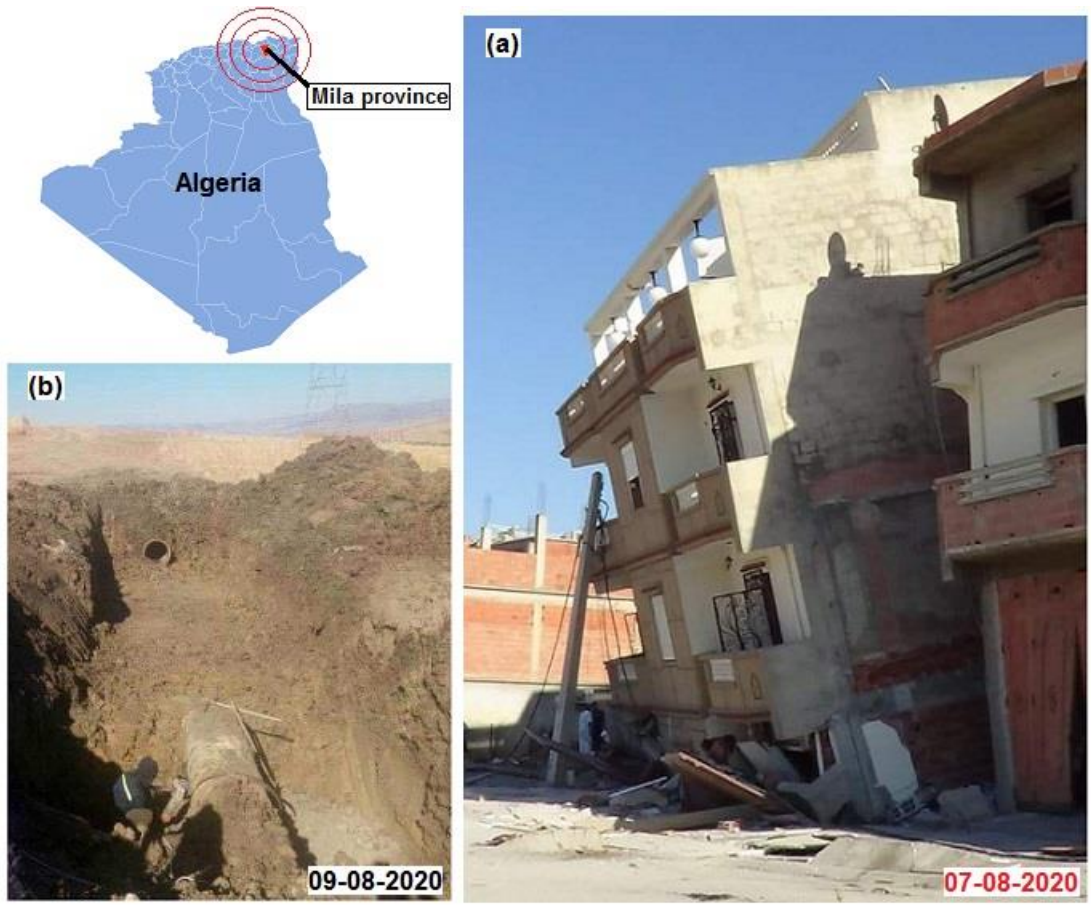

Figure 4-9. The7th august 2020 earthquake effects (a) damaged houses (b) pipeline repair operation

4.5. Numerical Model

The present study will investigate the behavior of Aine-Tine pipeline considering the same condition as shown in Figure 4-7(c) where the slip surface through the pipeline. The structural behavior of Aine-Tine water pipeline under a shallow sliding movement is studied numerically using the two dimensional computational software SIGMA/W. For this purpose, the cross section is investigated to simulate the interaction between the steel pipe and the surrounding soil medium. A uniform soil profile is assumed to extend down to 4 m depth under the naturel ground surface with a length of 8 m horizontally including the pipeline opening (Figure 4-10). Figure 4-10 shows the geometric dimensions of the numerical model adopted in this study. The top surface of the soil profile constitutes the naturel ground surface and the burial depth is assumed to be 2 m. The horizontal and vertical dimensions of the model are set to avoid the effects of boundary conditions; these dimensions are related directly to the pipeline diameter according to the recommendations presented in many published researches (Bouatia et al., 2020b) (Vazouras et al., 2015). The mesh is automatically generated with an available option in SIGMA/W where quadrilaterals and triangular elements are generated, forming thereby a unified mesh size of 0.25 m. For the pipe, the beam element perimeter is divided into 24 equal segments; the total number of elements in the model is thus equal to 1264 elements.

The numerical analysis is conducted following two steps. The first step is the generation of the geostatic stresses of the model using the in-situ option offered by the software and,

subsequently, in the second step, the permanent ground movement due to an eventual landslide is applied. The sliding plane is considered parallel to the ground surface and divides the soil model in two equal blocks of 8 m by 2 m horizontal and vertical dimensions for each one, respectively.

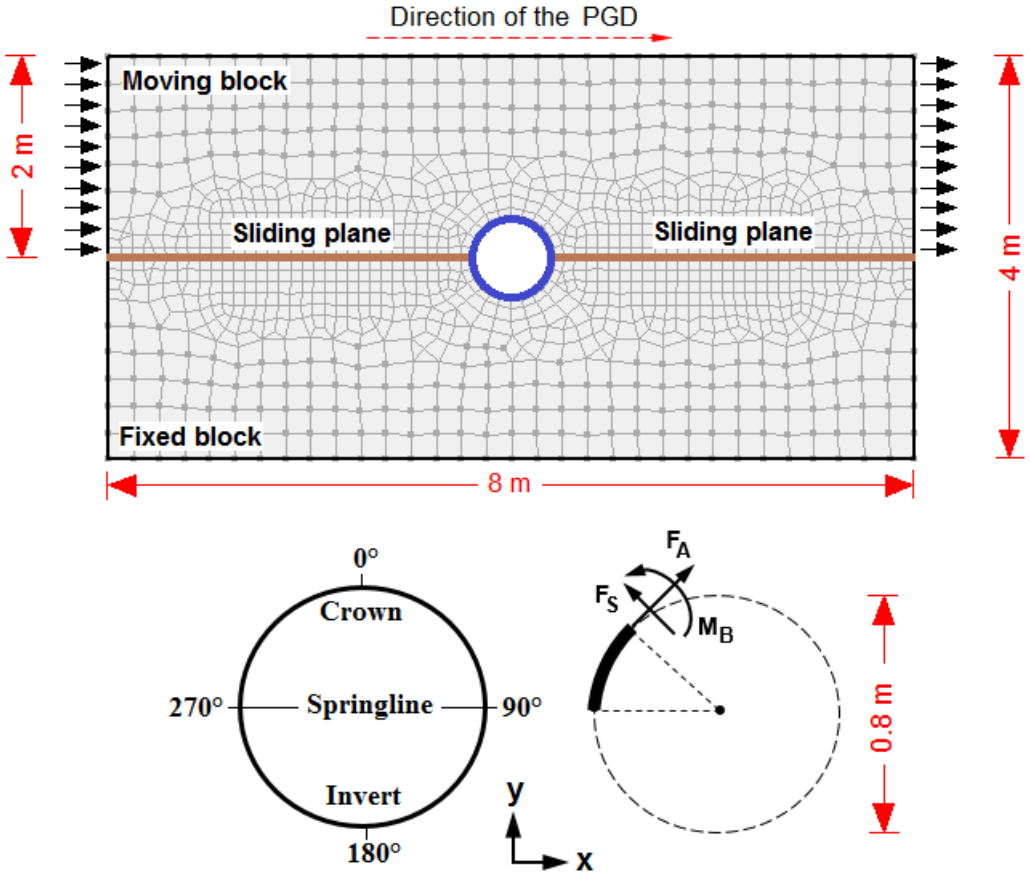

Figure 4-10. Finite element model and pipeline cross-section detail

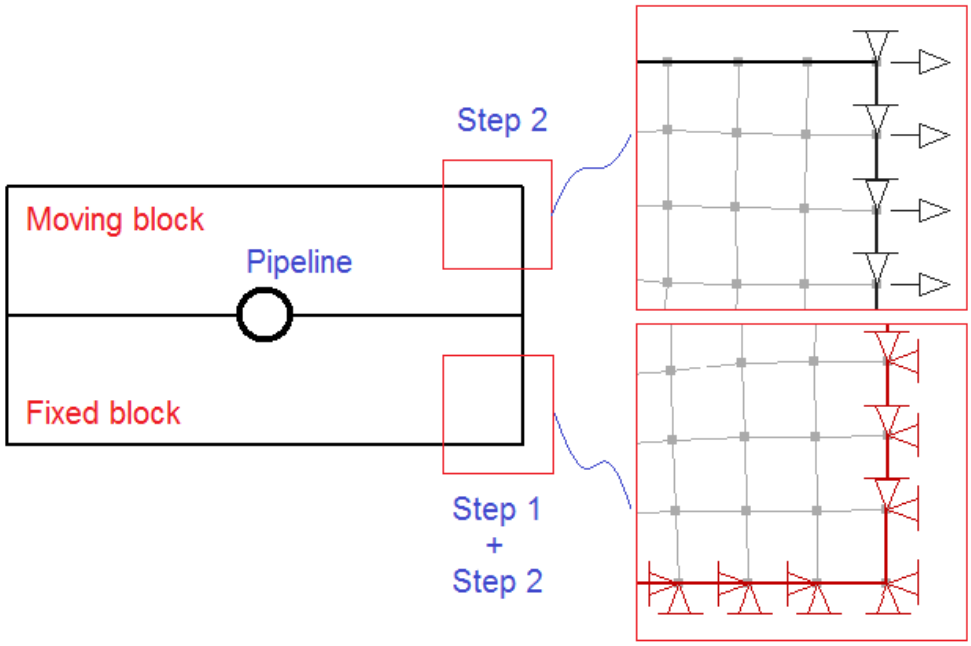

Figure 4-11. Details of boundary conditions

The boundary conditions of the model are: in the first step of the simulation (i.e., geostatic conditions), the left and right boundaries are fixed only in the x-direction and the bottom boundary is fixed in both the x and y directions. While, in the second step, the vertical boundary nodes of the bottom block remain fixed in the horizontal direction, whereas a uniform displacement due to the lateral sliding is applied to the external nodes of the top (moving) block in the horizontal x direction to simulate the induced permanent ground movement (Figure 4-11).

4.6. Material characteristics

4.6.1. Clay

Based on the results of the LNHC geotechnical reports carried out in 2015 and 2017 the soils of the surficial layer of Aine-Tine slope are classified according to USCS classification system as CH, which are inorganic clays of high plasticity with clay content equal to 52%. The geotechnical parameters used in the present study are summarized in Table 4-2. The integrated extended elastic-perfectly plastic Mohr-Coulomb (MC) constitutive model was used to model the clayey soil. It was successfully used to analyze soil-pipeline interaction problems (Robert et al., 2016) (Robert and Soga, 2013) (Al-Khazaali et al., 2018). The gravity is set to 9.81 m/s^2.

Table 4-2. Aine-Tine clay geotechnical parameters

Material	Soil property	Value
Clay	Total unit weight γ_t [KN/m3]	20
	Elastic modulus E [MPa]	3.5
	Poisson's ratio μ	0.33
	Angle of internal frictionφ [°]	15
	Cohesion c [kPa]	22
	USCS Classification	CH, Inorganic clay of high plasticity

4.6.2. Pipeline

Buried pipelines are subjected to a large variety of external loadings which are in this study the series of earthquakes followed by PGDs. The resulting PGD changes the stress state by generating a new shear and normal stress conditions, which result in: (1) the displacement of the pipeline away from its original location, (2) additional internal efforts (i.e., axial forces F_A, shear forces F_S and bending moment M_B), acting on the pipeline ring and (3) deformation of pipeline causing its ovalization. Considering the rigidity of these lifeline structures, they are classified by Moser and Folkman (2008) into two groups: flexible (i.e., polyethylene and steel pipes) and rigid (i.e., concrete and cast iron pipes) pipelines. The last earthquakes which affected the province of Mila damaged different diameter sizes of water transport pipelines which carry the water from the Beni-Haroun Dam to several destinations. The pipeline considered to perform the analysis is buried in Aine-Tine slope. The required geometric characteristics of the pipe are summarized in the Table 4-3. The burial depth is 2 m.

A beam element is used to model the pipeline ring behavior which ensures a continuous interaction with the surrounding soil. In Geomechanics, the rigidity is the only parameter that controls structures like buried pipelines where the soil-structure interaction is, therefore, a function of the geometric dimensions as well as the elastic characteristics of the material (i.e., Young's modulus E and Poisson's ratio μ). In accordance with the adopted values used by Al-Khazaali et al. (2018) to consider the rigidity effect on the response of buried pipelines subjected to ground movements induced by unsupported excavations, the used values of the young's modulus E, in this study, are as follow: 2 and 20 GPa to simulate flexible and rigid pipelines, respectively.

The cross section of Aine-Tine pipeline used to perform the present 2D plane-strain simulations is presented in Figure 4-10. The interfaces between the pipeline and the soil and at the sliding plane between the moving block (top) and fixed block (bottom) were created using line area option with much finer meshing because of the concentration of the expected stresses at these locations which will be subjected to large displacements. In the present study, the two interfaces were modelled using the same characteristics of the surrounding soil (see Table 4-2).

Table 4-3. Aine-Tine pipeline parameters

Material	Pipe property	Value	
Aine-Tine Pipeline	External diameter Q_{ext} [mm]	800	
	Thickness t [mm]	20	
	D/t	40	
	Young's modulus E [GPa]	Flexible	2
		Rigid	20

4.7. Results and discussion

The presentation of the results is divided into steps: (1) deformations and movement magnitudes of the pipeline and (2) the induced radial internal efforts that act on the perimeter of the Aine-Tine pipeline following the sliding displacements. The effect of the ground deformation on the pipeline is taken into account by considering the results of different magnitudes of sliding displacements equal to 0.1, 0.2, 0.3, 0.4, 0.5, 1 and 2 m considering the influence of two groups of pipeline rigidity, which are flexible and rigid pipeline.

4.7.1. Soil deformations.

The simulation of the PGD due to the earthquake stroke, as the triggering factor of the present study, is carried out by applying increment displacement in the x direction on the outer vertical edges of the top block (moving block). The applied movements will produce strains, which will be consequently seen as changes of the x and y stress components. Figure 4-12(a) and (b) show the contour of final displacements obtained after a magnitude equal to d= 2 m of the PGD for flexible and rigid pipeline, respectively.

The imposed displacement at the top block is accompanied by upward and downward vertical deformation of the top surface of the model, which correspond to the zones (a) and (b) shown in the Figure 4-13, and having approximately constant lengths equal to 4.75 m in the case of the

flexible pipeline while it is 4.5 m length in the case for the rigid pipeline. Looking to the results of the top surface displacement in the case of the flexible pipeline, it was observed that the upward displacements increase with the magnitude of the PGD where it starts from 2.4 cm under 0.2 m of PGD and reaches 37.5 cm after 2 m of PGD displacement. Simultaneously, the downwards movement occurred in the zone (b) increase with the PGD where the final values are equal to 12.1, 23.2 and 42.3 cm for PGD magnitudes equal to 0.5, 1 and 2 m, respectively.

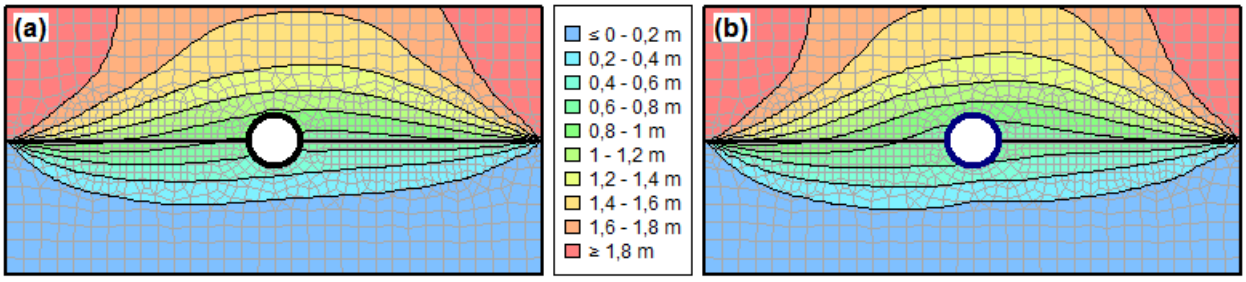

Figure 4-12. Contour of displacements after 2 m of sliding movement (a) flexible (b) rigid pipeline

In the case of the rigid pipeline, the same patterns of results were obtained but with different amplitudes. At the abscissa of 2 m the upward displacement, which corresponds to 0.5, 1 m and 2 m PGD magnitudes are, respectively equal to 8.9, 19.7 and 41.8 cm while for the same PGD magnitudes, the obtained downward displacements at the abscissa 7 m are as follow: 12.9, 24.3 and 43.1 cm. The zero vertical displacement locations are observed at 4.75 m and 4.5 m for flexible and rigid pipelines, respectively.

4.7.1. Pipeline displacements and ovalization

The deformed mesh after 0.5, 1 and 2m of PGD for flexible and rigid pipeline are shown in Figure 4-14. Figure 4-15 presents the results of the displacement and the deformation of the pipeline ring under different values of the PGD applied sliding movements which pass through the center of the pipeline body and horizontally divide the model into two equal parts and parallel to the ground surface. Considering the displacement of the pipeline center, the obtained displacement of the flexible pipeline reached 18.3, 35 and 72.5 cm for the magnitudes of PGD equal to 0.5, 1 and 2 m. On the other hand, for the same magnitudes the applied PGD movement, the rigid pipeline moved by 17, 33 and 71 cm, respectively.

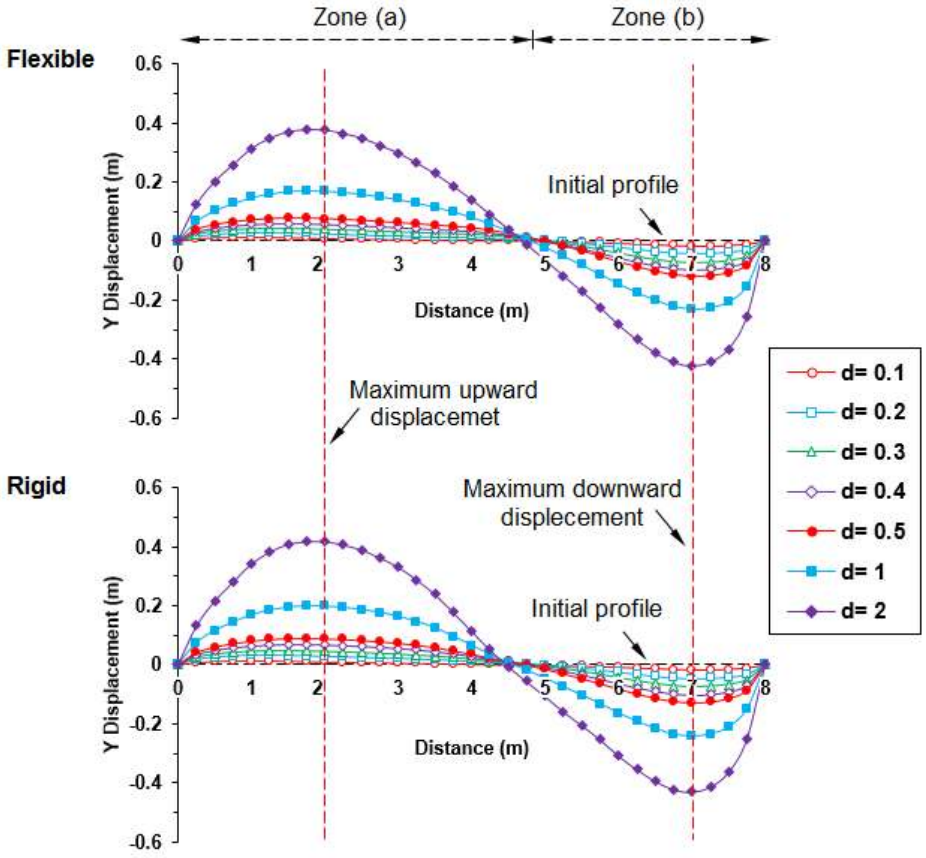

Figure 4-13. Vertical displacements at the ground surface

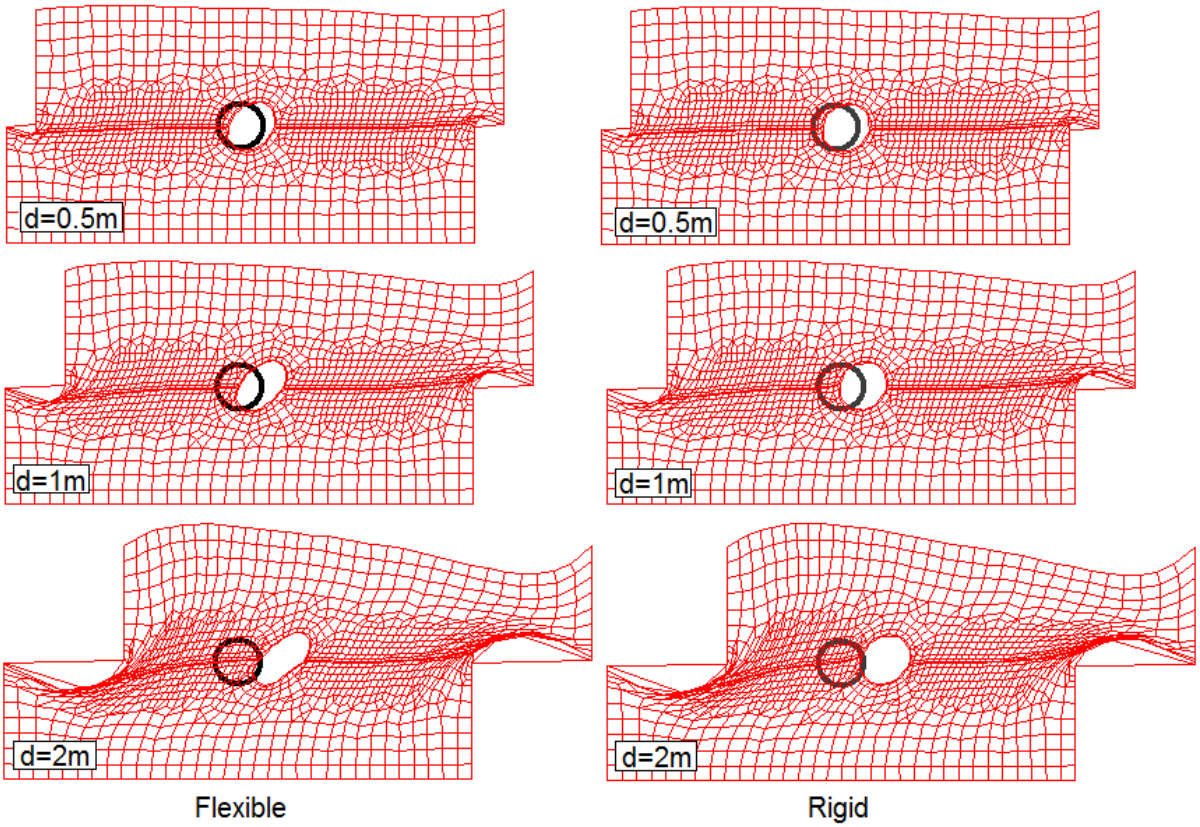

Figure 4-14. Deformed mesh after 0.5, 1 and 2m of PGD for flexible and rigid pipeline

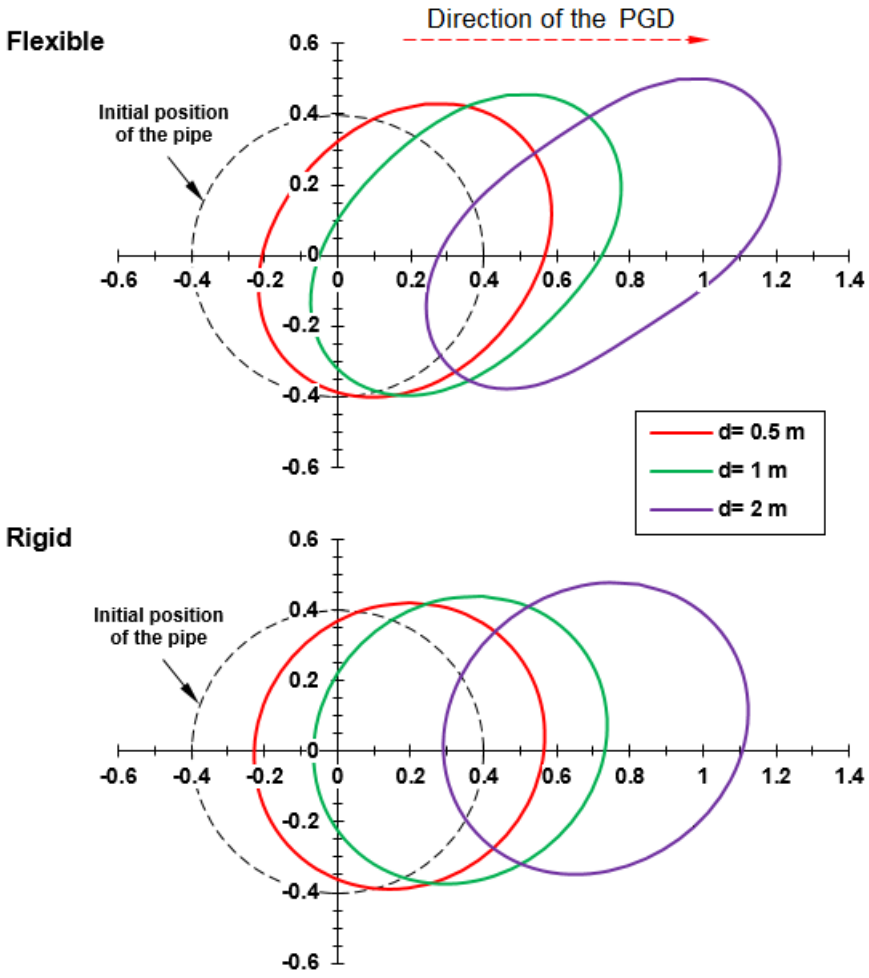

Figure 4-15. Displacement and deformation of pipeline and 0.5, 1 and 2 m PGD magnitudes

As a serviceability limit state, the cross-sectional ovalization of the pipe is one of the relevant conditions that are taken into consideration when designing buried pipeline to keep their normal operations. This condition can be expressed through the so-called flattering parameter f which written as follow $f = \Delta D/D$ where ΔD is the maximum variation of the pipeline diameter and D is the pipeline diameter. The Dutch specification NEN 3650 considers the value of 15% as the upper serviceability limit of ovalization when considering the latter as a criterion of performance.

The ovalization values calculated in the present study are summarized in the Table 4-4. The ovalization of the flexible pipeline are equal to 13, 24 and 39% for PGD magnitudes equal to 0.5, 1 and 2 m, respectively and they are higher by 23, 21 and 18 % than those calculated in the case of rigid pipeline for the same magnitudes of the PGD. Therefore, it can be concluded that the flexible pipelines are very sensitive to the shallow slope failures in terms of the ovalization serviceability limit state compared to the rigid pipelines where it is very clear that the values of ovalization obtained in the case of flexible pipeline are higher than the value of 15%.

Table 4-4. Ovalization values for flexible and rigid values under different PGD magnitudes.

PGD magnitude (m)	Cross-sectional ovalization [%]	
	Flexible	Rigid
0.5	13	3
1	24	5
2	39	7

The results shown in Figure 4-15 are consistent with those obtained in Figure 4-13 and Figure 4-14. In the case of rigid pipeline, the vertical displacements are slightly higher than those obtained with flexible pipeline because of the high deformations that happened on the ring of the flexible pipeline, which is resulted in the low magnitudes of the vertical displacements at the ground surface.

4.7.2. Radial forces

The radial internal efforts are an important element in the monitoring of the performance of buried pipelines and they are mainly related to the induced displacements within the surrounding soil. The calculated axial and shear forces as well as bending moments are presented in the following section. The PGD that follow slope failures triggered by natural hazards will produce stresses and strains on buried pipelines structures and subsequently lead to the application of additional internal efforts that can damage these structures.

4.7.2.1. Axial forces

The induced radial axial forces F_A calculated along the pipeline perimeter with two different Young's modulus equals to 2 and 20 GPa and assumed to be subjected to different magnitudes of shallow PGD ranging from 0.1 to 2 m are presented in Figure 4-16. It is clear that, for both flexible and rigid conditions, the pipeline ring is suffering compressive and tensile forces, where the maximum compression forces are shown as two positive peak values that are calculated at the angles 45° and 210° while the maximum tensile forces are calculated at the angles 135° and 300° and represented by negative peaks.

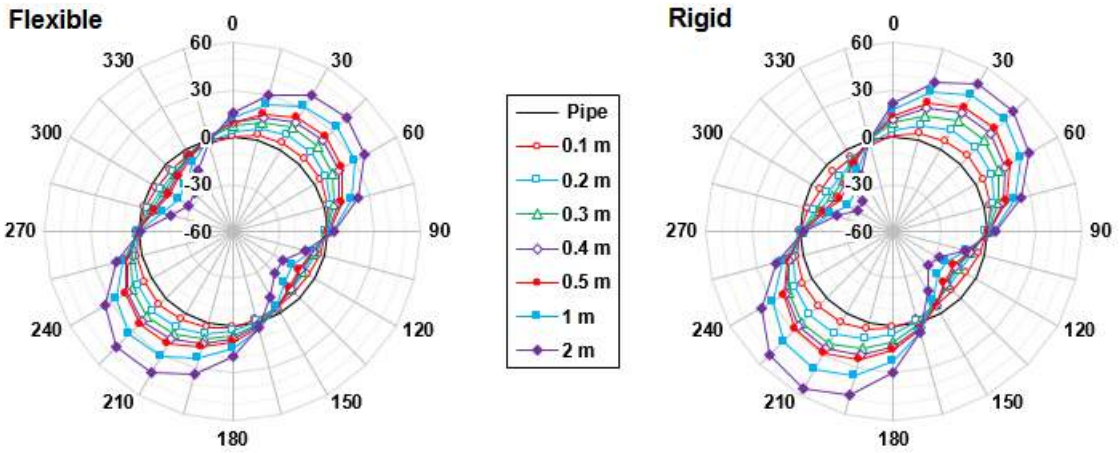

Figure 4-16. Axial force distribution [kN] for Flexible and Rigid pipeline under different PGDs.

The developed axial forces increase proportionally with the sliding movement, nevertheless they are slightly higher in the case of rigid pipeline than for the flexible pipeline because of the high rigidity which characterizes such buried structures. If one examines the flexible pipeline, the

applied lateral sliding movement on the top block increases the maximum tension forces at the angle 45° from 5.31 to 42.69 kN, which correspond to an increase of the PGD from 0.1 to 2 m. Simultaneously, they increase from 4.79 to 44.06 kN for those calculated at the angular location 210°. While in the case of the rigid pipeline, these values increase from 7.19 to 47.96 kN and from 6.92 to 54.82 kN, respectively at the same angular positions. For the same magnitudes of PGD (0.1 and 2 m), the compressive axial components increase from 4.82 to 22.5kN and from 4.29 to 27.9 kN at 135° and 300°, respectively.

4.7.2.2. Shear forces

The second component of the internal forces is the shearing forces F_S which can be seen in Figure 4-17. They are symmetrically distributed along the cross section of the pipeline where the peak values correspond with the null values of the axial forces. As for the axial forces, the shearing forces, which attempt to cut the pipeline wall perpendicularly to the tangent of the pipeline ring, have four peak values stated at 0°, 90°, 180° and 255°. The maximum values, which correspond to 0.5, 1 and 2 m of PGD magnitude, are recapitulated in the Table 4-5.

Table 4-5. Maximum shear forces at 0.5, 1 and 2m of PGD magnitudes (flexible and rigid pipeline)

PGD magnitude (m)	Maximum shear force [kN]	
	Flexible	Rigid
0.5	7.8	18.4
1	13.5	25.5
2	21.0	35.9

Based on the results of the Table 4-5 and on each of the plotted curves, one can conclude that the induced shear forces increase with respect to the pipeline rigidity as well as with the magnitude of the sliding movements.

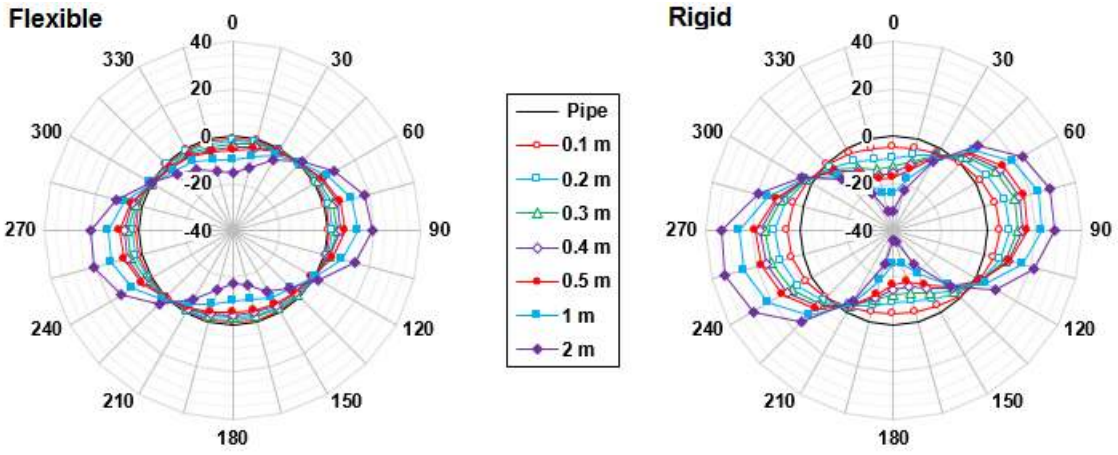

Figure 4-17. Shear force distribution [kN] for Flexible and Rigid pipeline under different PGDs.

4.7.2.3. Bending moment

The bending moment is the third required component for internal efforts investigation. The results of circumferential $M_B$calculated along the pipeline perimeter are illustrated in Figure 4-18 where they have the same trend with the previous results of internal forces (F_A and F_S) when

considering the proportionality of increasing with respect to both the (1) PGD magnitude and (2) the rigidity of the pipeline. In which concern the maximum values, they are obtained in the same angular location as in the axial forces but with opposite sign. In the case of flexible pipeline, the bending moment calculated after 2 m of PGD is equal to 6.66 kN.m, which is higher by 80% in the case of the rigid pipeline while the same comparison gives 105% and 161% considering 0.5 and 1 m of PGD magnitude, respectively. Reading attentively the Figure 4-16 – 17, it can be seen that at zero shear forces location, the peak values (positive and negative) of bending moments were obtained and at zero axial forces location, the peak values of the shearing forces were observed, which well consistent with the classic beam theory.

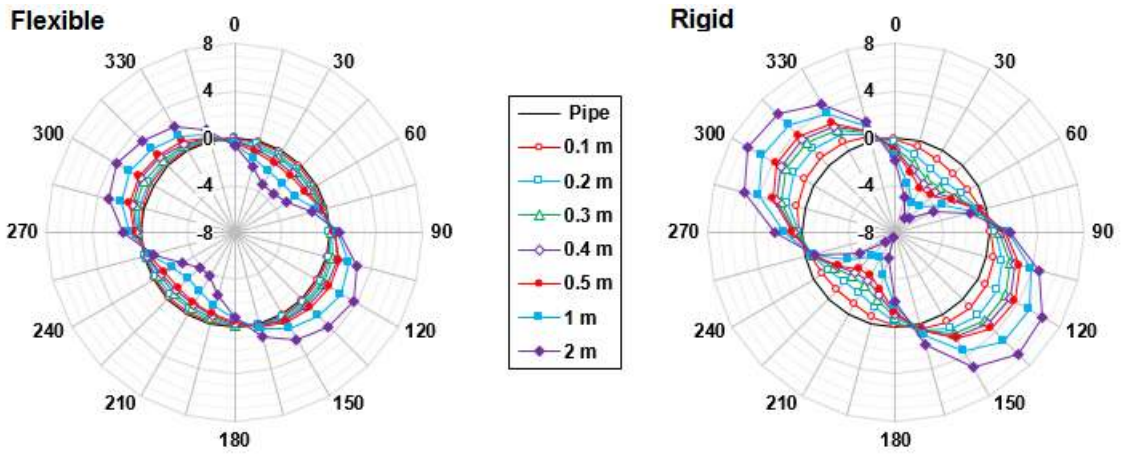

Figure 4-18. Bending moment distribution [kN.m] for Flexible and Rigid pipeline under different PGDs.

4.8. Conclusion

The analysis of the structural behavior of buried pipelines requires continuous monitoring of the various external loads that may affect the normal operations of these lifeline infrastructures. Using the SIGMA/W software in plane strain, the sliding movement such as the last PGD induced by the series of earthquakes happened in Mila province (Algeria) is carried out. The purpose of this study is to help engineers and planners to understand and predict the eventual external over loadings due to these sudden natural hazards. The development of the three induced components of the radial internal efforts, in terms of the magnitudes of the sliding displacement, are presented in the form of radial curves. The steel pipeline of water supply coming from the Beni-Haroun Dam, buried in Aine-Tine slopes (Mila, Algeria), is considered to study the performance of such buried structures under different magnitudes of shallow slope failures inducing PGD.

According to the numerical obtained results, it was found that:

- The deformation and ovalization of buried pipeline subjected to shallow slope failures are proportionally related to the magnitude of the induced PGD.
- The higher the PGD the higher the induced radial internal efforts.
- Based on the comparison between the internal efforts that occurred on the pipeline ring, it was found that rigid pipelines can resist high external loading than the flexible pipelines.

Finally, the present work will serve as an additional support to the engineers and planners to understand the behavior of Beni-Haroun pipelines networks, in the purpose to predict the main causes of the recorded damages.

4.9. References

ALA, 2005. Seismic Guidelines for Water Pipelines. American Lifelines Alliance, Federal Emergency Management Agency (FEMA).

Al-Khazaali, M., Vanapalli, S.K., 2020. A Novel Experimental Technique to Investigate Soil–Pipeline Interaction under Axial Loading in Saturated and Unsaturated Sands. Geotech. Test. J. 43, 70–93. https://doi.org/10.1520/GTJ20180059

Al-Khazaali, M., Vanapalli, S.K., Oh, W.T., 2018. Numerical investigation of soil–pipeline system behavior nearby unsupported excavation in saturated and unsaturated glacial till. Can. Geotech. J. 56, 69–88. https://doi.org/10.1139/cgj-2017-0411

Ariman, T., Muleski, G.E., 1981. A review of the response of buried pipelines under seismic excitations. Earthq. Eng. Struct. Dyn. 9, 133–152. https://doi.org/10.1002/eqe.4290090204

Bouatia, M., Demagh, R., Derriche, Z., 2020a. Structural Behavior of Pipelines Buried in Expansive Soils under Rainfall Infiltration (Part I: Transverse Behavior). Civ. Eng. J. 6, 1822–1838. https://doi.org/10.28991/cej-2020-03091585

Bouatia, M., Demagh, R., Derriche, Z., 2020b. Structural Behavior of Pipelines Buried in Expansive Soils under Rainfall Infiltration (Part I: Transverse Behavior). Civ. Eng. J. 6, 1822–1838. https://doi.org/10.28991/cej-2020-03091585

CRAAG, 2020. Centre de Recherche en Astronomie Astrophysique et Géophysique CRAAG [WWW Document]. RADP Ministère Intér. Collectiv. Locales. URL https://www.craag.dz/

Feng, W., Huang, R., Liu, J., Xu, X., Luo, M., 2015. Large-scale field trial to explore landslide and pipeline interaction. Soils Found. 55, 1466–1473. https://doi.org/10.1016/j.sandf.2015.10.011

IITK-GSDMA, 2007. GUIDELINES for SEISMIC DESIGN of BURIED PIPELINES. Indian Institute of Technology Kanpur - Gujarat State Disaster Management Authority, National Information Center of Earthquake Engineering, Kanpur, India.

Li, C., Wang, L., Jing, H., Liu, Q., 2013. Protection Control Scheme and Evaluation of Effectson Pipeline Crossing beneath Landslide Area. J. Pipeline Syst. Eng. Pract. 4, 41–48. https://doi.org/10.1061/(ASCE)PS.1949-1204.0000130

Moser, A.P., Folkman, S., 2008. Buried Pipe Design, Third Edition, 3rd ed. McGraw-Hill Education.

Ng, P.C.F., 1994. Behaviour of buried pipelines subjected to external loading. (phd). University of Sheffield.

O'Rourke, T.D., Jezerski, J.M., Olson, N.A., Bonneau, A.L., Palmer, M.C., Stewart, H.E., O'Rourke, M.J., Abdoun, T., 2008. Geotechnics of Pipeline System Response to Earthquakes, in: Geotechnical Earthquake Engineering and Soil Dynamics IV. Presented at the Geotechnical Earthquake Engineering and Soil Dynamics Congress IV, American Society of Civil Engineers, Sacramento, California, United States, pp. 1–38. https://doi.org/10.1061/40975(318)193

Rajani, B., Morgenstern, N., 1993. Pipelines and Laterally Loaded Piles in Elastoplastic Medium. J. Geotech. Eng. 119, 1431–1448. https://doi.org/10.1061/(ASCE)0733-9410(1993)119:9(1431)

Randeniya, C., Robert, D. j., Li, C.-Q., Kodikara, J., 2019. Large-scale experimental evaluation of soil saturation effect on behaviour of buried pipes under operational loads. Can. Geotech. J. 57, 205–220. https://doi.org/10.1139/cgj-2018-0544

Robert, D., Soga, K., 2013. Soil-Pipeline Interaction in Unsaturated Soils, in: Mechanics of Unsaturated Geomaterials. John Wiley & Sons, Inc., Hoboken, NJ USA, pp. 303–325. https://doi.org/10.1002/9781118616871.ch13

Robert, Soga K., O'Rourke T. D., Sakanoue T., 2016. Lateral Load-Displacement Behavior of Pipelines in Unsaturated Sands. J. Geotech. Geoenvironmental Eng. 142, 04016060. https://doi.org/10.1061/(ASCE)GT.1943-5606.0001504

Semmane, F., Abacha, I., Yelles-Chaouche, A.K., Haned, A., Beldjoudi, H., Amrani, A., 2012. The earthquake swarm of December 2007 in the Mila region of northeastern Algeria. Nat. Hazards 64, 1855–1871. https://doi.org/10.1007/s11069-012-0338-7

Shi, Y.-M., Wang, N., Gao, F.-P., Qi, W.-G., Wang, J.-Q., 2019. Physical modeling of the axial pipe-soil interaction for pipeline walking on a sloping sandy seabed. Ocean Eng. 178, 20–30. https://doi.org/10.1016/j.oceaneng.2019.02.059

Vazouras, P., Dakoulas, P., Karamanos, S.A., 2015. Pipe–soil interaction and pipeline performance under strike–slip fault movements. Soil Dyn. Earthq. Eng. 72, 48–65. https://doi.org/10.1016/j.soildyn.2015.01.014

Vazouras, P., Karamanos, S.A., 2017. Structural behavior of buried pipe bends and their effect on pipeline response in fault crossing areas. Bull. Earthq. Eng. 15, 4999–5024. https://doi.org/10.1007/s10518-017-0148-0

Vazouras, P., Karamanos, S.A., Dakoulas, P., 2012. Mechanical behavior of buried steel pipes crossing active strike-slip faults. Soil Dyn. Earthq. Eng. 41, 164–180. https://doi.org/10.1016/j.soildyn.2012.05.012

Vazouras, P., Karamanos, S.A., Dakoulas, P., 2010. Finite element analysis of buried steel pipelines under strike-slip fault displacements. Soil Dyn. Earthq. Eng. 30, 1361–1376. https://doi.org/10.1016/j.soildyn.2010.06.011

Wu, J., Zhou, R., Xu, S., Wu, Z., 2017. Probabilistic analysis of natural gas pipeline network accident based on Bayesian network. J. Loss Prev. Process Ind. 46, 126–136. https://doi.org/10.1016/j.jlp.2017.01.025

Wu, R., Mei, Y., Deng, Q., Pang, C., Fu, M., 2014. Comparative Analysis by Numerical Simulation on Natural Gas Pipelines in Different Positions of Landslide, in: ICPTT 2014. Presented at the International Conference on Pipelines and Trenchless Technology 2014, American Society of Civil Engineers, Xiamen, China, pp. 308–319. https://doi.org/10.1061/9780784413821.035

Zhang, W., Askarinejad, A., 2019. Behaviour of buried pipes in unstable sandy slopes. Landslides 16, 283–293. https://doi.org/10.1007/s10346-018-1066-1

SUMMARY AND CONCLUSIONS

Summary and Conclusions

Summary

The present thesis is carried out at the University of Mustafa ben Boulaid - Batna 2, Algeria with a long-term internship undertaken at the Johor campus of the Universiti de Teknologi Malaysia, Malaysia. The research aims to study the behavior of pipelines buried in the high unsaturated slopes that characterize the northern strip of Algerian territory with a semi-arid climate. The study focuses on the modeling of the behavior of the water pipes of the Beni Haroun dam which suffered repetitive and costly damage which actually disrupts the normal functioning of the water distribution to the east of Algeria. The section of pipeline passing through the Aine-Tine slope was used to carry out the numerical simulations considering the unsaturated behavior of the clayey soils of the Mila basin and extending the Mohr-Coulomb constitutive model to consider the effect of suction with its effective contribution to the strength and stiffness of unsaturated soils. The steel pipeline is 800 mm diameter and 20 mm thickness buried at 2 m depth which corresponds to the vadose zone of the region having a GWT located at 10-15 m depth.

For the first part of the work plan, and as the pipeline goes through a high sloping area, it was decided at the beginning to evaluate the stability of the Aine-Tine slope using the FLAC software to calculate the 2D and 3D factor of safety for long term conditions where it was found that the slope present a weak value of FoS turning about unity (~ 1). During the first evaluation many numerical tools were developed using the FISH programs to build subroutines that can construct complex geometries in 2D and 3D, affect various initial conditions (i.e., fixities, initial stresses etc.) and to show and control the obtained results in a very helpful way. These critical results of stability pushed us to deeper the investigations to consider the effect of the unsaturated conditions in the evaluation of the stability of the surficial layer of Aine Tine slope using the curves named the SWCC which relates the water content of unsaturated soils to the suction which contribute to the value of the apparent cohesion that characterize such soils. The SWCC has fitting parameters (i.e., a, n and m) it was decided for the first time to investigate the effect of each parameters considering the effect of depth of the surficial layers.

Conclusion

Based on the above discussion the following conclusions were obtained:

1. The suction present in unsaturated soils provides an additional cohesion and consequently increases the FoS of the unsaturated slopes in arid and semi-arid area and the provided cohesion is related to the SWCC's fitting parameters.
2. The parameter a has an increasing effect on the FoS in a determined range which is controlled by the parameters n and m. While the higher the parameter n and m, the lower the obtained additional cohesion and, consequently, the decrease of the FoS. in the other hand, it was found that for low values of n and m, the parameter n has a higher increasing effect on the FoS than the parameter m and vice-versa for high values.
3. Considering geometric factors, it was found that the FoS is inversely proportional to the sloping angle β. It was found that the higher the depth of calculation the lower the

obtained additional cohesion and consequently, the FoS due to (1) the decrease of the suction which inversely related the distance from the WT and (2) the increase of the mobilized shear stress which is proportional with the overburden stress.

For the second part of the work plan the pipeline will be considered. The behavior of this buried structure is modelled under the effect of two sources of displacements determined based on the literature review about the critical phenomenon that can possibly happen on the area and the deep discussion during and after numerous on-site visits during the geotechnical campaigns carried out by the LNHC laboratory and also other independent visits. The two sources are respectively:

a) The expansion of the clayey soils under the effect of a rainfall precipitation due the saturation of the surficial layers.
b) Large PGDs induced by surficial failures that can follow the losses of shear strength after precipitations or under seismic events.

These phenomena directly affected the water mains of the Beni-Haroun dam causing breaks and permanent leakages. To model the effects of these displacements the 2D plain strain module SIGMA/W of GeoStudio co ltd was used to develop simplified numerical models that can simulate and monitor the soil-pipeline interaction considering the unsaturated behavior of the burial medium and under the effect of mechanical (i.e., imposed displacement) and hydraulic (i.e., rainfall precipitations) boundary conditions. The analyze focused mainly on:

a) The monitoring of the development of the three component of internal forces (i.e., F_A, F_S and M_B) considering both transverse and longitudinal direction of the pipelines.
b) The prediction of displacements and deformations that occurred on the pipeline body.

The main conclusions that can be obtained from the analyses of the water main cross section behavior under rainfall events is that swelling movements can cause additional loads on buried pipelines in expansive soils because of the important role of the unsaturated behavior of such soils especially in arid and semi-arid regions where due to the soil saturation process caused by the progressive saturation of the soil, these soils exhibit volume changes associated with heave at the ground surfaces following decrease in suction indicating that the effect of the soil suction must be taken carefully into consideration, especially where the seasonal variation of moisture content is very high. It was also found that the induced soil heave and the radial forces exerted on the pipeline wall (Axial, Shear and Bending moment) increase with respect to the initial soil suction. From the results it can be concluded that the initial suction values worked out from the water table depth or from the degree of evapotranspiration and the rainfall precipitation are important factors that impact seriously the unsaturated behavior of the soil behavior as well as the response of the pipeline structure. The analyses of the pipeline cross-section ovalization can help related parts to expect logic reasons to many water leakage points along the paths of the Mila water supply pipelines including the one located in Aine-Tine site.

Considering the same variables as those used with the cross section analyses, simplified 2D plane strain numerical simulations of the longitudinal structural behavior of buried pipelines were

carried out simulating the Aine Tine pipeline as a straight beam with an equivalent moment of inertia. From the analyses of the effect of swelling movements on the buried pipelines which can occur in many site conditions such as the change of the geological formations and the change of sloping angle of the lands crossed by the pipeline which directly affect the ratio of the infiltrations of water and consequently influences the structural response of the pipeline which also can be one of the logic reasons of water leakage points along the pipeline routes.

In the last part of the work, as unsaturated slopes are prone to shallow failures which are mainly triggered by seepage or other factors such as earthquakes when they occur. The behavior of Aine-Tine pipeline cross section subjected permanent ground deformations that usually follow surficial failure was simulated. The main conclusions are as follow:

a) The purpose of this study is to help engineers and planners to understand and predict the eventual external over loadings due to these sudden natural hazards.
b) The deformation and ovalization of buried pipeline subjected to shallow slope failures are proportionally related to the magnitude of the induced PGD.
c) The higher the PGD the higher the induced radial internal efforts where it was found that rigid pipelines could support higher external loadings than the flexible pipelines.
d) Finally, the present work will serve as an additional support to the engineers and planners to understand the behavior of Beni-Haroun pipelines networks, in the purpose to predict the main causes of the recorded damages.

The results of the present study are very useful to understand the possible origin of the damages reported on the Ain-Tine water supply pipeline where the study made it clear that in order to achieve a realistic design of buried lifeline infrastructures, the unsaturated behavior of the embedding expansive du sol should be taken into consideration with respect to the climatic conditions of the region including the aridity and the rainfall precipitation.

Recommendations for future works:

The study was a plane strain numerical simulations ignoring of the effect of the third axis with some assumptions which leads to conservative results of the real behavior of the pipeline structure under simplified hypotheses including the used constitutive models, boundary conditions and geometrical characteristics of the area (i.e., real profiles of the land).

In order to achieve more realistic results,

** A representative daily precipitation data (i.e., intensity, duration and frequency) would be used instead.

** In addition, many types of the pipelines such as rigid, flexible, welded and jointed and with different diameter are buried to transport fluids and which need to be considered in the future studies.

** It would be also interesting to study the longitudinal and transverse behaviors of the pipeline using three dimensional numerical models using more sophisticated constitutive models which can imply the softening and hardening behavior of soils

** It is also helpful to consider the real geometry of slopes which will really generate more realistic initial stresses and provide more realistic loadings on the pipelines bodies.

** The study of the interaction of the pipelines with other infrastructures like roads in the case of their duplication which is the case considering the national highway RN79 in Mila basin.

REFERENCES

REFERENCES

[1]. Abramson, L.W., Lee, T.S., Sharma, S., Boyce, G.M., 2002. Slope stability and stabilization methods, 2nd ed. ed. Wiley, New York.

[2]. Adem, H.H., Vanapalli, S.K., 2013. Constitutive modeling approach for estimating 1-D heave with respect to time for expansive soils. Int. J. Geotech. Eng. 7, 199–204. https://doi.org/10.1179/1938636213Z.00000000024

[3]. Adem, H.H., Vanapalli, S.K., 2014. Elasticity moduli of expansive soils from dimensional analysis. Geotech. Res. 1, 60–72. https://doi.org/10.1680/gr.14.00006

[4]. Adem, H.H., Vanapalli, S.K., 2014. Prediction of the modulus of elasticity of compacted unsaturated expansive soils. Int. J. Geotech. Eng. 9, 163–175. https://doi.org/10.1179/1939787914Y.0000000050

[5]. Agus, S.S., Leong, E.C., Rahardjo, H., 2001. Soil–water characteristic curves of Singapore residual soils. Geotech. Geol. Eng. 19, 285–309. https://doi.org/10.1023/A:1013175913679

[6]. Akin, I.D., Likos, W.J., 2020. Suction Stress of Clay Over a Wide Range of Saturation. Geotech. Geol. Eng. 38, 283–296. https://doi.org/10.1007/s10706-019-01016-7

[7]. ALA, 2005. Seismic Guidelines for Water Pipelines. American Lifelines Alliance, Federal Emergency Management Agency (FEMA).

[8]. Al-Khazaali, M., 2019. Soil-Pile, Pile Group Foundations and Pipeline Systems Interaction Behavior Extending Saturated and Unsaturated Soil Mechanics (Thesis). Université d'Ottawa / University of Ottawa. https://doi.org/10.20381/ruor-23095

[9]. Al-Khazaali, M., Vanapalli, S.K., 2020. A Novel Experimental Technique to Investigate Soil–Pipeline Interaction under Axial Loading in Saturated and Unsaturated Sands. Geotech. Test. J. 43, 70–93. https://doi.org/10.1520/GTJ20180059

[10]. Al-Khazaali, M., Vanapalli, S.K., Oh, W.T., 2018. Numerical investigation of soil–pipeline system behavior nearby unsupported excavation in saturated and unsaturated glacial till. Can. Geotech. J. 56, 69–88. https://doi.org/10.1139/cgj-2017-0411

[11]. Anand, V., Satish Kumar, S.R., 2018. Seismic Soil-structure Interaction: A State-of-the-Art Review. Structures 16, 317–326. https://doi.org/10.1016/j.istruc.2018.10.009

[12]. Ariman, T., Muleski, G.E., 1981. A review of the response of buried pipelines under seismic excitations. Earthq. Eng. Struct. Dyn. 9, 133–152. https://doi.org/10.1002/eqe.4290090204

[13]. Athmania, D., Benaissa, A., Hammadi, A., Bouassida, M., 2010. Clay and Marl Formation Susceptibility in Mila Province, Algeria. Geotech. Geol. Eng. 28, 805–813. https://doi.org/10.1007/s10706-010-9341-5

[14]. Aung, K.K., Rahardjo, H., Leong, E.C., Toll, D.G., 2001. Relationship between porosimetry measurement and soil—water characteristic curve for an unsaturated residual soil, in: Unsaturated Soil Concepts and Their Application in Geotechnical Practice. Springer, pp. 401–416.

[15]. Azam, S., Shah, I., Raghunandan, M.E., Ito, M., 2013. Study on swelling properties of an expansive soil deposit in Saskatchewan, Canada. Bull. Eng. Geol. Environ. 72, 25–35. https://doi.org/10.1007/s10064-012-0457-0

[16]. Biot, M.A., 1941. General theory of three- dimensional consolidation. J. Appl. Phys. 12, 155–164.

[17]. Bishop, A.W., 1959. The principles of effective stress. Tech. Ukebl. 106(9), 859–863.

[18]. Bishop, A.W., Blight, G.E., 1963. Some Aspects of Effective Stress in Saturated and Partly Saturated Soils. Géotechnique 13, 177–197. https://doi.org/10.1680/geot.1963.13.3.177

[19]. Bouatia, M., Demagh, R., 2019. Numerical Assessment of Slope Stability of Ain-Tinn Mila Province (Algeria), in: Shehata, H., Desai, C.S. (Eds.), Advances in Numerical Methods in Geotechnical Engineering, Sustainable Civil Infrastructures. Springer International Publishing, Cham, pp. 133–143. https://doi.org/10.1007/978-3-030-01926-6_10

[20]. Bouatia, M., Demagh, R., Derriche, Z., 2020. Structural Behavior of Pipelines Buried in Expansive Soils under Rainfall Infiltration (Part I: Transverse Behavior). Civ. Eng. J. 6, 1822–1838. https://doi.org/10.28991/cej-2020-03091585

[21]. Brackley, I.J., 1971. Partial collapse in unsaturated expansive clay. CSIR.

[22]. Brooks, R.H., Corey, A.T., 1964. Hydraulic Properties of Porous Media and Their Relation to Drainage Design. Trans. ASAE 7, 0026–0028. https://doi.org/10.13031/2013.40684

[23]. Burland, J.B., 1964. Correspondence. Géotechnique 14, 64–68. https://doi.org/10.1680/geot.1964.14.1.64

[24]. Chettah, W., 2009. Investigation des propriétés minéralogiques et géomécaniques des terrains en mouvement dans la ville de Mila « Nord-Est d'Algérie » (Thèse de Magistère). University of Batna 1 Hadj Lakhdhar, Batna, Algérie.

[25]. Chowdhury, R., 2010. Geotechnical Slope Analysis.

[26]. Clark, C.M., 1971. Expansive-Soil Effect on Buried Pipe. J. - AWWA 63, 424–427. https://doi.org/10.1002/j.1551-8833.1971.tb04116.x

[27]. Cooper, R.G., Ballantyne, C.K., Jarman, D., 2007. Mass movements in Great Britain, Geological conservation review series. Joint Nature Conservation Committee, Peterborough.

[28]. CRAAG, 2020. Centre de Recherche en Astronomie Astrophysique et Géophysique CRAAG [WWW Document]. RADP Ministère Intér. Collectiv. Locales. URL https://www.craag.dz/

[29]. Crofts, J.E., Menzies, B.K., Tarzi, A.I., 1977. Lateral displacement of shallow buried pipelines due to adjacent deep trench excavations. Géotechnique 27, 161–179. https://doi.org/10.1680/geot.1977.27.2.161

[30]. Cruden, D.M., 1991. A simple definition of a landslide. Bull. Int. Assoc. Eng. Geol. 43, 27–29. https://doi.org/10.1007/BF02590167

[31]. Dahal, R.K., Hasegawa, S., Nonomura, A., Yamanaka, M., Dhakal, S., 2008. DEM-based deterministic landslide hazard analysis in the Lesser Himalaya of Nepal. Georisk Assess. Manag. Risk Eng. Syst. Geohazards 2, 161–178. https://doi.org/10.1080/17499510802285379

[32]. Dawson, E.M., Roth, W.H., Drescher, A., 1999. Slope stability analysis by strength reduction. Géotechnique 49, 835–840. https://doi.org/10.1680/geot.1999.49.6.835

[33]. de Blasio, F.V., 2011. Introduction to the Physics of Landslides. Springer Netherlands, Dordrecht. https://doi.org/10.1007/978-94-007-1122-8

[34]. Dikau, R., Brunsden, D., Schrott, L., Ibsen, M.-L., 1996. Landslide recognition: identification, movement, and causes, Publication / International Association of Geomorphologists. Wiley, Chichester ; New York.

[35]. Doumbouya, L., Guan, C.S., Bowa, V.M., 2020. Influence of Rainfall Patterns on the Slope Stability of the Lumwana (the Malundwe) Open Pit. Geotech. Geol. Eng. 38, 1337–1346. https://doi.org/10.1007/s10706-019-01094-7

[36]. Duncan, J.M., Wright, S.G., Brandon, T.L., 2014. Soil strength and slope stability, Second edition. ed. John Wiley & Sons Inc, Hoboken, New Jersey.

[37]. Feng, W., Huang, R., Liu, J., Xu, X., Luo, M., 2015. Large-scale field trial to explore landslide and pipeline interaction. Soils Found. 55, 1466–1473. https://doi.org/10.1016/j.sandf.2015.10.011

[38]. Fredlund, D.G., Morgenstern, N.R., 1976. Constitutive relations for volume change in unsaturated soils. Can. Geotech. J. 13, 261–276. https://doi.org/10.1139/t76-029

[39]. Fredlund, D.G., Morgenstern, N.R., Widger, R.A., 1978. The shear strength of unsaturated soils. Can. Geotech. J. 15, 313–321. https://doi.org/10.1139/t78-029

[40]. Fredlund, D.G., Rahardjo, H., 1993. Soil mechanics for unsaturated soils. John Wiley & Sons.

[41]. Fredlund, D.G., Xing, A., 1994. Equations for the soil-water characteristic curve. Can. Geotech. J. 31, 521–532. https://doi.org/10.1139/t94-061

[42]. Fredlund, D.G., Xing, A., Fredlund, M.D., Barbour, S.L., 1996. The relationship of the unsaturated soil shear strength to the soil-water characteristic curve. Can. Geotech. J. 33, 440–448. https://doi.org/10.1139/t96-065

[43]. Fredlund, D.G., Xing, A., Huang, S., 1994. Predicting the permeability function for unsaturated soils using the soil-water characteristic curve. Can. Geotech. J. 31, 533–546. https://doi.org/10.1139/t94-062

[44]. Fredlund, M.D., Fredlund, D.G., Zhang, L., 2018. Moving from 2D to a 3D Unsaturated Slope Stability Analysis, in: PanAm Unsaturated Soils 2017. Presented at the Second Pan-American Conference on Unsaturated Soils, American Society of Civil Engineers, Dallas, Texas, pp. 136–145. https://doi.org/10.1061/9780784481691.014

[45]. Fredlund, M.D., Wilson, G.W., Fredlund, D.G., 2002. Use of the grain-size distribution for estimation of the soil-water characteristic curve. Can. Geotech. J. 39, 1103–1117.

[46]. Gallage, C.P.K., Chan, D., Kodikara, J., 2012. Response of a plastic pipe buried in expansive clay. Proc. Inst. Civ. Eng. - Geotech. Eng. 165, 45–57. https://doi.org/10.1680/geng.9.00037

[47]. Gardner, W.R., 1958. SOME STEADY-STATE SOLUTIONS OF THE UNSATURATED MOISTURE FLOW EQUATION WITH APPLICATION TO EVAPORATION FROM A WATER TABLE: Soil Sci. 85, 228–232. https://doi.org/10.1097/00010694-195804000-00006

[48]. GeoSlope International Ltd, 2007. SIGMA/W user's guide for stress-deformation analysis. GEO-SLOPE International Ltd. Calgary, AB, Canada.

[49]. Gerard, C.J., 1965. The Influence of Soil Moisture, Soil Texture, Drying Conditions, and Exchangeable Cations on Soil Strength 1. Soil Sci. Soc. Am. J. 29, 641–645. https://doi.org/10.2136/sssaj1965.03615995002900060017x

[50]. Gresnigt, A.M., 1986. Plastic design of buried steel pipelines in settlement areas. Heron Delft 31, 1–113.

[51]. Han, Z., Vanapalli, S.K., 2016. Stiffness and shear strength of unsaturated soils in relation to soil-water characteristic curve. Géotechnique 66, 627–647. https://doi.org/10.1680/jgeot.15.P.104

[52]. Han, Z., Vanapalli, S.K., Kutlu, Z.N., 2016. Modeling Behavior of Friction Pile in Compacted Glacial Till. Int. J. Geomech. 16. https://doi.org/10.1061/(ASCE)GM.1943-5622.0000659

[53]. Highland, L., 2004. Landslide types and processes. Fact Sheet. https://doi.org/10.3133/fs20043072

[54]. Holtz, R.D., Kovacs, W.D., 1981. An Introduction to Geotechnical Engineering. Prentice-Hall.

[55]. Huang, S., Barbour, S.L., Fredlund, D.G., 1998. Development and verification of a coefficient of permeability function for a deformable unsaturated soil. Can. Geotech. J. 35, 411–425. https://doi.org/10.1139/t98-010

[56]. Huang, S.L., Bray, M.T., Akagawa, S., Fukuda, M., 2004. Field Investigation of Soil Heave by a Large Diameter Chilled Gas Pipeline Experiment, Fairbanks, Alaska. J. Cold Reg. Eng. 18, 2–34. https://doi.org/10.1061/(ASCE)0887-381X(2004)18:1(2)

[57]. Huang, S.L., Yang, K., Akagawa, S., Fukuda, M., Kanie, S., 2015. Frost Heave Induced Pipe Strain of an Experimental Chilled Gas Pipeline, in: Innovative Materials and Design for Sustainable Transportation Infrastructure. Presented at the International Symposium on Systematic Approaches to Environmental Sustainability in Transportation, American Society of Civil Engineers, Fairbanks, Alaska, pp. 405–416. https://doi.org/10.1061/9780784479278.037

[58]. Hungr, O., Leroueil, S., Picarelli, L., 2014. The Varnes classification of landslide types, an update. Landslides 11, 167–194. https://doi.org/10.1007/s10346-013-0436-y

[59]. IITK-GSDMA, 2007. GUIDELINES for SEISMIC DESIGN of BURIED PIPELINES. Indian Institute of Technology Kanpur - Gujarat State Disaster Management Authority, National Information Center of Earthquake Engineering, Kanpur, India.

[60]. ITASCA, 2005. User's manuel, FLAC3D (Fast Lagrangian Analysis of Continua).

[61]. Ito, M., Azam, S., Hu, Y., 2014. A two stage model for moisture-induced deformations in expansive soils. Environ. Syst. Res. 3, 19. https://doi.org/10.1186/s40068-014-0019-5

[62]. Jiang, X., Wu, L., Wei, Y., 2020. Influence of Fine Content on the Soil–Water Characteristic Curve of Unsaturated Soils. Geotech. Geol. Eng. 38, 1371–1378. https://doi.org/10.1007/s10706-019-01096-5

[63]. Karube, D., Kawai, K., 2001. The role of pore water in the mechanical behavior of unsaturated soils. Geotech. Geol. Eng. 19, 211–241. https://doi.org/10.1023/A:1013188200053

[64]. Kausel, E., 2010. Early history of soil–structure interaction. Soil Dyn. Earthq. Eng. 30, 822–832. https://doi.org/10.1016/j.soildyn.2009.11.001

[65]. Khalili, N., Khabbaz, M.H., 1998. A unique relationship for χ for the determination of the shear strength of unsaturated soils. Géotechnique 48, 681–687. https://doi.org/10.1680/geot.1998.48.5.681

[66]. Khemissa, M., 2006. Méthodes d'analyse de la stabilité et techniques de stabilisation des pentes. Actes JNGG.

[67]. Kouretzis, G.P., Karamitros, D.K., Sloan, S.W., 2015. Analysis of buried pipelines subjected to ground surface settlement and heave. Can. Geotech. J. 52, 1058–1071.

[68]. Kristo, C., Rahardjo, H., Satyanaga, A., 2017. Effect of variations in rainfall intensity on slope stability in Singapore. Int. Soil Water Conserv. Res. 5, 258–264. https://doi.org/10.1016/j.iswcr.2017.07.001

[69]. Kumar, S., Sahu, A.K., Naval, S., 2020. Influence of Jute Fibre on CBR Value of Expansive Soil. Civ. Eng. J. 6, 1180–1194. https://doi.org/10.28991/cej-2020-03091539

[70]. Lambe, T.W., Whitman, R.V., 1969. Soil mechanics, Series in soil engineering. Wiley, New York.

[71]. Leonards, G., Roy, M., 1976. Predicting Performance of Pipe Culverts Buried in Soil, Phase 1 : Interim Report (No. FHWA/IN/JHRP-76/15, 1(12) Pt 2). Purdue University, West Lafayette, IN. https://doi.org/10.5703/1288284313924

[72]. Leong, E.-C., Rahardjo, H., 1997. Permeability Functions for Unsaturated Soils. J. Geotech. Geoenvironmental Eng. 123, 1118–1126. https://doi.org/10.1061/(ASCE)1090-0241(1997)123:12(1118)

[73]. Li, C., Wang, L., Jing, H., Liu, Q., 2013. Protection Control Scheme and Evaluation of Effectson Pipeline Crossing beneath Landslide Area. J. Pipeline Syst. Eng. Pract. 4, 41–48. https://doi.org/10.1061/(ASCE)PS.1949-1204.0000130

[74]. Li, W.C., Lee, L.M., Cai, H., Li, H.J., Dai, F.C., Wang, M.L., 2013. Combined roles of saturated permeability and rainfall characteristics on surficial failure of homogeneous soil slope. Eng. Geol. 153, 105–113. https://doi.org/10.1016/j.enggeo.2012.11.017

[75]. Lian, B., Peng, J., Wang, X., Huang, Q., 2020. Moisture content effect on the ring shear characteristics of slip zone loess at high shearing rates. Bull. Eng. Geol. Environ. 79, 999–1008. https://doi.org/10.1007/s10064-019-01597-w

[76]. Lin, H., Zhong, W., 2019. Influence of Rainfall Intensity and Its Pattern on the Stability of Unsaturated Soil Slope. Geotech. Geol. Eng. 37, 615–623. https://doi.org/10.1007/s10706-018-0631-7

[77]. Liu, H., 2004. Pipeline Engineering. CRC Press.

[78]. Liu, Y., Cai, Y., Huang, S., Guo, Y., Liu, G., 2019. Effect of water saturation on uniaxial compressive strength and damage degree of clay-bearing sandstone under freeze-thaw. Bull. Eng. Geol. Environ. https://doi.org/10.1007/s10064-019-01686-w

[79]. LNHC Batna, 2016. Rapport d'etude de sol (2015) (Rapport d'etude de sol No. 127/2015). GENEST, Batna, Algérie.

[80]. LNHC Batna, 2016. Rapport d'Etude de Sol (No. 01). LNHC Batna, Ain Tinn, Mila, Algeria.

[81]. LNHC Batna, 2017. Rapport d'etude de sol (2017).

[82]. Lu, N., Kaya, M., 2014. Power Law for Elastic Moduli of Unsaturated Soil. J. Geotech. Geoenvironmental Eng. 140, 46–56. https://doi.org/10.1061/(ASCE)GT.1943-5606.0000990

[83]. Marston, Anderson, 1913. The Theory of Loads on Pipes in Ditches and Tests of Cement and Clay Drain Tile and Sewer Pipes.

[84]. Matyas, E.L., Radhakrishna, H.S., 1968. Volume Change Characteristics of Partially Saturated Soils. Géotechnique 18, 432–448. https://doi.org/10.1680/geot.1968.18.4.432

[85]. McKee, C.R., Bumb, A.C., 1987. Flow-Testing Coalbed Methane Production Wells in the Presence of Water and Gas. SPE Form. Eval. 2, 599–608. https://doi.org/10.2118/14447-PA

[86]. Mebarki, A., 2005. HYDROLOGIE DES BASSINS DE L'EST ALGERIEN : RESSOURCES EN EAU, AMENAGEMENT, ET ENVIRONNEMENT (thèse de doctorat d'etat). University of Mentouri, Constantine.

[87]. Meilani, I., Rahardjo, H., Leong, E.-C., 2005. Pore-water pressure and water volume change of an unsaturated soil under infiltration conditions. Can. Geotech. J. 42, 1509–1531. https://doi.org/10.1139/t05-066

[88]. Mohitpour, M., Golshan, H., Murray, A., 2007. Pipeline design & construction: a practical approach, 3rd ed. ed. ASME Press, New York.

[89]. Moser, A.P., Folkman, S., 2008. Buried Pipe Design, Third Edition, 3rd ed. McGraw-Hill Education.

[90]. Murray, E.J., Sivakumar, V., 2010. Unsaturated Soils: A fundamental interpretation of soil behaviour. John Wiley & Sons, New York.

[91]. Ng, P.C.F., 1994. Behaviour of buried pipelines subjected to external loading. (phd). University of Sheffield.

[92]. Nguyen, T.S., Likitlersuang, S., 2019. Reliability analysis of unsaturated soil slope stability under infiltration considering hydraulic and shear strength parameters. Bull. Eng. Geol. Environ. 78, 5727–5743. https://doi.org/10.1007/s10064-019-01513-2

[93]. O'Rourke, T.D., Jezerski, J.M., Olson, N.A., Bonneau, A.L., Palmer, M.C., Stewart, H.E., O'Rourke, M.J., Abdoun, T., 2008. Geotechnics of Pipeline System Response to Earthquakes, in: Geotechnical Earthquake Engineering and Soil Dynamics IV. Presented at the Geotechnical Earthquake Engineering and Soil Dynamics Congress IV, American Society of Civil Engineers, Sacramento, California, United States, pp. 1–38. https://doi.org/10.1061/40975(318)193

[94]. Oghabi, M., Khoshvatan, M., Marto, A., 2017. Evaluation of the Response of Buried Steel Pipelines Subjected to the Strike-slip Fault Displacement. Civ. Eng. J. 3, 661–671. https://doi.org/10.21859/cej-03093

[95]. Oh, W.T., Vanapalli, S.K., Puppala, A.J., 2009. Semi-empirical model for the prediction of modulus of elasticity for unsaturated soils. Can. Geotech. J. 46, 903–914. https://doi.org/10.1139/T09-030

[96]. Ozer, M., Ulusay, R., Isik, N.S., 2012. Evaluation of damage to light structures erected on a fill material rich in expansive soil. Bull. Eng. Geol. Environ. 71, 21–36. https://doi.org/10.1007/s10064-011-0395-2

[97]. Palmer, A.C., Tebboth, L., Miles, D., Calladine, C.R., 1999. Instability of Pipelines on Slopes. J. Appl. Mech. 66, 794–799. https://doi.org/10.1115/1.2791757

[98]. Patil, U.D., Puppala, A.J., Hoyos, L.R., Banerjee, A., 2018. Strength, Stiffness and Radial Anisotropy of Compacted Silty Sand Under Suction-Controlled Axisymmetric Shearing. Geotech. Geol. Eng. 36, 3945–3960. https://doi.org/10.1007/s10706-018-0590-z

[99]. Potts, D.M., Zdravković, L., 2001. Finite Element Analysis in Geotechnical Engineering: Volume two - Application. Thomas Telford Publishing. https://doi.org/10.1680/feaigea.27831

[100]. Qi, S., Vanapalli, S.K., 2015. Hydro-mechanical coupling effect on surficial layer stability of unsaturated expansive soil slopes. Comput. Geotech. 70, 68–82. https://doi.org/10.1016/j.compgeo.2015.07.006

[101]. Qi, S., Vanapalli, S.K., 2016. Influence of swelling behavior on the stability of an infinite unsaturated expansive soil slope. Comput. Geotech. 76, 154–169. https://doi.org/10.1016/j.compgeo.2016.02.018

[102]. Rahardjo, H., Melinda, F., Leong, E.C., Rezaur, R.B., 2011. Stiffness of a compacted residual soil. Eng. Geol. 120, 60–67. https://doi.org/10.1016/j.enggeo.2011.04.006

[103]. Rajani, B., Morgenstern, N., 1993. Pipelines and Laterally Loaded Piles in Elastoplastic Medium. J. Geotech. Eng. 119, 1431–1448. https://doi.org/10.1061/(ASCE)0733-9410(1993)119:9(1431)

[104]. Rajani, B., Zhan, C., Kuraoka, S., 1996. Pipe-soil interaction analysis of jointed water mains. Can. Geotech. J. 33, 393–404. https://doi.org/10.1139/t96-061

[105]. Rajeev, P., Chan, D., Kodikara, J., 2012. Ground–atmosphere interaction modelling for long-term prediction of soil moisture and temperature. Can. Geotech. J. 49, 1059–1073. https://doi.org/10.1139/t2012-068

[106]. Rajeev, P., Kodikara, J., 2011. Numerical analysis of an experimental pipe buried in swelling soil. Comput. Geotech. 38, 897–904. https://doi.org/10.1016/j.compgeo.2011.06.005

[107]. Rampino, C., Mancuso, C., Vinale, F., 2000. Experimental behaviour and modelling of an unsaturated compacted soil. Can. Geotech. J. 37, 748–763. https://doi.org/10.1139/t00-004

[108]. Randeniya, C., Robert, D. j., Li, C.-Q., Kodikara, J., 2019. Large-scale experimental evaluation of soil saturation effect on behaviour of buried pipes under operational loads. Can. Geotech. J. 57, 205–220. https://doi.org/10.1139/cgj-2018-0544

[109]. Robert, D., Soga, K., 2013. Soil-Pipeline Interaction in Unsaturated Soils, in: Mechanics of Unsaturated Geomaterials. John Wiley & Sons, Inc., Hoboken, NJ USA, pp. 303–325. https://doi.org/10.1002/9781118616871.ch13

[110]. Robert, D.J., Soga, K., O'Rourke, T.D., 2016a. Pipelines Subjected to Fault Movement in Dry and Unsaturated Soils. Int. J. Geomech. 16. https://doi.org/10.1061/(ASCE)GM.1943-5622.0000548

[111]. Robert, D.J., Soga, K., O'Rourke, T.D., Sakanoue, T., 2016b. Lateral Load-Displacement Behavior of Pipelines in Unsaturated Sands. J. Geotech. Geoenvironmental Eng. 142, 04016060. https://doi.org/10.1061/(ASCE)GT.1943-5606.0001504

[112]. Roy, K., Hawlader, B., Kenny, S., Moore, I., 2016. Finite element modeling of lateral pipeline–soil interactions in dense sand. Can. Geotech. J. 53, 490–504. https://doi.org/10.1139/cgj-2015-0171

[113]. Saadeldin, R., Hu, Y., Henni, A., 2015. Numerical analysis of buried pipes under field geo-environmental conditions. Int. J. Geo-Eng. 6, 6. https://doi.org/10.1186/s40703-015-0005-4

[114]. Satyanaga, A., Rahardjo, H., Leong, E.-C., Wang, J.-Y., 2013. Water characteristic curve of soil with bimodal grain-size distribution. Comput. Geotech. 48, 51–61. https://doi.org/10.1016/j.compgeo.2012.09.008

[115]. Sawangsuriya A., Edil T. B., Bosscher P. J., 2009. Modulus-Suction-Moisture Relationship for Compacted Soils in Postcompaction State. J. Geotech. Geoenvironmental Eng. 135, 1390–1403. https://doi.org/10.1061/(ASCE)GT.1943-5606.0000108

[116]. Semmane, F., Abacha, I., Yelles-Chaouche, A.K., Haned, A., Beldjoudi, H., Amrani, A., 2012. The earthquake swarm of December 2007 in the Mila region of northeastern Algeria. Nat. Hazards 64, 1855–1871. https://doi.org/10.1007/s11069-012-0338-7

[117]. Shen, H., Klapperich, H., Abbas, S.M., Ibrahim, A., 2012. Slope stability analysis based on the integration of GIS and numerical simulation. Autom. Constr. 26, 46–53. https://doi.org/10.1016/j.autcon.2012.04.016

[118]. Sheng, D., Zhou, A., Fredlund, D.G., 2011. Shear Strength Criteria for Unsaturated Soils. Geotech. Geol. Eng. 29, 145–159. https://doi.org/10.1007/s10706-009-9276-x

[119]. Shi, Y.-M., Wang, N., Gao, F.-P., Qi, W.-G., Wang, J.-Q., 2019. Physical modeling of the axial pipe-soil interaction for pipeline walking on a sloping sandy seabed. Ocean Eng. 178, 20–30. https://doi.org/10.1016/j.oceaneng.2019.02.059

[120]. Taber, S., 1929. Frost Heaving. J. Geol. 37, 428–461. https://doi.org/10.1086/623637

[121]. Teimouri, A.B.B., Khalkhali, A.B., 2018. Stability Control of Narmab Dam and Sensitivity Analysis of Reliability Coefficients. Civ. Eng. J. 4, 2197-2209–2209. https://doi.org/10.28991/cej-03091150

[122]. Timošenko, S.P., Goodier, J.N., 1970. Theory of elasticity, 3rd ed, Engineering societies monographs. McGraw-Hill, Auckland.

[123]. Timoshenko, S., 1968. Résistance des matériaux. Dunod, Paris.

[124]. UNESCO Working Party On World Landslide Inventory, 1993. A suggested method for describing the activity of a landslide. Bull. Int. Assoc. Eng. Geol. 47, 53–57. https://doi.org/10.1007/BF02639593

[125]. Uzundurukan, S., Keskin, S.N., Yıldırım, H., Göksan, T.S., Çimen, Ö., 2014. Suction and Swell Characteristics of Compacted Clayey Soils. Arab. J. Sci. Eng. 39, 747–752. https://doi.org/10.1007/s13369-013-0852-2

[126]. van Genuchten, M.Th., 1980. A Closed-form Equation for Predicting the Hydraulic Conductivity of Unsaturated Soils. Soil Sci. Soc. Am. J. 44, 892–898. https://doi.org/10.2136/sssaj1980.03615995004400050002x

[127]. Van Terzaghi, K., 1936. The shearing resistance of saturated soils, in: Proc. 1st. Int. Conf. Soil Mech. Found. Eng., Cambridge, Mass. pp. 54–56.

[128]. Vanapalli, S., Oh, W., 2010. A model for predicting the modulus of elasticity of unsaturated soils using the soil-water characteristic curve. Int. J. Geotech. Eng. 4, 425–433. https://doi.org/10.3328/IJGE.2010.04.04.425-433

[129]. Vanapalli, S.K., Al-Khazaali, M., 2019. Axial Load-Displacement Behavior of Energy Pipeline Systems in Sand, in: Latha G., M. (Ed.), Frontiers in Geotechnical Engineering, Developments in Geotechnical Engineering. Springer Singapore, Singapore, pp. 121–138. https://doi.org/10.1007/978-981-13-5871-5_7

[130]. Vanapalli, S.K., Fredlund, D.G., Pufahl, D.E., Clifton, A.W., 1996. Model for the prediction of shear strength with respect to soil suction. Can. Geotech. J. 33, 379–392. https://doi.org/10.1139/t96-060

[131]. Vazouras, P., Dakoulas, P., Karamanos, S.A., 2015. Pipe–soil interaction and pipeline performance under strike–slip fault movements. Soil Dyn. Earthq. Eng. 72, 48–65. https://doi.org/10.1016/j.soildyn.2015.01.014

[132]. Vazouras, P., Dakoulas, P., Karamanos, S.A., 2015. Pipe–soil interaction and pipeline performance under strike–slip fault movements. Soil Dyn. Earthq. Eng. 72, 48–65. https://doi.org/10.1016/j.soildyn.2015.01.014

[133]. Vazouras, P., Karamanos, S.A., 2017. Structural behavior of buried pipe bends and their effect on pipeline response in fault crossing areas. Bull. Earthq. Eng. 15, 4999–5024. https://doi.org/10.1007/s10518-017-0148-0

[134]. Vazouras, P., Karamanos, S.A., Dakoulas, P., 2010. Finite element analysis of buried steel pipelines under strike-slip fault displacements. Soil Dyn. Earthq. Eng. 30, 1361–1376. https://doi.org/10.1016/j.soildyn.2010.06.011

[135]. Vazouras, P., Karamanos, S.A., Dakoulas, P., 2012. Mechanical behavior of buried steel pipes crossing active strike-slip faults. Soil Dyn. Earthq. Eng. 41, 164–180. https://doi.org/10.1016/j.soildyn.2012.05.012

[136]. Vu, H.Q., Fredlund, D.G., 2004. The prediction of one-, two-, and three-dimensional heave in expansive soils. Can. Geotech. J. 41, 713–737. https://doi.org/10.1139/t04-023

[137]. Vu, H.Q., Fredlund, D.G., 2006. Challenges to modelling heave in expansive soils. Can. Geotech. J. 43, 1249–1272. https://doi.org/10.1139/t06-073

[138]. Vu, H.Q., Fredlund, D.G., 2011. Challenges to modelling heave in expansive soils. Can. Geotech. J. https://doi.org/10.1139/t06-073

[139]. Watkins, R.K., Anderson, L.R., 2000. Structural mechanics of buried pipes. CRC Press, Boca Raton, FL.

[140]. Williams, 1982. The surface of the Earth, an introduction to geotechnical science. Longman Inc, New York.

[141]. Wu, J., Zhou, R., Xu, S., Wu, Z., 2017. Probabilistic analysis of natural gas pipeline network accident based on Bayesian network. J. Loss Prev. Process Ind. 46, 126–136. https://doi.org/10.1016/j.jlp.2017.01.025

[142]. Wu, R., Mei, Y., Deng, Q., Pang, C., Fu, M., 2014. Comparative Analysis by Numerical Simulation on Natural Gas Pipelines in Different Positions of Landslide, in: ICPTT 2014. Presented at the International Conference on Pipelines and Trenchless Technology 2014, American Society of Civil Engineers, Xiamen, China, pp. 308–319. https://doi.org/10.1061/9780784413821.035

[143]. Xie, M., Esaki, T., Cai, M., 2004. A GIS-based method for locating the critical 3D slip surface in a slope. Comput. Geotech. 31, 267–277. https://doi.org/10.1016/j.compgeo.2004.03.003

[144]. Xie, M., Esaki, T., Qiu, C., Wang, C., 2006. Geographical information system-based computational implementation and application of spatial three-dimensional slope stability analysis. Comput. Geotech. 33, 260–274. https://doi.org/10.1016/j.compgeo.2006.07.003

[145]. Yilmaz, I., 2007. The effect of swelling clays on a water transport canal between Köklüce HPP and Erbaa HPP (Turkey). Bull. Eng. Geol. Environ. 66, 467–472. https://doi.org/10.1007/s10064-007-0086-1

[146]. Zeng, L., Xiao, L.-Y., Zhang, J.-H., Gao, Q.-F., 2020. Effect of the characteristics of surface cracks on the transient saturated zones in colluvial soil slopes during rainfall. Bull. Eng. Geol. Environ. 79, 699–709. https://doi.org/10.1007/s10064-019-01584-1

[147]. Zhang, J., Peng, J., Li, J., Zheng, J., 2018. Variation of Resilient Modulus with Soil Suction for Cohesive Soils in South China. Int. J. Civ. Eng. 16, 1655–1667. https://doi.org/10.1007/s40999-018-0315-y

[148]. Zhang, L.L., Fredlund, D.G., Zhang, L.M., Tang, W.H., 2004. Numerical study of soil conditions under which matric suction can be maintained. Can. Geotech. J. 41, 569–582. https://doi.org/10.1139/t04-006

[149]. Zhang, L.L., Zhang, J., Zhang, L.M., Tang, W.H., 2011. Stability analysis of rainfall-induced slope failure: a review. Proc. Inst. Civ. Eng. - Geotech. Eng. 164, 299–316. https://doi.org/10.1680/geng.2011.164.5.299

[150]. Zhang, W., Askarinejad, A., 2019. Behaviour of buried pipes in unstable sandy slopes. Landslides 16, 283–293. https://doi.org/10.1007/s10346-018-1066-1

[151]. Zhang, X., Briaud, J.-L., 2015. Three dimensional numerical simulation of residential building on shrink–swell soils in response to climatic conditions. Int. J. Numer. Anal. Methods Geomech. 39, 1369–1409. https://doi.org/10.1002/nag.2360